Engineering Innate Immune Activators for Intratumoral Immunotherapy

By

Kyle Michell Garland

Dissertation

Submitted to the Faculty of the

Graduate School of Vanderbilt University

in partial fulfillment of the requirements

for the degree of

DOCTOR OF PHILOSOPHY

in

Chemical Engineering

December 18, 2021

Nashville, Tennessee

Approved:

John T. Wilson, Ph.D.

Craig L. Duvall, Ph.D.

Marjan Rafat, Ph.D.

Young J. Kim, Ph.D.

Scott A. Guelcher, Ph.D.

Copyright © 2021 Kyle Michell Garland
All Rights Reserved

This work is dedicated to my friends and family.

ACKNOWLEDGMENTS

I am immensely fortunate to have had so much support all throughout my graduate career. First, I would like to thank my advisor, Prof. John T. Wilson for everything that he gives to ensure that his students and employees succeed in their endeavors. His remarkable enthusiasm for science and his endless devotion to the ImmunoEngineering Laboratory have created an incredibly secure foundation for scientific research as well as personal growth. I am extremely grateful to my other committee members, Prof. Craig L. Duvall, Prof. Marjan Rafat, Prof. Young J. Kim, and Prof. Scott A. Guelcher, who have also provided invaluable feedback and guidance. The mentorship that I have received from my committee has sculpted me into the passionate scientist that I am today.

I would like to thank all of the current members and alumni of the ImmunoEngineering Laboratory. In our research collaborations, I received exceptional mentorship and technical support from Sema Sevimli, Lihong Wang-Bishop, and Karan Arora. I am grateful for Sema's guidance during my first two years in the lab. She gave me the skills I needed to succeed as a scientist by teaching me to work effectively and efficiently in the lab. I am thankful for my undergraduate mentee, Casey Van Kaer, who assisted me with several experiments one summer and gave me the valuable experience of teaching and training a passionate student.

In terms of both research and mentoring, I have learned so much from my fellow graduate students in the ImmunoEngineering Laboratory: Dan Shae, Max Jacobson, Frances Knight, Carcia Carson, Christian Palmer, Jessalyn Baljon, Lucinda Pastora, Taylor Sheehy, Hayden Pagendarm, Payton Stone, and our honorary lab members, Jonah Rosch and Bonnie Walton. Dan offered me invaluable advice and insight toward both research and a career in industry. I thoroughly enjoyed game nights hosted by Max and our all-you-can-eat sushi escapades. My trips to the Flying Saucer

with Frances and pet-sitting her cat, Rosie always brightened my day. I was so lucky to join the lab with Carcia and Christian, both of whom helped me gain my footing in the lab. It has been an absolute pleasure getting to work closely with Carcia on our projects together. Her kind spirit and compliments about my growth as a scientist has meant more to me than she could ever imagine. Christian has been such a great peer in both the ChBE program and the ImmunoEngineering Laboratory; I will fondly remember our lunches together, playing with his cat, Ruca, and the time we got to our immunology class early only to find a couple cold and refreshing surprises. Jessalyn has been an amazing friend and coworker; I'll always strive for her level of organization and I am truly grateful that she and her cohort have been so welcoming. I appreciate them letting me tag along on their trips to the Flying Saucer. I also love that Bonnie Walton has been able to come to so many of the Wilson Lab outings, as she is a great friend and keeps life interesting. After work, I would sometimes get the chance to walk with Lucinda back towards our apartments near Hillsboro Village. I always found our walks quite enjoyable and cathartic, as we would catch up, discuss our research, and occasionally vent to each other. It was also always such a treat to hang out at Lucinda's apartment with her and her boyfriend, Brian and their cats, Dante and Loki. I wish that Taylor could have joined the Wilson Lab earlier, as she has been such a positive presence at work. Our review paper, written together with Prof. Wilson, is one of my proudest accomplishments, and I think that Taylor and I complemented each other very well on it. I have also enjoyed getting to pet-sit her dog, Tucker. My dog, Max has enjoyed Tucker's company as well! While my time in the Immunoengineering Laboratory has not overlapped very long with Hayden and Payton, I have enjoyed mentoring them some and I am very impressed with their abilities to learn quickly and execute their experiments. Jonah was always my "plus one" for all Wilson Lab social events, as he has been there for me from my very first day, when he hosted me

on my recruitment visit, through the end of my graduate studies. Even after he graduated and moved away, I have been able to count on him to lend an ear and offer advice. I don't think that I have ever met someone with more of my sense of humor. I will always remember our many adventures: at the dog park with Max and Lila, in my apartment playing Jeopardy on Alexa and drinking espressos in the mornings before work, and out on the town earning his reputation as the department's party animal.

For maintaining my work-life-balance, I am grateful to my Chemical and Biomolecular Engineering graduate student classmates: Christian Palmer, Sarah Sacco, Greg Lowen, Ray Matsumoto, Dustin Groff, Alex Yang, Kazi Tasneem, Debayon Dutta, Eden Paul, Zach Jenkins, Shauna Harbison, as well as my other friends from outside of lab (*e.g.* on the tennis courts, at pub trivia, at department happy hours, *etc.*): Mohsin Rahim, Michael Marin, Joe Weinstein-Webb, Katie Ozgun, Allison Bosworth, Natalie Noll, Ella Hoogenboezem, Prarthana Patil, Dickie D'Arcy, Carli DeJulius, Jesse Beckner, Bryan Dollinger, Isom Kelly, Brock Fletcher, Shrusti Patel, Will Tierney, Jordan Hill, Alex Sorets, Josh McCune, Harris Manning Jr., Krysta Waldrop, Michael Crocker, Tom Spoonmore, Bradley Baker, Emma Hollmann Neal, Michael Kosson, Josh Passantino, and Amy Zheng. I am constantly amazed by Mohsin's kindness and his broad scope of knowledge and I am grateful to have him as such a close friend. I am thankful to have befriended Allison, Katie, and Natalie and to have enjoyed movie nights, murder-mystery games, and camaraderie at their home. Their company was always warm and uplifting. I am thankful that Ella moved into my apartment complex and grateful that we have become so close and spent so much great time together. I could always count on Ella to watch Max when I needed to travel, and I could rest assured that Max would have fun with her and her dog, Nina while I was away. I am thankful that Prarthana has been a wonderful friend to me, living nearby me for most of my time in graduate

school and often hosting fun and exciting gatherings at her abode. I am grateful to have met Dickie, who is a truly brilliant scientist and an even better friend. Carli and Jesse are beautiful power couple, and I am so lucky to have become so close to both of them.

Finally, I must thank my entire family. Above all, I am grateful to my mother, who is the most selfless person that I know and has done more for my success than anyone else, including me. She is my role model, and I aspire to be like her. I am grateful to my father, for ensuring my education and for all of the advice he has given me. For their love and support, I am grateful to my siblings and their nuclear families: my sister, Alison, her husband, Lance, and their children, Charlotte, Logan (my godson), and Molly; my eldest brother, David, his wife, Sylvia, and their child, Claire; my other older brother, Taylor, his wife Tori, and their child, Ben; my younger brother, Ian. I am grateful to my loving and caring partner, Brittany Partain and our dogs, Max and Leo. Having spent the last five years living apart, our daily phone calls and her positive attitude have kept me sane. Through Brittany, I have met so many amazing people, who have also helped me along the way: her mother, Emmy; her step-father, David; her sister, Lauren; her brother-in-law, Michael; her godfather, Randy. None of this dissertation would have been possible without the love and support that I received from all of my family and friends.

TABLE OF CONTENTS

LIST OF TABLES

LIST OF FIGURES

CHAPTER I

INTRODUCTION

Significance

Cancer is a devastating disease that caused ~ 10 million deaths worldwide in 2020 alone[1]. In the United States, cancer is the second leading cause of death with ~ 1,900,000 new cancer cases and ~ 610,000 cancer deaths projected to occur in 2021[2]. While the total number of deaths per year due to cancer has continued to rise, the rate of cancer deaths within the United States has significantly declined over the past two decades, which has been largely attributed to reductions in smoking, advances in early detection, and better treatment options, notably including enhanced interventional radiology and the relatively recent clinical success of cancer immunotherapy[2].

The development of cancer occurs when immunosuppression sufficiently inhibits the naturally occurring process through which the immune system recognizes and eliminates cancerous cells (*i.e.* the cancer-immunity-cycle). While clinically used strategies to lessen immunosuppression, such as immune checkpoint blockade (ICB) therapy, can be extraordinarily effective at eliminating cancer, they only work in patients who already possess a certain degree of antitumor immunity. Indeed, the patients who do respond well to ICB therapy typically have tumors that possess a significant presence of certain cancer-killing immune cells[3]. This dissertation describes the development of novel platforms for local immunomodulation, which have been designed for intratumoral administration and are intended to address those limitations of the current standard-of-care cancer immunotherapies.

Innovation

I. Cytosolic Delivery of Nucleic Acids to Enhance the Cancer-Immunity-Cycle

For the early detection of diseased cells and the generation of disease-eliminating adaptive immunity, the immune system largely relies on a network of pattern recognition receptors (PRRs), which are germline-encoded cell-associated proteins that can initiate innate immunity by sensing and responding to various "danger signals" (*i.e.* anomalies that are indicative of cellular stress). PRRs recognize the aberrant cellular localization of exogenous pathogen-derived molecules as well as endogenous molecules derived from cellular damage. Notably, PRRs can be exploited to prime the immune system, even in the absence of a true threat. For example, the administration of vaccines, which usually comprise PRR-specific activators (*i.e.* adjuvants) along with disease-specific molecular cues (*i.e.* antigens), can mimic natural infection and thereby confer artificially generated immune protection against an encoded disease. Accordingly, certain PRRs are also attractive therapeutic targets for cancer immunotherapy, as they can be similarly exploited to galvanize antitumor immunity against tumors that exhibit low immunogenicity.

While there exist many PRRs that can stimulate innate immunity, most PRRs recognize distinct molecules and relay varied immunological effects, which can result in drastically different disease outcomes[4]. Notably, there are several PRRs (*e.g.* cGAS, RIG-I, TLR3, TLR9, *etc.*) that can promote antitumor immunity by triggering type-I interferon (IFN)-driven innate immune programs in response to mislocalized nucleic acids[5]. Thus, in the proper context, nucleic acids can jump-start the cancer-immunity-cycle by activating such pattern recognition receptors (PRRs).

In addition to their capacity for immunostimulation, nucleic acids can also provide a means for the removal of existing immunosuppression within the tumor microenvironment (TME). Indeed, small interfering RNA (siRNA) can bind the ubiquitously expressed RNA-induced

silencing complex (RISC) within the cytosol of cells and thereby inhibit specific protein translation via RNA interference (RNAi)[6]. Accordingly, the expression of immunosuppressive proteins that threaten the continuity of the cancer-immunity-cycle can be specifically reduced via RNAi. Therefore, since nucleic acids can push the cycle forward and release the cycle from restrictive immunosuppression, therapeutic strategies involving the cytosolic delivery of nucleic acids are well poised to propagate the cancer-immunity-cycle and are a main focus of this dissertation.

II. Intratumoral Administration of Cationic Nanoparticles

Many nucleic acid sensors (*e.g.* PRRs, RISC, *etc.*) reside within intracellular locations that are not easily druggable with exogenous nucleic acids. Indeed, nucleic acids are particularly inefficient at independently penetrating cell membranes as a result of their inherent hydrophilic composition, relatively large size, and overall negative charge[6]. In this work, the well-established pH-responsive diblock copolymer, poly(dimethylaminoethyl methacrylate)-*b*-poly(propylacrylic acid-*co*-dimethylaminoethyl methacrylate-*co*-butyl methacrylate) (D-PDB) was employed to overcome numerous barriers that inhibit the cytosolic delivery of nucleic acids (***Figure 1.1***).

D-PDB is a non-viral vector that was originally developed for the cytosolic delivery of siRNA[7, 8]. At the physiological pH of 7.4, D-PDB self-assembles into stable micelles that are solely dependent on electrostatic complexation for nucleic acid cargo loading, and therefore the polymer can also function as a carrier for other negatively charged multivalent compounds (*e.g.* DNA). Indeed, in this work, D-PDB is used not only for siRNA delivery, but also for the cytosolic delivery of various immunostimulatory nucleic acids, including cGAS-activating double-stranded DNA (dsDNA) molecules. Following cellular uptake, D-PDB loses its micellar morphology, as the encapsulating endosomes acidify. Freed polymer strands then trigger endosomal escape of the nucleic acid into the cytosol, where activation of RISC and/or PRRs can occur (***Figure 1.1***).

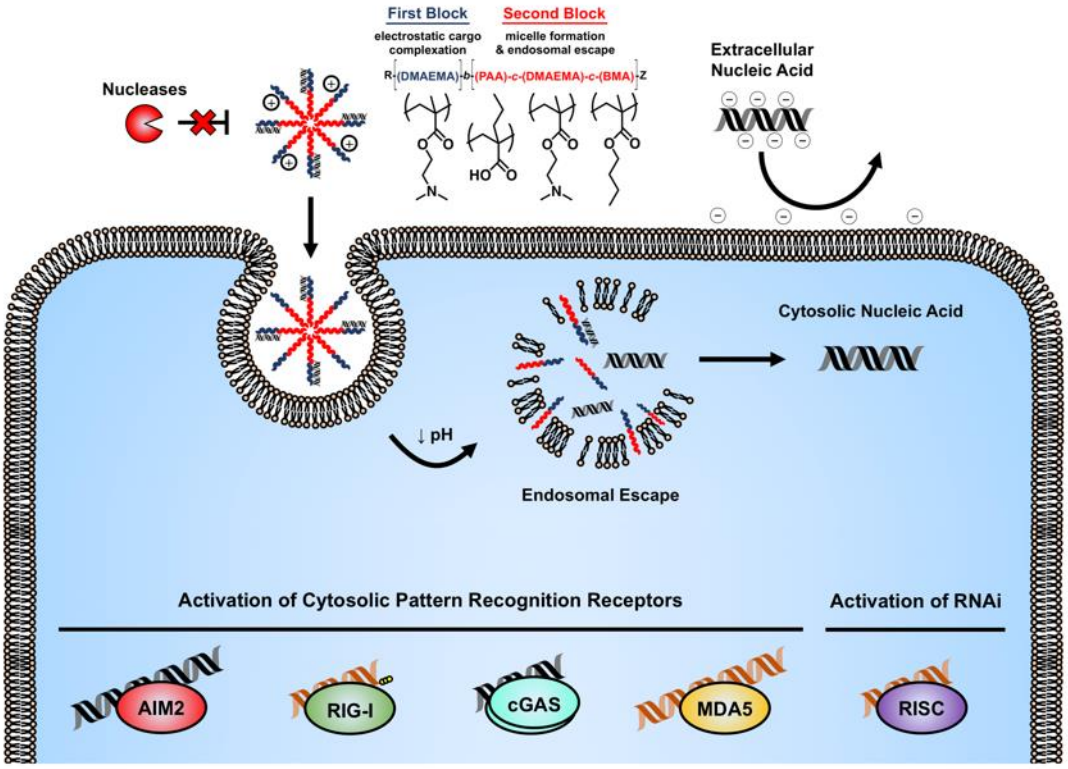

Figure 1.1. Employing the endosomolytic nanoparticle, D-PDB to overcome delivery barriers for therapeutic nucleic acids. Potential cytosolic targets are shown as well as the chemical and functional properties of D-PDB.

Having a hydrodynamic diameter of ~ 60 nm and a positive surface charge of ~ +15 mV, D-PDB nanoparticles exhibit optimal characteristics for efficient cellular association and uptake[9]. Nevertheless, cationic delivery vehicles, such as D-PDB, exhibit poor pharmacokinetic properties upon systemic administration. Indeed, when injected intravenously, cationic delivery vehicles exhibit exceptionally short half-lives (*e.g.* ~ 3 minutes in BALB/c mice)[10] and severe dose-limiting toxicities[11]. While in many cancer treatment settings, systemic delivery can be advantageous over a direct intratumoral injection in terms of a drug reaching undetectable metastatic tumor sites, cancer immunotherapy is unique in that, in theory, a single cellular interaction can generate a systemic immune response that is capable of clearing distal anenestic metastases (*i.e.* abscopal effect). Thus, the local administration of anticancer drugs is well-suited for cancer immunotherapy.

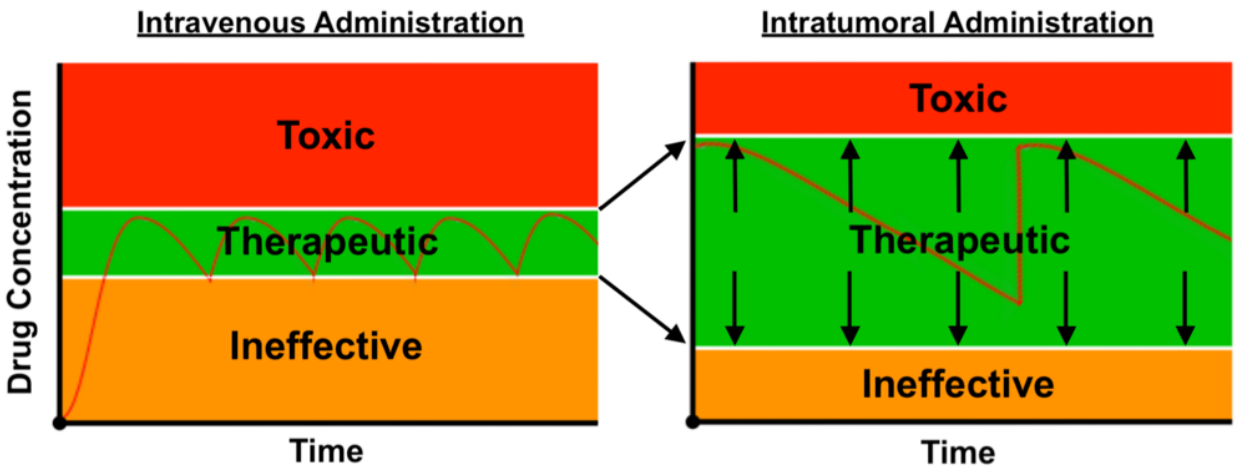

Figure 1.2. The therapeutic windows and intratumoral drug concentration profiles for intravenous and intratumoral administration routes.

Local therapy also offers much better control over drug concentrations within the TME. While intravenous delivery of cancer therapeutics typically results in low tumor accumulation due to off-target clearance[12, 13], intratumoral injections represent the most efficient form of delivery for cancer immunotherapeutics that exhibit their primary effector function within solid tumors. Indeed, intratumoral injections have great potential to efficiently kick-start the cancer-immunity-cycle, since all of an intratumorally injected dose will immediately encounter a TME. In addition to facilitating more complete and efficient delivery, intratumoral injections are also associated with better safety profiles relative to systemic administration. Accordingly, intratumoral therapeutic administration expands both boundaries of a drug's therapeutic window (***Figure 1.2***).

On one end of the therapeutic window, intratumoral injections increase dose potency as a result of more drug reaching its effector site within the TME, which can limit the need for excessive additional injections. Decreasing the number of injections required for a therapeutic effect is usually desirable, as it can increase practicality, clinical relevance, patient compliance, and economic availability[14]. On the other end of the therapeutic window, the intratumoral injection of

drugs can reduce the potential systemic toxicity of a drug, since only a fraction of the injected drug is likely to enter systemic circulation. Indeed, intratumorally injected drugs can experience multiple clearance routes, including cellular uptake in the TME, retention and/or degradation in a tumor's interstitial space, lymphatic drainage, and escape into systemic circulation (***Figure 1.3***).

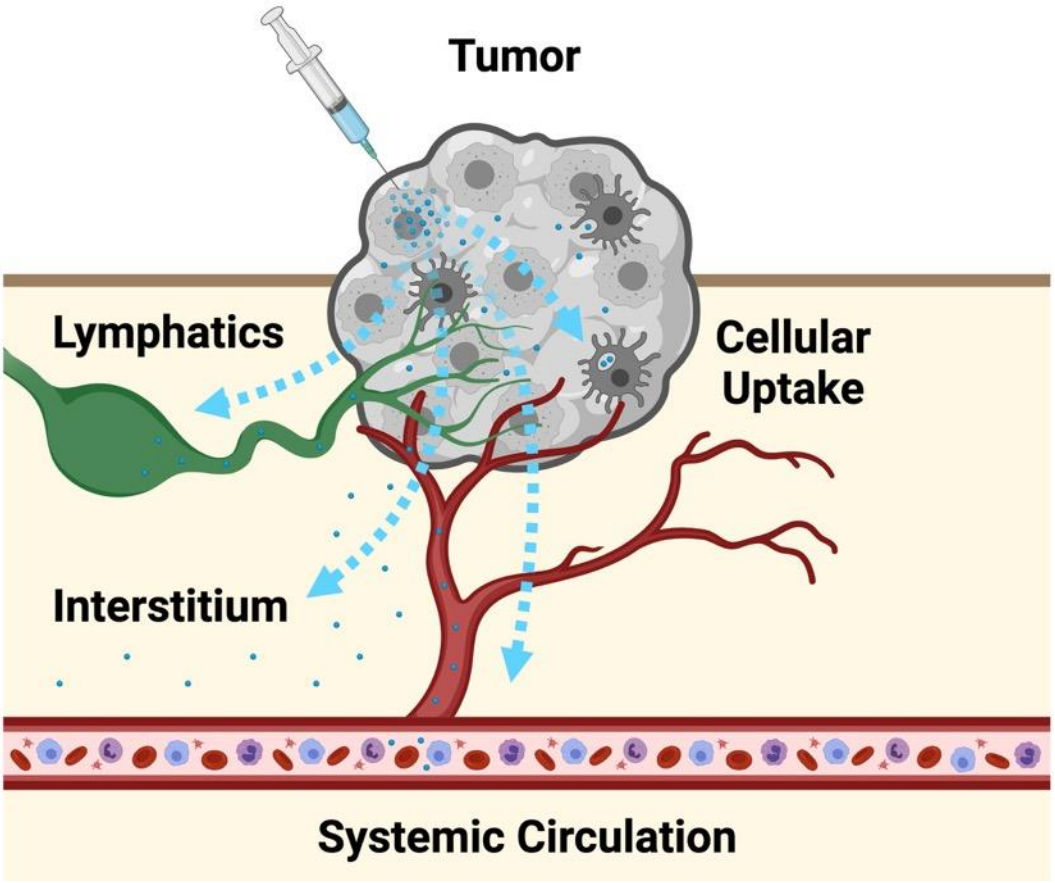

Figure 1.3. Potential clearance routes of intratumorally injected therapeutics. Figure created with *biorender.com*.

Accordingly, intratumoral administration can enable enhanced evaluation of drug efficacy, since higher drug doses can be explored with less risk of systemic toxicity. This is particularly important for cancer immunotherapy, because treatment-related toxicity often correlates with better responses to cancer immunotherapeutics[15]. Furthermore, due to recent advances in interventional radiology, endoscopy, and laparoscopic surgery, nearly every site/organ in the

human body can be biopsied and can therefore also accommodate a direct injection[16]. Thus, intratumoral immunotherapy is a broadly applicable strategy for the treatment of solid tumor cancers. Indeed, intratumoral immunotherapy has already demonstrated some success in generating durable and lasting therapeutic immune responses to many solid tumor cancers[17-20].

III. Pharmacological targeting of cGAS for Cancer Immunotherapy

While the STING protein has been the main focus for therapeutic strategies that seek to activate the cGAS/STING pathway, the cGAS protein at the forefront of the signaling pathway, has been relatively unexplored as a target, despite several potential advantages:

- Therapeutic adjuvants that target cGAS would more closely mimic microbial infection and self dsDNA sensing relative to adjuvants that target the STING protein.
- The cGAS enzyme overs more control over the degree of STING signaling relative to the STING protein, since cGAS activity can be tuned by altering the length of dsDNA ligands.
- Autophagy and other regulatory mechanisms prevent long-term activation of the STING protein within cells and consequently necessitate multiple injections of STING-targeting therapeutics to achieve therapeutic efficacy. Alternatively, cGAS activity has potential to support *in situ* propagation of STING signaling. Indeed, cGAMP may vacate its cell of origin and thereby activate cGAS in neighboring cells within the TME.
- High concentrations of STING agonists can inhibit antitumor immunity via T-cell toxicity. Adjuvants that target cGAS through nanoparticle-mediated delivery of dsDNA have potential to mitigate T-cell toxicity, since T cells do not efficiently endocytose nanoparticles and are therefore less likely to experience the toxic overactivation of STING.
- The cGAS protein also has an established regulatory role identifying internal genome instability; DNA damage in the nucleus can trigger the nuclear translocation of cGAS from the cytosol. cGAS is recruited to double-stranded breaks, where it then inhibits homologous recombination. Nuclear cGAS has been shown to promote tumorigenesis as a result of its role in suppressing DNA repair. Since activated cGAS induces a liquid-like phase separation that presumably restricts cGAS to the cytosol, pharmacologically activating cGAS with dsDNA might impede the nuclear migration of cGAS and thereby allow for DNA repair in mutated tumor cells, ultimately inhibiting tumorigenesis.
- Natural and synthetic STING agonists are typically more expensive to produce than cGAS agonists (i.e. dsDNA), thus cGAS agonists would likely be more accessible/scalable.

Motivated by these considerations, a potent cGAS adjuvant, comprised of a synthetic cGAS ligand (*i.e.* 95-BP phosphorothioate-capped dsDNA) and a well-established endosomolytic polymer (*i.e.* D-PDB), was engineered to elicit robust STING-driven gene expression and was subsequently used to explore the pharmacological activation of cGAS for cancer immunotherapy.

IV. Role of TREX1 in cGAS Activation

TREX1 (*i.e.* DNase III) is a major deoxyribonuclease that localizes to the cytosol of cells and prevents the gradual accumulation of cytosolic dsDNA under resting conditions. Interferonopathies arising from mutations in the *TREX1* gene have indicated that the nuclease prevents excessive STING signaling from overactivation of the cGAS protein[21]. Although TREX1 has been recognized as a major negative regulator of cGAS and proposed as an immunotherapeutic target[22], it has not yet been extensively studied in the context of pharmacological cGAS activation.

The enzyme is an exonuclease that initiates degradation at the 3′ ends of dsDNA strands. Notably, the nuclease activity of TREX1 can be inhibited by phosphorothioate linkages as well as oxidized guanine residues (*i.e.* 8-hydroxyguanine) and abasic nucleotides, and therefore selective incorporation of such modifications into dsDNA molecules can be employed to study the effects of TREX1 on the functional activity of various cGAS ligands.

In this work, synthetic and PCR-amplified dsDNA were modified with various levels of phosphorothioate modifications and 8-hydroxyguanine tails on the 3′ ends of the dsDNA strands, respectively. The chemically modified dsDNA was then formulated with D-PDB and characterized *in vitro* using reporter cell assays for IFN-I activity. The experimental results demonstrated that phosphorothioate capping of relatively short cGAS ligands (*i.e.* 20 – 95 BP dsDNA) could significant increase maximum efficacy relative to unprotected size-matched dsDNA. Conversely,

larger PCR-amplified dsDNA (*i.e.* 5000-BP dsDNA) that had been 3′ tailed with 8-hydroxyguanine did not significantly alter the maximum efficacy of the cGAS ligands relative to unprotected size-matched dsDNA. Thus, this work supports the hypothesis that protecting longer dsDNA from TREX1-mediated degradation provides little to no benefit in terms of increasing the magnitude of STING signaling upon cytosolic delivery. This work also agrees with a previous report that TREX1 has much less influence over the IFN-I response for longer cGAS ligands[23].

Collectively, these findings have notable implications for mitochondrial DNA (*i.e.* ~15,000-BP dsDNA), which is a major source of endogenous cGAS/STING activation. Indeed, this work would suggest that mitochondrial DNA is not appreciably regulated by TREX1, and therefore TREX1 is likely not an appropriate target for therapies that seek to modulate cGAS/STING signaling following such endogenous activation of the pathway.

V. Therapeutic Delivery of Alu RNA for Cancer Immunotherapy

Alu elements are relatively short transposable elements (*i.e.* ~ 300-BP in length) and constitute the most abundant repetitive elements in the human genome, having been introduced over 50 million years ago[24]. Indeed, it is estimated that over 10% of the human genome consists of Alu sequences[24]. While Alu elements do not encode for protein products and their main function is thought to be self-reproduction, Alu RNA intermediates can alter the expression of certain genes and thereby affect cell function[24]. Recently, our collogues in the Aune Lab at Vanderbilt University determined that certain double-stranded Alu RNAs contribute to elevated IFN-I expression in circulating leukocytes of patients with relapsing remitting multiple sclerosis (RRMS)[25]. They also found that some of the double-stranded Alu RNAs associated with RRMS can trigger the production of IFN-I and other proinflammatory cytokines through the activation of the RNA-

sensing PRRs, RIG-I and TLR3[26]. Notably, the cytokine signature from these PRRs is similar to that of STING signaling, and these PRRs have been previously successfully targeted for cancer immunotherapy[27-30]. This work is the first to demonstrate that immunostimulatory Alu RNAs can be packaged and delivered with D-PDB to relay a therapeutic benefit in a non-immunogenic murine tumor model (*i.e.* B16.F10 melanoma) upon intratumoral administration.

VI. Enhanced Retention of Endosomolytic Nanoparticles within Tumors

Intratumoral drug delivery depots have been utilized in this work, as they offer much utility for the administration of cancer immunotherapeutics. Drug delivery depots that are greater than 500 nm in diameter experience restricted transport within the extracellular matrix[9], resulting in their local retention at an injection site. Additionally, drug delivery depots can maintain high local drug concentrations over time by shielding their cargo from degradation prior to drug release. Thus, while nanoparticulate drugs tend to clear rapidly from an intratumoral injection site (*e.g.* half-life less then 24 hours), drug delivery depots can allow for prolonged drug retention as well as local drug release over time.

The drug retention afforded by drug delivery depots can enhance both the efficacy and safety already conferred by intratumoral immunotherapy. Indeed, temporal increases in drug availability typically correlate with more efficacious cancer therapies where toxicity and target saturation are not applicable. Treatments with improved efficacy have potential to reduce the number of drug administrations required for complete therapeutic responses, which consequently can decrease patient expenses as well as increase patient compliance. Moreover, drugs that are toxic at high concentrations in various parts of the body can be largely confined to the area surrounding drug delivery depots and thereby minimize drug accumulation in off-target sites, effectively further increasing the relative dose-limiting toxicities in cancer patients.

In this work, biocompatible poly(lactic-co-glycolic acid) (PLGA) microparticle depots were employed to enable sustained local release of immunotherapeutic nanoparticles following intratumoral administration. Relatively high nanoparticle loading (*i.e.* 1.8 ± 0.05 μg nucleic acid per mg PLGA) was demonstrated, and sustained nanoparticle efficacy was observed both *in vitro* using reporter cells and *in vivo* using murine tumor models.

On a separate note, the work in this dissertation is also the first to show that, in the absence of a drug delivery depot, larger nucleic acids (*e.g.* 95-BP dsDNA) loaded on D-PDB exhibit increased local retention relative to smaller nucleic acid strands (*e.g.* siRNA) loaded on D-PDB. The prolonged retention of larger nucleic acids loaded on D-PDB is likely attributable to increased valency of the electrostatic complexation, since freely administered uncomplexed D-PDB was also found to exhibit a comparably long retention profile (*i.e.* half-life ~ 60 days). Notably, the increased retention of larger nucleic acids complexed to D-PDB was however not associated with sustained local activity, since the *in vivo* activity of the freely administered nanoparticles was only detectable for a short time period (*i.e.* on the order of days). Thus, it is likely that the nanoparticles experience some form of inhibition over time that causes them to eventually become inactive despite their continued presence. This further motivates the use of drug depots, as protection from such inhibitory mechanisms and gradual local release can potentially resolve such issues.

Specific Aims

Specific Aim 1: Develop cell-penetrating cGAS agonists to stimulate antitumor immunity. To address limitations of current standard-of-care cancer immunotherapies, novel cGAS adjuvants were engineered using a library of synthetic dsDNA and the well-established endosomolytic polymer, D-PDB. The morphology, stability, and activity of the complexes were characterized. Design variables included polymer/DNA charge ratio, DNA length, and phosphorothioate modification of the dsDNA. Through several different screens for IFN-I activity, the most potent cGAS adjuvant (i.e. NanoISD) was identified and then further characterized *in vivo*. Notably, NanoISD demonstrated significant therapeutic efficacy in multiple murine tumor models.

Specific Aim 2: Repurpose endogenous Alu RNA to stimulate antitumor immunity. Several Alu RNAs have recently been identified as endogenous immunostimulatory molecules that can activate the RNA-sensitive PRRs, RIG-I and TLR3. Indeed, it was determined that certain Alu RNAs contribute to elevated IFN-I expression in circulating leukocytes of patients with relapsing remitting multiple sclerosis. In this work, Alu RNA was formulated with D-PDB and shown to stimulate innate immunity upon intratumoral administration in a murine model of melanoma.

Specific Aim 3: Develop a drug delivery depot to sustain the activity of cell-penetrating nanoparticles in tumors. Rapid clearance is a significant limiting factor for the efficacy and safety of various intratumorally administered immunotherapeutics (*e.g.* D-PDB polyplexes). To address this issue, poly(lactic-co-glycolic acid) microparticles were explored as intratumoral drug delivery depots for the controlled release of cell-penetrating nanoparticles, comprising D-PDB and various nucleic acids. A capacity for sustained release was observed *in vitro* with no loss of nanoparticle functionality. Moreover, these findings were conserved *in vivo* using murine tumor models.

CHAPTER II

THE cGAS/STING PATHWAY

Text for Chapter II is adapted from:

Garland KM, Sheehy TL, Wilson JT. Chemical and Biomolecular Strategies for STING Pathway Activation in Cancer Immunotherapy. *In Review.* (2021).

Abstract

The stimulator of interferon genes (STING) cellular signaling pathway is well-recognized as a promising target for cancer immunotherapies. Activation of the intracellular STING protein triggers the production of a multifaceted array of immunostimulatory cytokines, which in the proper context, can drive dendritic cell maturation, T cell priming and activation, natural killer cell activation, and/or cancer cell death, resulting in tumor eradication and antitumor immune memory. Accordingly, there is a significant amount of ongoing research towards further understanding the role of the STING pathway in cancer immune surveillance as well as the development of specific modulators of the pathway as a strategy to stimulate antitumor immunity. Yet, the efficacy of STING agonists is limited by many drug delivery and pharmacological challenges. Depending on the class of STING agonist and the desired administration route, these may include poor drug stability, immunocellular toxicity, immune-related adverse events, limited tumor or lymph node targeting and/or retention, low cellular uptake and intracellular delivery, and a complex dependence on the magnitude and kinetics of STING signaling. This chapter provides a concise summary of the STING pathway, highlighting the recent biological developments, key features, and implications for drug delivery. This chapter also offers a critical analysis of various chemical strategies that have been employed to enhance the efficacy, safety, and/or clinical utility of STING pathway agonists and lastly draws attention to several opportunities for therapeutic advancements.

Introduction

The stimulator of interferon genes (STING) cellular signaling pathway has profound importance for the health and survival of a large diversity of organisms (*e.g.* humans, sea anemones, fruit flies, *etc.*)[31], due to its critical role in the immune-mediated elimination of numerous pathogens and diseases[32]. Accordingly, elements of the STING pathway have been evolutionarily conserved within metazoans for over 600 million years through natural selection[33-35]. Since the relatively recent scientific discovery of the STING protein in 2008, the pathway has been extensively characterized, and a growing number of infectious pathogens and diseases have been found to stimulate host immune responses by initiating STING signaling[36-40].

The STING pathway continuously monitor the cytosol of cells for certain "danger signals" (*i.e.* anomalies that are indicative of cellular stress) as part of a network of cytosolic pattern recognition receptors of the innate immune system – referred to as cytosolic immune surveillance. Molecular recognition of such irregularities within the cytosol initiates STING signaling (***Figure 2.1***), which then propagates a coordinated distress signal that is directed by the cellular production of various proinflammatory cytokines[31, 41, 42]. The distress signal ultimately summons an innate immune response that can galvanize the immune system to address a myriad of potential threats. Notably, the immunostimulatory attributes of STING signaling distinguish the pathway as a prime target for applications in cancer immunotherapy (*i.e.* therapies that either involve or use components of the immune system for the treatment of cancer patients).

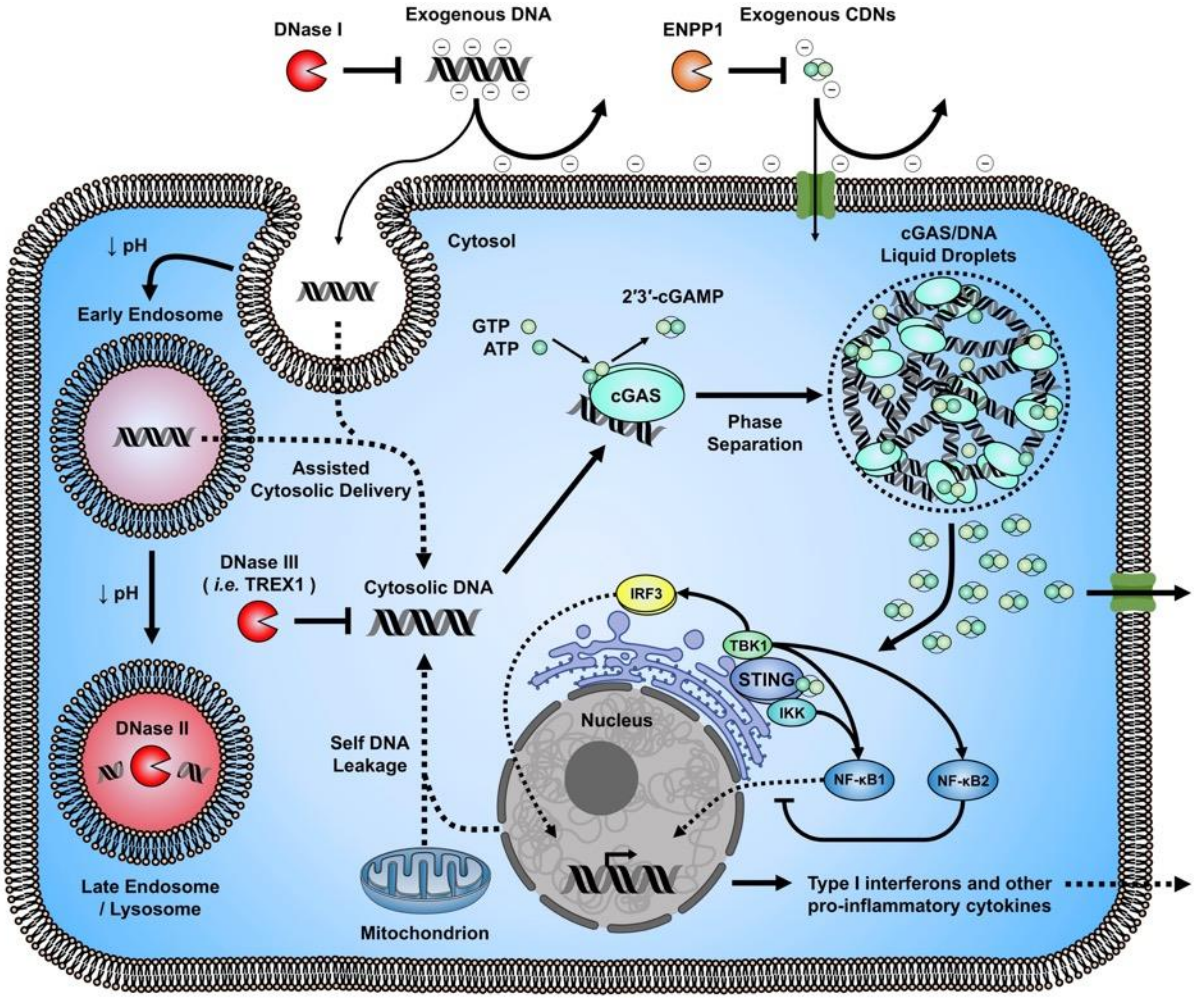

Figure 2.1. The stimulator of interferon genes (STING) cellular signaling pathway. The cGAS enzyme surveils the cytosol of cells for the accumulation of double-stranded DNA, which serves an indicator of cellular malfunction or infection. Notably, cytosolic double-stranded DNA may arise intrinsically (*e.g.* self-DNA leakage from nucleus or mitochondria) or extrinsically (*e.g.* pathogen-derived). Upon recognition (*i.e.* binding) of double-stranded DNA in the cytosol, cGAS oligomerizes into liquid-like droplets and catalyzes the production of 2′3′-cGAMP, which can bind and activate the STING protein on the endoplasmic reticulum to initiate downstream signaling, primarily through TBK1 and IKK. Notably, STING activation typically leads to the activation of the transcription factors, IRF3 and NF-κB1 as well as NF-κB2, which is known to partially inhibit the activity of NF-κB1. STING signaling results in the production of IFN-I and various other proinflammatory cytokines, the profile of which largely depends on context. Lastly, 2′3′-cGAMP can also vacate its cell of origin through various transport mechanisms and function as an immunotransmitter that can locally propagate STING signaling in neighboring cells. To pharmacologically activate the signaling pathway, STING pathway agonists (*i.e.* cGAS agonists and STING agonists) must cross the cell membrane, access the cytosol, and evade degradation by various deoxyribonucleases (DNases) and phosphatases. Due to its relatively large size and negative charge, exogenous DNA requires assistance (*e.g.* pathogen-mediated delivery) to penetrate cellular membranes and gain access the cytosol. Furthermore, DNA is highly susceptible

to degradation by DNase I in the extracellular space, DNase II (*i.e.* Acid DNase) during natural endolysosomal trafficking, and DNase III (*i.e.* TREX1) in cytosols. Alternatively, CDNs can utilize various membrane channels and transporters to access the cytosol, though the use of such transfer modalities is relatively inefficient and typically requires high local concentrations of CDNs. Moreover, certain naturally occurring CDNs, including 2′3′-cGAMP, are highly susceptible to degradation by ENPP1 in the extracellular space. Figure created with *biorender.com*.

The specific downstream effects of STING pathway activation can be largely variable, as they depend heavily on cellular context as well as signal intensity and duration[43]. However, a distinctive feature of mammalian STING signaling is the secretion of interferons (IFNs)[44], especially type I IFNs (IFN-I) such as IFN-β[45, 46], which is known to exhibit pleiotropic effects on cell function[47-49]. Notably, the type I IFN signature of STING activation has been linked to enhanced antigen-specific T cell responses[44, 47, 48] and natural killer (NK) cell responses[50] that collectively drive cell-mediated immunity. In certain settings, STING signaling can also induce various forms of programmed cell death, such as autophagy, apoptosis, necroptosis, and lysosomal cell death[51, 52]. Thus, the versatile nature of downstream STING signaling imparts cells with the ability to elicit a context-dependent immune response that can ultimately result in the clearance of diseased cells[45, 53, 54].

Table 2.1. Clinical Trials of STING agonists for Cancer Therapy.

Phase 2 Clinical Trials:	**Active Compound**	**Route of Delivery**	**Sponsor and *Collaborators***	**Trial Identifier**	**Status**
MIW815 +/- Pembrolizumab in Head and Neck Cancer	MIW815 (ADU-S100): Synthetic CDN STING Agonist	Intratumoral	Aduro Biotech, Inc.	NCT03937141	Active; Not Recruiting
MK-1454 +/- Pembrolizumab in Head and Neck Cancer	MK-1454: Synthetic CDN STING Agonist	Intratumoral	Merck Sharp & Dohme Corp.	NCT04220866	Active; Not Recruiting
Phase 1/2 Clinical Trials:	**Active Compound**	**Route of Delivery**	**Sponsor and *Collaborators***	**Trial Identifier**	**Status**
CDK 002 in Advanced/Metastatic, Recurrent, Injectable Solid Tumors	CDK 002 (exoSTING): PTGFRN-Targeted Exosome containing Synthetic CDN STING Agonist	Intratumoral	Codiak BioSciences	NCT04592484	Recruiting
Phase 1 Clinical Trials:	**Active Compound**	**Route of Delivery**	**Sponsor and *Collaborators***	**Trial Identifier**	**Status**
MIW815 +/- Spartalizumab in Advanced Solid Tumors or Lymphomas	MIW815 (ADU-S100): Synthetic CDN STING Agonist	Intratumoral	Novartis Pharmaceuticals	NCT03172936	Completed
MIW815 +/- Ipilimumab in Advanced Solid Tumors or Lymphomas	MIW815 (ADU-S100): Synthetic CDN STING Agonist	Intratumoral	Aduro Biotech, Inc. *Novartis Pharmaceuticals*	NCT02675439	Active; Not Recruiting
E7766 in Non-muscle Invasive Bladder Cancer	E7766: Synthetic CDN STING Agonist	Intravesical	Eisai Inc. *H3 Biomedicine Inc.*	NCT04109092	Withdrawn
E7766 in Advanced Solid Tumors or Lymphomas	E7766: Synthetic CDN STING Agonist	Intratumoral	Eisai Inc. *H3 Biomedicine Inc.*	NCT04144140	Recruiting
MK-1454 +/- Pembrolizumab in Advanced Solid Tumors or Lymphomas	MK-1454: Synthetic CDN STING Agonist	Intratumoral	Merck Sharp & Dohme Corp.	NCT03010176	Active; Not Recruiting
MK-2118 +/- Pembrolizumab in Advanced Solid Tumors or Lymphomas	MK-2118: STING Agonist	Intratumoral / Subcutaneous	Merck Sharp & Dohme Corp.	NCT03249792	Recruiting
SB 11285 +/- Nivolumab in Advanced Solid Tumors	SB 11285: Synthetic CDN STING Agonist	Intravenous	Spring Bank Pharmaceuticals, Inc.	NCT04096638	Recruiting
GSK3745417 in Advanced Solid Tumors	GSK3745417: Small Molecule STING Agonist	Intravenous	GlaxoSmithKline	NCT03843359	Recruiting
BMS-986301 +/- Nivolumab or Ipilimumab in Advanced Solid Cancers	BMS-986301: Small Molecule STING Agonist	Intratumoral / Intramuscular	Bristol-Myers Squibb	NCT03956680	Recruiting
SYNB1891 +/- Atezolizumab in Advanced Solid Tumors and Lymphoma	SYNB1891: *E. coli* STING Agonist	Intratumoral	Synlogic *IQVIA Biotech*	NCT04167137	Recruiting
BI 1387446 +/- Ezabenlimab in Advanced Solid Tumors	BI 1387446 (BI-STING): Synthetic CDN STING Agonist	Intratumoral	Boehringer Ingelheim	NCT04147234	Recruiting
TAK-676 +/- Pembrolizumab in Advanced Solid Tumors	TAK-676: Small Molecule STING Agonist	Intravenous	Takeda	NCT04420884	Recruiting
SNX281 +/- Pembrolizumab in Advanced Solid Tumors	SNX281: Small Molecule STING Agonist	Intravenous	Stingthera, Inc.	NCT04609579	Recruiting
IMSA101 +/- Immune Checkpoint Inhibitor in Advanced Treatment-Refractory Malignancies	IMSA101: Synthetic CDN STING Agonist	Intratumoral	ImmuneSensor Therapeutics Inc.	NCT04020185	Recruiting

In 2012, it was discovered that the therapeutic efficacy of the small molecule cancer therapeutic, 5,6-Dimethylxanthenone-4-acetic acid (DMXAA) was STING-dependent, establishing that pharmacological activation of STING signaling in solid tumors could promote antitumor responses in mice with established cancer[55]. Shortly thereafter, in 2014, the STING pathway was found to have a central role in preventing the onset of cancer in mice through tumor immune surveillance[56]. The STING pathway was thus identified as a promising target for cancer immunotherapy owing to its natural role in initiating and propagating endogenous immune responses to cancer. Moreover, it has now also been shown that many standard-of-care cancer treatments (*e.g.* DNA-damaging chemotherapies and radiotherapy) may promote additional therapeutic benefits through iatrogenic STING pathway activation[57-59]. Collectively, these findings have inspired the development of synthetic STING pathway agonists for cancer immunotherapy. Preclinical research using STING agonists to treat cancer has been exceptionally successful for generating antitumor immunity against a wide range of cancer types, which has prompted numerous clinical trials, many of which are ongoing (***Table 1.1***).

While STING pathway agonists offer considerable promise for cancer immunotherapy as both a monotherapy and an adjunct to current standard-of-care cancer treatments, none have yet reached the pharmaceutical market. As will be described, the clinical landscape of STING pathway agonists is rapidly evolving with a number of promising candidates in clinical trials that may soon yield the first approval of a STING agonist for cancer immunotherapy by the US Food and Drug Administration (FDA). Nonetheless, both the efficacy and safety of STING-activating therapeutics are restricted by many drug delivery and pharmacological challenges, including poor drug stability, immunocellular toxicity, immune-related adverse events, limited tumor or lymph node (LN) targeting and/or retention, low cellular uptake and intracellular delivery, and a complex

dependence on the magnitude and kinetics of STING signaling[60, 61]. In this chapter, a detailed summary of the STING pathway as well as a synopsis of chemical strategies to enhance the efficacy, safety, and/or clinical utility of STING pathway agonists are presented.

Biochemistry and Biology of the cGAS/STING Pathway

There are a number of ways through which STING signaling can be initiated. However, activation of the intracellular STING protein, or more specifically, translocation of STING to the Golgi is invariably required for the downstream STING signaling that can trigger innate immune activation[62-65]. In its resting state, the STING protein is localized on the surface of the endoplasmic reticulum[66] and is canonically activated by cyclic dinucleotides (CDNs)[67]. Alternatively, STING can also be directly bound and activated by several other chemical agents, many of which will be discussed in detail in this review.

Endogenous activation of the STING protein is largely dependent upon the recognition (*i.e.* binding) of the self-derived CDN, 2′3′-cyclic guanosine monophosphate – adenosine monophosphate (2′3′-cGAMP)[68, 69]. At the forefront of the STING pathway, 2′3′-cGAMP is produced intracellularly by cGAMP synthase (cGAS) after the enzyme detects the aberrant presence of double-stranded DNA (dsDNA) in the cytosol of cells. Thus, both cGAS and STING act as general sensors (*i.e.* pattern recognition receptors) for pathogens and pathologies that induce the cytosolic accumulation of such danger signals[70].

Recognition of Cytosolic DNA by cGAS

Under normal conditions, the cytosol of cells is largely DNA free, and any nominal amount of DNA that may be present is rapidly degraded by cytosolic nucleases. Accordingly, the

accumulation of DNA within the cytosol is indicative of pathogenic threats or compromised cellular states. Mammals express numerous DNA sensors that are capable of detecting and communicating such breaches in cellular homeostasis. Many of these DNA sensors can provoke IFN-I responses to activate innate immunity in response to the abnormal accumulation of either extrinsic or misplaced-self dsDNA within the cytosol[71]. Extrinsic DNA can infiltrate the cytosol through a variety of mechanisms (*e.g.* tumor-derived exosomes, viral infection, *etc.*), while intrinsic, self-DNA derived from mitochondria, chromosomes, or endogenous retroelements can accumulate in the cytosol in response to cellular stress or genetic mutation (***Figure 2.1***) [40, 72-75]. Notably, many cancerous cells have an established capacity for leading endogenous nuclear DNA into the cytosol[76-78], which likely contributes to the natural role of the cGAS/STING pathway in both tumor immune surveillance and spontaneous antitumor immunity.

Upstream of STING in the pathway, cGAS is considered to be the predominant contributor to endogenous STING activation following the detection of cytosolic DNA. However, some of the other cytosolic DNA sensors (*e.g.* DDX41, IFI16, DAI, RNA pol III, LRRFIP1, *etc.*) can also initiate IFN-I responses through STING signaling[79], either in conjunction with cGAS or even in the absence of cGAS[80]. Notably, cGAS is itself an IFN-stimulated gene (ISG)[81], and therefore, in cells with low baseline cGAS expression, cytosolic DNA can initially trigger other DNA sensors. The resultant IFN-I response can then lead to local cGAS production and subsequent cGAS activation if the DNA persists long enough within the cytosol (*e.g.* prolonged viral challenge), thereby increasing the magnitude of the IFN-I response in a positive feedback manner.

The activation of cGAS by dsDNA has been extensively characterized through many structural and biochemical studies[82-87]. Briefly, cGAS exhibits an autoinhibited conformation in its unbound, monomeric form. Positively charged sites on the C-terminal domain (CTD) of cGAS

bind the sugar-phosphate backbone of dsDNA. Steric interactions between cGAS and the bound DNA induce conformational transitions in cGAS that open the nucleotide binding pocket, which is also located on the CTD. The DNA strands serve as natural crosslinkers to promote cGAS oligomerization[84]. The dsDNA/cGAS oligomeric complexes undergo liquid–liquid phase separations within the cytosol, forming liquid-like droplets that function as intracellular microreactors for 2′3′-cGAMP production[42, 88]. The activated cGAS enzymes catalyze the production of 2′3′-cGAMP from intracellular adenosine triphosphate (ATP) and guanosine triphosphate (GTP)[68, 69]. The enzymatic synthesis occurs in a stepwise manner through the initial generation of 5′-pppG(2′,5′)pA prior to cyclization to c[G(2′,5′)pA(3′,5′)p][87]. Notably, 2′3′-cGAMP has mixed 2′,5′ and 3′,5′ phosphodiester bonds (c[G(2′,5′)pA(3′,5′)p]) in contrast to bacteria-derived CDNs, which exclusively have two uniform 3′,5′ phosphodiester bonds[87, 89, 90] (***Figure 2.2***). The biological consequences of CDN linkage orientation are discussed in detail in ***Section 4.1***.

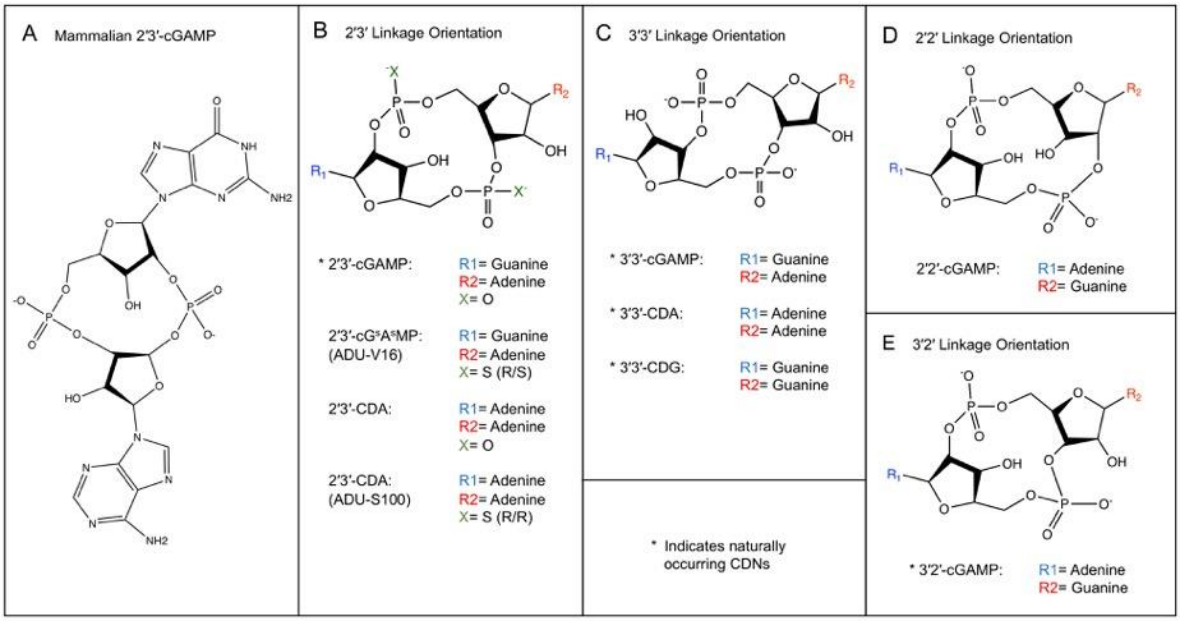

Figure 2.2. Chemical structures of cyclic dinucleotide (CDN) STING agonists. **(A)** Mammalian 2′3′-cGAMP. **(B)** Various naturally occurring or synthetic CDNs with the noncanonical 2′3′ linkage orientation that is produced by mammals. **(C)** Various naturally occurring CDNs with the

canonical 3′3′ linkage orientation that is produced by bacteria. **(D)** Synthetic 2′2′-cGAMP with the noncanonical 2′2′ linkage orientation that has not yet been found in nature. **(E)** Naturally occurring 3′2′-cGAMP with the noncanonical 3′2′ linkage orientation that is produced by *Drosophila melanogaster* (*i.e.* fruit flies).

The recognition of dsDNA by cGAS is largely sequence-independent, and the length of dsDNA that is empirically required *in vitro* for minimal cGAS activation in cell-based assays varies by species (*e.g.* ~ 45 base pairs (bp) in humans, ~ 20 bp in mice)[91, 92]. With only a few exceptions[93], short strands of dsDNA under these length thresholds cannot activate cGAS in any meaningful way, as they are unable to induce the formation of the liquid-like droplets that stabilize the dsDNA/cGAS complex through multivalent interactions[88]. This is largely due to the relatively low affinity of dsDNA for cGAS, the dissociation constant (K_D) of which has been estimated to be ~ 1−2 μM[82, 84]. Notably, the phase-separation of the liquid-like droplets stabilizes the dsDNA/cGAS complexes through more than just enhanced colocalization. The liquid-like droplets sequester the cGAS and dsDNA molecules, thereby providing a barrier that limits the physical access of DNA nucleases that would otherwise degrade the dsDNA ligands[94]. Prolonged protection from such negative regulators is especially important for cGAS, as it is considered an unusually slow enzyme with one round of cGAMP synthesis taking ~ 20 seconds[95].

The cGAS enzyme is allosterically activated by dsDNA in a length-dependent manner, such that binding longer strands of dsDNA increases the presence and stability of the active dsDNA/cGAS biocondensates and thereby increases the local production of 2′3′-cGAMP[23, 96]. Accordingly, the length of cytosolic dsDNA is a critically important determinant of both the magnitude and profile of the resultant immune response. The length-dependent cGAS activation is most pronounced at physiologically relevant low dsDNA concentrations that are comparable to that of self dsDNA sensing and viral infection (*e.g.* ~ 17 fg/cell for herpes simplex virus 1)[23, 43].

At low dsDNA concentrations (*e.g.* 15 ng/mL), which are representative of natural exposure, dsDNA that is technically above the length threshold for activation (*e.g.* 100 BP) fails to induce a measurable response, while much longer dsDNA (*e.g.* 2000 BP) is still capable of efficiently inducing STING signaling[23]. Notably, at the high dsDNA concentrations (*e.g.* 1 µg/mL or greater) that are often assessed *in vitro*, cGAS activity can be saturated using a relatively low molecular weight dsDNA (*e.g.* ~ 60 kDa), likely through substrate exhaustion (*i.e.* depletion of cellular ATP and/or GTP)[23].

Cytosolic dsDNA can also activate the protein known as absent in melanoma 2 (AIM2)[97], which has noteworthy implications for STING signaling. AIM2 is another prominent pattern recognition receptor for cytosolic dsDNA and is known to modulate STING signaling[98-103]. Activation of AIM2 characteristically results in pyroptosis-mediated cell death and the release of IL-1β and IL-18 via the AIM2 inflammasome. Concurrent activation of AIM2 and cGAS in antigen presenting cells (APCs) broadens the resultant cytokine response, but it also reduces the magnitude of STING-specific cytokines produced[99]. The dampened STING signaling caused by simultaneous AIM2 activation is largely due to the pyroptosis induced by AIM2. At the onset of AIM2-induced pyroptosis, gasdermin D pokes small holes in the cellular membrane. The pores in the cellular membrane enable a potassium efflux from the cell, which then inhibits cGAS activation prior to cell death[103].

Unlike cGAS, AIM2 evolved relatively recently as a nucleic acid sensor within mammals[104] and is entirely orthologous between murine and human species[105]. Notably, AIM2 is minimally activated by relatively longer dsDNA (*i.e.* ~ 80 bp)[106, 107]. Robust activation of cGAS and AIM2 at *in vitro* concentrations of ~ 1 µg/mL generally requires dsDNA lengths of at least ~ 100 bp and ~ 200 bp, respectively[96, 108-112]. Though, as previously stated, dsDNA length thresholds

for *in vitro* activation do not necessarily directly correspond with thresholds for *in vivo* activation, because cells within a living organism do not naturally experience such high cytosolic dsDNA concentrations even under stressed cellular conditions. Future research investigating the interplay between cGAS/STING signaling and the AIM2 inflammasome in a cancer setting will be necessary to define the impact of such dual activation on antitumor immunity.

The primary effector function of AIM2 activation is to induce cell-death, which is a non-tunable process that does not depend on an allosteric equilibrium[113, 114]. The AIM2 inflammasome does not disassemble after it has formed on sufficiently long cytosolic dsDNA, and the assembly of the AIM2 inflammasome is reinforced by multiple positive feedback loops, which supports a binary signaling response[112]. Conversely, cGAS activation is tunable and the downstream response can be quite variable and setting specific[43, 115, 116]. STING signaling can evoke diverse stress responses that range from the suppression of viral replication to apoptosis depending on signal strength, signaling duration, and cellular context[40, 43, 45, 117-119].

Regulation of cGAS

Mammalian DNA is primarily packaged and compartmentalized inside the nuclei and mitochondria of cells and therefore typically avoids contact with cGAS[120]. However, nominal amounts of self dsDNA routinely enter the cytosol under normal cellular conditions[40, 72-75]. Mammals have evolved to locally restrict intrinsic activation of pattern recognition receptors to a baseline level by constitutively expressing deoxyribonucleases (DNases)[40, 121, 122]. DNase I, DNase II, and TREX1 (*i.e.* DNase III) actively degrade dsDNA in systemic circulation, lysosomes, and cytosols, respectively[74, 123-125]. The cytosolic exonuclease, TREX1 directly affects the length, concentration, and persistence of dsDNA within the cytosol, and consequently, is critically

important for negatively regulating cGAS activity[126-129].

TREX1 deficiency has been linked to many type I interferonopathies caused by overactive STING signaling. Most notably, mutations in the *TREX1* gene cause Aicardi-Goutières syndrome (AGS) and have also been associated with many other autoimmune diseases, including both familial chilblain lupus and systemic lupus erythematosus[129]. Interestingly, the genes encoding cGAS and TREX1 are both prominent ISGs and thus they contribute to local regulatory feedback loops that can either amplify or restrict the subsequent immune response in various settings[81, 130]. Recently, the intratumoral inhibition of TREX1 has even been proposed as a novel immunotherapeutic strategy to promote local STING signaling for the treatment of cancer[22]. Notably, radiotherapy-induced tumor immunogenicity is strongly negatively regulated by TREX1 at high doses of radiation (*i.e.* 12−18 gray)[131, 132]. It has been shown that reactive oxygen species (ROS), a biproduct of ionizing radiation[133] can oxidize intracellular DNA bases[134], which can then partially inhibit TREX1-mediated degradation through steric hindrance to perpetuate STING signaling during radiotherapy[135, 136]. However, TREX1 inhibition via oxidized bases is contingent upon low TREX1 concentrations (*e.g.* ~ 50 nM or less); high concentrations of TREX1 (*e.g.* ~ 200 nM or greater) can efficiently degrade DNA containing oxidized bases[137]. Thus, the observed dose-dependent regulation of radiotherapy-induced tumor immunogenicity by TREX1 may be explained by dose-dependent ISG expression, where higher doses of radiation lead to higher concentrations of TREX1, which can then degrade oxidized dsDNA and thereby limit the extent of cGAS activation. In support of this theory, it was determined that consecutive low doses of radiation (*i.e.* 3x 8 gray) could circumvent TREX1-mediated cGAS inhibition[131]. Nevertheless, TREX1 represents a formidable obstacle for all DNA-based cGAS-activating cancer therapies and must therefore be given careful consideration when designing such therapeutic approaches.

In addition to TREX1, there are numerous other factors that can significantly influence the intensity of STING signaling in a particular tissue and therefore alter the nature of the resultant immune response. The activity of cGAS is known to be intricately regulated by many different post-translational modifications of cGAS, such as acetylation, glutamylation, phosphorylation, sumoylation, and ubiquitination[138-143]. Post-translational modifications are heavily dependent on environmental conditions and therefore likely contribute to cell-type specific STING signaling. cGAS activation is also vitally dependent on the ability of cGAS to encounter its dsDNA substrate, which is undoubtedly a function of the protein's spatiotemporal distribution within cells.

The subcellular localization of cGAS is currently a subject of controversy and seems to be quite dynamic in nature depending on cell cycle phase, cell type, and environmental conditions[144]. Until recently, cGAS has generally been regarded as a strictly cytosolic protein[68]; however, recent studies have challenged this theory. In murine bone marrow-derived macrophages (BMDMs) and in human THP1 monocytes, it was determined that cGAS primarily resides on the interior of the plasma membrane due to the electrostatic interactions of the N terminus of cGAS with the membrane-bound $PI(4,5)P_2$ phospholipid[145]. The intracellular localization of cGAS to the plasma membrane was found to limit the recognition of self dsDNA by spatial segregation from the nucleus and simultaneously maximize the potential response to viral infection by allowing for a more rapid encounter with exogenous DNA.

cGAS has also been identified within the nuclei of mammalian cells[68, 146-148]. Outside of the canonical STING signaling axis, cGAS has an established secondary function, where it operates as a negative regulator of DNA repair, inhibiting homologous recombination in the nucleus[149, 150]. Several research groups currently contend that cGAS is constitutively present in the nuclei of cells at steady state[150-152]. One study found that the non-catalytic N terminal domain of

cGAS was responsible for an association of cGAS with the centromeres of chromosomes within the nuclear compartment[151]. More recently, another study has asserted that cGAS is predominantly a nuclear protein that is tethered tightly to intact chromatin by a salt-resistant interaction in its resting state[152]. The researchers found that cGAS was resistant to standard salt-based elution, requiring relatively high salt concentrations for complete solubilization (*e.g.* 0.75 M NaCl compared to the 420 mM NaCl that is typically used to isolate nuclear proteins). They have suggested that the observed tight interactions of cGAS in the nucleus cannot be explained by its relatively low intrinsic affinity for DNA (*e.g.* $K_D \sim 1{-}2\ \mu M$).

These disparate findings indicated that the N terminus of cGAS was dispensable for nuclear localization; instead, the core of human cGAS, composed of a bilobed nucleotidyltransferase structure bridged by an alpha-helical spine, was required for the observed nuclear tethering. It was noted that the amino acid residues, which are important for nuclear tethering, partially overlap with one of the DNA-binding surfaces of cGAS. Consequently, a model of "regulated desequestration" was proposed, which proclaims that cGAS is inactive while chromatin-bound and that there exists an unknown regulated step prior to the assembly of cGAS onto dsDNA that enables its release from chromatin and subsequent activation.

Chromatin tethering is indeed one of several regulatory mechanisms that can inhibit cGAS activation at times where immune activation is unnecessary (*e.g.* cell division)[138, 153, 154]. Specifically, chromatin tethering can prevent the oligomerization of cGAS that is necessary for liquid-like droplet formation and efficient 2′3′-cGAMP synthesis[154]. Accordingly, the tethering of cGAS to chromatin actually increases during mitosis when the nuclear envelope breaks down, so as to prevent spurious activation of cGAS while DNA is exposed to the cytosol[147, 155]. Further research in this area may lead to the discovery and characterization of the aforementioned unknown

regulatory mechanism that is responsible for the release of cGAS from nuclear chromatin, which may thereby enable targeted strategies for controlling the degree of cGAS activation to enhance cancer therapies.

Regulation of STING

After cGAS catalyzes the synthesis of 2′3′-cGAMP, the CDN acts as a second messenger that binds and activates STING proteins on the endoplasmic reticulum[66, 69, 89]. STING comprises four transmembrane helices coupled to a cytoplasmic ligand-binding and signaling domain[156]. The transmembrane and cytoplasmic regions naturally interact to form a domain-swapped homodimer in its resting form[157]. Two intertwined STING molecules take the shape of an opened butterfly with the head toward the membrane (***Figure 2.3-A***)[158]. Upon binding 2′3′-cGAMP, the STING homodimer undergoes extensive conformational rearrangements. While 2′3′-cGAMP induces closure of the ligand-binding domain, it is important to note that not all agonists of STING provoke a closed lid confirmation (***Figure 2.3-B***). Indeed, several STING agonists (*e.g.* the bacteria-derived CDN, cyclic di-guanosine monophosphate (c-di-GMP)) promote STING oligomerization and exhibit immunostimulatory activity without rearrangement of the lid region (***Figure 2.3-C***)[159-161].

Activated STING proteins oligomerize, are ubiquitinated, and then traverse the Golgi apparatus, whereupon they are palmitoylated and traffic to submicrometer-sized perinuclear vesicles (*i.e.* STING translocators)[62, 162-166]. Following translocation though the Golgi body, TANK-binding kinase 1 (TBK1) binds and phosphorylates STING[167, 168]. Notably, TBK1 recruitment to STING has been identified as essential for STING-mediated antitumor immunity[169]. The STING/TBK1 complex phosphorylates interferon regulatory factor 3 (IRF3), which then homodimerizes and navigates into the nucleus to induce target gene expression[164, 170-172].

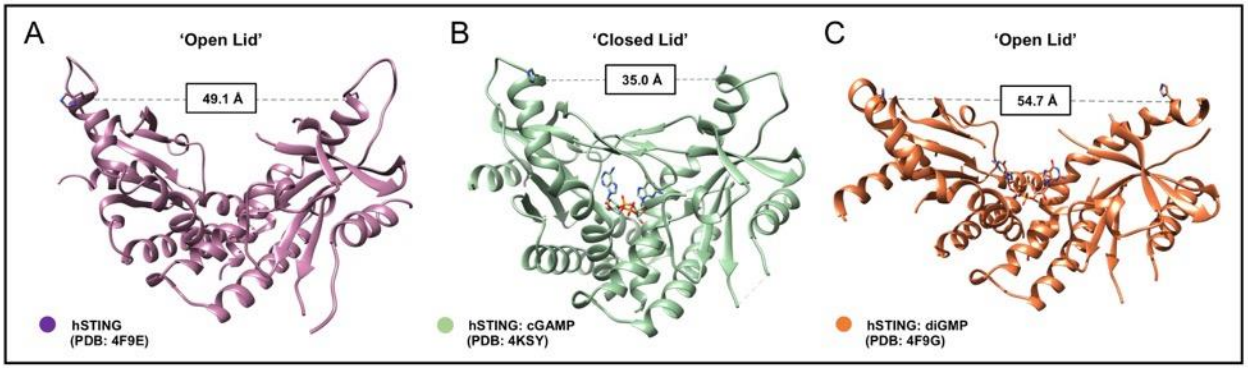

Figure 2.3. Crystal Structures of symmetrical human STING dimers. **(A)** The resting 'Open Lid' configuration of an apo (*i.e.* unbound) human STING dimer. Adapted from reference[173] (PDB ID: 4F9E)[159]. **(B)** The 'Closed Lid' configuration of a holo (*i.e.* ligand bound) human STING dimer bound to 2′3′-cGAMP. Adapted from reference[173] (PDB ID: 4KSY)[89]. **(C)** The 'Open Lid' configuration of a holo (*i.e.* ligand bound) human STING dimer bound to 3′3′-diGMP. Adapted from reference[173] (PDB ID: 4F9G)[159].

Similar to the liquid phase condensation of cGAS that is triggered by activation of the endogenous STING pathway[88], untranslocated ER-resident STING can also undergo a liquid-liquid phase separation[174]. However, unlike the liquid-like droplets of activated cGAS that enhance STING signaling, the STING condensates contain inactive STING proteins and negatively regulate the pathway by preventing the translocation of STING that is necessary for downstream signaling[175]. When intracellular 2′3′-cGAMP concentrations reached a certain threshold (*e.g.* 1 µg/mL *in vitro*), which is above the threshold for the initial activation of STING by 2′3′-cGAMP (*e.g.* K_D ~ 4.59 nM), STING condensates form as micrometer-sized granules that colocalize with the ER. Additionally, when present in an exceptionally high concentration (*e.g.* 6 µg/mL *in vitro*), 2′3′-cGAMP also further induces a fluid-to-gel transition of the STING condensates that significantly decreases their internal molecular mobility. Notably, the STING condensates also formed in response to the bacterial CDN, c-di-GMP. It is currently unclear whether the phase separation of STING occurs in response to all of the known STING agonists or just CDNs. It is also unknown if constitutively active STING mutants trigger the STING phase-separator.

While most hydrogels of biocondensates formed by protein liquid-liquid phase separation are largely disordered or assemble into polymeric fibrils[176, 177], the STING condensates, now termed the STING phase-separator, surprisingly comprise a highly organized membranous structure that resembles jigsaw puzzles. Following DNA virus infection, formation of active STING translocators occurred 3 hours post infection and peaked at 8 hours, whereas inhibitory STING condensates peaked at 20 hours. Thus, formation of the STING phase-separator is a partially delayed response and serves to prevent overactivation of STING and inhibit excessive innate immune signaling.

Additional transcription factors synergize with IRF3 to direct context-dependent antiviral gene expression[178]. In various settings, STING signaling has been associated with the activation of canonical and non-canonical nuclear factor κB (NF-κB), mitogen-activated protein (MAP) kinases, and signal transducer and activator of transcription (STAT) transcription factors[66, 179-182]. Notably, efficient production of IFN-β, a hallmark of STING signaling, relies on the cooperative assembly of the enhanceosome, a higher order transcription enhancer complex[183, 184]. Individual transcription factors of the enhanceosome, such as IRF3 and canonical NF-κB, cannot initiate IFN-β gene expression by themselves[185, 186]. Instead, they must work in conjunction with each other and several other enhancer components for maximal gene transcription[46]. Indeed, a 50% decrease in IFN-β production was observed in primary mouse embryonic fibroblast cells when canonical NF-κB expression was partially silenced via RNA interference (RNAi)[179].

The intricacy of the enhanceosome elegantly highlights the importance of synergy between multiple inducible transcription factors[187]. Thus, in addition to post-translational modifications of STING pathway constituents, the combinatorial regulation of gene transcription likely contributes to cell-type specific STING signaling, as it is largely responsible for the selective protein

expression that occurs in various environmental conditions. Accordingly, a better understanding of the transcriptional regulation that ensues STING activation in various cell types could lead to more efficacious cancer immunotherapies designed to differentially regulate the expression of certain STING-stimulated proteins to enhance antitumor effects and minimize unnecessary off-target effects.

Single nucleotide polymorphisms in the STING protein are responsible for existence of distinct human STING (hSTING) isoforms that exhibit variable intrinsic activity as well as distinctive reactivity to various STING agonists[87, 188, 189]. The five most prominent haplotypes of hSTING are known as **WT** (R232), **HAQ** (R71H, G230A, R293Q), **REF** (R232H), **AQ** (G230A, R293Q), and **Q** (R293Q), and their allelic frequencies in the human population are 57.9%, 20.4%, 13.7%, 5.2%, and 1.5%, respectively[45, 189]. Relative to the other major variants, hSTING^{HAQ} generally exhibits lower intrinsic IFN-I and NF-κB activity, which has been attributed to the R71H substitution that likely affects the protein's resting localization to the endoplasmic reticulum[189-191].

There are many agonist-specific differences in the recognition and activation of the various STING isoforms that can be attributed to the unique chemical structures of the STING agonists. While bacteria-derived CDNs can activate murine STING (mSTING) and certain hSTING variants, they do not appreciably activate the hSTING^{REF} or hSTING^{Q} isoforms[45, 188, 189]. Alternatively, endogenous 2′3′-cGAMP can activate mSTING as well as all 5 of the major hSTING variants[45, 89]. However, whether 2′3′-cGAMP is a weak agonist for certain hSTING isoforms is currently a controversial topic. Some researchers have reported that for hSTING^{REF}, 2′3′-cGAMP is weaker agonist, exhibiting reduced IFN-I activity, despite generating comparable NF-κB activity[189, 192]. Conversely, others have shown that 2′3′-cGAMP engenders no significant difference in its inducible IFN-I activity with the hSTING^{REF} isoform[45]. Furthermore, the small

molecule, DMXAA potently activates mSTING, but is unable to activate any of the hSTING variants[193]. Thus, the isoforms of STING represent a crucial design consideration for the clinical development of any STING agonist, as translatability will favor universal STING agonists.

Regulation of 2′3′-cGAMP

In addition to binding STING within the cell of origin, endogenous 2′3′-cGAMP can also vacate the native cell and thereby function as an immunotransmitter to neighboring cells[194, 195]. The accumulation of intracellular cGAMP that follows robust cGAS activation creates a strong electrochemical gradient that promotes cGAMP expulsion[196, 197]. The distribution of cGAMP to nearby cells can occur in several different ways, either directly (*e.g.* cell-to-cell) or indirectly (*e.g.* secretion followed by proximal cellular uptake). Direct cell-to-cell transfer of cGAMP may occur through connexin-dependent intercellular gap junctions, cellular fusion, and phagocytosis of dead or dying cells[77, 198-204]. Notably, the predominant gap junction protein involved in cGAMP transfer, connexin-43 (Cx43) is also established as a tumor suppressor in many types of cancer[205-207]. Although cGAMP transfer has not yet been directly linked to the anticancer role of Cx43, facilitating STING signaling in a time of cellular stress could potentially support a tumor suppressor function via the activation of innate immunity. In contrast to the direct transfer of cGAMP, indirect transfer may be mediated by ion channels, transport proteins, virions, and extracellular vesicles released from infected or apoptotic cells[195-197, 208-215].

Many of these cGAMP transfer modalities have limited functionality in various settings, as several are largely dependent on cellular context, viability, and/or infection status. Indeed, the unidirectional cell membrane transporter, SLC19A1 was shown to be important for cGAMP import in U937 monocyte-derived cells and monocytic THP1 cells, but was also found to be

minimally expressed in many other cell types[195, 209]. Additionally, SLC46A2 has more recently been identified as the dominant cGAMP importer in primary human monocytes and monocyte-derived macrophages[215]. Conversely, gap junctions containing Cx43 and volume-regulated anion channels (VRACs) have important roles in cell survival and are therefore ubiquitously expressed in human cells[207, 216-218].

Gap junctions form intercellular channels in appositional cellular membranes and thereby promote direct cellular communication and nutrient exchange, both of which are essential to cellular physiology[207]. VRACs also help maintain cellular homeostasis, though they do so by counteracting dynamic cytoplasmic pressures[218-220]. Leucine-rich repeat-containing 8 (LRRC8) protein heteromers associate to form VRACs, with LRRC8A being an essential subunit that must combine with at least one other LRRC8 member (B–E)[221]. Of the various potential combinations of VRAC subunits, LRRC8A:C and LRRC8A:E contribute the most to cGAMP flux, though LRRC8E expression is somewhat restricted in humans[196, 197, 218]. Gap junctions and VRACs are both capable of two-way molecular transit, unlike some transporters that are simply unidirectional (*e.g.* the cell-specific cGAMP importers, SLC19A1 and SLC46A2)[195-197, 209, 215]. Thus, gap junctions and VRACs represent the main cGAMP transfer mechanisms in humans, though the contribution of each is likely tissue specific. Gap junctions were recently found to be essential for cGAMP transfer in lungs upon nanoparticulate STING agonist administration and also in livers following alcohol-induced hepatocyte injury[201, 202]. Alternatively, VRACs were identified as the dominant cGAMP importer in human microvascular endothelial cells, which are characteristic of many tumor microenvironments (TMEs)[197].

Notably, gap junctions enable transfer of cGAMP to a limited number of connected cells, while VRACs allow for secretion into the extracellular space and likely enable cGAMP transmission to a larger number of cells via paracrine signaling. Indeed, VRACs were found to be responsible for ~ 50−70% of cGAMP uptake in a wide variety of cell types[196]. While cGAMP and other CDN STING agonists may enter cells through these portals, the efficiency of cellular import appears to be quite low for these compounds. Notably, when cells are treated *in vitro* with cGAMP or other CDNs, dose-response studies for STING pathway activation typically yield values for the half-maximal effective concentration (EC_{50}) in the high micromolar range, suggesting inefficient CDN entry into the cytosol via the membrane transporters as well as poor cell membrane permeability due to their polar nature and negative charge[222]. This cytosolic delivery barrier has inspired the development of nanotechnology to enhance the intracellular delivery of exogenous STING agonists (***Figure 2.4***).

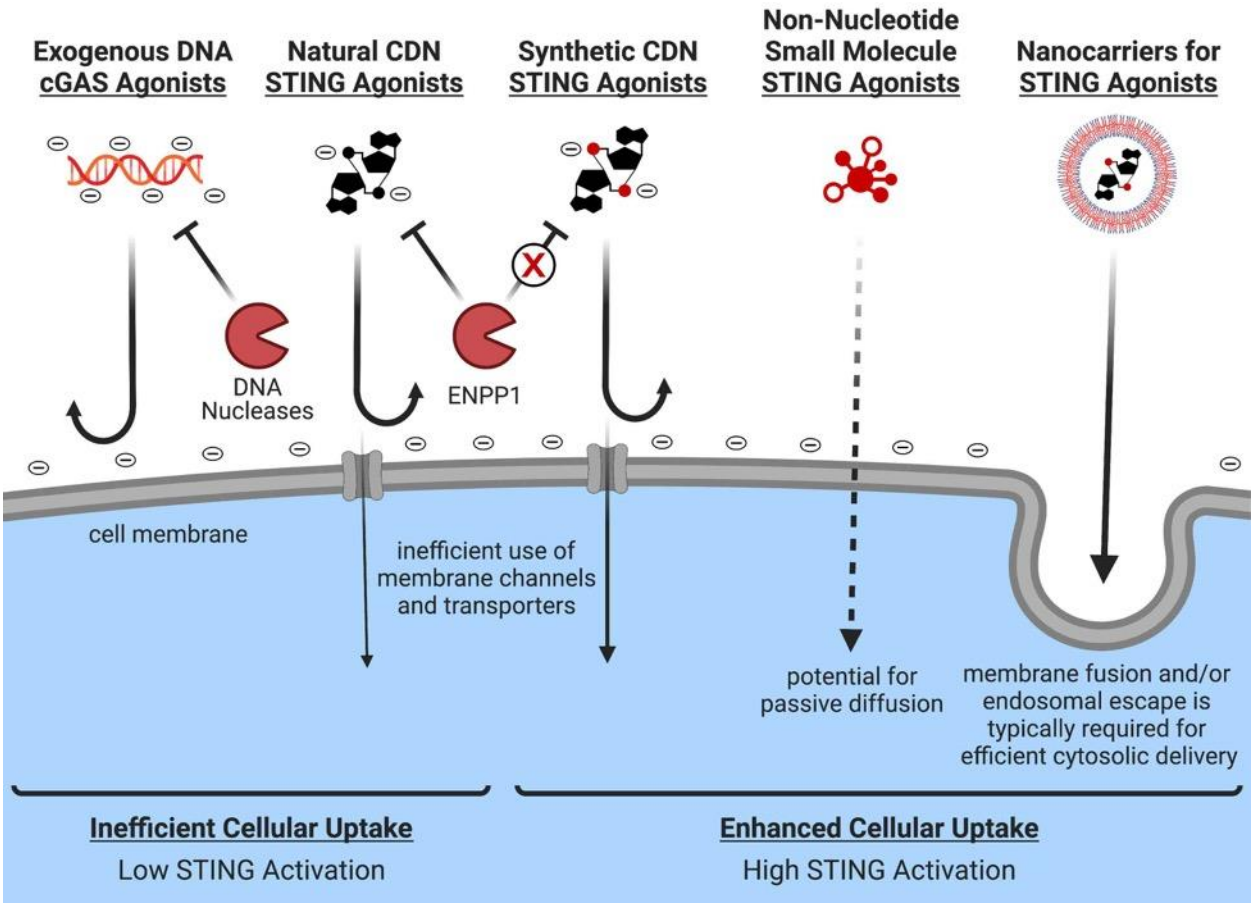

Figure 2.4. Intracellular delivery challenges for STING pathway agonists. Exogenous DNA and CDNs are negatively charged and hydrophilic and consequently cannot readily access the cytosol to activate the STING pathway. While both natural and synthetic CDNs are small enough to infiltrate the cytosol through the use of membrane channels and transporters, these transport modalities are inefficient. Furthermore, extracellular nuclease and phosphatases quickly degrade exogenous DNA and natural CDNs, respectively. Accordingly, relatively high concentrations of CDNs are required to elicit measurable STING activation. Non-nucleotide, small molecule agonists of the STING pathway have potential to passively diffuse across the cell membrane and therefore are an attractive alternative to the natural agonists. Lastly, certain nanocarriers can improve the efficacy and safety of STING pathway agonists by promoting intracellular delivery. Figure created with *biorender.com*.

Currently, there is no indication that extracellular cGAMP preferentially spreads into any particular cell type, since gap junctions and VRACs are so broadly expressed. Rather, cGAMP likely distributes indiscriminately, but predominantly enters local cells due to the presence of ecto-nucleotide pyrophosphatase phosphodiesterase 1 (ENPP1) in the extracellular space[194, 223]. ENPP1

hydrolyzes extracellular cGAMP and thus prevents extensive spread[223, 224]. Elevated expression of ENPP1 has even been correlated with tumor development in several cancer types[194, 225, 226]. Accordingly, inhibitors of ENPP1 are currently being developed for cancer immunotherapy[194, 227]. Synthetic STING agonists without phosphodiester bonds have also been engineered to avoid degradation by ENPP1 and thereby enhance drug stability. Phosphorothioate modifications are commonly employed as they are resistant to ENPP1 degradation and may even enhance cellular uptake and cytosolic delivery[45, 223, 228, 229]. Though the development of nonhydrolyzable analogs of cGAMP has circumvented the issue of extracellular degradation, evading ENPP1 remains an important design criterion for therapies that exploit natural cGAMP from endogenous STING signaling (*e.g.* radiotherapy).

The manner in which cGAMP is transferred also uniquely affects the mechanism of action for subsequent STING signaling. Unlike intracellular CDNs that trigger classical cGAS/STING signaling, extracellular CDNs can activate an alternative cGAS/STING signaling pathway[230]. Liu *et al.* found that cells primarily endocytose extracellular CDNs in a clathrin-dependent manner. Endocytosed CDNs were released into the cytosol through an unidentified mechanism that required endosome maturation and acidification, whereupon the internalized extracellular CDNs bound cGAS directly. A CDN/cGAS/STING complex was subsequently formed and ultimately activated IRF3. Exceptionally similar downstream effects have been observed between this alternative pathway and the classical pathway, though overall protein expression seems to differ in magnitude with intracellular CDNs and the classical pathway evoking a greater response[230, 231]. *In vivo* cancer therapies that use CDN STING agonists without a cytosolic delivery agent likely activate this alternative STING signaling pathway and consequently may not maximize their immunostimulatory potential.

The duration of STING pathway stimulation is also a critically important consideration, as it can dramatically influence immunological outcomes (***Figure 2.5***). While, acute and localized activation of the STING pathway generally supports a healthy level of immune activation for disease eradication, chronic STING signaling can elicit many inflammation-driven diseases. Such diseases include monogenic autoinflammatory syndromes (*e.g.* STING-associated vasculopathy with onset in infancy (SAVI), AGS, familial chilblain lupus, *etc.*), autoimmune diseases (*e.g.* systemic lupus erythematosus and rheumatoid arthritis), neurological disorders (*e.g.* ischaemic brain injury, Parkinson disease, Huntington disease, age-dependent macular degeneration, *etc.*), metabolic diseases (*e.g.* nonalcoholic steatohepatitis (NASH), alcoholic liver disease, *etc.*), inflammatory diseases (*e.g.* sepsis), cardiovascular diseases (*e.g.* myocardial infarction), cancer (*e.g.* metastases), as well as senescence and aging[21].

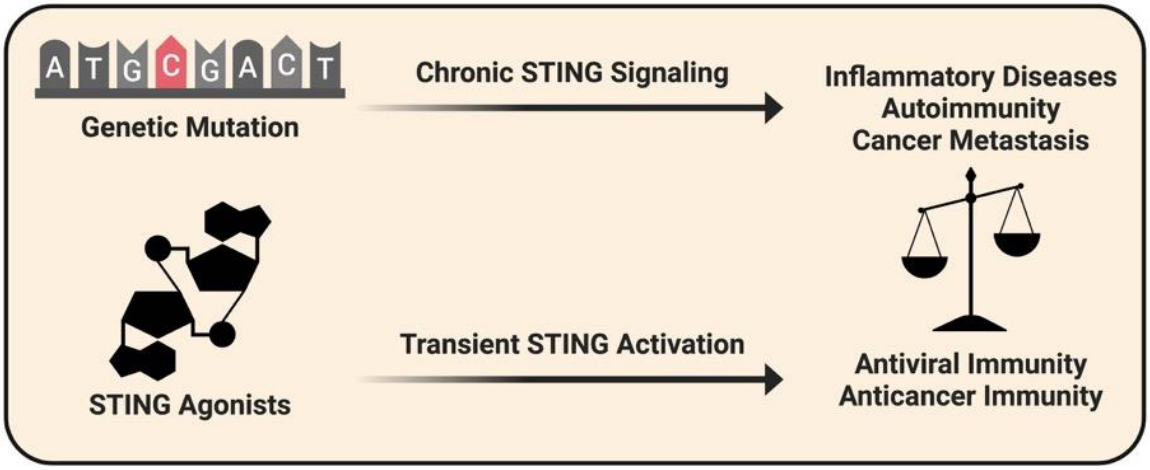

Figure 2.5. The importance of STING signaling kinetics. The distinct outcomes of STING activation are balanced by signal persistence. Chronic STING signaling, which is quite often the result of genetic mutations, can lead to numerous IFN-driven inflammatory diseases, autoimmunity, and even cancer metastasis. Conversely, transient STING signaling, which can be induced by the acute STING activation from STING pathway agonists, can galvanize robust antiviral and/or anticancer immunity. Figure created with *biorender.com*.

Prolonged stimulation of the STING pathway can lead to lethal inflammatory disease[179] as well as cancer development and metastasis in certain settings[232-234]. Thus, the degree and persistence at which cGAMP is able to spread and activate STING in neighboring cells can play a role in tumorigenesis. Indeed, STING-induced metastasis in the context of brain cancer has been observed and attributed to the continuous transfer of cGAMP from cancerous cells to neighboring astrocytes via gap junctions[77]. Therefore, in order to avoid promoting disease progression, careful thought should be given to treatment regimen and the cellular context of the treatment location when designing cancer therapies that exploit cellular transfer of cGAMP.

STING and the Cancer-Immunity-Cycle

Intrinsic STING Signaling and Innate Antitumor Immunity

The main process through which the immune system recognizes and eliminates cancer has been described as the cancer-immunity-cycle[235]. The cancer-immunity-cycle summarizes how antitumor cellular immune responses are initiated and propagated through cooperation between the innate and adaptive immune systems. In principal, the cycle perpetually functions to inhibit cancer formation and growth through the following major steps: 1) Antigen Processing and Presentation, 2) Lymphatic Trafficking, 3) T Cell Priming and Activation, 4) Systemic Trafficking of T Cells, 5) Infiltration of T Cells into Tumors, 6) Immune Recognition of Cancer Cells, and 7) Killing of Cancer Cells / Antigen Release.

Spontaneous cancer-immunity-cycle operations that prevent the immune escape of pre-cancerous cells can be largely dependent on STING signaling[236, 237]. Mechanistic studies using genetically engineered mouse models of immunodeficiencies have identified STING signaling as an integral mechanism for innate immune sensing of immunogenic cancers. Notably, wildtype

mice with functional STING signaling exhibited attenuated tumor growth relative to mice that were deficient in various STING pathway components[53, 56]. In accordance with the cancer-immunity-cycle, the innate antitumor effects of intrinsic STING signaling have been primarily attributed to enhanced tumor antigen-specific T cell responses[238, 239]. While the STING pathway was found critical to the spontaneous priming of antitumor T cells in certain murine tumor models, several other pattern recognition receptor pathways, including RIG-I and various Toll-like receptors (TLRs) were less essential for generating cell-mediated antitumor immunity despite their conserved ability to induce the production of type I IFNs[56]. Additionally, in accordance with the dependence of immune checkpoint blockade (ICB) on spontaneous T cell responses, it has been established that functional STING signaling is critical for the maximal efficacy of ICB in murine tumors[56, 240, 241].

The development of cancer is often the result of immunosuppression that impedes the favorable progression of the cancer-immunity-cycle. Indeed, selective pressure can lead to the deregulation of STING signaling, a prevalent mechanism by which cancer cells evade intrinsic antitumor immunity[36, 37]. Notably, the genes encoding cGAS and STING are seldom mutated in cancer (*i.e.* less than 1% of tumors exhibit such mutations)[242, 243]. Instead, epigenetic silencing of cGAS and/or STING is the predominant cause of the STING signaling dysfunction that is observed in the immune escape of various cancers[36, 37, 41, 242]. The cellular transfer of cGAMP and/or tumor-derived dsDNA to stromal cells (*e.g.* myeloid cells, endothelial cells) becomes particularly important for innate antitumor immunity when STING signaling becomes deregulated in cancer cells.[132, 204]. Extrinsic STING signaling may then be employed to promote the immune recognition and eradication of such cancer cells.

It has been suggested that the STING protein may facilitate the intracellular clearance of

cGAMP[122]. Therefore, cGAMP could be prone to accumulate more rapidly in the cytosol when expression of the STING protein is suppressed in cancer cells. Such accumulation of cGAMP in tumor cells could generate high intracellular concentrations that would promote cGAMP transfer to surrounding cell populations. Thus, tumorigenesis could be prevented by activation of antitumor immunity, provided the degree of cGAMP spread was sufficiently high to stimulate innate immune activation. However, this is clearly insufficient to prevent the development of all cancers, since deregulated STING is a common feature of many immune-evasive tumors. Factors such as ENPP1 may critically inhibit the degree of extrinsic STING signaling despite an increased efflux of cGAMP from cancer cells. Restricted cGAMP transfer in such cases might even contribute to the development of tumors with deregulated STING, as sustained low-level STING signaling may actually promote tumor growth and metastasis[77, 180, 232, 244], especially for tumors with low antigenicity[245].

Therapeutic Effects of Type I Interferons

As previously mentioned, generation of antitumor innate and adaptive immunity is considered the primary mechanism by which STING activation can combat cancers[183]. Indeed, in response to STING agonist treatment, antitumor immunity is mainly responsible for the tumor regression observed in murine tumor models as well as the sustained protection against disease recurrence demonstrated by efficacy in tumor rechallenge experiments[53, 54, 246]. Such therapeutic responses have been largely attributed to type I IFN signaling in addition to other proinflammatory cytokines (*e.g.* TNF-α) downstream of STING activation.

Type I IFNs (*i.e.* IFN-α and IFN-β) are signature cytokines of STING activation and are considered a primary effector induced by STING signaling[44]. Type I IFNs directly regulate the

transcription of over 100 genes that influence protein synthesis, autophagy, apoptosis, angiogenesis, and immunity[47]. Notably, the direct administration of type I IFNs into solid tumors has demonstrated clinical efficacy, and in 1986, recombinant IFN-α2 became the first human immunotherapeutic approved by the FDA for the treatment of cancer. Many mechanisms of action have been proposed for the therapeutic effect of type I IFNs in the treatment of cancer, including both immune-mediated and immune-independent mechanisms. In various settings, type I IFNs have been found to directly inhibit tumor cell proliferation[247-249], disrupt tumor vasculature[250, 251], prompt the maturation of various APCs[252-254], induce CTL responses[255, 256], and activate NK cells[249, 257, 258].

For any IFN-driven cancer therapy (*e.g.* targeted STING pathway activation), the dosing of type I IFN and/or type I IFN inducers is a critically important therapeutic design consideration, as they can directly influence the mechanism of antitumor activity[48, 259]. Cancer treatments that implement high levels of intratumoral type I IFN can result in significant tumor regression that is largely independent of host adaptive immunity and instead depends heavily upon disruption of the tumor vasculature[250]. This high-dose ablative effect on tumors has also been observed with STING agonists[260] and may be related to the type I IFN component of downstream STING signaling. Similar to the dose-dependence of type I IFN treatment, robust antitumor T cell responses are achieved in murine tumor models with lower, more immunogenic doses of STING agonists, and excessive STING activation fails to sufficiently generate the antitumor immunity that can prevent tumor growth upon rechallenge.

In addition to dosing, timing of intratumoral type I IFN administration and/or induction can affect the development of antitumor immunity, which is essential for durable responses and long-term survival[48, 259]. As stated previously, type I IFNs induce DC maturation[252-254]. When DCs

undergo maturation, they lose their phagocytic ability, thereby preventing the capture of new antigens in favor of an increased ability to cross-prime naïve $CD8^+$ T cells that are specific for antigens previously internalized by the DCs[261]. Accordingly, Tzeng *et al.* found that generation of antigenic tumor debris must precede the induction of type I IFNs in order to efficiently prime long-term antitumor immunity[262].

Though type I IFNs have demonstrated efficacy in the treatment of cancer, they have also been associated with systemic adverse effects, which have limited their clinical use. The observed side effects for type I IFN therapies included fever and chills upon initial administration and fatigue, depression, and anorexia with continued treatment[263, 264]. While the production of type I IFNs is a critically important component of STING signaling for promoting antitumor immunity, other IFN-independent signaling pathways downstream of STING activation (*e.g.* NF-κB signaling) are also important for immune regulation[265] and can act to balance and resolve the resultant immune response[266].

Immunological Effects of STING Pathway Activation

The cancer-immunity-cycle can be considered as the "central dogma" of cancer immunotherapy; in order to work effectively, cancer immunotherapies must harness the cancer-immunity-cycle and promote it, either by pushing the cycle forward or by removing the restraints that impede the proper operation of the cycle. Accordingly, the great potential of STING pathway agonists for cancer immunotherapy arises from their exceptional capacity to bolster antitumor immune responses by promoting each phase of the CIC (***Figure 2.6***). Indeed, STING has been described as a master regulator of the cancer-immunity-cycle[267].

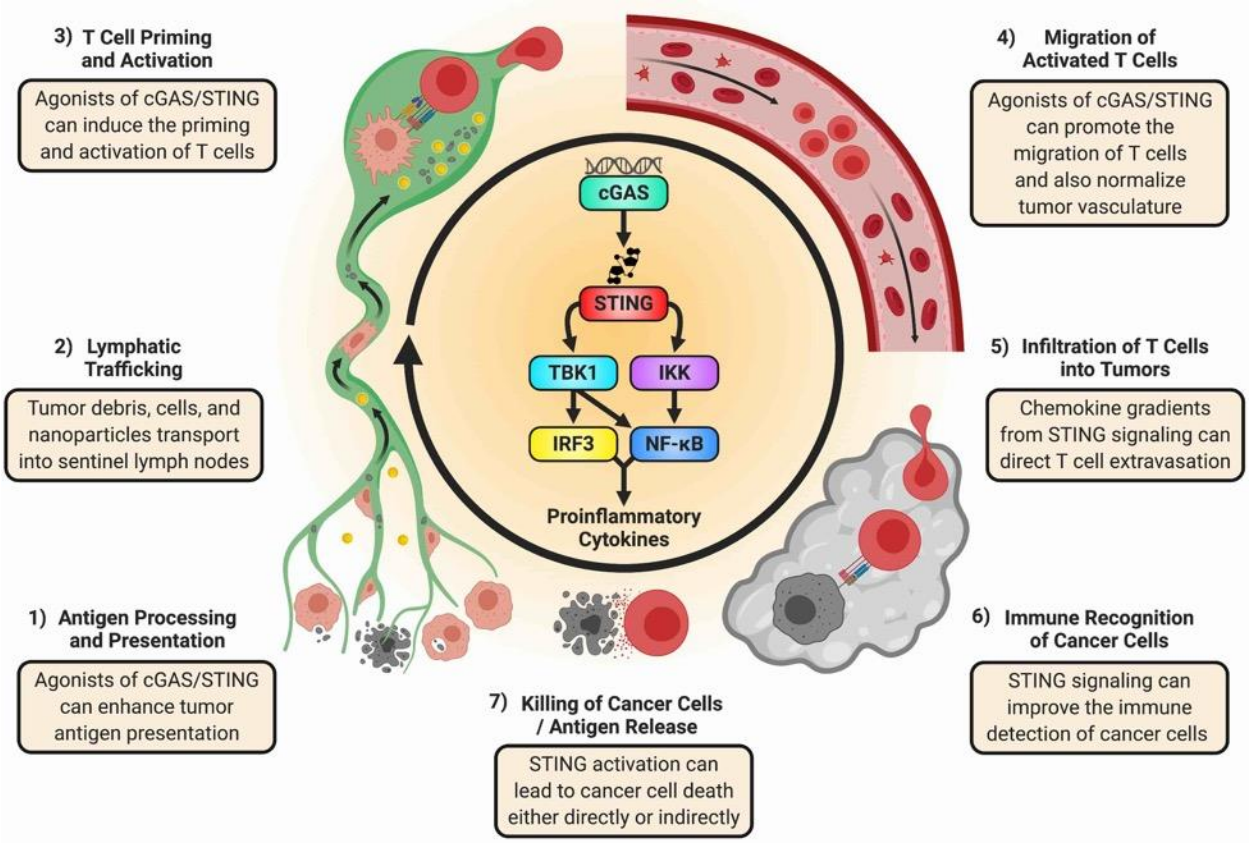

Figure 2.6. STING and the Cancer-Immunity-Cycle. STING can promote antitumor immunity via the Cancer Immunity Cycle by promoting each of the following steps: 1) Antigen processing and presentation, 2) Lymphatic trafficking, 3) T cell priming and activation, 4) Systemic trafficking of T cells, 5) Infiltration of T cells into tumors, 6) Immune recognition of cancer cells, and 7) Killing of cancer cells / antigen release. Figure created with *biorender.com*.

The production of type I IFNs is essential for the STING-mediated propagation of the cancer-immunity-cycle. Type I IFNs prompt the maturation of various APCs, promoting the expression of the major histocompatibility complex (MHC), costimulatory molecules, and various other proinflammatory cytokines that are required for T cell priming and activation[268]. Indeed, STING signaling has been found to stimulate antigen processing and presentation in a type I IFN dependent manner[269, 270].

A particular subset of DCs known as $CD8\alpha^+$ Batf3 DCs have been described as the main APCs responsible for generating antitumor T cells[271, 272]. $CD8\alpha^+$ Batf3 DCs typically reside in

secondary lymphoid tissues and are characterized by an exceptional capacity for antigen cross-presentation (*i.e.* the process of antigen internalization and subsequent antigen presentation in complex with MHC-I to $CD8^+$ T cells). Notably, type I IFN production within solid tumors, like that induced by targeted STING activation, promotes the intratumoral accumulation of $CD8\alpha^+$ Batf3 DCs from surrounding tissues[256]. Additionally, interferon-alpha/beta receptor (IFNAR) signaling within tumor-infiltrating $CD8\alpha^+$ Batf3 DCs is required for successful cross-priming of tumor antigen–specific $CD8^+$ T cells and subsequent immune control of tumor growth[256, 273].

Matured APCs, especially matured DCs, upregulate CC-chemokine receptor 7 (CCR7), causing them to enter the lymphatic vasculature, which expresses the CCR7 ligand, CC-chemokine ligand 21 (CCL21)[274, 275]. The APCs then further migrate to the tumor draining lymph nodes (tdLNs), where they can interact with naïve T cells. While T cell activation typically occurs in tdLNs, it has been suggested that intratumoral expression of type I IFNs may also prompt tumor-infiltrating $CD8\alpha^+$ Batf3 DCs to cross-prime $CD8^+$ T cells within the TME, thus bypassing the need for migration to the tdLNs[271]. Indeed, the direct activation of naïve T cells in tumors has been observed in mice that were treated with a T cell recirculation blocker[276] as well as in mice that were devoid of LNs and spleens[277]. Furthermore, targeted STING activation within B16-F10 murine melanoma tumors has been reported to induce the intratumoral formation of tertiary lymphoid structures, which may also serve as a local site for T cell priming to occur[278].

In addition to the type I IFN effects of STING signaling, there are other downstream effects of STING activation that can also enhance tumor antigen processing and presentation. Notably, STING activation typically results in the production of other proinflammatory cytokines (*e.g.* IL-6 and TNF-α) and nitric oxygen species that can promote M1-like polarization of macrophages[279, 280]. Moreover, STING signaling can even repolarize the phenotype of existing tumor resident

macrophages from M2 to M1[280, 281]. While M2 macrophages tend to be immunosuppressive and protumor, M1 macrophages are exceptionally conducive to effective cancer treatments, as they can inhibit the proliferation of surrounding cells via paracrine signaling[279] and even induce lysis in various types of cancer cells[282, 283].

Generally, three signals are required from APCs to activate naïve T cells: protein antigen displayed on MHC for recognition by the T cell receptor (TCR), co-stimulatory molecules, and certain proinflammatory cytokines, all of which can be enhanced by STING activation as just described. Thus, T cell priming and activation in the tdLNs naturally follow the STING-mediated APC response.

The two major types of effector T cells are MHC-I–restricted $CD8^+$ T cells, which are known as *cytotoxic T lymphocytes* (CTLs) and MHC-II–restricted $CD4^+$ T cells, which are known as *helper T lymphocytes*. A main function of CTLs is to directly kill diseased cells that express and present their cognate antigen[284], while helper T lymphocytes tend to regulate the function of other immune cells via paracrine signaling[285]. Notably, functional APC responses from STING signaling can enhance the activation of both CTLs[256, 270] and helper T lymphocytes[269, 286]. The CTLs are generally considered to be the primary driver of the antitumor immune responses that are stimulated by STING signaling[238, 239]. However, the helper T lymphocytes are known to support CTL function and cytolytic activity. Indeed, in response to STING signaling, the helper T lymphocytes exhibit a balanced Type 1 / Type 2 (Th1/Th2) phenotype, with slightly greater Th1 activity[287], which promotes supportive M1 macrophage polarization[288, 289].

In addition to stimulating T cell responses through the activation of innate immunity, STING signaling can also directly influence antitumor T cell function. STING signaling within T cells has been shown to have varied effects depending on the degree and duration of the stimulus.

Hyperactivation of STING can drive antiproliferative and apoptotic signaling within T cells[115, 290, 291]. Some lesser degree of STING signaling within T cells can however maintain $CD8^+$ T cell stemness, which can improve T cell-mediated tumor clearance[239]. In light of this dichotomous role of STING signaling in T cells, careful evaluation of how STING pathway agonists impact antitumor T cell viability and effector function will be critical to maximizing immunotherapeutic responses.

Before CTLs can recognize and kill cancer cells, they must egress the tdLNs and traffic to tumor sites. Like matured DCs, naïve T cells are largely attracted to and retained within LNs through their expression of CCR7[292]. Activated T cells migrate out of LNs and into systemic circulation by downregulating CCR7 and simultaneously upregulating the receptor for sphingosine1-phosphate (S1P)[293], which is a signaling sphingolipid that is present in the blood at much higher concentrations than in lymphoid organs[294, 295]. Once activated T cells accumulate in the bloodstream, they require additional signals for direction to their effector site. STING signaling generates a chemokine gradient (*e.g.* CXCL9 and CXCL10) that can guide T cell extravasation into solid tumors[256, 272, 296]. Notably, CXCL9 and CXCL10 are also capable of driving NK cell recruitment, activation, and maturation[297]. Moreover, activated NK cells can augment adaptive antitumor immunity by recruiting additional DCs to the TME[298].

Despite the powerful effects of chemokine gradients, dysfunctional tumor vasculature, a common feature of many cancers, can still act as a major barrier to immune cell infiltration and function[299]. However, vascular normalization, a reversal of tumor vessel abnormalities, has been shown to increase T cell infiltration and restore T cell function[299]. In addition to promoting chemokine gradients, STING activation can also normalize tumor vasculature and thereby further enhance T cell infiltration into tumors. Specifically, the direct injection of STING agonists into

solid murine tumors results in reduced blood vessel density and vascular sprouts as well as an increase in pericyte coverage and an upregulation of endothelial-leukocyte adhesion molecules[300]. The normalized tumor vasculature that ensues STING activation has been found to facilitate the intratumoral trafficking of effector T cells across the endothelial barrier and condition the TME to enhance antitumor immunity[278, 300]. Notably, while other agents can also normalize tumor vasculature, STING-activating therapeutics offer the potential for coordinating vascular remodeling with reprogramming of the immune microenvironment, which can allow T cells to more efficiently home to tumor sites and perform their effector function.

STING signaling can trigger tumor elimination either by directly inducing cell death programs in cancer cells[301] or indirectly via mechanisms involving the immune system, particularly CTLs[56] and NK cells[50, 302]. Notably, the direct induction of cell death programs in cancer cells appears to be most pronounced in hematopoietic malignant cells, such as B cell and T cell lymphomas[115]. As demonstrated by numerous murine tumor models where immune cells have been knocked out or inhibited, antitumor immune responses are the primary cancer elimination mechanism promoted by STING signaling[183].

Antitumor immunity can be enhanced by intratumoral STING signaling in a multitude of ways. STING signaling can promote the expression of MHC-I on the surface of cancer cells to enhance the recognition of cancer cells by CTLs, which promotes CTL-mediated cancer cell death[303]. Some tumors can however evade this cellular response through loss of MHC-I expression or lack of neoantigens[304-306]. NK cells can act to overcome such evasion mechanisms by recognizing stress-induced cells, particularly those that have lost MHC-I, and eliciting a cytotoxic response[304, 305]. NK cells have also been reported to drive tumor cell killing in cancers with poor antigenicity[49]. Indeed, it has recently been described that NK cells mediate the clearance of CTL-

resistant tumors in response to STING agonists[307]. Furthermore, STING signaling within cancer cells has also been shown to upregulate ligands for the NK cell-specific immunoreceptor, NKG2D, which increases NK cell recognition and elimination of cancer cells[308]. Cancer cell death can result in the release of additional tumor antigens, which leads to epitope spreading and recommencement of the cancer-immunity-cycle.

Iatrogenic STING Activation by Classical Cancer Therapies

As previously mentioned, indirect STING activation is a consequence of many classical cancer treatments (***Figure 2.7***), including many DNA-damaging chemotherapies (*e.g.* cisplatin[309], camptothecin[310], doxorubicin[311], paclitaxel[155, 312], etoposide[313-316], *etc.*), radiotherapy[317], and therapies that compromise the DNA damage response (*e.g.* poly(ADP)-ribose polymerase 1 (PARP) inhibitors[318-322], ataxia telangiectasia and Rad3-related protein (ATR) inhibitors[323], *etc.*). The inadvertent STING activation within tumor cells from such cancer therapies is primarily caused by micronuclei formation and subsequent cGAS recognition of cytosol-accessible dsDNA[57, 58]. Notably, inhibitors of DNA methyltransferases are another class of cancer therapeutics, which have been approved for the treatment of acute myeloid leukemia[324] and are known to work well in combination with radiation and various chemotherapies in preclinical cancer models[325]. Recent findings suggest that the pharmacological inhibition of DNA methylation caused by a DNA methyltransferase inhibitor (*i.e.* 5-aza-2'-deoxycytidine) can also promote STING signaling by reversing the epigenetic silencing of both cGAS and STING that is commonly observed in a variety of cancer types[326].

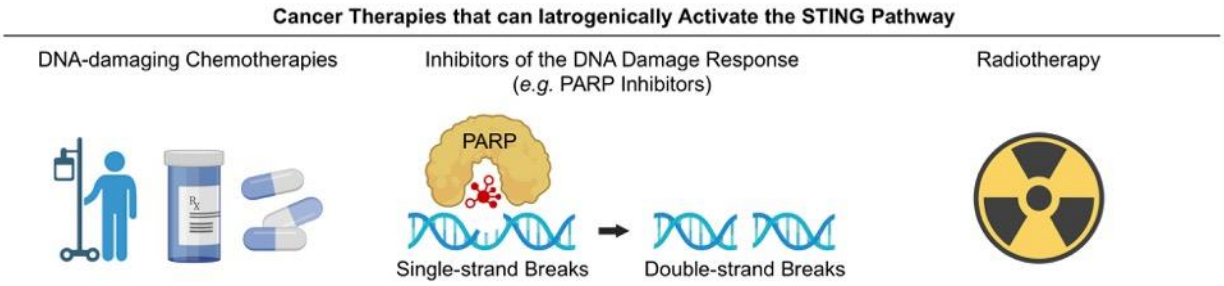

Figure 2.7. Cancer therapies that can iatrogenically activate the STING pathway. STING activation is a known biological consequence of many classical cancer treatments, including DNA-damaging chemotherapies, therapies that compromise the DNA damage response, and radiotherapy. While the effects of classical cancer treatments are multifaceted, therapies that also induce STING signaling have potential to enhance overall therapeutic efficacy by providing a supportive inflammatory context for generating antitumor immunity. Figure created with *biorender.com*.

While the effects of classical cancer treatments are multifaceted, therapies that also induce STING signaling have potential to enhance overall therapeutic efficacy by providing a supportive inflammatory context for generating antitumor immunity. Indeed, it has been reported that STING signaling actively contributes to immune-mediated tumor growth inhibition in murine tumor models treated with a growing number of classical cancer treatments, notably including topotecan[327], viral oncolytic therapy[36], PARP inhibition[318, 320, 328], and radiotherapy[317]. Additionally, STING agonists were found to synergize well with radiotherapy in murine pancreatic tumors by promoting inflammatory pathways following tumor antigen release by radiotherapy[329].

STING signaling has also been implicated in the response to classical cancer treatments even in the absence of immune-mediated mechanisms. STING activation in cancer cells induced by antimitotic chemotherapies (*e.g.* taxane drugs) has been shown to trigger a proapoptotic secretory phenotype, which promotes BCL-xL-dependent apoptotic priming in untreated cancer cells[312]. It was confirmed that the STING-dependent apoptotic effects are required for the

antitumor response to paclitaxel *in vivo*. Additionally, autophagy caused by STING-activating chemotherapies can clear diseased cells directly in addition to promoting desirable antitumor immune responses by triggering ATP release and immunogenic cell death (ICD)[330, 331]. In the context of radiotherapy, the cGAS protein can also directly contribute to cancer cell clearance by initiating cell death programs and accelerating γ-irradiation-induced cell ablation[150].

The functional significance of iatrogenic STING activation in human cancer patients is currently unclear. As previously discussed, the magnitude and context of STING signaling are critically important determinants of antitumor immune responses, and therefore iatrogenic STING activation may not be optimal for maximizing therapeutic impact. Furthermore, many classical cancer treatments target tumors indiscriminately and thus likely also impact immune cells within the TME. Therefore, the balance of STING activation, degree and type of tumor cell death, and the effect of the treatment on immune cells are all important variables to consider, as they will likely influence therapeutic outcomes[332]. Nevertheless, research has already begun to explore the employment of nanotechnology for enhancing STING-activating chemotherapies, strategies that not only address drug delivery challenges but also seek to simultaneously reinforce antitumor immunity within the TME[333].

cGAS Agonists

While the STING protein has appropriately garnered much interest as a druggable target for cancer immunotherapy, cGAS has been largely overlooked despite the potential of cGAS activation to more closely mimic the endogenous STING pathway[334]. Indeed, cGAS agonists may offer more control over the level and kinetics of local STING signaling, which may be tailored to optimize antitumor immunity[108]. As mentioned previously, dsDNA in the cytosol can elicit tiered

immune responses, the phenotype of which is determined by the physiochemical composition of the dsDNA[108]. The molecular weight of the cGAS-bound dsDNA (*i.e.* BP length) influences the prevalence and size of the resultant liquid-like droplets, which function as miniature bioreactors for the efficient production of 2′3′-cGAMP[88]. Accordingly, the localized production of 2′3′-cGAMP is tightly regulated, and the liquid-like droplets essentially act as *in situ* drug delivery depots that confer tunability over the degree of 2′3′-cGAMP production, which may be useful for promoting and controlling antitumor immunity. The lack of development behind cGAS agonists could be ascribed to the complexity of cGAS activation as well as the challenges facing nucleic acid delivery.

In theory, small molecule cGAS agonists could circumvent the delivery issues that are associated with the negative charge, hydrophilicity, and relatively large molecular weight of dsDNA. While no small molecule cGAS agonists have been reported to date, Hall *et al.* have identified a potential small molecule binding site on the cGAS enzyme that may cause catalytic activation of cGAS and is certainly worth investigation[335]. However, phase separation does require multivalent interactions for the assembly of macromolecular complexes[336], and therefore a small molecule activator of cGAS may not be able to induce the same liquid-like phase transition that is dependent on DNA-bridging. A small molecule agonist would likely have to exhibit self-multimerization to achieve efficient 2′3′-cGAMP production via cGAS oligomerization, which adds another level of complex requirements for the design and development of a small molecule cGAS agonist. Most small molecules would seemingly be unlikely to generate the intracellular microreactors for 2′3′-cGAMP production without assistance from other molecules, and this is perhaps the primary reason that the development of small molecule cGAS agonists has not yet been reported. Notably, DNA-bridging is not required for cGAS *inactivation*, and there already

exist several small molecule cGAS inhibitors that have been developed for applications outside of cancer (*e.g.* autoimmunity)[138, 334, 337, 338].

While not a canonical small molecule per se, the metal ion, manganese (Mn^{2+}) is worth discussing as it has recently been shown to be capable of independently activating monomeric cGAS in the absence of dsDNA without the need for oligomerization[339]. Mn^{2+} can affect STING signaling in several unique ways, and this will be discussed in greater detail in *Section 7.1* along with other potentiators of the STING pathway. While Mn^{2+} possesses the capacity for oligomerization-free cGAS activation, Mn^{2+} also sensitizes cGAS to DNA binding and oligomerization. Thus, the recently reported therapeutic efficacy of Mn^{2+} as a STING pathway potentiator for cancer therapy[340] cannot be solely attributed to oligomerization-free cGAS activation. It remains to be determined whether any cGAS activator that does not somehow induce cGAS oligomerization and droplet formation could achieve therapeutically relevant STING activation and whether they would allow for control over the degree of STING signaling.

In addition to Mn^{2+}-encompassing therapies, DNA delivery strategies offer great promise for the pharmacological activation of cGAS. Since freely administered dsDNA is rapidly cleared and degraded with minimal cellular uptake[5], vehicles for efficient cytosolic delivery must to be employed for dsDNA-based cGAS agonists. Targeted cGAS activation via intracellular dsDNA delivery has been only modestly explored by just a few research groups, all reporting significant but limited success[341-344]. As with STING agonists, the development of cGAS agonists for cancer immunotherapy will likely require the employment of nanotechnology and molecular engineering approaches to overcome drug delivery barriers[345, 346].

Therapeutic Potentiators of the cGAS/STING Pathway

There is a growing list of known STING pathway potentiators (***Figure 2.8***), which currently includes certain metal ions (*e.g.* Mn^{2+} and Mg^{2+}), cGAS-binding proteins, inhibitors of DNA methyltransferases, various inhibitors of NF-κB signaling, as well as ENPP1 inhibitors for therapies that utilize endogenous 2′3′-cGAMP (*e.g.* radiotherapy). These therapeutic agents have potential to improve the efficacy and/or safety of STING pathway activation for cancer immunotherapy and could be utilized in combination with STING pathway agonists either through local co-administration or by rational co-incorporation into drug delivery platforms.

It is well established that transition metals can regulate the function of enzymes. Indeed, nearly half of all enzymes utilize metal cofactors[347, 348]. Manganese, one of the most abundant metals within mammalian tissues, has recently been identified as a natural, triggerable potentiator of the STING pathway[349]. At cellular steady-state, the majority of Mn^{2+} within cells is confined to membrane-enclosed organelles, such as the Golgi and mitochondria[349]. Viral infection can induce the release of Mn^{2+} into the cytosol, whereupon Mn^{2+} is then disposed to bind the cGAS and/or STING proteins[349]. Mn^{2+} is capable of sensitizing both cGAS and STING to activation and consequently lowers the threshold for STING pathway activation by several orders of magnitude[349]. Shortly thereafter, it was determined that Mn^{2+} is also essential in the innate immune sensing of tumors and that combining it with ICB synergistically boosted antitumor immunity[340]. Furthermore, a phase 1 clinical trial investigating the combination of Mn^{2+} and anti-PD-1 antibody yielded promising efficacy in patients with advanced metastatic solid tumors[340] (NCT03991559).

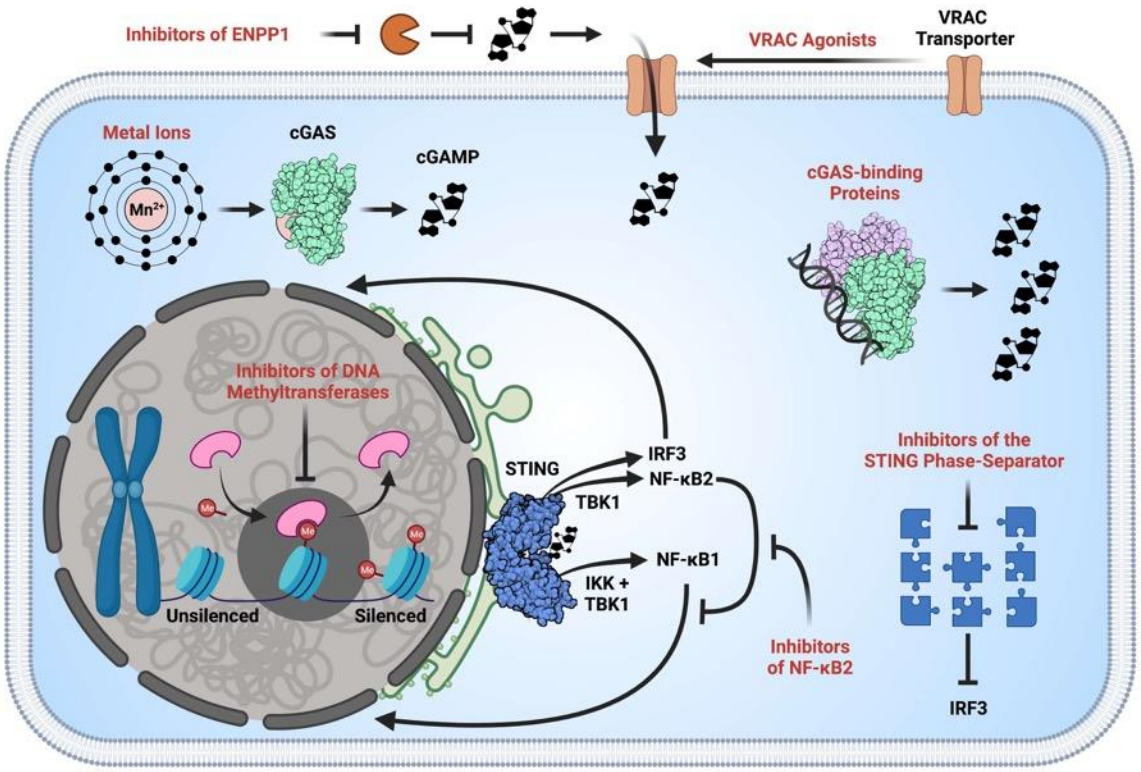

Figure 2.8. Strategies for potentiating STING signaling. The magnitude of STING-driven gene expression and/or profile of the resultant immune response can be modulated by many different biochemical agents (*i.e.* potentiators). Some notable potentiators of the cGAS/STING pathway include certain metal ions (*e.g.* Mn^{2+} and Mg^{2+}), inhibitors of DNA methyltransferases, various inhibitors of NF-κB signaling, inhibitors of the STING phase-separator, cGAS-binding proteins, VRAC agonists, and inhibitors of ENPP1. Figure created with *biorender.com*.

Cytosolic Mn^{2+} has been reported to potentiate STING signaling in several unique ways: 1) Mn^{2+} can independently activate monomeric cGAS in the absence of dsDNA without the need for cGAS oligomerization[95, 339]; 2) In conjunction with the ATP/GTP substrate pair, Mn^{2+} enhances the dsDNA binding capacity of cGAS. Conversely, dsDNA enhances the Mn^{2+} binding capacity of cGAS, which is also amplified by larger molecular weight dsDNA. Thus, Mn^{2+} and dsDNA act in a concerted manner for maximal cGAS-substrate recognition[95]; 3) Mn^{2+} accelerates the overall catalytic activity of dsDNA-bound cGAS resulting in much greater production of cGAMP[95, 349]; 4) Mn^{2+} increases the binding affinity of cGAMP to STING[174, 349]. Collectively, these attributes make cytosolic Mn^{2+} an exceptionally potent STING pathway potentiator.

Several research groups have already begun to develop nanotechnology and/or depots for Mn^{2+} delivery to promote enhanced pharmacological STING pathway activation for cancer immunotherapy[343, 350-354]. Wang *et al.* reported a biomaterial-based delivery approach that coupled the divalent cation chelator, alginate with Mn^{2+} in the context of radiotherapy[350]. The researchers found that IT injections of Mn^{2+} by itself could indeed enhance the antitumor immune response following RT, but that the timing of administration was critical for efficacy. Free Mn^{2+} was metabolized out from tumors within minutes and DNA did not accumulate in the cytosol of cells until ~ 24 hours post RT treatment. Accordingly, Mn^{2+} injected IT immediately after RT was unable to enhance the therapy, while IT injection 24 hours after RT did demonstrate efficacy. They subsequently employed alginate to act as a depot to control the release of Mn^{2+} for up to 72 hours. Administration of the alginate-manganese complexes 24 hour after RT lead to 90% tumor inhibition rate and a significantly extended average survival time.

Hou *et al.* created a multifaceted NP for STING pathway activation in tumors[351]. Doxorubicin (DOX) was encapsulated within amorphous porous manganese phosphate (APMP) NPs, which were then coated them with phospholipids (PL) for improved stability in systemic circulation and triggerable phospholipase-mediated degradation within tumor cells. When administered IV, the resultant PL/APMP-DOX NPs navigated to tumors, released DOX to induce DNA damage and subsequent cGAS activation, and released Mn^{2+} to augment cGAS/STING activity. The PL/APMP-DOX NP treatment boosted DC maturation and increased tumor infiltration of both cytotoxic T cells and NK cells in the 4T1 murine breast cancer model.

Zhou *et al.* also developed a multifunctional NP platform, which likely operates in a similar manner to the PL/APMP-DOX NPs (*i.e.* delivering DOX and potentiating the STING pathway with manganese)[343]. Their NP platform was prepared by co-assembling dsDNA-gold conjugates

and DOX onto Mn_3O_4 nanoflowers. 59 bp poly(dA):poly(dT) was chosen as the dsDNA to activate the STING pathway. The poly(dT) single-stranded DNA was pre-conjugated onto AuNP through an Au-S bond and then annealed with complementary strand. This was then loaded onto Mn_3O_4 nanoflowers via a noncovalent attachment method. Finally, DOX was loaded onto the complex, resulting in a final particle diameter of ~ 354 nm and a surface charge of −7.7 mV. Following IV administration, manganese and gold from the nanoflower NPs were detected in B16-F10 tumors, suggesting some level of passive targeting. It was reported that the dsDNA stimulated the immune response by activating the STING pathway via cGAS, while the DOX exerted its chemotherapeutic antitumor activity. Though not addressed by the authors, it is likely that the DOX also contributed indirectly to the STING pathway activation via its DNA-damaging capacity and that the Mn^{2+} degradation product of nanoflower enhanced the STING signaling within the tumors. The combination particles significantly inhibited tumor growth and prolonged survival in the 4T1 tumor model and successfully demonstrated potential for synergy between a STING-pathway agonist and a chemotherapy.

Chen *et al.* reported a thiolated and Mn^{2+} coordinated CDN nanovaccine (termed Mn-cGAMP NVs) that facilitates the cytosolic co-delivery of 2′3′-cGAMP and Mn^{2+} to potentiate an antitumor immune response against B16-F10 murine melanoma following IT administration[352]. They utilized polymerized guanidine-containing disulfides to assemble with 2′3′-cGAMP and then coordinate with Mn^{2+} ions, forming particles that were ~ 176 nm in diameter. The Mn-cGAMP NVs attenuated primary tumor growth, inhibited distal tumor growth, and improved responses when administered in combination with anti-PD-L1 monoclonal antibody treatment.

Yang *et al.* engineered a biomimetic nanoplatform using cancer cell membranes extracted from B16-F10 cells to co-encapsulate manganese dioxide (MnO_2) NPs and the established

photothermal therapy sensitizer, 1,1′-Dioctadecyl-3,3,3′,3′-tetramethylindotricarbocyanine iodide (DiR)[353]. Interestingly, manganese was the sole adjuvant in their system and it was used to induce STING signaling via cGAS activation. The resultant vesicles had a diameter of ~ 125 nm and displayed a negative surface charge of −19 mV. Notably, the researchers found that slightly acidic conditions (*e.g.* pH ~ 6.8) with high concentrations of hydrogen peroxide (*e.g.* 2.5 mM H_2O_2) triggered the release of Mn^{2+} from the vesicles and that the vesicles promoted the tumor accumulation of both Mn^{2+} and DiR following IV injection. The systemic administration of their construct coupled with targeted photothermal therapy enabled partial tumor regression in primary tumors, multinodular tumors, metastatic tumors, and recurrent tumors. Additionally, transcriptomic analysis of the tumors following treatment demonstrated the upregulation of STING-driven genes, supporting on-target STING activation *in vivo*.

Gao *et al.* described the development and characterization of PEGylated manganese phosphate (MnP-PEG) nanoclusters for cancer immunotherapy[354]. The particles were fabricated by mixing Mn^{2+} and PO_4^{3-} ions in solution followed by the addition of a phosphate-functionalized 5 kDa PEG polymer. The MnP-PEG nanoclusters were ~ 150 nm in diameter with a negative surface charge of −11 mV. It was determined that the nanoparticles could mediate endocytosis, acid-triggered Mn^{2+} release, and STING signaling. Furthermore, intratumoral administration of the MnP-PEG nanoclusters in the B16-F10 tumor model enhanced the tumor infiltration of DCs and macrophages as well as activated (*i.e.* $CD69^+$) tumor-infiltrating $CD8^+$ and $CD4^+$ T cells and NK cells. The treatment also resulted in antitumor efficacy as a monotherapy and improved responses to ICB (*i.e.* anti-PD-1 therapy).

There exist several known cGAS-binding proteins that also bind DNA and thereby promote cGAS activity[355-358]. By providing additional binding sites for cytosolic DNA, these cGAS-binding

proteins enhance the recognition of DNA by cGAS, which augments 2′3′-cGAMP production and STING signaling. Polyglutamine binding protein 1 (PQBP1) has been described as a proximal innate sensor of a human immunodeficiency virus type 1 (HIV-1) infection, as it was found to enhance the IRF3-dependent innate response in primary human monocyte-derived DCs (MDDCs) by directly binding reverse-transcribed HIV-1 DNA and cGAS[355]. The CCHC-type zinc-finger (ZF) protein, ZCCHC3 was similarly reported as a co-sensor of cGAS, capable of improving the innate immune response to cytosolic dsDNA and the DNA viruses, herpes simplex virus 1 (HSV-1) and vaccinia virus[356]. GTPase-activating protein SH3 domain-binding protein 1 (G3BP1) was identified as another positive regulator of cGAS activity with the inhibition of G3BP1 partially rescuing cGAS-mediated autoinflammation in a *Trex1*$^{-/-}$ mouse model[357]. Lastly, the secreted bacterial protein, streptavidin was recently reported to bind both DNA and cGAS to promote cGAS-dependent immune responses against the DNA virus, HSV-1[358]. Notably, streptavidin exhibits exceptionally strong noncovalent interactions with biotin and has accordingly been extensively used for many biotechnological applications, such as molecular purification, molecular detection, and drug delivery. Therefore, the unique interaction of streptavidin with cGAS and DNA, which can lead to immunostimulation, complicates the clinical and biotechnological usage of streptavidin. Indeed, careful consideration should be given when choosing to use streptavidin in certain applications. However, since enhanced STING signaling is beneficial for many cancer types, these cGAS-binding proteins have potential for therapeutic use in combination with cGAS-activating cancer therapies, though nanotechnology would likely need to be employed for *in vivo* delivery of these molecules.

As briefly mentioned in ***Section 3.4***, inhibitors of DNA methyltransferases are approved for the treatment of certain cancers and are also capable of improving intratumoral STING

signaling and tumor immunogenicity[324, 326]. Indeed, Falahat *et al.* recently determined that promoter hypermethylation of cGAS and STING genes mediates transcriptional silencing and impairs STING signaling function in melanoma, which disrupts tumor antigen presentation and the accumulation of tumor infiltrating lymphocytes[326]. By inhibiting DNA methylation with a clinically available DNA methyltransferase inhibitor (*i.e.* 5-aza-2'-deoxycytidine), the researchers were able to restore the activity of cGAS and STING and thereby improve antigenicity through the augmentation of MHC class I surface expression and antigen presentation. This ultimately resulted in enhanced T cell recognition of melanoma. Therefore, inhibitors of DNA methyltransferases could possibly be used along with STING pathway agonists to improve antitumor immune responses in cancers where STING is epigenetically silenced.

Recent studies conducted by Hou *et al.* have demonstrated that irradiation-induced STING signaling activates both canonical NF-κB (*i.e.* NF-κB1) and noncanonical NF-κB (*i.e.* NF-κB2) in tumor-localized DCs[266]. Interestingly, the researchers also found that the NF-κB2 pathway negatively regulates NF-κB1–mediated gene transcription and that they could enhance the antitumor effect of irradiation in murine models by inhibiting downstream signaling of the noncanonical pathway with intratumoral injections of a specific NF-κB2 inhibitor (*i.e.* SN52). Thus, targeted inhibition of NF-κB2 represents another possible strategy for potentiating the therapeutic effects of STING signaling in cancer. Tuning the downstream signaling that follows STING activation holds tremendous promise, because it may yield outcomes where beneficial effects of STING signaling (*e.g.* antitumor immunity) are maximized and negative effects (*e.g.* toxicity, immune regulation, *etc.*) are minimized. Interestingly, an inhibitor of downstream NF-κB1 signaling (*i.e.* SN50) has recently been characterized in combination with vaccine adjuvants and was described as an immune potentiator capable of decreasing markers associated with poor

tolerability and improving the protective response of vaccination[359], which suggests that therapeutic context is certainly important as well.

Carozza *et al.* found that many cancer cells continuously export endogenous 2′3′-cGAMP and that 2′3′-cGAMP is rapidly degraded by ENPP1 in the extracellular space[194]. They also determined that depletion of extracellular 2′3′-cGAMP by intratumoral injection of wildtype STING decreased the tumor infiltration of immune cells and eliminated the curative effects of tumor irradiation. Moreover, intratumoral administration of ENPP1 inhibitors elevated extracellular 2′3′-cGAMP concentrations and promoted improved responses to radiation therapy as demonstrated by delayed tumor growth. Notably, ENPP1 inhibitors would also limit levels of immunosuppressive adenosine in addition to elevate the levels of 2′3′-cGAMP[226]. Accordingly, ENPP1 inhibitors are currently being explored in preclinically with cGAS-activating therapies[360], as they are likely to synergize with therapies that involve endogenous 2′3′-cGAMP.

In addition to the established potentiators of the STING pathway, there are still many other possible agents that might also propagate STING signaling, such as inhibitors of the STING phase-separator and VRAC agonists, both of which could synergize with cGAS-activating therapies by enhancing the production and spread of 2′3′-cGAMP. Though such agents have not yet been directly explored in the context of STING signaling and cancer immunotherapy, future investigation is certainly warranted.

CHAPTER III

NanoISD

Text for Chapter III is adapted from:

Garland KM, Rosch JC, Carson CS, Wang-Bishop L, Hanna A, Sevimli S, Van Kaer C, Balko JM, Ascano M, Wilson JT. Pharmacological Activation of cGAS for Cancer Immunotherapy. *Frontiers in Immunology* (2021).

Abstract

When compartmentally mislocalized within cells, nucleic acids can be exceptionally immunostimulatory and can even trigger the immune-mediated elimination of cancer. Specifically, the accumulation of double-stranded DNA in the cytosol can efficiently promote antitumor immunity by activating the cGAMP synthase (cGAS) / stimulator of interferon genes (STING) cellular signaling pathway. Targeting this cytosolic DNA sensing pathway with interferon stimulatory DNA (ISD) is therefore an attractive immunotherapeutic strategy for the treatment of cancer. However, the therapeutic activity of ISD is limited by several drug delivery barriers, including susceptibility to deoxyribonuclease degradation, poor cellular uptake, and inefficient cytosolic delivery. Here, we describe the development of a nucleic acid immunotherapeutic, NanoISD, which overcomes critical delivery barriers that limit the activity of ISD and thereby promotes antitumor immunity through the pharmacological activation of cGAS at the forefront of the STING pathway. NanoISD is a nanoparticle formulation that has been engineered to confer deoxyribonuclease resistance, enhance cellular uptake, and promote endosomal escape of ISD into the cytosol, resulting in potent activation of the STING pathway via cGAS. NanoISD mediates the local production of proinflammatory cytokines via STING signaling. Accordingly, the intratumoral administration of NanoISD induces the infiltration of natural killer cells and T

lymphocytes into murine tumors. The therapeutic efficacy of NanoISD is demonstrated in preclinical tumor models by attenuated tumor growth, prolonged survival, and an improved response to immune checkpoint blockade therapy.

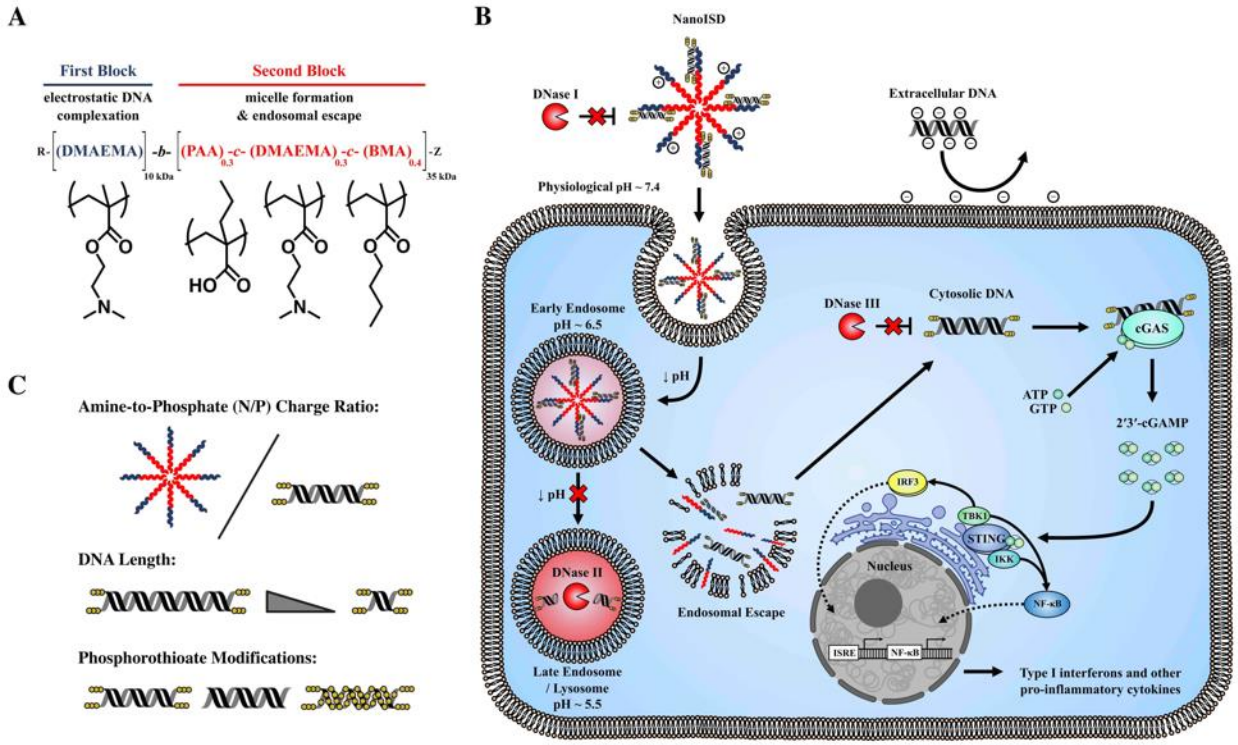

Figure 3.1. NanoISD – A nanoscale activator of the cGAS/STING pathway. NanoISD is fabricated via the self-assembly of an optimized interferon stimulatory DNA (ISD) sequence in complex with endosome-destabilizing polymer nanoparticles. **(A)** Chemical composition of poly[(DMAEMA)-*block*-(PAA-*co*-DMAEMA-*co*-BMA)] (D-PDB). **(B)** Schematic diagram of NanoISD activating cytosolic cGAS by evading major deoxyribonuclease and mediating cellular uptake and endosomal escape. **(C)** Design variables explored for DNA/polymer complexes include N/P charge ratio, dsDNA length, and degree and location of phosphorothioate backbone modifications.

Introduction

Nucleic acid sensing is a fundamental part of the innate immune system that can galvanize immune responses against pathogens and diseased cells[361]. During cellular homeostasis, DNA is largely sequestered from the cytosol inside the nucleus and mitochondria[120]. Accordingly, the

abnormal accumulation of DNA inside the cytosol is indicative of cellular distress. The aberrant presence of such "danger signals" within the cytosol can trigger various pattern recognition receptors (PRRs) and lead to a myriad of immunological responses[362]. Moreover, the physiochemical properties of cytosolic DNA (*e.g.* nucleotide sequence, base pair (BP) length, *etc.*) can drastically influence the nature of the resultant immune response by modulating PRR activation[108].

The stimulator of interferon genes (STING) cellular signaling pathway is a major DNA sensing pathway that bridges the gap between innate and adaptive immunity. The STING protein is located on the endoplasmic reticulum[66] and is directly activated by cyclic dinucleotides (CDNs)[90], such as the endogenous second messenger, 2′3′-cyclic guanosine monophosphate–adenosine monophosphate (cGAMP)[89]. Molecules of cGAMP are produced intracellularly by cGAMP synthase (cGAS) when the enzyme detects double-stranded DNA (dsDNA) in the cytosol[68, 69, 89, 188]. Notably, the recognition of cytosolic dsDNA by cGAS is independent of nucleotide sequence[40], and therefore this DNA sensing pathway is broadly applicable to a vast number of microbial infections as well as the detection of self dsDNA leakage resulting from cellular malfunction, a common feature of many precancerous cells.

STING activation results in the local production of type-I interferons (IFN-I) and various other proinflammatory cytokines, the specific profile of which depends on cellular context as well as the type, intensity, and duration of the stimulant[43]. This dynamic cytokine response generally creates an inflammatory microenvironment, which in certain settings, can promote robust cellular immune responses towards pathogens and diseases[363]. Notably, localized STING signaling has been identified as critical for the spontaneous induction of antitumor immunity[56]. Indeed, STING knockout (KO) mice (*i.e. Tmem173* $^{-/-}$) exhibit defective tumor control in some murine tumor

models and demonstrate a significantly reduced therapeutic response to immune checkpoint blockade (ICB) therapy relative to wildtype mice[56]. Moreover, these preclinical findings have corresponded with clinical data from human cancer patients that has positively correlated cGAS/STING activation with the presence of tumor infiltrating T lymphocytes (*i.e.* T cells)[364] as well as T cell–inflamed tumors with increased overall survival[365] and responsiveness to ICB therapy[366, 367].

Under the proper conditions, STING signaling can mediate cancer cell death either directly[52, 368] or indirectly by supporting cytotoxic T lymphocyte (CTL)[45] and natural killer (NK) cell[50, 307] responses. Additionally, the STING pathway is iatrogenically activated by many of the classical cancer therapies (*e.g.* radiation, certain chemotherapies, *etc.*) and may contribute to enhanced therapeutic responses in such cases[58, 369]. Indeed, in murine tumor models, antitumor immune responses generated by STING signaling are essential to achieving maximum therapeutic efficacy in response to radiotherapy[317]. These discoveries have collectively motivated the development of synthetic STING pathway agonists for applications in cancer immunotherapy.

Numerous preclinical studies using synthetic STING agonists have now shown that targeted activation of the STING pathway within established murine tumors can shift the immune profile of an immunosuppressive tumor microenvironment (TME) toward an immunogenic state that is conducive to productive antitumor immunity and to enhancing the therapeutic efficacy of multiple immunotherapeutic modalities[45, 183, 240]. Accordingly, many synthetic STING agonists are currently being explored as cancer therapeutics in human clinical trials[59, 370]. However, it is worth noting that all of the STING pathway agonists currently in clinical development are direct activators of the STING protein or inhibit antagonists of the pathway[183]. Compared to the STING protein, cGAS has been relatively underappreciated as a druggable target for cancer

immunotherapy[371], despite the potential of a cGAS-targeting therapeutic to more closely mimic endogenous STING signaling by simulating natural, endogenous DNA sensing.

There are many drug delivery challenges that must be overcome to activate cGAS with interferon stimulatory DNA (ISD), which may explain why the development of cGAS agonists has been remarkably limited thus far. Efficient cytosolic delivery of ISD is critical to the pharmacological activation of cGAS, yet freely administered ISD experiences negligible cellular uptake and is quickly cleared and degraded[5]. Furthermore, cGAS possesses several DNA-length dependencies that affect both the activation of the pathway[91] and the strength of STING signaling (*i.e.* the amount of STING-driven gene expression)[23]. Here, we have engineered a nucleic acid immunotherapeutic, NanoISD, which can target cGAS and exploit the DNA sensing pathway in the context of local cancer immunotherapy via the cytosolic delivery of noncoding, immunostimulatory dsDNA.

The well-established, endosomolytic polymer, poly[(DMAEMA)-*block*-(PAA-*co*-DMAEMA-*co*-BMA)] (D-PDB)[7, 8, 27, 28, 372-384] was used to electrostatically complex dsDNA into environmentally responsive nanoparticles capable of achieving cytosolic delivery. The DNA/polymer complexes were characterized using a library of synthetic ISD to study the effects of both N/P charge ratio (*i.e.* molar amount of protonated amines on the polymer corona / molar amount of phosphates on the nucleic acid backbone) and dsDNA composition on nanoparticle stability, transfection efficiency, cGAS activation, and antitumor immunity. *In vitro* screening of various DNA/nanoparticle complexes resulted in the identification of an optimized cGAS adjuvant, a phosphorothioate-capped 95-BP dsDNA / D-PDB complex, termed NanoISD. NanoISD is a nanoparticle formulation that confers deoxyribonuclease resistance, cellular uptake, endosomal escape, and potent activation of the STING pathway via cGAS (***Figure 3.1***). Notably,

the direct injection of NanoISD into murine tumors triggers the production of proinflammatory cytokines, which leads to the tumor infiltration of both NK cells and T lymphocytes. Finally, the therapeutic efficacy of NanoISD is demonstrated in preclinical tumor models by attenuated tumor growth, increased survival, and an improved therapeutic response to ICB therapy.

Results and Discussion

Engineering DNA/Polymer Nanoparticles for Intracellular Activation of cGAS

A library of synthetic ISD was created with a distinct set of design principles intended to yield structurally optimized cGAS ligands (***Supplementary Figure A.S1***). The library contains 4 dsDNA sequences of different lengths (*i.e.* 20-BP, 45-BP, 70-BP, and 95-BP dsDNA). To the extent possible, based on the designated dsDNA length, the individual ISD strands comprise poly(AC) and poly(AAC) repeats, which are each 20 nucleotides in length and are interspersed with random sequence spacers that are each 5 nucleotides in length. This unique composition of the ISD sequences should provide enough footing to minimize strand slippage. Additionally, the individual ISD strands exhibit positive free energies for secondary structure formation and are therefore not disposed to hairpins and self-dimerization. Moreover, the ISD has melting temperatures that are sufficiently high to maintain double-stranded morphologies at biologically relevant temperatures (*i.e.* 37 ºC). Lastly, the synthetic ISD sequence contains three terminal phosphorothioate bonds (*i.e.* "caps") on both ends of each complementary DNA strand to inhibit exonuclease degradation, a known feature of such modifications[385].

To overcome the delivery barriers that limit the activity of ISD, we employed a diblock copolymer, D-PDB, which has previously been used primarily for the cytosolic delivery of small-interfering RNA (siRNA)[7, 8, 27, 28, 372-384]. Under a physiological pH of ~ 7.4, D-PDB self-assembles

into colloidally stable, nanoparticle micelles with a cationic corona that can electrostatically load nucleic acids. In response to the decrease in endosomal pH that follows cellular uptake, these nanoparticles disassemble. The hydrophobic moieties of the polymer become accessible and then disrupt the endosomal membrane, whereupon the exogenous nucleic acid cargo escapes from the endosome into the cytosol of the cell. While nuclear localization is required for most applications of intracellular DNA delivery (*e.g.* gene therapy), DNA delivery to the cytosol is adequate and perhaps better for pharmacologically targeting cGAS, since the PRR is primarily activated by DNA within the cytosol[68]. Thus, in terms of maximizing cGAS activation, D-PDB has potential to be advantageous relative to nanocarriers that are designed to deliver their nucleic acid cargo to the nucleus of cells.

To determine an ideal N/P charge ratio (*i.e.* molar amount of protonated amines on the polymer corona / molar amount of phosphates on the nucleic acid backbone) for the ISD and polymer, polymeric micelles of D-PDB were complexed with varying concentrations of phosphorothioate-capped 95-BP dsDNA, one of the ISD molecules from the starting library. The resultant complexes were then analyzed *in vitro* via agarose gel electrophoresis, dynamic light scattering (DLS), and reporter cell assays for IFN-I production (***Figure 3.2***).

Agarose gel electrophoresis was run to determine the N/P charge ratio at which complete complexation is achieved (***Figure 3.2-A***). Consistent with previous findings for D-PBD with shorter double-stranded RNA molecules[7, 28], it was determined that N/P charge ratios of 1 and greater enabled complete loading of the phosphorothioate-capped 95-BP dsDNA. Conversely, an N/P charge ratio of 0.5 exhibited incomplete complexation, as demonstrated by the migration of unbound DNA, which formed a band corresponding to that of the free DNA.

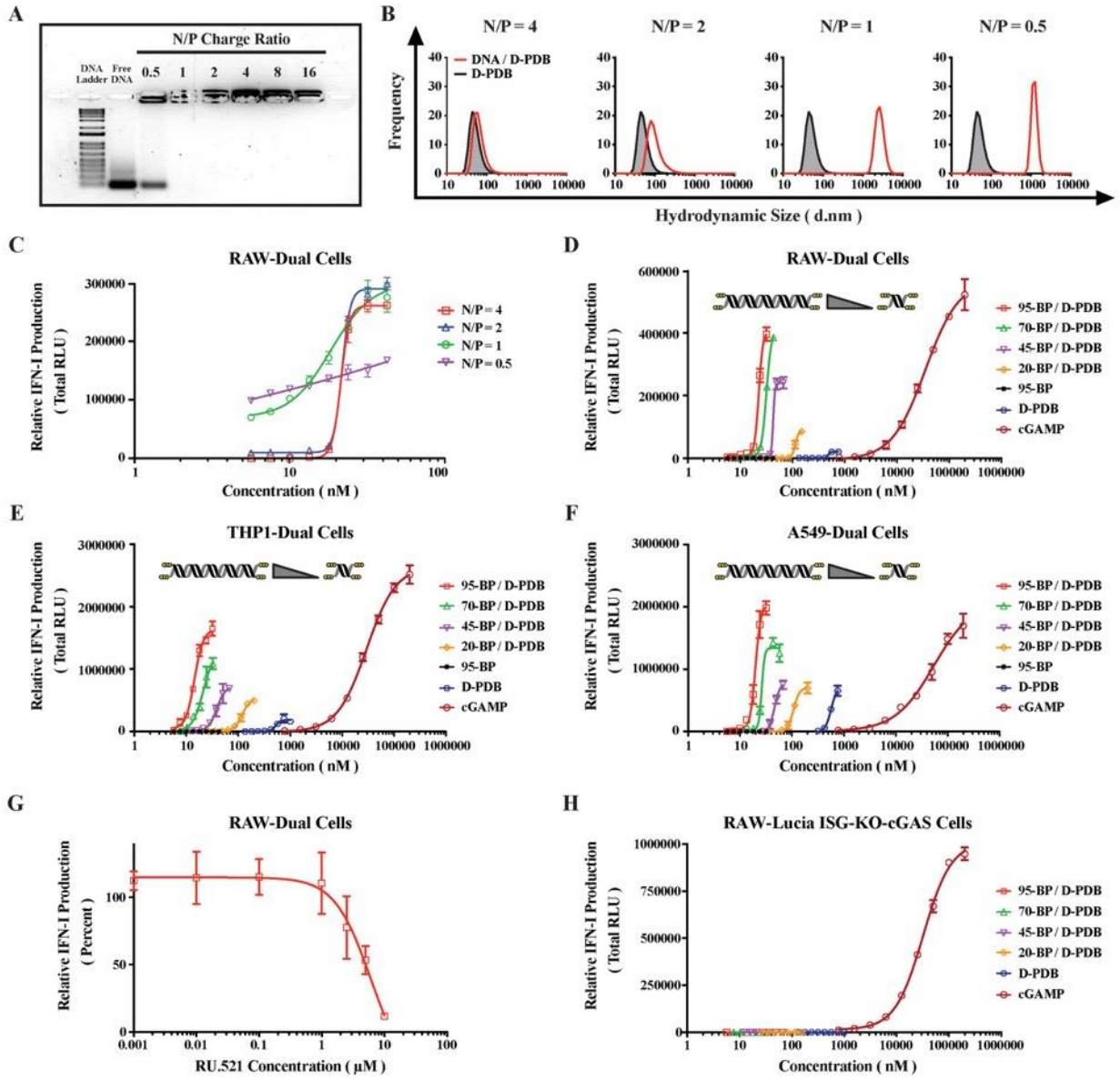

Figure 3.2. Engineering DNA/Polymer Nanoparticles for Intracellular Activation of cGAS. **(A)** Agarose gel image. DNA Ladder refers to the TrackIt^{TM} 1 Kb Plus DNA Ladder, and Free DNA refers to uncomplexed phosphorothioate-capped 95-BP dsDNA. Lanes comprise 1 µg DNA mixed with the indicated amount of D-PDB. **(B)** DLS analysis of phosphorothioate-capped 95-BP dsDNA / D-PDB complexes at varying N/P charge ratios. Frequency indicates the number-based particle size distribution. Hydrodynamic size indicates the particle diameter in nm. **(C)** RAW-Dual reporter cell assay of phosphorothioate-capped 95-BP dsDNA / D-PDB complexes at varying N/P charge ratios. **(D)** RAW-Dual reporter cell assay of synthetic, variable-length ISD library complexed to D-PDB at an N/P charge ratio of 4, and indicated experimental controls were used. (**E**) THP1-Dual reporter cell assay of synthetic, variable-length ISD library complexed to D-PDB at an N/P charge ratio of 4, and indicated experimental controls were used. **(F)** A549-Dual reporter cell assay of

synthetic, variable-length ISD library complexed to D-PDB at an N/P charge ratio of 4, and indicated experimental controls were used. **(G)** Dose response of the cGAS inhibitor, RU.521 in RAW-Dual reporter cells. After a 4 hour incubation with RU.521, cells were treated with 25 nM phosphorothioate-capped 95-BP dsDNA complexed to D-PDB at an N/P charge ratio of 4. **(H)** RAW-Lucia ISG-KO-cGAS reporter cell assay of synthetic, variable-length ISD library complexed to D-PDB at an N/P charge ratio of 4, and indicated experimental controls were used. The dose response curves for free D-PDB are positioned along the x-axis in terms of the molar amount of polymer chains rather than molar amount of loaded dsDNA, and each dose response that utilized the polymer was administered using equivalent D-PDB concentrations.

DLS was subsequently performed to characterize the size and polydispersity of the complexes (***Figure 3.2-B***). DLS analysis demonstrated that uncomplexed D-PDB micelles are ~ 45-60 nm in diameter and that loading phosphorothioate-capped 95-BP dsDNA at an N/P charge ratio of 4 results in slightly larger nanoparticles that are ~ 60-90 nm in diameter. As the N/P charge ratio was lowered, the measured hydrodynamic size significantly increased to micrometer diameters that are indicative of particle aggregation. Notably, larger particles (*i.e.* greater than 100 nm) are not ideal for *in vivo* cancer applications, since particle permeability and distribution within tumors are known to decrease with increasing particle size[386].

To determine the *in vitro* activity of the complexes, a reporter cell assay for cellular IFN-I production was utilized (***Figure 3.2-C***). The reporter cells stably express a secreted luciferase downstream of interferon-stimulated response elements, and therefore luminescence can be used to track relative IFN-I production. RAW-Dual murine macrophages were treated with phosphorothioate-capped 95-BP dsDNA / D-PDB complexes that were formulated at different N/P charge ratios. Supernatants were collected 24 hours after the cells were treated, and the relative IFN-I production was quantified via luminescence. Notably, immunostimulatory activity was detected from all of the complexes. A maximum efficacy of ~ 275,000 Relative Light Units (RLU) was consistent for N/P charge ratios of 4, 2, and 1. Alternatively, the maximum efficacy for the N/P charge ratio of 0.5 over the same concentration range was substantially lower at ~ 170,000

RLU, which is likely due to the incomplete loading of the DNA that was observed in the agarose gel assay. Additionally, half-maximal effective concentration (EC_{50}) values were determined for each dose response curve to allow for the comparison of *in vitro* potency. The calculated EC_{50} values for the N/P charge ratios of 4, 2, 1, and 0.5 were 22 nM, 22 nM, 15 nM, and 3 nM, respectively. Since *in vitro* potency is inversely related to EC_{50} values, the potency is greater for the N/P charge ratios of 1 and 0.5, both of which also exhibit larger sizes as determined by DLS. The apparent increase in potency accompanied by an increase in particle size is consistent with a recent report that larger, micrometer-sized polyplexes enhance *in vitro* transfection efficiency relative to compositionally-equivalent nanometer-sized polyplexes due to increased gravitational sedimentation[387]. Interestingly, we characterized a second ISD library of relatively larger PCR-amplified dsDNA (***Supplementary Figure A.S2***) with D-PDB and found that the effects of N/P charge ratio on particle complexation, size, and activity were well conserved with dsDNA up to at least 5000-BP in length (***Supplementary Figure A.S3***). Based on these initial *in vitro* characterizations of the complexes, an N/P charge ratio of 4 was selected for all complexes used in the subsequent studies.

The degree of cGAS activation is directly proportional to the length of dsDNA recognized by cGAS[23, 88], yet larger molecular weight dsDNA can also compromise the colloidal stability of non-viral vectors[388] and thereby limit transfection efficiency. Moreover, there exist DNA-length thresholds for cGAS activation that are species-specific due to some small variations in the amino acid composition of the protein[91]. For *in vitro* cell-based assays, a minimum dsDNA length of ~ 45-BP is required to activate human cGAS (hcGAS)[91], whereas dsDNA as low as ~ 20-BP in length can activate murine cGAS (mcGAS)[84, 92]. Thus, the entire library of variable-length, synthetic ISD was evaluated, so that the molecular weight (*i.e.* BP length) of the ISD in complex

with D-PDB micelles could be optimized.

DLS analysis of D-PDB and the synthetic ISD library revealed that while keeping the N/P charge ratio consistent at 4, particle size slightly increased as the BP length of the DNA increased (***Supplementary Figure A.S4***). This relationship was also observed for D-PDB complexed to the second ISD library of larger PCR-amplified dsDNA, though size appeared to plateau at ~ 140 nm in diameter once a dsDNA length of 1250-BP was reached (***Supplementary Figure A.S5***). For the N/P charge ratio of 4, colloidal stability of the complexes was lost when dsDNA length reached 10,000-BP, as evident from the complex's nonuniform and highly polydisperse size range.

Reporter cell assays for IFN-I production were again utilized to evaluate *in vitro* activity of the complexes. RAW-Dual murine macrophages (***Figure 3.2-D***), THP1-Dual human monocytes (***Figure 3.2-E***), and A549-Dual adenocarcinomic human alveolar basal epithelial cells (***Figure 3.2-F***) were all treated with each of the varied-length, synthetic ISD complexed to D-PDB over a range of ISD concentrations to generate dose response curves. The endogenous STING ligand, 2′3′-cGAMP was used as a positive control for IFN-I induction, and free D-PDB (*i.e.* not loaded with dsDNA) was used as a vehicle control. Additionally, free phosphorothioate-capped 95-BP dsDNA was used as a negative control to demonstrate the importance of the polymeric drug delivery vehicle. Maximum efficacy and EC_{50} values for each of the treatments can be found in the supplementary information (***Supplementary Figure A.S6***). Consistent with previous observations that cGAS is activated in a dsDNA length dependent manner[23], both the potency and efficacy of the complexes generally increased with increasing BP length of the dsDNA cargo in all three reporter cell lines. Interestingly, free D-PDB demonstrated a small but significant dose response, suggesting that the polymer has an intrinsic capacity for stimulating some degree of IFN-I production. Notably, potency normalized to polymer concentration is exceptionally consistent

for free D-PDB and all of its dsDNA-loaded counterparts, which suggests that the transfection efficiency of D-PDB is relatively fixed and independent of loaded dsDNA length for the colloidally stable DNA/polymer complexes formed at the N/P charge ratio of 4.

In accordance with the established dsDNA length thresholds for species-specific cGAS activation, the phosphorothioate-capped 20-BP dsDNA complexed to D-PDB (*i.e.* 20-BP / D-PDB) enhanced maximum efficacy relative to that of free D-PDB in the murine RAW-Dual reporter cells (*i.e.* ~ 85,000 vs. ~ 20,000 RLU, respectively) and did not affect baseline efficacy in the human A549-Dual reporter cells (*i.e.* both treatments ~ 70,000 RLU). However, in the human THP1-Dual reporter cells, the 20-BP / D-PDB treatment did slightly outperform free D-PDB in terms of maximum efficacy (*i.e.* ~ 50,000 RLU vs ~ 20,000 RLU, respectively), despite the 20-BP dsDNA being shorter than the empirically established threshold for human cGAS activation (*i.e.* ~ 45-BP)[91]. This subtle discrepancy may be due to cell line–specific phenomenon coupled with the phosphorothioate modifications of the ISD, as the threshold established in previous reports was determined using unmodified dsDNA[96, 172].

The role of cGAS in the immunostimulatory activity of the compounds was investigated in the RAW-Dual reporter cells by pretreating the cells with a dose response of the established small molecule inhibitor of cGAS, RU.521[91, 337, 389] (***Figure 3.2-G***). Four hours after incubation with RU.521, the cells were treated with the EC75 concentration of 95-BP / D-PDB (*i.e.* 25 nM), a treatment known to be consistently active. Analysis of the supernatant 24 hours after treatment revealed that the cGAS-specific inhibitor was able to significantly diminish the IFN-I signal at the higher concentrations, suggesting that the observed activity of the DNA / polymer complexes is indeed cGAS-dependent. Notably, RU.521 exhibited a half-maximal inhibitory concentration (IC_{50}) value of ~ 5 μM.

To further explore the dependence of cGAS on the activity of the treatments, RAW-Lucia ISG-KO-cGAS reporter cells, which do not express cGAS, were treated with each of the varied-length, synthetic ISD complexed to D-PDB (***Figure 3.2-H***). Free D-PDB and cGAMP were again used as controls for the experiment. While cGAMP, which activates STING downstream of cGAS, retained its IFN-I activity, no activity was detected from DNA/polymer complexes, suggesting that the activity from those treatments observed in the wildtype reporter cells were largely, if not entirely, cGAS-dependent. These findings also suggest that if alternative IFN-inducing DNA sensors, such as IFI204 (*e.g.* the murine ortholog of IFI16), are involved in the response to the DNA/polymer complexes, they must operate as dependent cofactors of cGAS. Interestingly, the activity of free D-PDB was also completely abolished in the RAW-Lucia ISG-KO-cGAS reporter cells. While D-PDB is unlikely to be a direct cGAS ligand, D-PDB may indirectly activate cGAS in the wildtype reporter cells by inducing the cytosolic accumulation of mitochondrial DNA. Indeed, cationic nanocarriers have been linked to toll-like receptor 9 (TLR9) (*i.e.* a PRR for unmethylated DNA rich in CpG motifs) and STING activation via their intrinsic capacity for mitochondrial damage and the subsequent release of mitochondrial DNA[390, 391].

Similar cGAS-dependent activity in the RAW-Dual reporter cells was also demonstrated for the larger PCR-amplified dsDNA library complexed to D-PDB (***Supplementary Figure A.S7***). The DNA length–dependent trends were conserved for the larger PCR-amplified dsDNA library in the wildtype reporter cells, though the maximum efficacy of the DNA/polymer complexes did saturate at ~ 615,000 RLU when a dsDNA length of 625-BP was reached. Additionally, the colloidally unstable 10,000-BP / D-PDB complexes exhibited a reduced maximum efficacy of ~ 470,000 RLU over the same concentration range, which could be attributed to its extensive polydispersity of size. Furthermore, the synthetic phosphorothioate-capped 95-BP dsDNA

complexed to D-PDB, which had a maximum efficacy of ~ 1,000,000 RLU, drastically outperformed all of the PCR-amplified dsDNA complexed to D-PDB in terms of maximum efficacy, which is likely a consequence of its exonuclease resistance and highlights the importance of such modifications for enhancing cGAS activation.

STING signaling induces the activation of two main transcription factors: IFN-regulatory factor 3 (IRF3) and nuclear factor kappa-light chain enhancer of activated B cells (NF-κB)[392]. Notably, in mammals, the NF-κB signaling from STING activation is fairly modest relative to its IRF3-driven IFN-I signaling[393]. Alternatively, certain DNA agonists of TLR9 can trigger substantial NF-κB activity[394]. Thus, high levels of NF-κB activity can be indicative of off-target PRR activation. Accordingly, to explore potential off-target effects of the ISD and the polymer, we treated RAW-Dual reporter cells for 24 hours and then quantified relative NF-κB activity from the supernatants of the treated cells via absorbance (***Supplementary Figure A.S8***). The TLR9 agonist, CpG DNA (*i.e.* ODN 1826) was used as a positive control for NF-κB activity.

We found that the phosphorothioate-capped 95-BP dsDNA did not exhibit significant NF-κB activity, which is consistent with its complete lack of CG sites (*i.e.* inability to engage TLR9). The PCR-amplified 5000-BP dsDNA with and without D-PDB also did not induce significant NF-κB activity. While PCR-amplified 5000-BP dsDNA sequence does contain CpG motifs, every DNA molecule containing CpG motifs must be considered as a separate agent capable of eliciting differing levels of efficacy[394]. Indeed, the lack of NF-κB activity for the larger ISD may simply be due to its unique composition, as the PCR-amplified dsDNA also contains many CpG neutralizing motifs (*e.g.* CG sites preceded by a C and/or followed by G) that can antagonize the stimulatory effects of CpG DNA[395]. Lastly, NF-κB activity was insignificant for free D-PDB, suggesting that the potential contribution of D-PDB to TLR9 activation/signaling is negligible.

We note that while the CpG DNA potently induces NF-κB activity, the same molecule complexed to D-PDB loses most, if not all, of its *in vitro* NF-κB activity. This result is consistent with reports that have found that nucleic acid –binding polymers can inhibit the activation of TLRs[396, 397]. It is also possible that this particular polymer (*i.e.* D-PDB) mediates cytosolic delivery of the CpG DNA before it can be sensed by TLR9, which is localized to endosomes[398]. Indeed, endosomal maturation has been described as a necessary event for successful TLR9 signaling by CpG DNA[399]. However, we do note that a version of this polymer loaded with CpG DNA has demonstrated efficacy *in vivo*[400], which suggests that such complexes may behave differently *in vivo* and emphasizes the importance of multiple modes of therapeutic characterization.

The starting ISD library used for the experiments in ***Figure 3.2*** comprised synthetic dsDNA molecules that were produced via solid-phase phosphoramidite-based synthesis, which can accommodate routine, scalable production of dsDNA up to ~ 95-BP in length as well as the molecular modification of dsDNA[401, 402]. Conversely, PCR-mediated amplification of dsDNA utilizes polymerase-based synthesis that does not allow for site-specific DNA modification outside of the primer sequence, and therefore PCR-mediated amplification of dsDNA is not readily amenable to phosphorothioate-capping. Accordingly, we took an alternative strategy to protect the larger ISD from exonuclease degradation and then study its effects on cGAS activity.

Oxidized guanine nucleotides (*i.e.* 8-hydroxyguanine) have recently been identified as inhibitors of TREX1 degradation[135]. Since TREX1 degradation initiates at the 3′ ends of dsDNA strands, we "capped" the long ISD (*i.e.* PCR-amplified 5000-BP dsDNA) post-synthesis with 8-hydroxyguanine using terminal transferase, an enzyme that can selectively add nucleotides to the 3′ ends of dsDNA strands. Various feed ratios were used, and successful addition of the 8-hydroxyguanine was confirmed by an ELISA for 8-hydroxyguanine (***Supplemental Figure A.S9-***

A). The efficacy of the PCR-amplified dsDNA capped with 8-hydroxyguanine was then tested in IFN-I reporter cells (***Supplemental Figure A.S9-B***). The "capped" large dsDNA achieved only a modest increase in efficacy in both RAW Duals and THP1 Duals. In the RAW Dual reporter cells, the PCR-amplified dsDNA capped with 8-hydroxyguanine exhibited a maximum efficacy of ~ 400,000 RLU, which matched that of the phosphorothioate capped 95-BP dsDNA. These studies support the hypothesis that TREX1 is more of a limiting factor for shorter cGAS ligands. Thus, the synthetic, phosphorothioate-capped 95-BP dsDNA became the lead cGAS ligand, and the nanoparticle complex of D-PDB and the phosphorothioate-capped 95-BP dsDNA at an N/P charge ratio of 4, herein referred to as NanoISD, was employed as a potent cGAS adjuvant for the subsequent studies investigating its utility in cancer immunotherapy.

NanoISD Exhibits Deoxyribonuclease Resistance

Mammalian cells constitutively express many deoxyribonucleases (DNases) to prevent the potentially inflammatory accumulation of DNA outside of protective organelles. Notably, DNA present in systemic circulation, lysosomes, and cytosols is degraded by DNase I, DNase II (*i.e.* Acid DNase), and DNase III (*i.e.* TREX1), respectively[74, 123-125]. The inhibition of such nucleases can allow immunostimulatory dsDNA to remain intact for an extended period of time during delivery, which can lead to improved functionality. Notably, the length of cytosolic dsDNA directly influences the rate and extent of cGAS activation and thereby the amount of cGAMP produced[23]. Thus, when dsDNA strands are not rapidly broken down into smaller fragments, they can exploit the length-dependence of the protein to promote maximal STING signaling. As the stability of DNA is essential for cGAS activation, the deoxyribonuclease resistance of NanoISD was evaluated (***Figure 3.3***).

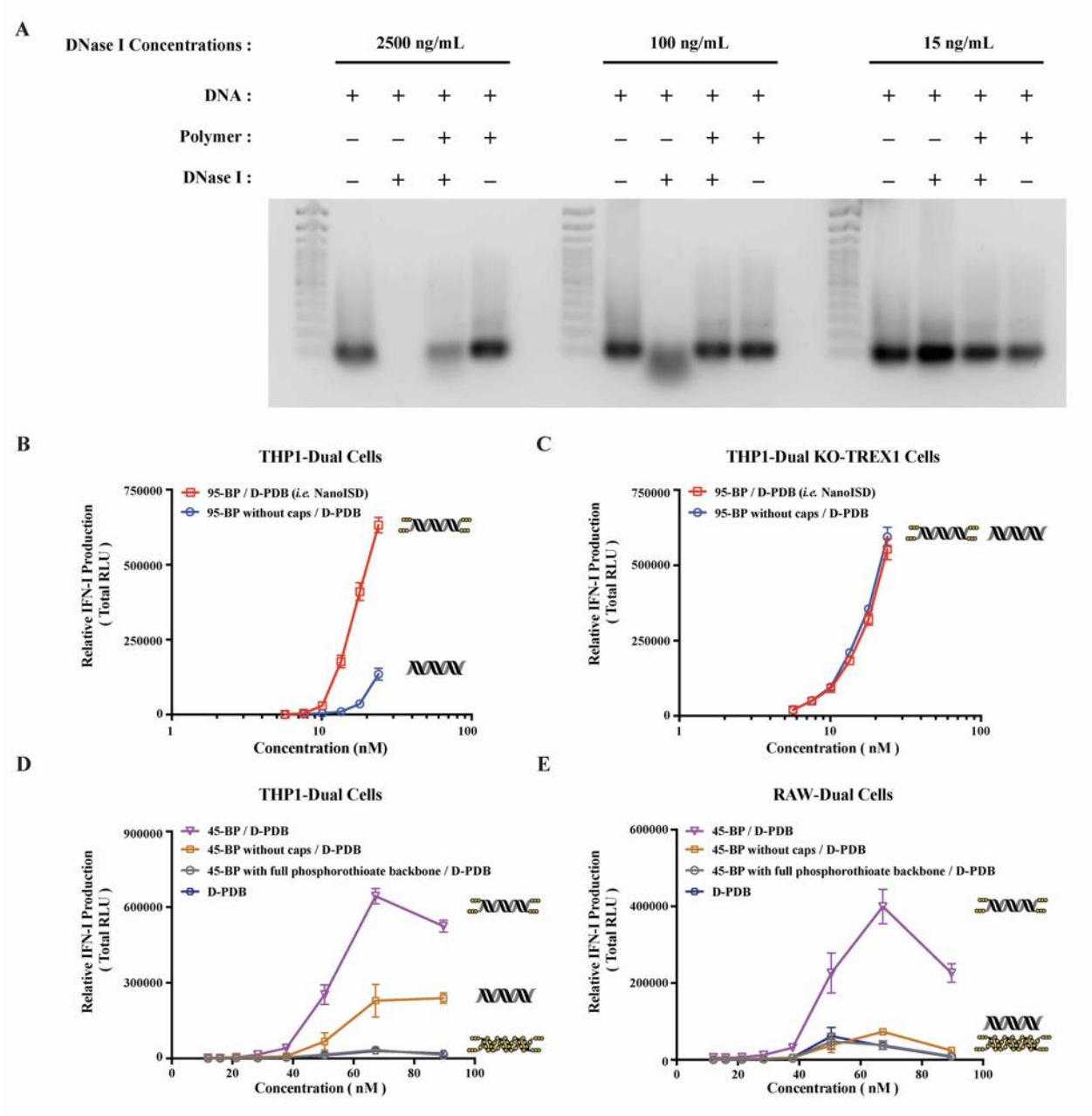

Figure 3.3. NanoISD Exhibits Deoxyribonuclease Resistance. **(A)** Agarose gel image. Lanes are as indicated. The TrackIt^{TM} 100 bp DNA Ladder was used for reference. The DNA used in these studies was the phosphorothioate-capped 95-BP dsDNA at a concentration of 1 µg DNA/lane, and the polymer used was D-PDB at an N/P charge ratio of 4. **(B)** THP1-Dual reporter cell assay of 95-BP dsDNA with and without phosphorothioate caps complexed to D-PDB at an N/P charge ratio of 4. **(C)** THP1-Dual KO-TREX1 reporter cell assay of 95-BP dsDNA with and without phosphorothioate caps complexed to D-PDB at an N/P charge ratio of 4. **(D)** THP1-Dual reporter cell assay of synthetic 45-BP dsDNA complexed to D-PDB at an N/P charge ratio of 4, and D-PDB was used as an experimental control. Each 45-BP / D-PDB treatment comprised DNA with varying levels of phosphorothioate incorporation as indicated. **(E)** RAW-Dual reporter cell assay of synthetic 45-BP dsDNA complexed to D-PDB at an N/P charge ratio of 4, and D-PDB was used

as an experimental control. Each 45-BP / D-PDB treatment comprised DNA with varying levels of phosphorothioate incorporation as indicated. The dose response curves for free D-PDB are positioned along the x-axis corresponding to their equivalent dsDNA-loaded treatments, as each dose response that utilized the polymer was administered using equivalent D-PDB concentrations.

Both free phosphorothioate-capped 95-BP dsDNA and NanoISD were incubated with three different concentrations of the endonuclease, DNase I (***Figure 3.3-A***). 15 ng/mL was selected as it is the physiological level of DNase I in human serum[403], 100 ng/mL was selected as it is the concentration of recombinant human DNase I that can mediate the effective removal of DNA from blood circulation[404], and 2500 ng/mL was selected as an extreme high-dose control. Following incubation with DNase I, samples were heat-inactivated, and SDS was added to break apart the complexes. The samples were then run on a gel along with free phosphorothioate-capped 95-BP dsDNA and NanoISD that were not exposed to DNase I. While free phosphorothioate-capped 95-BP dsDNA was susceptible to degradation by the higher concentrations of DNase I, NanoISD exhibited marked protection of its DNA cargo from deoxyribonuclease degradation, which is likely due to polymer-mediated steric hindrance of the nuclease (*i.e.* nanoparticle packaging).

Since cGAS activation is greatly dependent on the length, concentration, and persistence of dsDNA in the cytosol, a particularly important negative regulator of the STING pathway is the exonuclease, TREX1 (*i.e.* DNase III). Indeed, it was recently discovered that DNA oxidized by reactive oxygen species (ROS) can significantly impede the exonuclease activity of TREX1, and such TREX1 inhibition was found to significantly potentiate STING signaling[135]. Accordingly, the inhibition of TREX1 has recently been proposed as an immunotherapeutic strategy for the treatment of cancer[22].

The phosphorothioate caps of the synthetic ISD were implemented to boost immunostimulatory activity by obstructing the TREX1-mediated degradation of dsDNA that limits

STING pathway activation. To further test the deoxyribonuclease resistance of the chemically modified ISD, reporter cell assays for IFN-I production were once again utilized. Phosphorothioate-capped 95-BP dsDNA and 95-BP dsDNA without caps were complexed with D-PDB micelles and incubated with THP1-Dual cells (***Figure 3.3-B***) and THP1-Dual KO-TREX1 cells (***Figure 3.3-C***).

In the wildtype reporter cells, the efficacy and potency of NanoISD were both significantly increased relative to D-PDB loaded with 95-BP dsDNA without phosphorothioate caps. As the caps inhibit TREX1 activity, it is likely that they enable a prolonged presence of the dsDNA in the cytosol and thereby enhance cGAS activation. This theory is supported by the finding that phosphorothioate caps on a 45-BP dsDNA also enhanced activity relative to 45-BP dsDNA without caps when delivered with D-PDB micelles to wildtype reporter cells (***Figures 3.3-D and 3.3-E***). Notably, it was also demonstrated that complete phosphorothioate modification of the dsDNA backbone rendered 45-BP dsDNA inactive, which is consistent with previous observations that phosphodiester bonds on dsDNA are required for cGAS activation[172, 405]. One possible future opportunity for further enhancing the efficacy and potency of the ISD might involve incorporating intermittent phosphorothioate modifications along the DNA strands, which could potentially improve the deoxyribonuclease resistance and stability of the DNA while also maintaining a capacity for cGAS oligomerization/activation. The distance between each modification would likely need to be optimized to avoid deleterious effects on cGAS activation.

Moreover, in the TREX1 (*i.e.* DNase III) KO reporter cells, the efficacy and potency of the nanoparticles loaded with dsDNA lacking phosphorothioate caps were insignificantly different from that of NanoISD (***Figure 3.3-C***), suggesting that in the wildtype reporter cells, TREX1 is mainly responsible for the reduced *in vitro* activity of the nanoparticles carrying unprotected

dsDNA. Thus, in addition to the deoxyribonuclease resistance afforded by nanoparticle packaging, deoxyribonuclease activity was found to be further inhibited through the chemical modification of the synthetic dsDNA.

Notably, the IFN-I activity of the synthetic ISD library in the THP1-Dual reporter cells is entirely lost when delivered with the non-endosomolytic polymer, poly[(DMAEMA)-*block*-(BMA)] (D-B) at a consistent DNA concentration and N/P charge ratio (***Supplementary Figure A.S10***). D-B forms micelles that do not disassemble at low pH, and accordingly the polymer does not facilitate the cytosolic delivery of nucleic acid[28], which is necessary for cGAS activation. Conversely, D-PDB mediates endosomal escape at the onset of endosomal acidification due to the composition of the polymer[7] and the resultant loss of particle morphology under minimally acidic conditions (*e.g.* pH ~ 6.5), which leads to endosomal membrane disruption[28]. Therefore, the dsDNA cargo loaded on D-PDB is likely released into the cytosol before endosomes can fully acidify. Since DNase II is mostly active under highly acidic conditions (*e.g.* pH ~ 5.5)[406], it is probable that the enzyme has a reduced opportunity to degrade the ISD when delivered with D-PDB. Indeed, the observed cGAS activation from NanoISD treatment is evidence that the dsDNA ligands are not appreciably degraded by DNase II in lysosomes. Thus, the chemical and physical composition of NanoISD as well as its intrinsic delivery route protect its cGAS ligand from three major deoxyribonucleases and thereby constitute NanoISD as an exceptionally potent cGAS adjuvant.

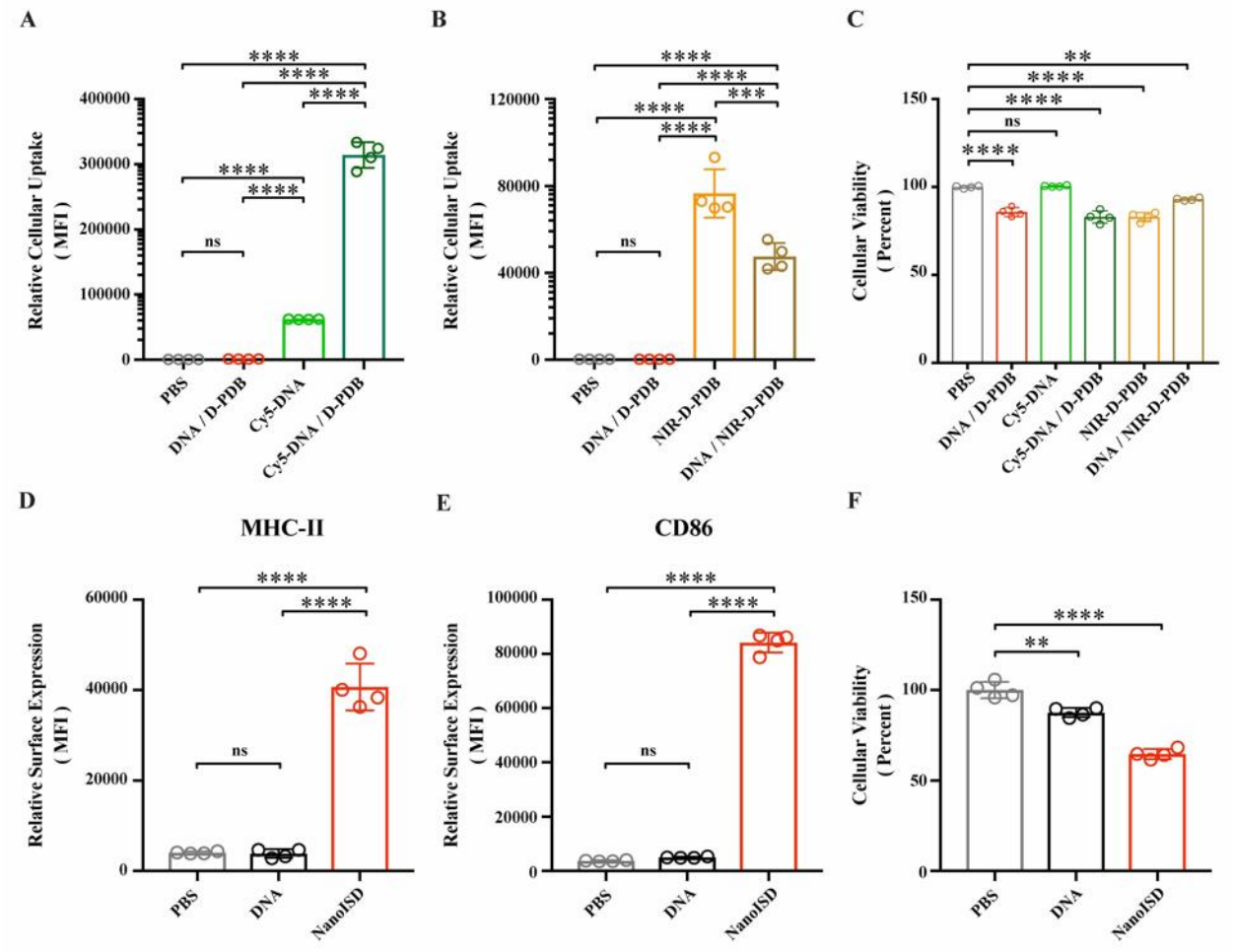

Figure 3.4. NanoISD Enhances Cellular Uptake and Immunostimulatory Activity of ISD In Vitro. **(A)** Flow cytometry analysis on the cellular uptake of 45 nM DNA (*i.e.* Cy5-labeled phosphorothioate-capped 95-BP dsDNA). Flow cytometry was conducted 4 hours after indicated treatment. The median fluorescence intensity (MFI) of Cy5-labeled DNA was quantified. **(B)** Flow cytometry analysis on the cellular uptake of 1.1 μM D-PDB (*i.e.* NIR-D-PDB), which corresponds to 45 nM DNA for a N/P charge ratio of 4. Flow cytometry was conducted 4 hours after indicated treatment. The MFI of NIR-664-labeled D-PDB was quantified. **(C)** Cellular viability determined 4 hours after indicated treatment as assessed by DAPI staining. Percent viable is relative to cells treated with PBS. **(D)** Flow cytometry analysis of the BMDC maturation marker, MHC-II conducted 24 hours after treatment of either PBS, 45 nM DNA (*i.e.* phosphorothioate-capped 95-BP dsDNA), or NanoISD at a dose corresponding to 45 nM. The MFI of anti-MHC-II-APC-Cy7 was quantified. **(E)** Flow cytometry analysis of the BMDC maturation marker, CD86 conducted 24 hours after treatment of either PBS, 45 nM DNA (*i.e.* phosphorothioate-capped 95-BP dsDNA), or NanoISD at a dose corresponding to 45 nM. The MFI of anti-CD86-PE-Cy7 was quantified. **(F)** Cellular viability determined 24 hours after indicated treatment as assessed by DAPI staining. Percent viable is relative to cells treated with PBS. A one-way ANOVA with Tukey test was used for statistical analysis.

NanoISD Enhances Cellular Uptake and Immunostimulatory Activity of ISD In Vitro

DNA by itself does not readily pass through the negatively-charged plasma membrane of cells due to the relatively large, negatively-charged, and hydrophilic nature of DNA[407]. However, when ISD is complexed at an N/P charge ratio of 4 with D-PDB micelles that exhibit a positive surface charge of +16.27 mV, the resultant DNA-loaded nanoparticles also exhibit a positive surface charge (***Supplementary Figure A.S11***) and can be efficiently endocytosed by DC2.4 dendritic cells *in vitro* as determined by flow cytometry analysis of fluorescently-labeled phosphorothioate-capped 95-BP dsDNA (*i.e.* Cy5-DNA) (***Figure 3.4-A***). It is likely that the overall positive surface charge of NanoISD (*i.e.* +14.87 mV) afforded by D-PDB drives the cellular uptake of the nanoparticles, especially since free fluorescently-labeled D-PDB (*i.e.* NIR-D-PDB) is also efficiently endocytosed (***Figure 3.4-B***). The positive charge of NanoISD does however dictate that the therapeutic be administered locally, as positively charged nanoparticles are typically poorly tolerated when administered systemically[408]. There are many advantages to using local administration, especially for the delivery of a cancer immunotherapeutic[409]. Indeed, while the direct injection of many classical cancer therapeutics (*e.g.* various chemotherapies) into solid tumors often results in therapeutic responses that are limited to the treated tumors, the local administration of a cancer immunotherapeutic can generate a systemic immune response with potential to clear untreated metastatic tumors (*i.e.* abscopal effect). Additionally, D-PDB treatment also confers a minor but significant degree of toxicity relative to cells treated with phosphate buffered saline (PBS) (***Figure 3.4-C***). Notably, some toxicity may actually be beneficial in the context of killing cancer cells following local administration[410] and releasing tumor antigens, which can then be processed by APCs to promote the cancer-immunity-cycle[235].

The activation of APCs is a key feature of many innate immune agonists and is essential

for cancer immunotherapies that are aimed at promoting antitumor T cells[411]. Since STING pathway activation has been linked to APC maturation and T cell activation[269, 270], NanoISD was evaluated for its ability to promote APC maturation. Murine bone marrow-derived dendritic cells (BMDCs) were treated with either PBS, DNA (*i.e.* phosphorothioate-capped 95-BP dsDNA), or NanoISD. Markers of BMDC maturation (*i.e.* cell surface expression of CD86 and MHC-II) were quantified via flow cytometry 24 hours post treatment. It was determined that NanoISD evokes significantly enhanced maturation *in vitro* as compared to PBS-treated BMDCs and DNA-treated BMDCs (***Figures 3.4-D and 3.4-E***). Additionally, viability of the BMDCs after NanoISD treatment was comparable to that of the DC2.4 cells treated with the same concentration of NanoISD (***Figure 3.4-F***).

NanoISD Enhances Delivery and Immunostimulatory Activity of ISD In Vivo

By packaging dsDNA into cationic nanoparticles, it was hypothesized that NanoISD would address the rapid clearance of dsDNA by promoting local cellular uptake at the site of injection. To evaluate this, NanoISD and free ISD were injected subcutaneously into mice and the *in vivo* retention was evaluated via IVIS imaging using both fluorescently-labeled phosphorothioate-capped 95-BP dsDNA (*i.e.* Cy5-DNA) and fluorescently-labeled D-PDB (*i.e.* NIR-D-PDB) (***Figures 3.5-A and 3.5-B***). As anticipated, the free ISD was rapidly cleared from the injection site (*i.e.* half-life < 6 hours). Interestingly, D-PDB was retained at the injection site for an extended timeframe (*i.e.* half-life ~ 50 days) and also dramatically enhanced the retention of the dsDNA (*i.e.* half-life ~ 50 days).

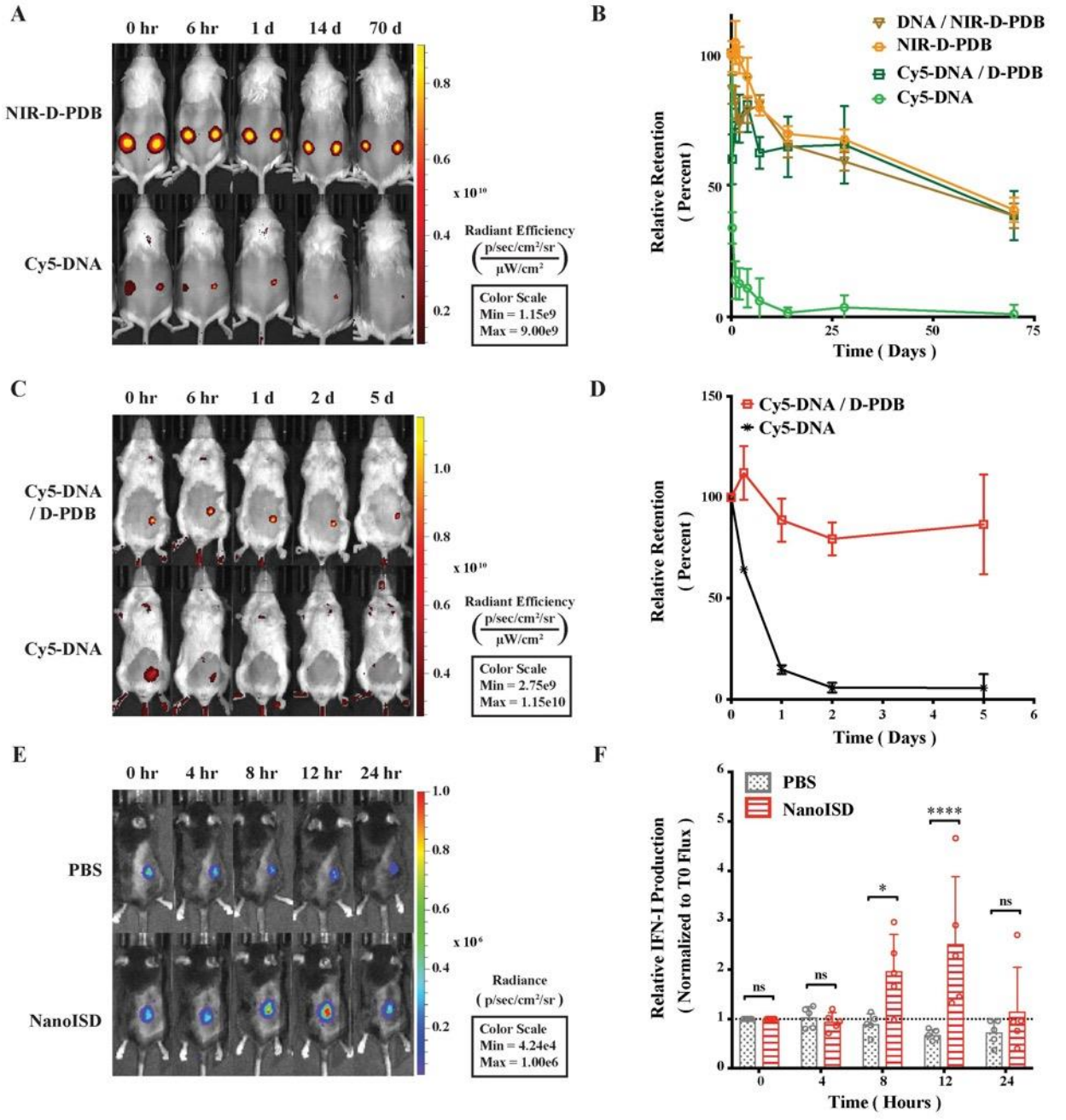

Figure 3.5. NanoISD Enhances Delivery and Immunostimulatory Activity of ISD In Vivo. **(A)** Representative fluorescence IVIS images evaluating the subcutaneous retention of NanoISD in CD-1 mice. D-PDB labeled with NIR-664-iodoacetamide (*i.e.* NIR-D-PDB) was used to track the polymer, and phosphorothioate-capped 95-BP dsDNA labeled with Cy5 (*i.e.* Cy5-DNA) was used to track the DNA. On the left flank of each mouse, individual uncomplexed agents were administered, and on the right flank of each mouse, complexes at an N/P charge ratio of 4 with the indicated fluorescent agent were administered. A subcutaneous injection was given as a single 100

µL dose of 2 µg DNA and/or 36 µg of polymer. **(B)** Retention profiles of NIR-D-PDB and Cy5-DNA either uncomplexed or complexed with unlabeled counterparts following subcutaneous administration in CD-1 mice. **(C)** Representative fluorescence IVIS images evaluating the tumor retention of NanoISD in BALB/cJ mice bearing orthotopic 4T1 tumors. Phosphorothioate-capped 95-BP dsDNA labeled with Cy5 (*i.e.* Cy5-DNA) was used to track the DNA. Cy5-DNA was administered by itself or in complex with D-PDB at an N/P charge ratio of 4. An intratumoral injection was given as a single 100 µL dose of 2 µg DNA. **(D)** Retention profiles of Cy5-DNA complexed to D-PDB and free Cy5-labeled DNA following intratumoral administration into orthotopic 4T1 breast tumors growing in BALB/c mice. **(E)** Representative luminescence IVIS images evaluating tumor IFN activity in C57BL/6J mice bearing B16.F10 IFN-LUC tumors. An intratumoral injection was given as a single 100 µL dose of either PBS or NanoISD at a dose corresponding to 2 µg DNA. **(F)** Longitudinal analysis of IFN activity following treatment. A two-way ANOVA with Sidak test was used for statistical analysis.

The intratumoral retention of the fluorescently-labeled phosphorothioate-capped 95-BP dsDNA (*i.e.* Cy5-DNA) with and without the polymeric carrier (*i.e.* D-PDB) was then investigated using a murine orthotopic tumor model of 4T1 breast cancer (***Figures 3.5-C and 3.5-D***). Consistent with the subcutaneous retention data, the free ISD dispersed quickly (*i.e.* half-life ~ 12 hours), and the ISD complexed to the polymer (*i.e.* NanoISD) exhibited sustained retention (*i.e.* half-life > 5 days). The matching pharmacokinetic clearance profiles of free D-PDB and the ISD complexed to D-PDB is consistent with prolonged *in vivo* association of the two species. Additionally, this finding is disparate with previous data that has consistently reported a short retention profile (*e.g.* half-life < 1 day) for siRNA complexed to the same polymer[377, 382-384]. This discrepancy is likely attributable to the higher valency of the polymer interaction with the significantly larger dsDNA cargo and/or the extra deoxyribonuclease resistance afforded by the phosphorothioate caps of the dsDNA. Notably, the local delivery of many innate immune agonists (*e.g.* CpG DNA, CDN STING agonists, *etc.*) results in widespread dissemination that can cause systemic inflammation and contribute to relatively low dose-limiting toxicities[412-414], while the enhanced local retention of NanoISD inherently limits the escape of nanoparticles into systemic circulation and therefore reduces the potential for systemic toxicity.

B16.F10 murine melanoma cells, which had been previously engineered to express luciferase upon IFN induction (*i.e.* B16.F10 IFN-LUC cells)[231], were next employed to assess whether the immunostimulatory activity of NanoISD was conserved in the non-immune, cancer cells and if so, to identify the *in vivo* kinetics of signaling. By quantifying luminescence via IVIS imaging following exposure to the substrate, D-luciferin, it was established that an *in vitro* treatment of NanoISD could activate luciferase production (*i.e.* IFN production) in the melanoma reporter cells, suggesting that the immunostimulatory capacity of the dsDNA was indeed conserved in the B16.F10 cell line (***Supplementary Figure A.S12***).

An intravital kinetics study of IFN production was subsequently performed to study the pharmacodynamics of NanoISD (***Figures 3.5-E and 3.5-F***). Mice were subcutaneously inoculated with the B16.F10 IFN-LUC cells, and when the tumors were ~ 50 mm^3, mice were given a single intratumoral injection of either PBS or NanoISD. At preselected timepoints, mice were administered D-luciferin, and luminescence was measured 15 minutes thereafter. The longitudinal IVIS imaging confirmed *in vivo* IFN production with peak protein production occurring 12 hours post treatment. The level of *in vivo* IFN signaling returned to baseline at 24 hours post treatment despite the extended local retention profile of NanoISD. Therefore, though NanoISD is likely still present and intact within the tumor, we suspect that over time other factors, such as inhibitory pathways within cells or extracellular exclusion (*e.g.* fibrotic entrapment), might inactivate the nanoparticle complex and/or locally down regulate IFN signaling. Moreover, cancer cell stress or death induced by the treatment may also contribute to the decreased IFN signal over time, especially since the cancer cells are serving as the IFN reporter. Regardless, the acute IFN activity of NanoISD *in vivo* motivates the use of a therapeutic dosing regimen involving multiple injections spaced days apart (*e.g.* every three days (*q3d*)).

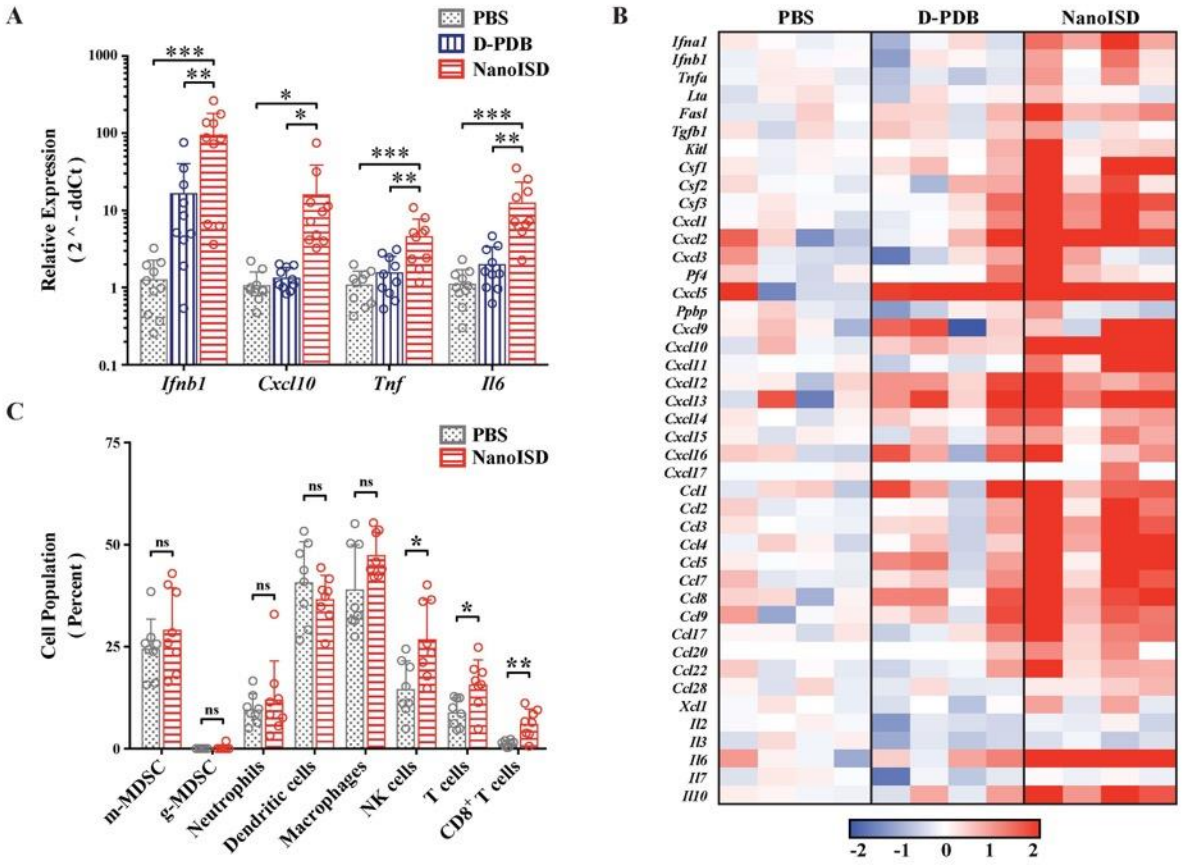

Figure 3.6. NanoISD Reprograms the Immune Profile of the Tumor Microenvironment. **(A)** Quantitative polymerase chain reaction (qPCR) analysis of B16.F10 tumors 6 hours following a single 100µL intratumoral treatment of either PBS, D-PDB, or NanoISD at a dose corresponding to 2 µg DNA. A one-way ANOVA with Tukey test was used for statistical analysis. **(B)** NanoString analysis of B16.F10 tumors 6 hours following a single 100µL intratumoral treatment of either PBS, D-PDB, or NanoISD at a dose corresponding to 2 µg DNA. Data is presented as log2 fold change relative to PBS treatment. **(C)** Flow cytometry analysis of the cellular composition of B16.F10 tumors treated intratumorally with 100 µL of either PBS or NanoISD at a dose corresponding to 2 µg DNA. Tumors were harvested 48 hours after the third intratumoral injection of a *q3d* dosing regimen. Data is presented as percent of $CD45^+$ live cells. A two-way ANOVA with Sidak test was used for statistical analysis.

NanoISD Reprograms the Immune Profile of the Tumor Microenvironment

The immunological effects of intratumorally administered NanoISD were initially quantified by measuring changes in the gene expression of certain signature cytokines for STING pathway activation. B16.F10 tumors were harvested 6 hours after a single intratumoral treatment

of either PBS, D-PDB, or NanoISD, and the relative mRNA levels of *Ifnb1*, *Cxcl10*, *Tnf*, and *Il6* in the tumor were determined via quantitative polymerase chain reaction (qPCR) (***Figure 3.6-A***). The relative gene expression of these proinflammatory molecules was significantly elevated as compared to that of tumors treated with either PBS or free D-PDB, which is in accordance with STING pathway activation in the TME[234]. Free D-PDB also exhibited increased *Ifnb1* expression, though not to the extent of NanoISD treatment, which is consistent with the *in vitro* activity assays that indicated that the D-PDB polymer acts as a weak cGAS adjuvant.

NanoString gene expression analysis was subsequently performed to provide a more robust transcriptomic analysis of the immune response in the treated tumors (***Figure 3.6-B***). Using a slight variation of a gene expression panel that had been previously developed for myeloid cell characterization[415], exact mRNA levels were quantified for 43 different immunomodulatory cytokines. As determined by one-way ANOVA main effect, a single intratumoral NanoISD treatment upregulated the myeloid activation markers of the panel relative to PBS treatment (*i.e.* $p = 0.0376$) and D-PDB treatment (*i.e.* $p = 0.0596$). Notably, cytokines involved in myeloid recruitment (*i.e. Cxcl1*, *Cxcl2*, *Cxcl3*), myeloid differentiation (*i.e. Csf1*, *Csf2*, *Csf3*), and T cell recruitment (*i.e. Cxcl9*, *Cxcl10*, *Cxcl11*, *Cxcl12*) were markedly upregulated in the TME after NanoISD treatment. Additionally, D-PDB treatment was insignificantly different from PBS treatment (*i.e.* $p = 0.9809$) with regard to the myeloid activation markers of the panel. These results from the NanoString study further support the qPCR findings and provide additional insight into the immune profile of the treated tumors, demonstrating that a proinflammatory phenotype is indeed induced by intratumorally administered NanoISD.

To characterize the immunocellular changes within the TME that were likely to follow the local cytokine response, flow cytometry was conducted on B16.F10 tumors 48 hours after the final

injection of a three treatment *q3d* dosing regimen (***Figure 3.6-C***). Cell populations of interest were quantified using a myeloid cell panel (***Supplementary Figure A.S13***) and a T cell panel (***Supplementary Figure A.S14***). No marked changes occurred for the tumor populations of macrophages (*i.e.* $CD45^+$ $CD11b^+$ $F4/80^+$), dendritic cells (*i.e.* $CD45^+$ $CD11c^+$ $MHC\text{-}II^+$), monocytic myeloid-derived suppressor cells (m-MDSCs) (*i.e.* $CD45^+$ $CD11b^+$ $Ly6C^+$), granulocytic MDSCs (g-MDSCs) (*i.e.* $CD45^+$ $CD11b^+$ $Ly6G^+$ SSC^{hi}), and neutrophils (*i.e.* $CD45^+$ $CD11b^+$ $Ly6G^+$, SSC^{lo}). However, the relative concentrations of NK cells (*i.e.* $CD45^+$ $NK1.1^+$), total T cells (*i.e.* $CD45^+$ $CD3^+$), and $CD8^+$ T cells (*i.e.* $CD45^+$ $CD3^+$ $CD8^+$) within the tumor were significantly elevated following NanoISD treatment, consistent with the established effects of STING pathway activation in tumors[50, 56, 307, 317]. Thus, NanoISD can also propagate the adaptive arm of the cancer-immunity-cycle via the initial activation of innate immunity.

In addition to altering the migration and proliferation of lymphoid-derived immune cells, STING activation can also lead to improved cytotoxic immune responses by repolarizing immunosuppressive M2-like macrophages to M1-like macrophages that can promote antitumor immunity[280, 281]. Thus, while not assessed in this work, it is possible that NanoISD also induces the M1-like phenotype in tumor macrophages, thereby further enhancing the antitumor immunity that is stimulated by NanoISD. Future work could study how NanoISD affects macrophage polarization and the importance of such effects.

NanoISD Exerts Antitumor Effects

Cancer therapy studies were conducted in murine tumor models to establish the therapeutic effect of NanoISD. Initially, the antitumor effects of NanoISD and free D-PDB were investigated in a poorly immunogenic B16 model of melanoma that has been engineered to express the foreign

antigen, OVA (*i.e.* B16-OVA) in order to increase its antigenicity and therefore potential to respond to cancer immunotherapies. Mice bearing B16-OVA murine melanoma tumors were intratumorally treated with either PBS, D-PDB, or NanoISD for a total of three injections administered *q3d* (***Supplementary Figure A.S15***). Notably, NanoISD significantly restricted tumor growth and prolonged survival relative to both free D-PDB and PBS, which is consistent with a previous finding that phosphorothioate-capped dsDNA delivered intratumorally with a cationic transfection agent can mediate antitumor immune effects in the B16-OVA tumor model[204]. Additionally, while D-PDB acts as a weak cGAS adjuvant, the free polymer did not demonstrate therapeutic efficacy *in vivo*, suggesting that the intrinsic effects of the D-PDB are insufficient to initiate STING-driven antitumor immune programs in the TME.

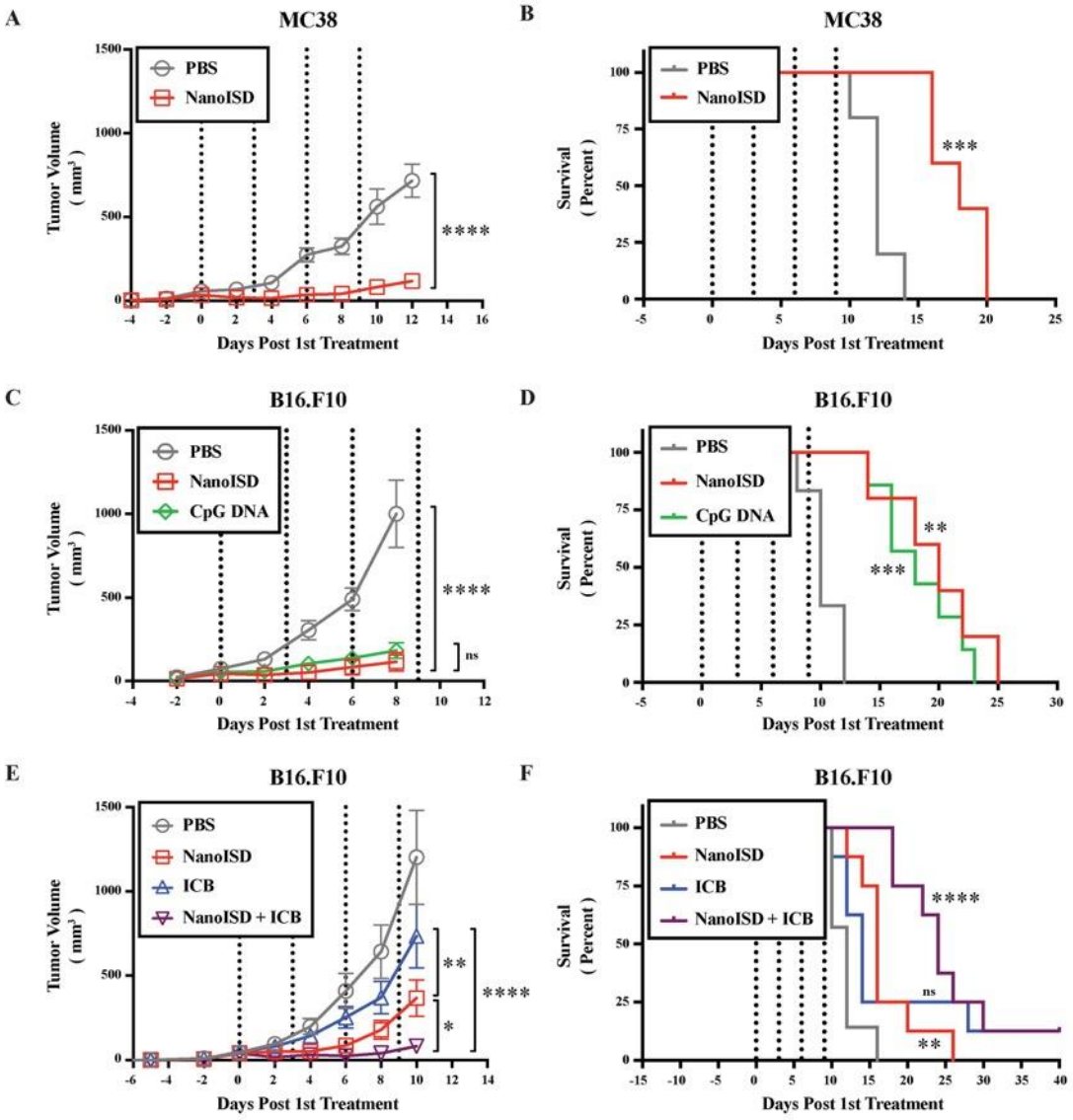

Figure 3.7. NanoISD Exerts Antitumor Effects. **(A)** Tumor growth plot for MC38 tumors intratumorally treated with 100 µL of either PBS or NanoISD at a dose corresponding to 2 µg DNA (n = 5 per treatment group). Treatments were administered four times *q3d* as indicated by the dotted lines. Tumor growth curves were truncated to the first day that a mouse in any treatment group reached the study endpoint. A two-way ANOVA with Sidak test was used for statistical analysis. The statistical analysis presented is for the final day shown (*i.e.* day 12). **(B)** Kaplan-Meier survival curve for MC38 tumors intratumorally treated with 100 µL of either PBS or NanoISD. Log rank (Mantel-Cox) test was used for statistical analysis. **(C)** Tumor growth plot for B16.F10 tumors intratumorally treated with 100 µL of either PBS, CpG DNA (*i.e.* ODN 1826), or NanoISD (n = 5 or greater per treatment group). Both the CpG DNA and NanoISD doses corresponded to 2 µg DNA. Treatments were administered four times *q3d* as indicated by the dotted lines. Tumor growth curves were truncated to the first day that a mouse in any treatment group reached the study endpoint. A two-way ANOVA with Tukey test was used for statistical

analysis. The statistical analysis presented is for the final day shown (*i.e.* day 8). **(D)** Kaplan-Meier survival curve for B16.F10 tumors intratumorally treated with 100 µL of either PBS, CpG DNA (*i.e.* ODN 1826), or NanoISD. Log rank (Mantel-Cox) test was used for statistical analysis. **(E)** Tumor growth plot for B16.F10 tumors treated with 100 µL of either PBS, ICB (*i.e.* anti-PD-1 + anti-CTLA-4 monoclonal antibody therapy), NanoISD, or NanoISD + ICB (n = 8 per treatment group). NanoISD and PBS were administered intratumorally, while ICB was administered intraperitoneally. The NanoISD dose corresponded to 2 µg DNA. The ICB treatment corresponded to 100 µg of both anti-PD-1 and anti-CTLA-4 monoclonal antibodies. Treatments were administered four times *q3d* as indicated by the dotted lines. Tumor growth curves were truncated to the first day that a mouse in any treatment group reached the study endpoint. A two-way ANOVA with Tukey test was used for statistical analysis. The statistical analysis presented is for the final day shown (*i.e.* day 10). **(F)** Kaplan-Meier survival curve for B16.F10 tumors treated with 100 µL of either PBS, ICB (*i.e.* anti-PD-1 + anti-CTLA-4 monoclonal antibody therapy), NanoISD, or NanoISD + ICB (*i.e.* anti-PD-1 + anti-CTLA-4 monoclonal antibody therapy). Log rank (Mantel-Cox) test was used for statistical analysis.

NanoISD was subsequently explored as a therapeutic treatment for the less immunogenic tumor models, B16.F10 murine melanoma and MC38 murine colon cancer, both of which lack the expression of a foreign antigen (***Figure 3.7***). Treatments were again intratumorally administered *q3d* for a total of four injections. Relative to PBS-treated controls, the NanoISD treatment attenuated tumor growth (***Figures 3.7-A and 3.7-C***), prolonged murine survival (***Figures 3.7-B and 3.7-D***), and was well-tolerated by mice as demonstrated by insignificant differences in total mouse weight over time (***Supplementary Figure A.S16***). Furthermore, in the B16.F10 model, NanoISD treatment performed comparably to the well-established innate immune activator, CpG DNA when administered at the same dose (*i.e.* 2 µg DNA) (***Figures 3.7-C and 3.7-D***).

TLR9 agonists can function in a similar manner to that of cGAS/STING pathway agonists by promoting the cancer-immunity-cycle. Indeed, CpG DNA can induce B16 tumor regression in mice via NK cell-dependent, tumor antigen-specific T cell cross-priming[416]. Accordingly, CpG DNA is also currently being investigated in human clinical trials for the treatment of cancer and they have recently demonstrated great potential for overcoming PD-1 blockade resistance in humans with advanced melanoma[417]. However, CpG DNA relies on the cellular expression of

TLR9, which is mostly restricted to plasmacytoid dendritic cells and B cells in humans[418]. Alternatively, both the cGAS and STING proteins are rather ubiquitously expressed in mammalian cells[419-421]. Moreover, TLR9 signaling can only occur in cells that are directly exposed to CpG DNA, while STING signaling can locally propagate from cell-to-cell via endogenous cGAMP transfer following DNA-induced cGAS activation[198, 422, 423]. Thus, the cGAS/STING pathway might represent a more accessible pathway for promoting antitumor immunity via cytosolic DNA sensing. Regardless, cGAS/STING pathway agonists increase the arsenal of potential immunotherapeutic treatments, which can dramatically enhance overall patient outcomes by providing more opportunities for application-specific treatments. For example, CpG-based immunotherapy can impair the antitumor activity of BRAF inhibitors in a B cell–dependent manner when used in combination to treat cancer[240], whereas STING agonists can actually sensitize melanoma cells to BRAF inhibitors[424] and might thereby improve therapeutic efficacy in such a scenario.

To determine the impact of NanoISD treatment on the therapeutic response to ICB treatment (*i.e.* combined anti-PD-1 and anti-CTLA-4 monoclonal antibody therapy), B16.F10-bearing mice were treated with either PBS, NanoISD, ICB, or a combination of NanoISD and ICB for a total of four injections administered *q3d* (***Figures 3.7-E and 3.7-F***). Notably, the NanoISD treatment outperformed the ICB treatment, and the combination treatment of NanoISD and ICB was most effective at inhibiting the growth of treated tumors, indicating that NanoISD treatment can indeed improve therapeutic responses to murine ICB therapy. We note that there is still much room for improvement regarding the therapeutic efficacy of NanoISD, as the treatment in combination with ICB resulted in only one complete response (*i.e.* complete tumor elimination), matching that of ICB alone.

Since NanoISD consists of a self-assembling multi-phasic structure and is highly amenable to the integration of reactive handles[425], it should support various chemical and biomolecular engineering strategies to co-deliver multiple therapeutic agents (*e.g.* potentiators of the cGAS/STING pathway). One potential strategy for increasing the efficacy of NanoISD could include coupling NanoISD treatment with MEK inhibition or CXCR2 inhibition in order to block the expression and/or function of potentially undesirable cytokines (*e.g.* CXCL1 and CXCL2) that can enhance MDSC activity[415] and thereby reduce immune-mediated tumor clearance. Indeed, such a strategy has been previously employed to alleviate certain immunosuppressive effects of STING signaling that can accompany STING agonists and radiotherapy[426].

Other future considerations for NanoISD might involve further improving upon the design of the cGAS ligand and/or the cytosolic delivery agent as well as exploring strategies that could enable intravenous administration and/or tumor targeting of the cGAS agonist.

One variable not examined in this work is whether NanoISD activates other intracellular DNA sensors, such as AIM2, which can limit the magnitude of STING signaling upon *in vitro* stimulation[99]. Future studies could investigate whether AIM2 is involved in the response to NanoISD. We note that it is unlikely that AIM2 plays a large role in the response to NanoISD, since the BP length threshold for robust AIM2 activation *in vitro* (*i.e.* ~ 150-BP) is greater than that of the optimized cGAS ligand (*i.e.* 95-BP)[108]. However, if AIM2 is involved in the response to NanoISD, strategies could be employed to reduce AIM2 activation with the goal of enhancing STING signaling.

In this work, D-PDB was employed because of its previous success as a vehicle for the cytosolic delivery of immunostimulatory nucleic acids. Indeed, in multiple murine tumor models, an intratumoral treatment regimen of D-PDB loaded with immunostimulatory 5′ triphosphate RNA

demonstrated significant therapeutic efficacy by promoting the activation of RIG-I (*i.e.* another cytosolic PRR that can drive antitumor immunity)[27, 28]. While the work in this paper demonstrates that D-PDB can also be used to induce a therapeutic response via the cytosolic delivery of ISD and the pharmacological activation of cGAS, it is possible that other nanocarriers may elicit enhanced ISD delivery and improved therapeutic responses. Thus, future work aimed at improving therapeutic efficacy could explore the comparison of other nanocarriers for the cytosolic delivery of the optimized ISD (*i.e.* phosphorothioate-capped 95-BP dsDNA).

Lastly, we note that NanoISD may also have utility in other therapeutic areas (*e.g.* vaccinations for infectious diseases), as the DNA/polymer complex is a versatile adjuvant that can indiscriminately generate a local proinflammatory response, which can be advantageous for treating various diseases.

Conclusion

Through an iterative experimental screen, the nucleic acid immunotherapeutic, NanoISD was engineered to trigger local cGAS/STING signaling via DNA-induced activation of the cGAS enzyme within the cytosol. The effects of formulation conditions (*i.e.* N/P charge ratio), DNA molecular weight (*i.e.* BP length), and DNA composition (*i.e.* phosphorothioate modifications) were investigated using a rationally designed synthetic ISD library in combination with a pH-responsive, endosome-destabilizing polymeric delivery vehicle. This yielded a potent nanoparticulate cGAS adjuvant that can evade major deoxyribonucleases, enhance cellular uptake, promote cytosolic delivery via endosomal escape, and trigger the cGAS/STING pathway in a cGAS-directed manner. Furthermore, NanoISD induces proinflammatory cytokine production, prompts the maturation of antigen presenting cells, promotes the tumor infiltration of NK cells and

$CD8^+$ T cells, reduces tumor burden, and enhances responses to ICB therapy. Thus, NanoISD represents a novel immunostimulant with clear indications for the treatment of immunologically cold cancers.

Materials and Methods

Polymer Synthesis and Characterization

Reversible addition-fragmentation chain transfer (RAFT) polymerization was employed to synthesize the amphiphilic diblock copolymer, *poly*[dimethylaminoethyl methacrylate]$_{10kDa}$-*block*-[(propylacrylic acid)$_{0.3}$-*co*-(dimethylaminoethyl methacrylate)$_{0.3}$-*co*-(butyl methacrylate)$_{0.4}$]$_{35kDa}$ (*p*[DMAEMA]$_{10kDa}$-*bl*-[PAA$_{0.3}$-*co*-DMAEMA$_{0.3}$-*co*-BMA$_{0.4}$]$_{35kDa}$; D-PDB) as previously described[8]. Briefly, the chain transfer agent (CTA) and mass initiator for the RAFT polymerizations were 4-cyano-4-(ethylsulfanylthiocarbonyl)sulfanylpentanoic acid (ECT; Boron Molecular) and 2,2'-azobis(4-methoxy-2,4-dimethyl valeronitrile) (V-70; Wako Chemicals), respectively. An analytical mass balance (XSE205DU DualRange; Mettler Toledo) was used for all mass measurements. Inhibitors were removed from monomer stocks by gravity filtration in columns that were packed with aluminum oxide.

For the first block of the polymer, filtered dimethylaminoethyl methacrylate (DMAEMA) was added to measured CTA in a glass vial with a target degree of polymerization of 100. A mass initiator stock was prepared by dissolving the initiator in the reaction solvent, dioxane. An appropriate amount of the mass initiator stock was added to the solution of CTA and DMAEMA at a molar ratio of 100:1:0.05 representing total monomer, CTA, and initiator, respectively. Additional dioxane was then added to the reaction vessel to attain a 40 wt% monomer solution. The solution was sealed and purged with nitrogen gas for 30 minutes on ice and then allowed to

react at 40 ºC in an oil bath.

The reaction was stopped after 22 hours by opening the reaction vessel and exposing the mixture to air. The resultant polymer was then purified by precipitation into cold pentane and subsequent dialysis. The crude product was precipitated six times by transferring the polymer solution into cold pentane. Centrifugation (5000 rpm, 5 min, 4 ºC) was used to pellet the polymer mixture, and the supernatant was then discarded. Small volumes of acetone were added to dissolve the pelleted polymer, thereby enabling the polymer to be transferred to new precipitation tubes. The polymer mixture was then collected in a 3.5 MWCO SnakeSkin^{TM} dialysis membrane (Cat. No. 68035; Thermo Fisher Scientific) and further purified via membrane dialysis against pure acetone (3x), half-acetone and half deionized water (2x), and then pure deionized water (2x) for 4 hour intervals each. Following dialysis, poly(DMAEMA) was frozen at -80 ºC for 5 hours and then lyophilized for 3 days.

For the second block of the polymer, poly(DMAEMA) was used as a macroCTA (mCTA). Filtered DMAEMA, PAA, and BMA (at a molar ratio of 30:30:40) were added to measured mCTA in a glass vial with a target degree of polymerization of 450. PAA was synthesized using diethyl propylmalonate as the precursor as previously described[427]. A mass initiator stock was prepared by dissolving the initiator in the reaction solvent, N,N-dimethylacetamide (DMAC). An amount of the mass initiator stock was added to the solution of mCTA and monomers at a molar ratio of 450:1:0.4 representing total monomer, mCTA, and initiator, respectively. Note that a greater Initiator/CTA ratio is required to get PAA to incorporate into the polymer chains. Additional DMAC was then added to the reaction vessel to attain a 40 wt% mCTA and monomer solution. The solution was sealed and purged with nitrogen gas for 30 minutes on ice and then allowed to react at 40 ºC in an oil bath.

The reaction was stopped after 24 hours by opening the reaction vessel and exposing the mixture to air. The resultant polymer was then purified by precipitation into cold pentane:ether (80:20) and subsequent dialysis. The crude product was precipitated six times by transferring the polymer solution into cold pentane:ether (80:20). Centrifugation (5000 rpm, 5 min, 4 ºC) was used to pellet the polymer mixture and remove the supernatant. Again, small volumes of acetone were added to dissolve the pelleted polymer, thereby enabling the polymer to be transferred to new precipitation tubes. The polymer mixture was then collected in a 10 MWCO SnakeSkin^{TM} dialysis membrane (Cat. No. 68100; Thermo Fisher Scientific) and further purified via membrane dialysis against pure acetone (3x), half-acetone and half deionized water (2x), and then pure deionized water (2x) for 4 hour intervals each. Following dialysis, poly(DMAEMA) was frozen at -80 ºC for 5 hours and then lyophilized for 3 days. All lyophilized polymer was stored at -20 ºC prior to use.

^{1}H NMR Spectroscopy ($CDCl_3$ with TMS, 400 MHz) was used to calculate the experimental degree of polymerization, polymer composition, and theoretical molecular weight of the polymers (***Supplementary Figure A.S17***). Subsequently, the experimental molecular weight and a polydispersity index were measured by gel permeation chromatography (GPC) (mobile phase HPLC-grade dimethylformamide (DMF) containing 0.1% LiBr) with inline light scattering (Wyatt Technology) and refractive index (Agilent) detectors (***Supplementary Figure A.S18***). The ASTRA V Software (Wyatt Technology) was used for all GPC-related calculations. Additionally, The *poly*(dimethylaminoethyl methacrylate)$_{10kDa}$-*block*-(butyl methacrylate)$_{34kDa}$ (*p*DMAEMA$_{10kDa}$-*bl*- BMA$_{34kDa}$; D-B) polymer was previously prepared[28].

Near-infrared D-PDB (NIR-D-PDB) was created by labeling D-PDB with NIR-664-iodoacetamide (CAS 149021-66-9; Santa Cruz) at a molar ratio of 1:1. Briefly, 72 µL of a 12.5 mg/mL stock of NIR-664-iodoacetamide dissolved in methanol was added to 50 mg of D-PDB

dissolved in 1 mL methanol. The mixture was vortexed, and the reaction was allowed to proceed at room temperature overnight while continuously stirring and protected from light. The mixture was then transferred to a 3.5 MWCO SnakeSkin™ dialysis membrane (Cat. No. 68035; Thermo Fisher Scientific) and purified via membrane dialysis against pure methanol (3x), half-methanol and half deionized water (2x), and then pure deionized water (2x) for 4 hour intervals each, all the while kept at 4 ºC and protected from light. Following dialysis, the sample was run through a PD-10 desalting column (17085101; Cytiva) into H_2O. The fully purified sample was frozen at -80 ºC for 5 hours and then lyophilized for 2 days. NIR-D-PDB was stored at -20 ºC prior to use.

Preparation of ISD Libraries

The synthetic library of phosphorothioate-capped dsDNA (***Supplementary Figure A.S1***) and other associated DNA sequences were purchased as a duplex from Integrated DNA Technologies (IDT) unless otherwise specified. The second ISD library of PCR-amplified dsDNA (***Supplementary Figure A.S2***) was prepared as follows. The 10,183-BP lentiGuide-Puro plasmid (Plasmid #52963; Addgene) was used to generate custom BP length dsDNA PCR products. In brief, the lentiGuide-Puro agar stab was spread over standard 0.5 mg/mL puromycin agar plates and placed in a 37 ºC bacteria incubator overnight. The following day, individual bacteria colonies were isolated and placed in liquid LB broth with 0.5 mg/mL puromycin, swirled, loosely covered with sterile cap, and left to incubate at 37 ºC for 12 hours. Bacteria growths were purified with the QIAprep Miniprep kit (Cat. No. 27104; Qiagen), resuspended in sterile H_2O, and DNA concentration was quantified by ultraviolet–visible (UV-Vis) spectroscopy (Nanodrop 2000 Spectrophotometer; Thermo Fisher Scientific).

Forward and reverse primers were designed using the NCBI Primer Blast tool for dsDNA

sequences of variable BP length (*i.e.* 95, 156, 313, 625, 1250, 2500, 5000, and 10000 BP). For the PCR-amplification of each length of dsDNA, individual reactions were set up with 4 µL of 5x Phusion GC Buffer, 0.4 µL of 10 mM dNTPs (D7295; MilliporeSigma), 1 µL of 10 µM forward primer, 1 µL of 10 µM reverse primer, 0.6 µL of DMSO, 0.2 µL of Phusion® High-Fidelity DNA Polymerase (M0530; New England Biolabs), 4 µL of 1 ng/µL (4 ng) of lentiGuide-Puro plasmid template DNA (Plasmid #52963; Addgene), and 8.8 µL of H_2O, per 20 µL reaction. Thermocycling conditions were 98 ºC for 30 seconds, followed by 35 cycles of 98 ºC for 10 seconds, 54 ºC for 30 seconds, 72 ºC for 30 seconds per kb of PCR length, followed by 72 ºC for 10 minutes. PCR products were concentrated using standard ethanol precipitation and clear bands were observed on a 2% agarose gel for each PCR length. Each PCR-amplified product was stored at -20 ºC prior to use.

Nanoparticle Formulation

Lyophilized D-PDB was dissolved in ethanol to 50 mg/mL. Aliquots of this polymer stock were then diluted in phosphate buffer (pH 7.0, 100 mM) to a concentration of 10 mg/mL, allowing the polymer chains to self-assemble into micelles. The 10 mg/mL polymer solution was then concentrated into PBS (pH 7.4; Gibco) through 4 cycles of centrifugal filtration with Amicon® Ultra 0.5 mL Centrifugal Filter Units (Ultracel® - 3K, Regenerated Cellulose 3,000 NMWL; MilliporeSigma) following manufacturer's instructions. The final concentrated polymer solution was collected, and an aliquot was taken to determine the polymer concentration relative to a standard curve. Using a 96-well plate (REF 655180; Greiner Bio-One), the polymer concentration was calculated from UV-vis spectroscopy (Synergy H1 Multi-Mode Microplate Reader; Biotek) based on absorbance at 310 nm. The micelle solution was diluted to 1 mg/mL with PBS and passed

through a 0.2 µm Whatman® Puradisc polyethersulfone sterile filter (WHA67801302; MilliporeSigma). A fixed amount of the sterile-filtered polymer stock was then added to an aqueous solution containing a set amount of nucleic acid, which corresponded to the desired N/P charge ratio. Again, note that the first block of the diblock copolymer composed of poly(DMAEMA) is estimated to exhibit 50% protonation at pH 7.4 for the purposes of determining N/P ratios. Upon the addition of the polymer micelles to the nucleic acid, the solution was rapidly mixed by pipetting and then incubated at room temperature for 20 minutes to allow for complete electrostatic complexation.

Nanoparticle Physical Characterization

Hydrodynamic size of the polymeric micelles and DNA/polymer complexes was measured via digital light scattering (DLS) using either the Zetasizer Nano ZS instrument (Malvern Panalytical) or the Litesizer 500 instrument (Anton Paar) as indicated in figure captions. Additionally, the zeta potential of the polymeric micelles and DNA/polymer complexes was determined using the Zetasizer Nano ZS instrument (Malvern Panalytical). Polymer concentrations were normalized to 1 mg/mL and samples were run at physiological pH 7.4. DNA concentrations correspond to the N/P charge ratios, which were set to 4 unless otherwise indicated.

2% agarose gels were prepared by dissolving 3 grams of UltraPure™ Agarose powder (16500100; Thermo Fisher Scientific) in 150 mL of 1x TAE buffer that had been diluted with deionized H_2O from a 10x TAE buffer stock (REF 46010CM; Corning). The mixture was microwaved in 30 second intervals until the agarose was fully dissolved. The solution was then cast into a gel. DNA and DNA/polymer complexes were then prepared. For the DNase I activity experiment, the indicated concentrations of DNase I (M0303; New England Biolabs) were

incubated with the indicated samples for 15 minutes at 37 ºC. The resultant mixtures and controls were then incubated at 75 ºC for 15 minutes to heat-inactivate the DNase I, and a volume of 10% sodium dodecyl sulfate (SDS) (RGE3230; K-D Medical) was subsequently added to the mixtures and controls such that a final concentration of 1% SDS was achieved, which allowed for decomplexation of the DNA from the polymer. All of the samples were mixed with a volume of glycerol such that a final concentration of 5% glycerol was achieved prior to gel loading. Samples were loaded into wells of the agarose gel at a concentration of 1 μg DNA/lane. Polymer concentrations correspond to the indicated N/P charge ratio. The TrackIt™ 100 bp DNA Ladder (Cat. No. 10488058; Thermo Fisher Scientific), the TrackIt™ 1 Kb Plus DNA Ladder (Cat. No. 10488085; Thermo Fisher Scientific), or the NEB 1 kb DNA Ladder (N3232; New England Biolabs) were used for references as indicated in figure captions. Gel electrophoresis was then performed at 120 V for 45 minutes. Gels were subsequently stained with SYBR Safe dye (S33102; Thermo Fisher Scientific) for 30 minutes while protected from light and then imaged with a Digital ChemiDoc MP system (Bio-Rad).

Cell Lines

All cell lines were maintained according to supplier specifications and/or technical data sheets. RAW-Dual cells (InvivoGen) and RAW-Lucia ISG-KO-cGAS cells (InvivoGen) were cultured in Dulbecco's Modified Eagle Medium (DMEM; Gibco) supplemented with 2 mM L-glutamine, 4.5 g/L glucose, 10% heat-inactivated fetal bovine serum (HI-FBS; Gibco), 100 U ml^{-1} penicillin / 100 μg ml^{-1} streptomycin (Gibco), and 100 μg/mL Normocin. For the continual selection of these cell lines, Zeocin was added on every other cell passage at a concentration of 200 μg/mL. THP1-Dual cells (InvivoGen) and THP1-Dual KO-TREX1 cells (InvivoGen) were cultured in Roswell

Park Memorial Institute (RPMI) 1640 Medium (Gibco) supplemented with 2 mM L-glutamine, 25 mM HEPES, 10% heat-inactivated fetal bovine serum (HI-FBS; Gibco), 100 U ml^{-1} penicillin / 100 µg ml^{-1} streptomycin (Gibco), and 100 µg/mL Normocin. For the continual selection of these cell lines, Blasticidin and Zeocin were added after every cell passage at concentrations of 10 µg/mL and 100 µg/mL, respectively. A549-Dual cells (InvivoGen) were cultured in Dulbecco's Modified Eagle Medium (DMEM; Gibco) supplemented with 2 mM L-glutamine, 4.5 g/L glucose, 10% heat-inactivated fetal bovine serum (HI-FBS; Gibco), 100 U ml^{-1} penicillin / 100 µg ml^{-1} streptomycin (Gibco), and 100 µg/mL Normocin. For the continual selection of this cell line, Blasticidin and Zeocin were added after every cell passage at concentrations of 10 µg/mL and 100 µg/mL, respectively. DC2.4 cells were cultured in Roswell Park Memorial Institute (RPMI) 1640 Medium (Gibco) supplemented with 2 mM L-glutamine, 1× non-essential amino acids (Cellgro), 10 mM HEPES (Invitrogen), 50 µM 2-mercaptoethanol (Gibco), 10% heat-inactivated fetal bovine serum (HI-FBS; Gibco), and 100 U ml^{-1} penicillin / 100 µg ml^{-1} streptomycin (Gibco). 4T1 cells (ATCC) were cultured in Dulbecco's Modified Eagle Medium (DMEM; Gibco) supplemented with 2 mM L-glutamine, 4.5 g/L glucose, 10% heat-inactivated fetal bovine serum (HI-FBS; Gibco), and 100 U ml^{-1} penicillin / 100 µg ml^{-1} streptomycin (Gibco). B16.F10 cells (ATCC) were cultured in Dulbecco's Modified Eagle Medium (DMEM; Gibco) supplemented with 2 mM L-glutamine, 4.5 g/L glucose, 10% heat-inactivated fetal bovine serum (HI-FBS; Gibco), and 100 U ml^{-1} penicillin / 100 µg ml^{-1} streptomycin (Gibco). B16.F10 IFN-LUC cells were cultured in Dulbecco's Modified Eagle Medium (DMEM; Gibco) supplemented with 2 mM L-glutamine, 4.5 g/L glucose, 10% heat-inactivated fetal bovine serum (HI-FBS; Gibco), and 100 U ml^{-1} penicillin / 100 µg ml^{-1} streptomycin (Gibco). Puromycin was added after every cell passage at a concentration of 10 µg/mL. B16-OVA cells were cultured in Dulbecco's Modified Eagle Medium

(DMEM; Gibco) supplemented with 2 mM L-glutamine, 4.5 g/L glucose, 10% heat-inactivated fetal bovine serum (HI-FBS; Gibco), and 100 U ml^{-1} penicillin / 100 µg ml^{-1} streptomycin (Gibco). For the continual selection of this cell line, Geneticin (G418; Gibco) was added after every cell passage at a concentration of 500 µg/mL. MC38 cells were cultured in Dulbecco's Modified Eagle Medium (DMEM; Gibco) supplemented with 2 mM L-glutamine, 0.1 mM non-essential amino acids (Cellgro), 10 mM HEPES (Invitrogen), 1 mM sodium pyruvate, 10% heat-inactivated fetal bovine serum (HI-FBS; Gibco), 100 U ml^{-1} penicillin / 100 µg ml^{-1} streptomycin (Gibco), and 50 µg/mL gentamicin sulfate (Gibco). All cells lines were tested for Mycoplasma contamination and kept in a humidified environment with 5% CO at 37 °C.

In Vitro Reporter Cell Assays

96-well plates (REF 655180; Greiner Bio-One) were used for screening the DNA/polymer complexes. Reporter cells were seeded at 50,000 cells/well in 100 µL media. When cells became ~ 80% confluent, treatments were administered in 100 µL PBS. Results were collected 24 hours after treatment. Quanti-Luc™ and Quanti-Blue™ (InvivoGen) assays were performed on cell supernatants following manufacturer's instructions. Luminescence and absorbance were quantified via plate reader (Synergy H1 Multi-Mode Microplate Reader; Biotek). Luminescence measurements were performed using white, opaque-bottom 96-well plates (REF 655073; Greiner Bio-One), and absorbance measurements were performed using standard, clear 96-well plates (REF 655180; Greiner Bio-One). The signal for each sample concentration was determined using 3 biological replicates, each with 3 technical replicates. For the *in vitro* IVIS assay with the B16.F10 IFN-LUC cells, black 96-well plates (REF 655096; Greiner Bio-One) were used, and luminescence measurements were performed on an IVIS Lumina III (PerkinElmer) 5 minutes after

the addition of Pierce™ D-Luciferin, Monopotassium Salt (88293; Thermo Fisher Scientific) reconstituted in PBS, such that the final concentration of D-luciferin was 150 µg/mL. The *in vitro* IVIS experiment included 3 biological replicates without technical replicates. All reporter cell measurements were normalized by subtracting the average value of a PBS-treated negative control group. All bell-shaped dose response curves were truncated at their plateau. The EC_{50} and IC_{50} values were calculated for each of the dose responses using curve fitting analysis in the GraphPad Prism software.

In Vitro Cellular Uptake Study

DC2.4 cells were seeded in 12-well plates (REF 665180; Greiner Bio-One) at 4 x 10^5 cells/well and allowed to adhere overnight. Treatments of either PBS, DNA / D-PDB, Cy5-DNA, Cy5-DNA / D-PDB, NIR-D-PDB, or DNA / NIR-D-PDB were administered to the cells for 4 hours at 37 ºC with 5% CO_2. Doses were set at 45 nM DNA (*i.e.* theoretical EC_{50} value for NanoISD in RAW-Dual cells normalized to surface area of the tissue culture area on the 12-well plate) and/or the corresponding concentration of polymer for an N/P charge ratio of 4. Following incubation, cells were trypsinized, washed, and resuspended with flow cytometry staining buffer (FACS buffer) (*i.e.* PBS + 2% FBS) supplemented with 1 µg/mL DAPI. Cells were then analyzed using an Amnis CellStream Luminex flow cytometer. Each treatment was performed with 4 technical replicates. Cellular uptake was also analyzed at 24 hours post treatment, and similar results were observed (***data not shown***).

In Vitro BMDC Maturation Study

Bone marrow cells were harvested from femurs and tibias of 6-8 week-old female

C57BL/6J mice by flushing them with cold PBS. Cells were centrifuged for 5 minutes at 450 x g and resuspended in complete BMDC culture media (*i.e.* RPMI 1640 medium supplemented with 10% HI FBS, 1% Pen-Strep (*i.e.* 100 U/mL penicillin and 100 µg/mL streptomycin)**,** 2 mM L-glutamine, 10 mM HEPES, 1 mM sodium pyruvate, 1x non-essential amino acids, 50 µM β-mercaptoethanol, and 20 ng/mL GM-CSF). The cell suspension was passed through a 70 µM sterile cell strainer (22363548; Fisherbrand™; Thermo Fisher Scientific), and the cells were then seeded in 100x15 mm non-tissue-culture-treated petri dishes (REF 351029; Corning) and incubated at 37 ºC with 5% CO_2. Fresh complete BMDC culture media was added on days 3, 5, and 7. On day 8, the percentage of $CD11c^+$ cells (*i.e.* BMDCs) was confirmed to be greater than 80% as measured with by flow cytometry using anti-CD11c-FITC (Clone N418; BioLegend), and the BMDCs were then seeded in 12-well plates (REF 665180; Greiner Bio-One) at 6 x 10^5 cells/well. Treatments of PBS, 45 nM phosphorothioate-capped 95-BP dsDNA (*i.e.* DNA), 2 µM MPLA, and 45 nM NanoISD (*i.e.* theoretical EC_{50} value for NanoISD in RAW-Dual cells normalized to surface area of the tissue culture area on the 12-well plate) were administered to the BMDCs for 24 hours at 37 ºC with 5% CO_2. Following incubation, cells were scrapped, washed with FACs buffer, incubated with Fc-block (anti-CD16/CD32, Clone 2.4G2; Tonbo) for 15 minutes at 4 ºC, and then stained with antibodies against the markers of DC activation, anti-CD86-PE/Cy7 (Clone GL-1; BioLegend) and anti-MHC-II-APC/Cy7 (Clone M5.114.15.2; BioLegend) for 1 hour at 4 °C. Cells were then washed 2x in FACS buffer, resuspended using FACS buffer supplemented with 1 µg/mL DAPI, and analyzed using an Amnis CellStream Luminex flow cytometer. Each treatment was performed with 4 technical replicates, and the experiment was conducted 3 times with similar results.

In Vivo Imaging Experiments

All *in vivo* imaging was performed on the IVIS Lumina III (PerkinElmer). Mice were anesthetized with isoflurane gas and shaved around the injection site as necessary. For all *in vivo* retention experiments, fluorescence was recorded longitudinally as indicated, and corresponding fluorophore-specific filter pairs were used. For the subcutaneous retention study, 6-8 week-old CD-1 mice (Charles River Laboratories) were administered a single 100 µL subcutaneous injection of either PBS, Cy5-DNA, Cy5-DNA / D-PDB, NIR-D-PDB, or DNA / NIR-D-PDB on each rear flank. Individual uncomplexed fluorescent agents were administered on the left flank of the mice, and the complexes at an N/P charge ratio of 4 with the indicated fluorescent agent were administered on the right flank of the mice. Each treatment contained 2 µg DNA and/or the corresponding amount of polymer for an N/P charge ratio of 4. For the intratumoral retention study, 6-8 week-old BALB/c mice (The Jackson Laboratory) were orthotopically inoculated with 4T1 tumors by injecting 1 x 10^6 cells suspended in 100 µL of a 1:1 mixture of PBS and Type 2 Cultrex Basement Membrane Extract (3532-005-02; R&D Systems) into the left inguinal mammary fat pad. When tumors were ~ 100 mm^3, the mice were administered a single 100 µL intratumoral injection of either PBS, Cy5-labeled phosphorothioate-capped 95-BP dsDNA (*i.e.* Cy5-DNA), or Cy5-DNA / D-PDB. Each treatment contained 2 µg DNA and/or the corresponding amount of polymer for an N/P charge ratio of 4.

For the *in vivo* IFN activity experiment, 6-8 week-old C57BL/6 mice (The Jackson Laboratory) were inoculated with B16.F10 IFN-LUC tumors by subcutaneously injecting 1 x 10^6 cells suspended in 100 µL of PBS into the rear right flank. When tumors were ~ 100 mm^3, the mice were administered a single 100 µL intratumoral injection of either PBS or NanoISD at a 2 µg DNA dose. Luminescence was recorded at set time points (*i.e.* 0, 4, 8, 12, and 24 hours). For

each timepoint, the mice were administered a dorsal subcutaneous 150 µL injection of 30 mg/mL Pierce™ D-Luciferin, Monopotassium Salt (88293; Thermo Fisher Scientific) reconstituted in PBS, and a luminescence image was captured 15 minutes thereafter.

Quantitative RT-PCR and NanoString Analysis

6-8 week-old C57BL/6 mice (The Jackson Laboratory) were inoculated with B16.F10 tumors by subcutaneously injecting 1 x 10^6 cells suspended in 100 µL of PBS into the rear right flank. When tumors were ~ 200 mm^3, the mice were administered a single 100 µL intratumoral injection of either PBS, D-PDB, or NanoISD at a 2 µg DNA dose. 6 hours after the intratumoral injection, mice were euthanized and tumors were harvested. Tumors were then homogenized using TissueLyser II (Qiagen), and tumor RNA was isolated using the RNeasy® Plus Mini Kit (Qiagen).

For the qPCR analysis of gene expression, 1 µg of the tumor RNA was reverse transcribed by an iScript cDNA synthesis kit (Bio-Rad) following the manufacturer's instructions. The qPCR was conducted on the generated cDNA using a Bio-Rad CFX Connect Real-time System, with the threshold cycle number determined by Bio-Rad CFX manager software V.3.0. The following TaqMan gene expression kits (Thermo Fisher Scientific) were used following the manufacturer's instructions: mouse *Ifnb1* (Mm00439552_s1); mouse *Cxcl10* (Mm00445235_ m1); mouse *Tnf* (Mm00443258_m1); mouse *Il6* (Mm00446190_m1); mouse *Ppib* (Mm00478295_m1). Reactions for each gene were performed in technical duplicate for ten biological samples per treatment group, and the threshold cycle numbers were averaged. Gene expression was normalized to the house-keeping gene, *Ppib* and then normalized to the PBS treatment values using the 2^{-ddCt} method of analysis.

For the NanoString analysis of gene expression, 100 ng of RNA isolated from tumor tissue

was hybridized to a myeloid panel of target-specific fluorescent barcodes. The hybridized samples were analyzed on the NanoString nCounter MAX Analysis system. Subsequent data processing was performed using the NanoString nSolver data analysis software.

In Vivo Tumor Therapy Experiments

6-8 week-old C57BL/6 mice (The Jackson Laboratory) were inoculated with B16-OVA, B16.F10, or MC38 tumors by subcutaneously injecting 1 x 10^6 cells suspended in 100 µL of PBS into the rear right flank. When tumors were ~ 50 mm^3, the mice were given four 100 µL intratumoral injections administered *q3d* with treatments of either PBS, D-PDB, CpG DNA (*i.e.* ODN 1826), or NanoISD at a 2 µg DNA dose. For the therapy study with ICB, certain mice were also given four 100 µL intraperitoneal injections on the same days as the intratumoral treatments (*i.e.* administered *q3d*) with a treatment of the monoclonal antibodies, anti-PD-1 (RMP1-14, BE0146; Bio X Cell) and anti-CTLA-4 (9d9, BE0164; Bio X Cell). Tumor volume, total murine mass, and murine well-being were recorded *qod* for the duration of the study. The study endpoint for maximum tumor volume (*i.e.* survival) was 1500 mm^3.

Flow Cytometry

6-8 week-old C57BL/6 mice (The Jackson Laboratory) were inoculated with B16.F10 tumors by subcutaneously injecting 1 x 10^6 cells suspended in 100 µL of PBS into the rear right flank. When tumors were ~ 50 mm^3, the mice were given three 100 µL intratumoral injections administered *q3d* with treatments of either PBS or NanoISD at a 2 µg DNA dose. 48 hours after the final intratumoral injection, mice were euthanized and tumors were harvested. The tumors were then mechanically dissociated with an OctoMACS separator, and digested in a solution of 125 µg

ml−1 Deoxyribonuclease I (Worthington) and 500 μg ml−1 Collagenase III (Worthington) in RPMI 1640 media for 30 minutes at 37 ºC. The digested tumors were strained through a 70 μM sterile cell strainer (22363548; Fisherbrand™; Thermo Fisher Scientific) and treated with ACK Lysing Buffer (Gibco).

The remaining tumor cells were washed and diluted to a concentration of 1×10^7 cells/ mL in FACS buffer supplemented with 50 nM dasatinib, and the cell suspension was aliquoted into a 96-well plate (REF 655180; Greiner Bio-One). 100 μl was add to each well with the number of wells filled corresponding to the number of flow cytometry tests to be performed. After another wash with FACS buffer supplemented with 50 nM dasatinib, the plated cells were incubated with Fc-block (anti-CD16/CD32, Clone 2.4G2; Tonbo) for 15 minutes at 4 ºC. The relevant fluorescent antibodies were then added for each flow cytometry test, and the cells were incubated for 45 minutes at 4 ºC while protected from light. Cells were washed twice, suspended in FACS buffer supplemented with 1 μg/mL DAPI, and then analyzed using a 5-laser LSRII flow cytometer (BD).

The samples were stained with the fluorescent antibodies of either a myeloid panel or T cell panel. The following antibodies were used for the myeloid panel: anti-CD45.2-APC (20-0454-U025; Tonbo), anti-CD11b-PerCp-Cy5.5 (550993; BD BioSciences), anti-NK-1.1-PE (108707; BioLegend), anti-F4/80-PE/Cy7 (123113; BioLegend), anti-MHC-II-APC/Cy7 (107628; BioLegend), anti-CD11c-PE/Cy5 (117316; BioLegend), anti-Ly-6G-A488 (127625; BioLegend), and anti-Ly-6C-BV605 (128035; BioLegend). The following antibodies were used for the T cell panel: anti-CD45.2-APC (20-0454-U025; Tonbo), anti-CD3e-PE/Cy7 (552774; BD BioSciences), and anti-CD8a-PE/Cy5 (100710; BioLegend). DAPI was used to discriminate live versus dead cells. Representative gating for each panel can be found in the Supplementary Information (***Supplementary Figures A.S13 and A.S14***).

Ethics Statement

All animal experiments were reviewed and approved by the Vanderbilt University Institutional Animal Care and Use Committee (IACUC), and all surgical and experimental procedures were performed in accordance with the regulations and guidelines of the Vanderbilt University IACUC. All mice were maintained at the animal facilities of Vanderbilt University under pathogen-free conditions.

Statistical Analysis

The significance for each experiment was determined as indicated in the corresponding figure caption. Statistical analyses were performed using GraphPad Prism software, version 7.0c. The plotted values represent the experimental means, and the error bars represent one standard deviation (SD), except for those in the tumor growth plots, which represent one standard error of the mean (SEM). **** $p < 0.0001$, *** $p < 0.005$, **$p < 0.01$, * $p < 0.05$. ns, not significant.

CHAPTER IV

ENDOGENOUS ALU RNA

Text for Chapter IV is adapted from:

Garland KM, Tossberg J, Aune T, Wilson JT. Repurposing Endogenous Alu RNA for Cancer Immunotherapy. *In Preparation.* (2021).

Abstract

Mammalian cells can identify invading pathogens as well as cellular malfunction through the detection of exogenous pathogen-derived RNA or mislocalized cellular RNA. Such RNA recognition can galvanize innate immunity for a stimulus-specific response that is coordinated through the activity of intracellular signaling pathways. It has recently been discovered that elevated IFN-I expression in circulating leukocytes of patients with relapsing remitting multiple sclerosis (RRMS) is at least partly attributable to an increased presence of endogenous double-stranded Alu RNA, which was found to concomitantly activate multiple RNA-sensing pathways. Moreover, a specific Alu RNA associated with the IFN-I signature of RRMS was identified as an exceptionally potent innate immune agonist. Here, that immunostimulatory Alu RNA is repurposed toward the treatment of cancer. The Alu RNA was formulated with an endosomolytic polymer to enable intracellular delivery of the RNA and targeted activation of RNA-sensing pathways. The Alu RNA / polymer complexes formed colloidally stable nanoparticles that exhibited immunostimulatory activity both *in vitro* and *in vivo*. Lastly, the therapeutic potential of Alu RNA for the treatment of cancer was demonstrated by attenuated tumor growth and prolonged survival in the B16.F10 murine melanoma tumor model.

Introduction

RNA sensing is a prominent defense mechanism employed by mammalian cells to maintain homeostasis[361, 428]. The abnormal accumulation of RNA at certain locations in and around a cell is a distinguishing feature of many forms of cellular distress (*e.g.* microbial infection, cellular malfunction, *etc.*)[120]. Accordingly, cells have evolved to express a class of pattern recognition receptors (PRRs) known as RNA-sensing PRRs, which can detect (*i.e.* bind) and respond to such irregularities by activating innate immunity[429-431]. Notably, each RNA-sensing PRR is associated with their own recognition requirements (*e.g.* RNA sequence, RNA morphology, RNA localization, *etc.*) and their own downstream effects, which can also depend on cellular context[5]. Once bound to RNA, the RNA-sensing PRRs trigger intracellular signaling cascades that direct the gene expression of the affected cell and ultimately shape an immune response in a stimulus-specific manner. Thus, PRRs have great potential as therapeutic targets for combating a large variety of diseases, since they can be manipulated to orchestrate host immune responses[432].

Under normal conditions, cellular RNAs tend to be immunologically inert and avoid spurious innate immune activation, since RNA-sensing PRRs can largely discriminate against them on the basis of the RNA's subcellular localization, composition, and local concentration. Furthermore, cellular RNAs are naturally processed in a variety of ways to evade immune recognition (*e.g.* 5′ capping, A-to-I editing, *etc.*). Certain diseases can however affect the natural processing of cellular RNA and thereby trigger the activation of RNA-sensing PRRs. Indeed, it has recently been discovered by Aune and colleagues that circulating leukocytes of patients with relapsing remitting multiple sclerosis (RRMS) exhibit elevated IFN-I levels accompanied by an increased presence of double-stranded Alu RNA derived from endogenous Alu elements in the human genome[25]. They determined that, while inactive in its edited single-stranded form, the Alu

RNA can be highly immunostimulatory in its unedited double-stranded form. The authors suggest that the observed increase in double-stranded Alu RNA could likely be attributed to loss of A-to-I editing, since such post-transcriptional modification can destabilize dsRNA structures[433]. In support of their working theory, they conducted a subsequent study and confirmed that Alu RNAs in RRMS patients do indeed experience widespread loss of A-to-I editing[26]. Furthermore, using RNA-seq analysis, they identified several Alu RNAs present at high levels in leukocytes with elevated levels of A-to-I editing in healthy patients relative to RRMS patients.

Of those endogenous Alu RNAs associated with RRMS, one particular double-stranded RNA of the AluJb class (chr17: 76,418,582 – 76,418,856 on the GrCh37 / hg19 assembly) was found to be exceptionally immunostimulatory as determined by a reporter cell screen for both IFN-I and NF-κB activity[26]. Using various KO reporter cells, they also determined that the immunostimulatory capacity of the AluJb RNA is primarily derived from its ability to activate both RIG-I and TLR3 (*i.e.* RNA-sensing PRRs). Notably, their results suggest that MDA5 (*i.e.* another RNA-sensing PRR) is not involved in the recognition of the AluJb RNA, despite the PRR's established involvement in the detection of other Alu RNAs. The lack of a response from MDA5 might be attributable to the relatively short length of the AluJb RNA (*i.e.* 274 nt), since longer double-stranded RNA molecules (*i.e.* greater than 300-BP) are required for MDA5 activation[361].

The cytokine signatures from RIG-I and TLR3 typically involve type I IFNs and other proinflammatory cytokines. Accordingly, while systemic inflammation from upregulated endogenous Alu RNA may be detrimental for RRMS patients, localized inflammation induced by therapeutic delivery of Alu RNA could be beneficial for the treatment of cancer in the context of promoting the cancer-immunity-cycle. Indeed, there are several immunostimulatory RNA therapeutics that activate either the RIG-I or TLR3 pathways now in preclinical and/or clinical

development for the treatment of solid tumor cancers[27-30]. Notably, Aune and colleagues have demonstrated that AluJb RNA can outperform poly(IC) RNA (*i.e.* TLR3 agonist) in terms of both IFN-I and NF-κB activity[26], which may suggest that the combined activation of RIG-I and TLR3 can enable heightened innate immune activation relative to the discrete activation of either PRR.

Here, we have repurposed endogenous Alu RNA by engineering a nucleic acid immunotherapeutic, AluJb RNA (Left Arm) / D-PDB, which can efficiently target RNA-sensing PRRs and exploit RNA sensing in the context of local cancer immunotherapy (***Figure 4.1***). The well-established, endosomolytic polymer, poly[(DMAEMA)-*block*-(PAA-*co*-DMAEMA-*co*-BMA)] (D-PDB)[7, 8, 27, 28, 372-384] was used to electrostatically complex double-stranded AluJb RNA into environmentally responsive nanoparticles capable of achieving intracellular delivery of the noncoding, immunostimulatory Alu RNA. The RNA/polymer nanoparticles were characterized for nanoparticle stability, transfection efficiency, IFN-I activity, and antitumor immunity. Notably, the direct injection of the nanoparticle formulation into murine tumors triggered the production of proinflammatory cytokines that are known to enhance the tumor infiltration of cancer-killing NK cells and T lymphocytes. Finally, the therapeutic efficacy of NanoISD was demonstrated in the B16.F10 murine melanoma tumor model by attenuated tumor growth and prolonged survival.

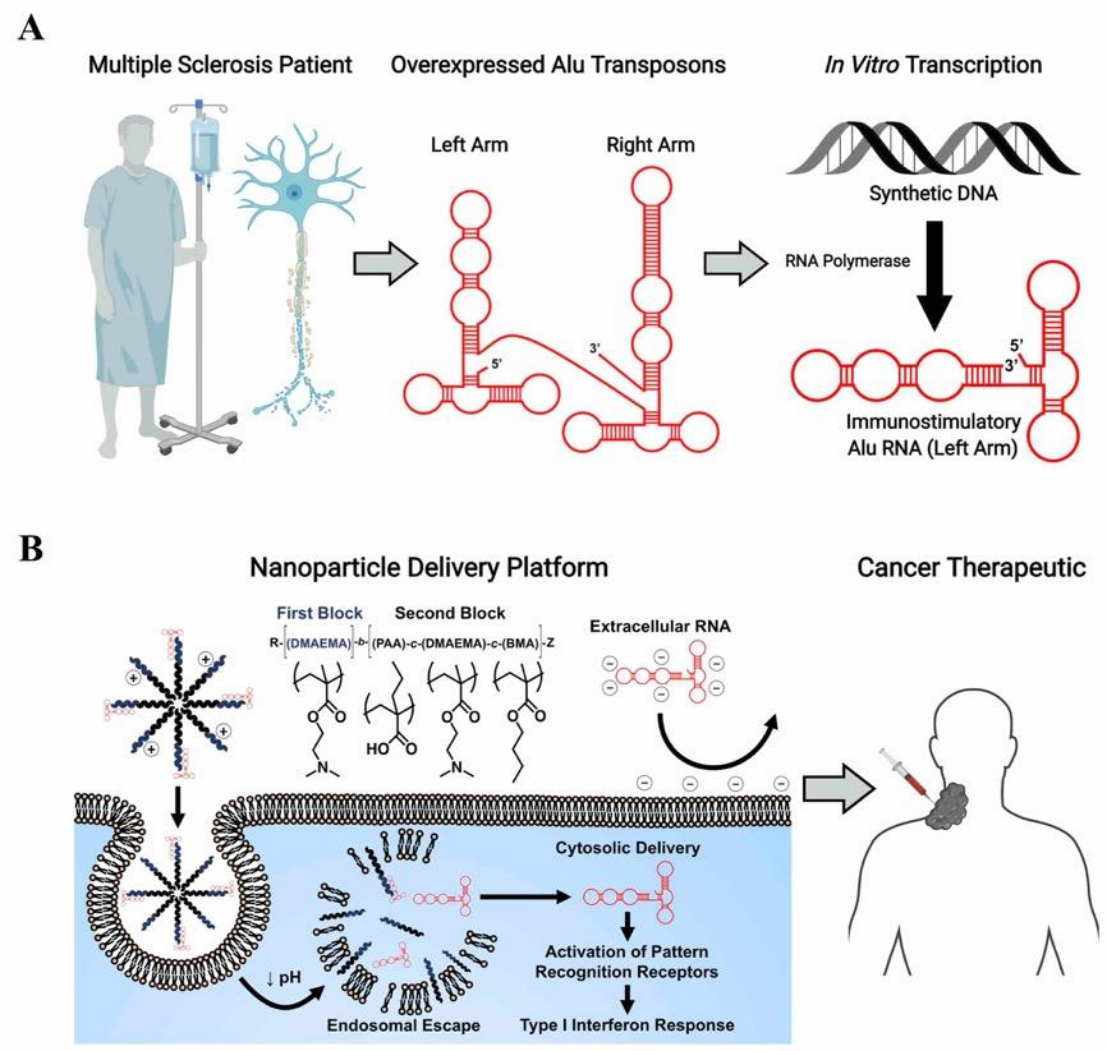

Figure 4.1. Repurposing endogenous Alu RNA for Cancer Immunotherapy. Immunostimulatory Alu RNA has been identified in circulating leukocytes of patients with relapsing remitting multiple sclerosis. *In vitro* transcription of synthetic Alu element DNA can reproduce the immunostimulatory left arm of the Alu RNA, which can then be formulated and delivered with an endosomolytic polymer for enhanced cytosolic delivery and PRR activation. Activation of innate immunity via Alu RNA represents a promising strategy to stimulate antitumor immunity with endogenous immunostimulants.

Results and Discussion

Engineering Alu RNA / Polymer Nanoparticles to Simulate Natural Alu RNA Expression

In their recent work, Aune and colleagues examined structure-function relationships of the highly immunostimulatory AluJb RNA[26]. Since Alu RNAs tend to form two intramolecular

double-stranded structures (*i.e.* left and right arms) separated by an intermediate linker sequence, they sought to determine the importance of each arm in regard to innate immune activation[26]. Each arm was individually *in vitro* transcribed and then screened with the reporter cells for IFN-I and NF-κB activity. It was determined that the left arm of the AluJb RNA conserved the same immunostimulatory capacity as the full sequence, while the right arm was completely inactive. As a result of this finding and coupled with the fact that shorter nucleic acid sequences are generally easier to load and deliver with nanocarriers, the AluJb RNA (Left Arm) was utilized for all of the *in vitro* and *in vivo* experiments investigating the therapeutic application of endogenous Alu RNA.

To explore whether endogenous Alu RNA could be repurposed to stimulate antitumor immunity, immunostimulatory AluJb RNA (Left Arm) was *in vitro* transcribed, and the well-established endosomolytic polymer, D-PDB was employed to mediate intracellular delivery of the innate immune activator (***Figure 4.1***). The synthetic AluJb RNA (Left Arm) was complexed with D-PDB at various N/P charge ratios (*i.e.* molar amount of protonated amines on the polymer corona / molar amount of phosphates on the nucleic acid backbone) to identify the ratio at which AluJb RNA (Left Arm) is fully loaded onto the polymeric micelles. Gel electrophoresis was performed on the resultant complexes (***Figure 4.2-A***), and complete complexation of AluJb RNA (Left Arm) and D-PDB was shown to occur at an N/P charge ratio of 4, which is consistent with previous findings for D-PDB and other nucleic acids[7, 28]. At an N/P charge ratio of 4, AluJb RNA (Left Arm) / D-PDB also demonstrated discrete particle packaging with a uniform particle size distribution centered at ~ 100 nm in diameter (***Figure 4.2-B***). The lack of particle aggregation also agrees with a previous report[434], which indicates that D-PDB and other similarly sized nucleic acids aggregate only at N/P charge ratios less than 4. Accordingly, an N/P charge ratio was used for all subsequent experiments involving AluJb RNA (Left Arm) / D-PDB complexes.

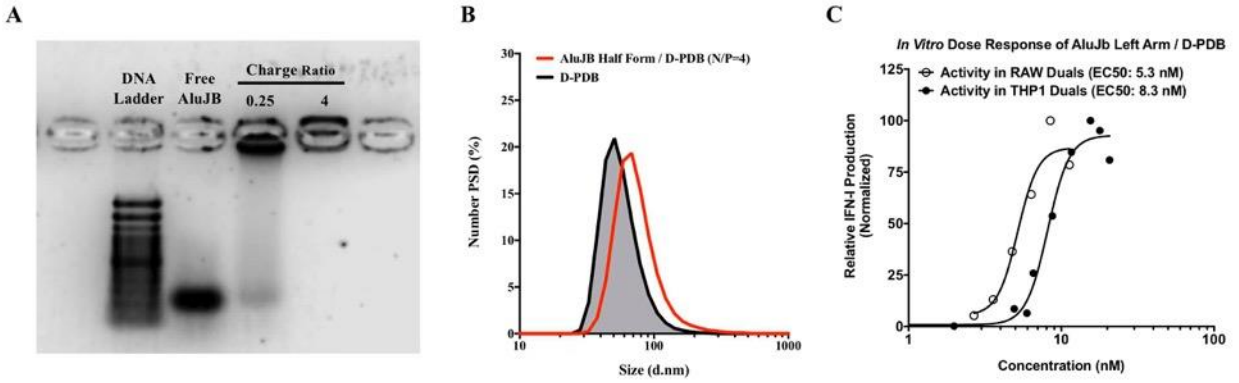

Figure 4.2. In vitro characterization of AluJb RNA (Left Arm) / D-PDB. **(A)** Agarose gel of AluJb RNA (Left Arm) with and without various amounts of D-PDB, as indicated. 1 μg RNA/lane. The TrackIt™ 100 bp DNA Ladder was used for reference. **(B)** DLS analysis of AluJb RNA (Left Arm) / D-PDB relative to D-PDB. **(C)** RAW-Dual and THP1-Dual reporter cell assays of AluJb RNA (Left Arm) / D-PDB. Curves are normalized to their respective maximum value.

The immunostimulatory activity of AluJb RNA (Left Arm) / D-PDB was then investigated using *in vitro* activity assays. AluJb RNA (Left Arm) / D-PDB complexes were administered to IFN-I reporter cells that stably express a secreted luciferase downstream of interferon-stimulated response elements, and 24 hours after treatment, the relative IFN-I production was measured via luminescence (***Figure 4.2-C***). In both murine RAW-Dual macrophages and human THP1-Dual monocytes, the AluJb RNA (Left Arm) / D-PDB complexes demonstrated potent induction of cellular IFN-I production with half-maximal effective concentration (EC50) values of 5.3 nM and 8.3 nM, respectively. These results are in stark contrast to the lack of immunostimulatory activity demonstrated *in vitro* by freely administered AluJb RNA (Left Arm) (***Figures 6.6-C and 6.7-A***). Thus, D-PDB was indeed able to simulate the overexpression of immunostimulatory Alu RNA associated with RRMS via intracellular delivery of AluJb RNA (Left Arm).

Alu RNA / Polymer Nanoparticles Stimulate Innate Immunity

To determine whether the complexes conserved their immunostimulatory activity when administered *in vivo*, AluJb RNA (Left Arm) / D-PDB was injected intratumorally *q3d* in mice bearing B16.F10 tumors, and 6 hours after the second treatment, tumor RNA was collected for qPCR analysis (***Figure 4.3-A***). Gene expression changes were quantified for various proinflammatory cytokines that are known to be associated with RIG-I activation (*i.e. Ifnb1*, *Cxcl10*, *Il6*, and *Tnf*). Intratumorally administered AluJb RNA (Left Arm) / D-PDB elicited significantly increased gene expression of *Ifnb1*, *Cxcl10*, and *Tnf* in the TME. The local expression of *Il6* was also partially elevated relative to PBS-treated tumors ($p = 0.0861$). Thus, AluJb RNA (Left Arm) / D-PDB could indeed stimulate innate immunity at the level of genomic regulation.

Subsequently, B16.F10 IFN-LUC tumors, which express luciferase upon IFN induction, were used to confirm proteomic expression of IFN in the TME and to study the kinetics of signaling in response to intratumorally administered AluJb RNA (Left Arm) / D-PDB (***Figures 4.3-B and 4.3-C***). At various timepoints following treatment, mice were anesthetized, administered D-luciferin, and imaged to quantify luminescent signal. The results demonstrate that AluJb RNA (Left Arm) / D-PDB can indeed stimulate significant IFN production with peak signal detected at 12–24 hours after treatment.

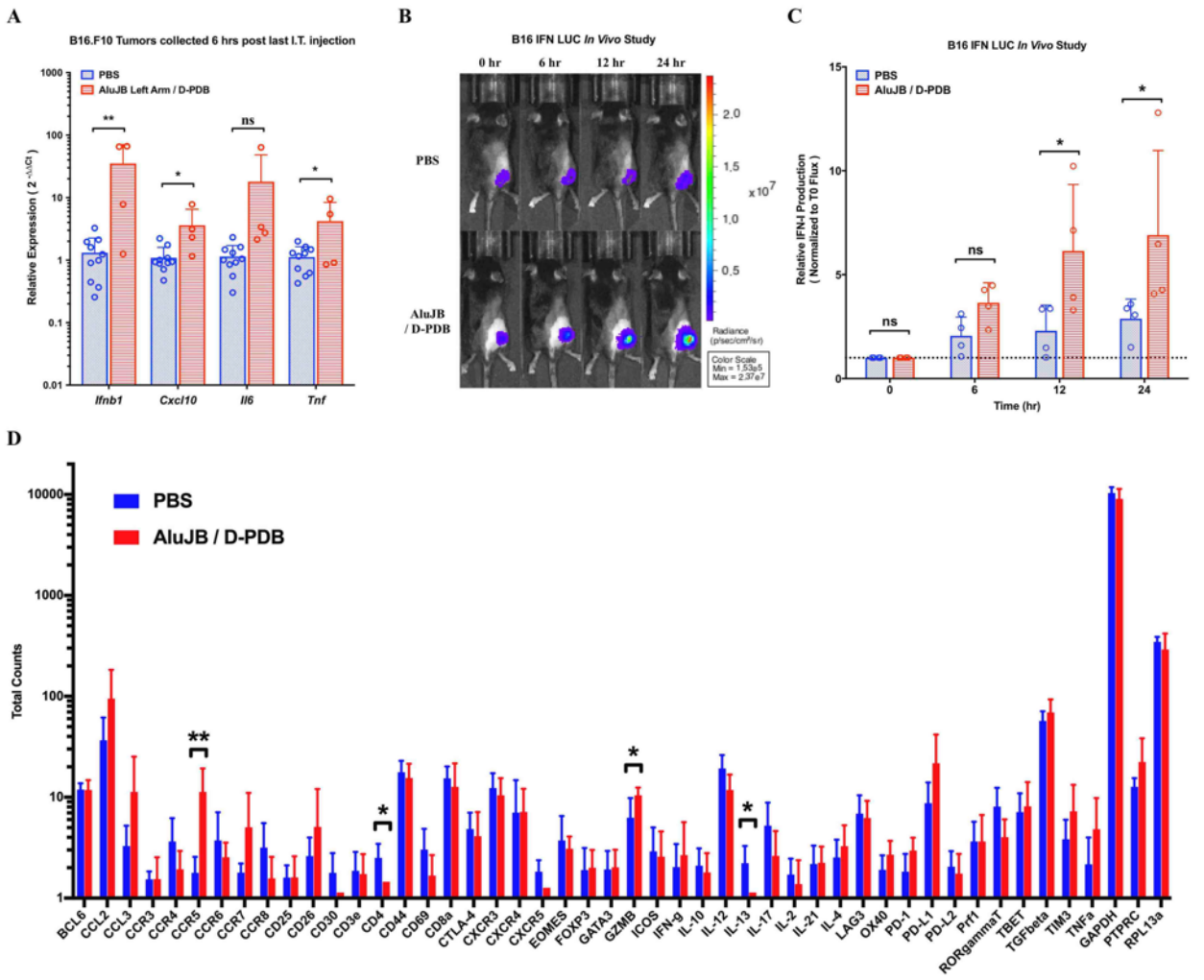

Figure 4.3. Effects of AluJb RNA (Left Arm) / D-PDB on the immune profile of the tumor microenvironment. **(A)** Quantitative polymerase chain reaction (qPCR) analysis of B16.F10 tumors treated intratumorally with 100 µL of either PBS or AluJb RNA (Left Arm) / D-PDB at a dose corresponding to 2 µg RNA. Tumors were harvested 6 hours after the second intratumoral injection of a *q3d* dosing regimen. An unpaired test was used for statistical analysis. **(B)** Representative luminescence IVIS images evaluating tumor IFN activity in C57BL/6J mice bearing B16.F10 IFN-LUC tumors. An intratumoral injection was given as single 100 µL dose of either PBS or AluJb RNA (Left Arm) / D-PDB at a dose corresponding to 2 µg RNA. **(C)** Longitudinal analysis of IFN activity following treatment. A two-way ANOVA with Sidak test was used for statistical analysis. **(D)** NanoString analysis of B16.F10 tumors treated intratumorally with 100 µL of either PBS or AluJb RNA (Left Arm) / D-PDB at a dose corresponding to 2 µg RNA. Tumors were harvested 6 hours after the second intratumoral injection of a *q3d* dosing regimen.

NanoString gene expression analysis was then performed to further characterize the immune profile of the TME following AluJb RNA (Left Arm) / D-PDB treatment (***Figure 4.3-D***). Tumor RNA was collected 6 hours after the second intratumoral treatment of a *q3d* dosing regimen, and the expression of 48 genes was quantified using a NanoString panel for T cell activity. For most genes in the panel, the difference in expression following AluJb RNA (Left Arm) / D-PDB treatment was not statistically significant relative to PBS-treated tumors. However, AluJb RNA (Left Arm) / D-PDB did induce significant upregulation of *Ccr5* and *Gzmb* as well as significant downregulation of *Cd4* and *Il-13*. Thus, some changes in T cell activity are detectable in response to AluJb RNA (Left Arm) / D-PDB treatment. Additionally, differences in the expression of several genes were approaching significance, including *Ccl2* ($p = 0.1211$), *Ccl3* ($p = 0.1583$), *Ccr7* ($p = 0.1757$), *Ox40* ($p = 0.1508$), *Pd-1* ($p = 0.0690$), *Pd-l1* ($p = 0.1249$), *Tim3* ($p = 0.1871$), and *Ptprc* ($p = 0.1418$) for upregulation as well as *Ccr4* ($p = 0.1932$), *Ccr8* ($p = 0.1887$), *Cd30* ($p = 0.1903$), *Cd69* ($p = 0.1697$), *Cxcr5* ($p = 0.0502$), *Il-12* ($p = 0.0651$), *Il-17* ($p = 0.1811$), and *Rorgammat* ($p = 0.0778$) for downregulation. While more T cell associated gene expression changes were expected to follow such innate immune activation, the minimal changes in T cell associated gene expression relative to that of PBS treatment may be explained by temporal dependencies. Indeed, the tumor infiltration of T cells has been shown to peak at 48 hours post IFN-I treatment in various murine models.

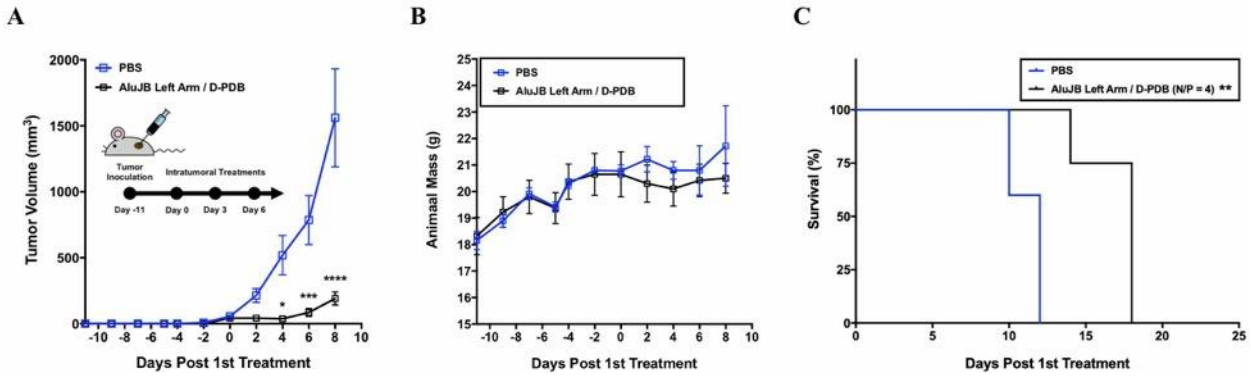

Figure 4.4. AluJb RNA (Left Arm) / D-PDB exerts antitumor effects. **(A)** Tumor growth plot for B16.F10 tumors intratumorally treated with 100 µL of either PBS or AluJb RNA (Left Arm) / D-PDB at a dose corresponding to 2 µg RNA (n = 4 or greater per treatment group). Treatments were administered three times *q3d* as indicated. Tumor growth curves were truncated to the first day that a mouse in any treatment group reached the study endpoint. A two-way ANOVA with Sidak test was used for statistical analysis. **(B)** Total mouse weight over time for the mice with B16.F10 tumors. A two-way ANOVA with Sidak test was used for statistical analysis. **(C)** Kaplan-Meier survival curve for B16.F10 tumors treated with 100 µL of either PBS or AluJb RNA (Left Arm) / D-PDB. Log rank (Mantel-Cox) test was used for statistical analysis.

Alu RNA / Polymer Nanoparticles Exert Antitumor Effects

A cancer therapy study was conducted in the B16.F10 murine melanoma tumor model to determine the therapeutic effect of AluJb RNA (Left Arm) / D-PDB (***Figure 4.4***). Mice bearing B16.F10 murine melanoma tumors were intratumorally treated with either PBS or AluJb RNA (Left Arm) / D-PDB for a total of three injections administered *q3d*. Relative to PBS treatment, AluJb RNA (Left Arm) / D-PDB treatment significantly restricted tumor growth (***Figure 4.4-A***), prolonged survival (***Figure 4.4-B***), and was well-tolerated by the mice as demonstrated by insignificant differences in total murine weight over time (***Figure 4.4-C***). Thus, endogenous Alu RNA can indeed be repurposed in the form of AluJb RNA (Left Arm) / D-PDB to stimulate antitumor immunity and serve as a potent cancer immunotherapeutic.

Conclusion

Endogenous double-stranded Alu RNA was repurposed as a novel cancer immunotherapy from its established role in RRMS-related inflammation. Specifically, immunostimulatory AluJb RNA (Left Arm) was formulated with the endosomolytic polymer, D-PDB to enable the intracellular delivery of RNA and targeted activation of RNA-sensing PRRs. At an N/P charge ratio of 4, AluJb RNA (Left Arm) / D-PDB complexes exhibited high RNA loading and formed uniform nanoparticles (*i.e.* approximately 100 nm in diameter) that could potently activate innate immune signaling pathways as determined with *in vitro* reporter cell assays. Upon intratumoral injection, AluJb RNA (Left Arm) / D-PDB induced changes in the expression of key immune-related genes, which altered the immune profile of the tumor microenvironments and relayed antitumor effects in the B16.F10 murine melanoma tumor model. To the best of our knowledge, this work is the first to demonstrate that immunostimulatory Alu RNAs can be therapeutically delivered with an endosomolytic polymer to stimulate antitumor immune responses.

Materials and Methods

Materials

D-PDB was synthesized via reversible addition-fragmentation chain transfer (RAFT) polymerization as previously described[8]. Alu RNA was reverse-transcribed using synthetic Alu DNA templates (IDT DNA) and MEGAscript SP6 (Invitrogen) in overnight reactions at 37 ºC. Reaction products were treated with Turbo DNase, precipitated with lithium chloride, and purified using the RNeasy MiniElute Cleanup Kit (Qiagen). Alu RNAs were not treated with phosphatases to remove 5′ phosphate groups. Absorbance was determined at 260 nm to quantitate yields. Gel electrophoresis was performed to ensure that the Alu RNAs were of the predicted size.

Nanoparticle Formulation

Lyophilized D-PDB was dissolved in ethanol to 50 mg/mL. Aliquots of this polymer stock were then diluted in phosphate buffer (pH 7.0, 100 mM) to a concentration of 10 mg/mL, allowing the polymer chains to self-assemble into micelles. The 10 mg/mL polymer solution was then concentrated into PBS (pH 7.4; Gibco) through 4 cycles of centrifugal filtration with Amicon® Ultra 0.5 mL Centrifugal Filter Units (Ultracel® - 3K, Regenerated Cellulose 3,000 NMWL; MilliporeSigma) following manufacturer's instructions. The final concentrated polymer solution was collected, and an aliquot was taken to determine the polymer concentration relative to a standard curve. Using a 96-well plate (REF 655180; Greiner Bio-One), the polymer concentration was calculated from UV-vis spectroscopy (Synergy H1 Multi-Mode Microplate Reader; Biotek) based on absorbance at 310 nm. The micelle solution was diluted to 1 mg/mL with PBS and passed through a 0.2 µm Whatman® Puradisc polyethersulfone sterile filter (WHA67801302; MilliporeSigma). A fixed amount of the sterile-filtered polymer stock was then added to an aqueous solution containing a set amount of nucleic acid, which corresponded to the desired N/P charge ratio. Again, note that the first block of the diblock copolymer composed of poly(DMAEMA) is estimated to exhibit 50% protonation at pH 7.4 for the purposes of determining N/P ratios. Upon the addition of the polymer micelles to the nucleic acid, the solution was rapidly mixed by pipetting and then incubated at room temperature for 20 minutes to allow for complete electrostatic complexation.

Nanoparticle Physical Characterization

The hydrodynamic size of the polymeric micelles and RNA/polymer complexes was

determined via digital light scattering (DLS) using the Zetasizer Nano ZS instrument (Malvern Panalytical). Polymer concentrations were normalized to 1 mg/mL and the samples were evaluated at physiological pH 7.4.

2% agarose gels were prepared by dissolving 3 grams of UltraPure™ Agarose powder (16500100; Thermo Fisher Scientific) in 150 mL of 1x TAE buffer that had been diluted with deionized H_2O from a 10x TAE buffer stock (REF 46010CM; Corning). The mixture was microwaved in 30 second intervals until the agarose was fully dissolved. The solution was then cast into a gel. RNA and RNA/polymer complexes were then prepared. The TrackIt™ 100 bp DNA Ladder (Cat. No. 10488058; Thermo Fisher Scientific) was used for reference. Gel electrophoresis was performed at 120 V for 45 minutes. Gels were subsequently stained with SYBR Safe dye (S33102; Thermo Fisher Scientific) for 30 minutes while protected from light and then imaged with a Digital ChemiDoc MP system (Bio-Rad).

Cell Lines

All cell lines were maintained according to supplier specifications and/or technical data sheets. RAW-Dual cells (InvivoGen) were cultured in Dulbecco's Modified Eagle Medium (DMEM; Gibco) supplemented with 2 mM L-glutamine, 4.5 g/L glucose, 10% heat-inactivated fetal bovine serum (HI-FBS; Gibco), 100 U ml^{-1} penicillin / 100 µg ml^{-1} streptomycin (Gibco), and 100 µg/mL Normocin. For the continual selection of these cell lines, Zeocin was added on every other cell passage at a concentration of 200 µg/mL. THP1-Dual cells (InvivoGen) were cultured in Roswell Park Memorial Institute (RPMI) 1640 Medium (Gibco) supplemented with 2 mM L-glutamine, 25 mM HEPES, 10% heat-inactivated fetal bovine serum (HI-FBS; Gibco), 100 U ml^{-1} penicillin / 100 µg ml^{-1} streptomycin (Gibco), and 100 µg/mL Normocin. For the continual

selection of these cell lines, Blasticidin and Zeocin were added after every cell passage at concentrations of 10 µg/mL and 100 µg/mL, respectively. B16.F10 cells (ATCC) were cultured in Dulbecco's Modified Eagle Medium (DMEM; Gibco) supplemented with 2 mM L-glutamine, 4.5 g/L glucose, 10% heat-inactivated fetal bovine serum (HI-FBS; Gibco), and 100 U ml^{-1} penicillin / 100 µg ml^{-1} streptomycin (Gibco). B16.F10 IFN-LUC cells were cultured in Dulbecco's Modified Eagle Medium (DMEM; Gibco) supplemented with 2 mM L-glutamine, 4.5 g/L glucose, 10% heat-inactivated fetal bovine serum (HI-FBS; Gibco), and 100 U ml^{-1} penicillin / 100 µg ml^{-1} streptomycin (Gibco). Puromycin was added after every cell passage at a concentration of 10 µg/mL. All cells lines were tested for Mycoplasma contamination and kept in a humidified environment with 5% CO at 37 °C.

In Vitro Reporter Cell Assays

96-well plates (REF 655180; Greiner Bio-One) were used for screening the RNA/polymer complexes. Reporter cells were seeded at 50,000 cells/well in 100 µL media. When cells became ~ 80% confluent, treatments were administered in 100 µL PBS. Results were collected 24 hours after treatment. The Quanti-Luc™ (InvivoGen) assay was performed on cell supernatants following manufacturer's instructions. Luminescence and absorbance were quantified via plate reader (Synergy H1 Multi-Mode Microplate Reader; Biotek). Luminescence measurements were performed using white, opaque-bottom 96-well plates (REF 655073; Greiner Bio-One). The signal for each sample concentration was determined using 3 biological replicates, each with 3 technical replicates. All reporter cell measurements were normalized by subtracting the average value of a PBS-treated negative control group. All bell-shaped dose response curves were truncated at their plateau. The EC_{50} values were calculated for each of the dose responses using curve fitting analysis

in the GraphPad Prism software.

In Vivo Imaging Experiments

The *in vivo* IFN activity experiment, was performed on the IVIS Lumina III (PerkinElmer). 6-8 week-old C57BL/6 mice (The Jackson Laboratory) were inoculated with B16.F10 IFN-LUC tumors by subcutaneously injecting 1 x 10^6 cells suspended in 100 µL of PBS into the rear right flank. When tumors were ~ 100 mm^3, the mice were administered a single 100 µL intratumoral injection of either PBS or AluJb RNA (Left Arm) / D-PDB at a 2 µg RNA dose. Luminescence was recorded at set time points (*i.e.* 0, 6, 12, and 24 hours). For each timepoint, the mice were administered a dorsal subcutaneous 150 µL injection of 30 mg/mL Pierce™ D-Luciferin, Monopotassium Salt (88293; Thermo Fisher Scientific) reconstituted in PBS, and a luminescence image was captured 15 minutes thereafter. Mice were anesthetized with isoflurane gas and shaved as necessary.

Quantitative RT-PCR and NanoString Analysis

6-8 week-old C57BL/6 mice (The Jackson Laboratory) were inoculated with B16.F10 tumors by subcutaneously injecting 1 x 10^6 cells suspended in 100 µL of PBS into the rear right flank. When tumors were ~ 200 mm^3, the mice were administered a single 100 µL intratumoral injection of either PBS or AluJb RNA (Left Arm) / D-PDB at a 2 µg RNA dose. 6 hours after the intratumoral injection, mice were euthanized and tumors were harvested. Tumors were then homogenized using TissueLyser II (Qiagen), and tumor RNA was isolated using the RNeasy® Plus Mini Kit (Qiagen).

For the qPCR analysis of gene expression, 1 µg of the tumor RNA was reverse transcribed

by an iScript cDNA synthesis kit (Bio-Rad) following the manufacturer's instructions. The qPCR was conducted on the generated cDNA using a Bio-Rad CFX Connect Real-time System, with the threshold cycle number determined by Bio-Rad CFX manager software V.3.0. The following TaqMan gene expression kits (Thermo Fisher Scientific) were used following the manufacturer's instructions: mouse *Ifnb1* (Mm00439552_s1); mouse *Cxcl10* (Mm00445235_ m1); mouse *Tnf* (Mm00443258_m1); mouse *Il6* (Mm00446190_m1); mouse *Ppib* (Mm00478295_m1). Reactions for each gene were performed in technical duplicate for at least 4 biological samples per treatment group, and the threshold cycle numbers were averaged. Gene expression was normalized to the house-keeping gene, *Ppib* and then normalized to the PBS treatment values using the 2^{-ddCt} method of analysis.

For the NanoString analysis of gene expression, 100 ng of RNA isolated from tumor tissue was hybridized to a myeloid panel of target-specific fluorescent barcodes. The hybridized samples were analyzed on the NanoString nCounter MAX Analysis system. Subsequent data processing was performed using the NanoString nSolver data analysis software.

In Vivo Tumor Therapy Experiments

6-8 week-old C57BL/6 mice (The Jackson Laboratory) were inoculated with B16.F10 tumors by subcutaneously injecting 1 x 10^6 cells suspended in 100 µL of PBS into the rear right flank. When tumors were ~ 50 mm^3, the mice were given three 100 µL intratumoral injections administered *q3d* with treatments of either PBS or AluJb RNA (Left Arm) / D-PDB at a 2 µg RNA dose. Tumor volume, total murine mass, and murine well-being were recorded *qod* for the duration of the study. The study endpoint for maximum tumor volume (*i.e.* survival) was 1500 mm^3.

Ethics Statement

All animal experiments were reviewed and approved by the Vanderbilt University Institutional Animal Care and Use Committee (IACUC), and all surgical and experimental procedures were performed in accordance with the regulations and guidelines of the Vanderbilt University IACUC. All mice were maintained at the animal facilities of Vanderbilt University under pathogen-free conditions.

Statistical Analysis

The significance for each experiment was determined as indicated in the corresponding figure caption. Statistical analyses were performed using GraphPad Prism software, version 7.0c. The plotted values represent the experimental means, and the error bars represent one standard deviation (SD), except for those in the tumor growth plots, which represent one standard error of the mean (SEM). **** $p < 0.0001$, *** $p < 0.005$, **$p < 0.01$, * $p < 0.05$. ns, not significant.

CHAPTER V

PLGA MICROPARTICLE DEPOTS

Text for Chapter V is adapted from:

Garland KM, Sevimli S, Kilchrist KV, Duvall CL, Cook RS, Wilson JT. Microparticle Depots for Controlled and Sustained Release of Endosomolytic Nanoparticles. *Cel. Mol. Bioeng.* 12, 429–442 (2019). PMID: 31719925

Abstract

Nucleic acids have gained recognition as promising immunomodulatory therapeutics. However, their potential is limited by several drug delivery barriers, and there is a need for technologies that enhance intracellular delivery of nucleic acid drugs. Furthermore, controlled and sustained release is a significant concern, as the kinetics and localization of immunomodulators can influence resultant immune responses. Here, we describe the design and initial evaluation of poly(lactic-*co*-glycolic) acid (PLGA) microparticle (MP) depots for enhanced retention and sustained release of endosomolytic nanoparticles that enable the cytosolic delivery of nucleic acids. Endosomolytic *p*[DMAEMA]$_{10kD}$-*bl*-[PAA$_{0.3}$-*co*-DMAEMA$_{0.3}$-*co*-BMA$_{0.4}$]$_{25kD}$ diblock copolymers were synthesized by reversible addition-fragmentation chain transfer polymerization. Polymers were electrostatically complexed with nucleic acids and resultant nanoparticles (NPs) were encapsulated in PLGA MPs. To modulate release kinetics, ammonium bicarbonate was added as a porogen. Release profiles were quantified *in vitro* and *in vivo* via quantification of fluorescently-labeled nucleic acid. Bioactivity of released NPs was assessed using small interfering RNA (siRNA) targeting luciferase as a representative nucleic acid cargo. MPs were incubated with luciferase-expressing 4T1 (4T1-LUC) breast cancer cells *in vitro* or administered intratumorally to 4T1-LUC breast tumors, and silencing via RNA interference was quantified via

longitudinal luminescence imaging. Endosomolytic NPs complexed to siRNA were effectively loaded into PLGA MPs and release kinetics could be modulated *in vitro* and *in vivo* via control of MP porosity, with porous MPs exhibiting faster cargo release. In vitro, release of NPs from porous MP depots enabled sustained luciferase knockdown in 4T1 breast cancer cells over a five-day treatment period. Administered intratumorally, MPs prolonged the retention of nucleic acid within the injected tumor, resulting in enhanced and sustained silencing of luciferase relative to a single bolus administration of NPs at an equivalent dose. This work highlights the potential of PLGA MP depots as a platform for local release of endosomolytic polymer NPs that enhance the cytosolic delivery of nucleic acid therapeutics.

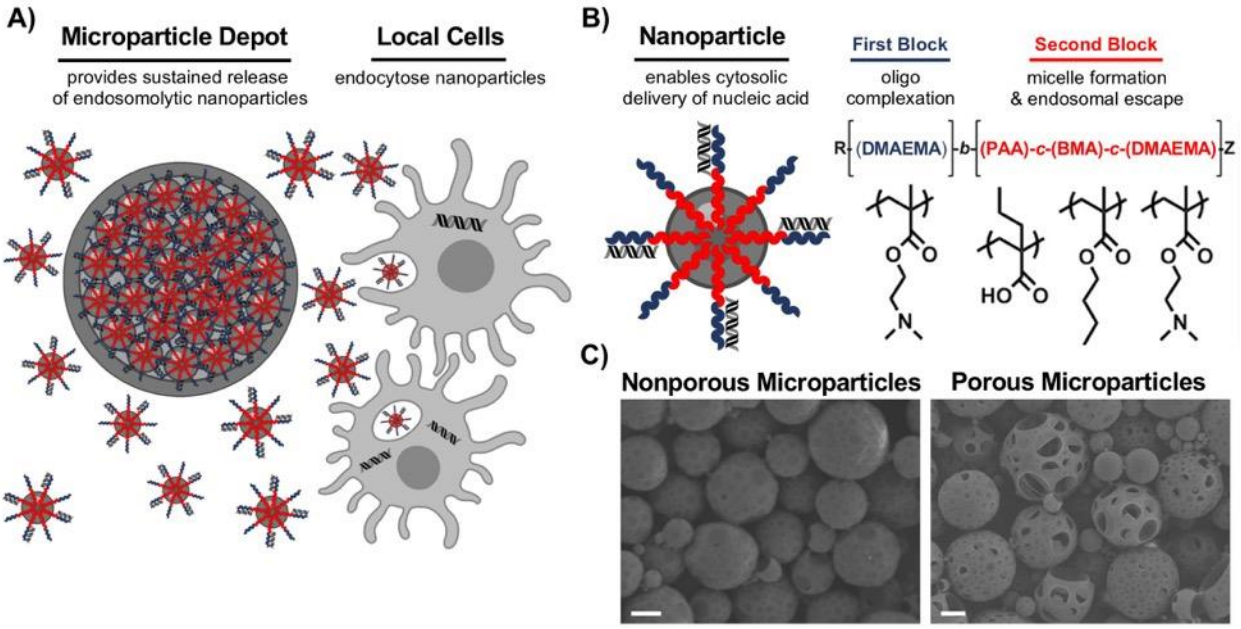

Figure 5.1. PLGA microparticle depots for controlled release of endosomolytic nanoparticles. **(A)** PLGA MP depots mediate local nanoparticle release and subsequent intracellular delivery of nucleic acid to local cell populations. **(B)** Structure and composition of the endosomolytic diblock copolymers used for cytosolic nucleic acid delivery. **(C)** Representative scanning electron microscopy (SEM) images of nonporous microparticles (left) and porous microparticles (right). Scale: 3 μm.

Introduction

Nucleic acids have emerged as a promising class of immunotherapeutics with potential to treat numerous diseases, including infections, inflammation, autoimmunity, and cancer[362, 435-440]. This broad and versatile class of biomacromolecular drugs can be leveraged to both activate and suppress the immune system. Notably, short-interfering RNA (siRNA) can be utilized to selectively inhibit expression of specific immunoregulatory proteins through RNA interference (RNAi)[6, 435, 436, 441, 442], allowing for precision tailoring of immune responses. Additionally, nucleic acids that chemically or structurally mimic pathogenic genetic material can be harnessed to activate the innate immune system by targeting various nucleic acid sensing pathways, which have evolved to detect viral or bacterial invasion[4, 362, 437-440, 443]. Nucleic acids have been widely explored as adjuvants to bolster responses to vaccines,[444] and more recently as cancer immunotherapeutics that initiate inflammatory programs at tumor sites to stimulate antitumor immunity.[204, 445] Despite their immense promise as immunomodulators, the clinical advancement of nucleic acid therapeutics has been relatively modest due to a multitude of challenges that hinder drug efficacy and/or patient safety[446, 447].

Inefficient intracellular delivery is a significant barrier to efficacy that is shared across virtually all types of nucleic acid therapeutics[6, 442, 447-450]. Nucleic acids do not passively diffuse across the plasma membrane, are cleared rapidly after administration, and are endocytosed with relatively low efficiency. Additionally, while several immunostimulatory nucleic acids (*e.g.* CpG DNA, poly(I:C)) act through receptors residing in endosomal membranes, a larger number must access cytosolic targets to exert their immunoregulatory effects. This includes more common classes of nucleic acid therapeutics that can be leveraged for immunotherapy, such as siRNA, miRNA, and mRNA, but also an emerging family of immunostimulatory agents that engage

cytosolic pattern recognition receptors (PRRs), such as RIG-I, MDA-5, cGAS, and STING.[27, 28, 204] This pervasive challenge has led to the widespread development of synthetic nucleic acid carriers that enhance cellular uptake and promote endosomal escape of associated cargo[451-453]. Our group, and others, have recently utilized pH-responsive, endosomolytic polymer nanoparticles (NPs) to enhance the cytosolic delivery and activity of siRNA and immunostimulatory 5'-triphosphate RNA[27, 28, 454, 455]. These NPs are assembled using amphiphilic diblock copolymers that self-assemble into micelles with a cationic dimethylaminoethyl methacrylate (DMAEMA) corona for electrostatic complexation of nucleic acids, and a pH-responsive, endosomolytic core comprising DMAEMA, butyl methacrylate (BMA), and propylacrylic acid (PAA) (***Figure 5.1-B***)[7, 454]. While highly efficient at cytosolic delivery, the cationic corona has restricted the use of such NPs to local delivery applications, including tissue regeneration, vaccine delivery, and intratumoral cancer immunotherapy[28, 375, 382, 456].

While systemic administration of nucleic acid therapeutics is necessary for many applications, directed, local delivery circumvents critical systemic delivery barriers and ensures sufficiently high doses reach target tissues, while also reducing systemic side effects[453, 457]. Indeed, local delivery is commonly used, and often preferred, for many immunotherapeutics, the most salient example being vaccines, which are delivered intradermally or intramuscularly[458, 459]. Additionally, image-guided, direct injection into lymph nodes (intranodal), considered the "command centers" of an immune response, is used clinically for treatment of allergy[460]. Finally, intratumoral injection of immunotherapeutics, including several different nucleic acids, has become increasingly prevalent in recent clinical trials among substantial preclinical evidence that local immunotherapy can generate systemic immunity capable of eliminating distal, untreated tumors (*e.g.* abscopal effect)[461, 462]. However, for nearly all of these applications, multiple, repeated

injections are necessary to stimulate desired immune responses and attendant therapeutic activitiy.[463-465] This requirement for multiple injections can pose a significant practical challenge for both physicians and patients and, in some cases, may not be feasible. Additionally, the timing, dose, and localization of immunomodulators plays a critical role in determining the magnitude and phenotype of the resultant immune response[14, 116, 466-468]. Yet, locally administered biomacromolecules, including nucleic acids, typically rapidly clear from the injection site, which not only limits local bioavailability but can also result in systemic distribution with an increased risk of toxicity[463, 464, 469]. These challenges have motivated the development of delivery technologies for controlled and sustained release of nucleic acid immunotherapeutics[470-475]. These drug delivery depots can be either injectable or implantable scaffolds or microparticles, and are typically composed of biodegradable materials that release cargo in a controlled and sustained manner[476]. Depots can also be engineered to exhibit a wide variety of drug release profiles by altering their chemical and physical properties[477].

The NP system used here has been previously used in sustained and controllable release scaffolds aimed toward wound healing applications[380, 382, 478]. Here, we describe an intratumorally-injectable nanoparticle-in-microparticle strategy for controlled, localized delivery of cytosolically-active nucleic acid therapeutics. Poly(lactic-*co*-glycolic) (PLGA) microparticle (MP) depots were designed for sustained release of endosomolytic NPs that can mediate the cytosolic delivery of various nucleic acids, exemplified here by intratumoral delivery of siRNA. Through enhanced retention, controlled and sustained release, and prolonged functionality of encapsulated NPs, this approach offers a simple and potentially universally applicable strategy for achieving enhanced spatial and temporal control of nucleic acid delivery for applications in immunotherapy.

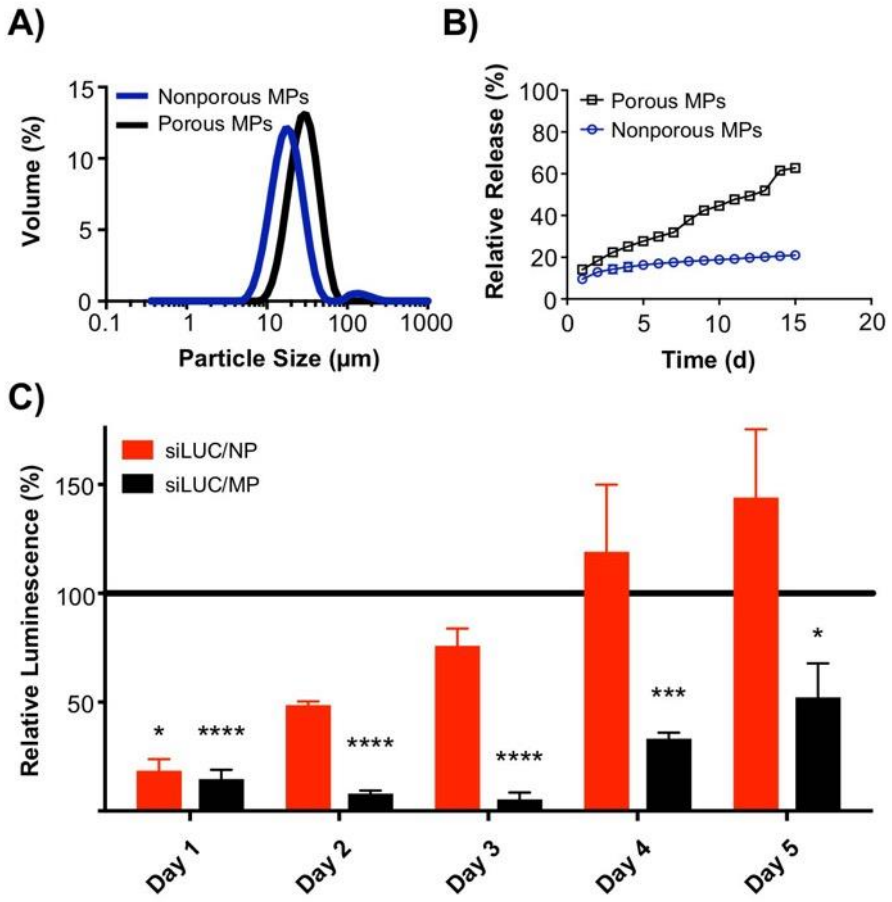

Figure 5.2. In vitro characterization of PLGA microparticle depots. **(A)** Particle size distribution of nonporous and porous MPs determined by laser diffraction particle sizing. **(B)** *In vitro* release profiles of NPs from porous and nonporous MP depots over a 15 day period. **(C)** Longitudinal analysis of luciferase silencing in 4T1-LUC breast cancer cells treated with a single administration of either free NPs or porous MPs. The NP treatments were removed after 24 hours, while MPs were left in coculture with the cells throughout the experiment to mimic biological residence. Luminescent signal for each treatment group was normalized to that of an analogous treatment containing scrambled negative control RNA substituted for luciferase siRNA.

Results and Discussion

Design and In Vitro Characterization of PLGA Microparticle Depots

To generate depots for controlled release of cytosolically-active nucleic acids, we encapsulated endosomolytic polymer NPs complexed with nucleic acid (either double-stranded DNA or siRNA) within MPs of PLGA, a biocompatible, hydrolytically-degradable, and commonly

used biomaterial for local and sustained therapeutic drug delivery[479-489]. PLGA MPs were synthesized using DCM as a nonpolar, volatile organic solvent and PVA as a surfactant in a $W_1/O/W_2$ double emulsion as previously described[490-493]. Sonication and homogenization were employed after the primary and secondary emulsions, respectively. NPs were incorporated into the W_1 aqueous phase, resulting in a drug loading of approximately 1.8 ± 0.05 µg nucleic acid per mg PLGA and an encapsulation efficiency of about 75 ± 2%. To generate porous MPs with a faster release profile, the effervescent salt ammonium bicarbonate was added to the W_1 aqueous phase. Following PLGA MP synthesis, SEM imaging was performed to characterize MP morphology, which confirmed that ammonium bicarbonate was an effective porogen for NP-loaded PLGA MPs (***Figure 5.1-C***). Laser diffraction size analysis was used to quantitatively characterize the particle size distribution (***Figure 5.2-A***). Nonporous MPs and porous MPs had an average diameter of 21.21 µm and 28.33 µm, respectively. An *in vitro* release assay was performed to characterize the release profiles of NPs from PLGA MP depots with varying porosity (***Figure 5.2-B***). As expected, the addition of pores and the associated increase in surface area within PLGA MPs resulted in faster release of the NP cargo, likely reflecting the shorter diffusion distance for release. While cationic excipients, such as polyethyleneimine or polyamines, have been incorporated into PLGA to increase nucleic acid loading and intracellular delivery[494-497], this represents the first demonstration of a PLGA MP depot used for sustained release of endosomolytic nanoparticles that enhance cytosolic nucleic acid delivery.

In Vitro RNAi Luciferase Silencing

An *in vitro* RNAi protein knockdown assay was performed to demonstrate that PLGA MP depots could sustain the release and biological activity of nucleic acid-loaded NPs (***Figure 5.2-C***).

As a model nucleic acid cargo, siRNA specific for luciferase (siLUC) or a scrambled negative control siRNA (siNC) were complexed with D-PDB micelles (siRNA/NP) and loaded into porous MPs (siRNA/MP). 4T1-LUC breast cancer cells, engineered to constitutively express luciferase, were treated with free NP or porous MPs each complexed to either siLUC or siNC at 50 nM siRNA per well. Free NPs were removed after 24 hours to approximate a transient residence time at an injected site, whereas cells were incubated with MP depots for an additional four days. Bioluminescence imaging was used to quantify luciferase expression each day, following an administration of D-luciferin. While comparable silencing was observed between free siLUC/NP and siLUC/MP after 1 day (~75% knockdown), continuous incubation with depots resulted in significantly greater knockdown on days 2-5. The luciferase expression of the cells treated for 24 hours with siLUC/NP returned to near baseline intensity within 3 days. Due to the short doubling time of 4T1 cells, cultures approached confluence within 5 days, which precluded evaluation of knockdown at later timepoints. Nonetheless, these data demonstrate the capacity of PLGA MP depots to sustain the release and silencing activity of encapsulated siRNA/NP complexes.

Cytotoxicity is a well-established challenge of all polycationic nucleic acid delivery platforms that can indeed limit their utility in local delivery applications. However, this may be advantageous or detrimental depending on the intended application of the system; for example, in an intratumoral setting, some toxicity can galvanize cancer cell antigen release and may therefore be beneficial toward priming an anti-cancer immune response. Notably, we observed similar expression of bioluminescence in both the NP and MP negative control groups, suggesting that there is no difference in cell viability between the various treatments and that the PLGA used to entrap the NPs does not contribute to cellular toxicity, which is consistent with its high cytocompatibility.

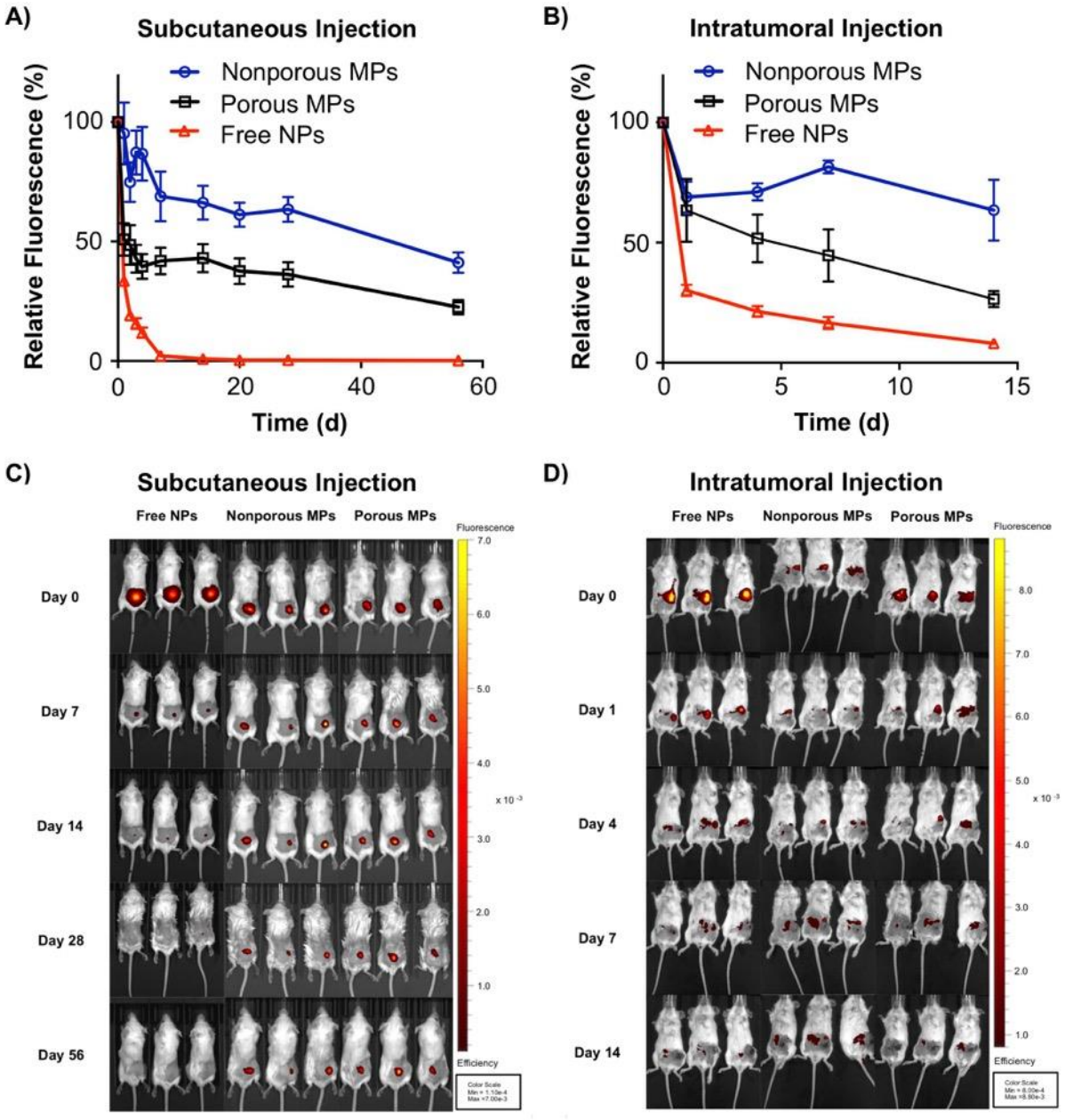

Figure 5.3. In vivo retention and release of NPs from PLGA microparticles. *In vivo* analysis of injection site localization of free NPs, nonporous MP depots, and porous MP depots in BALB/c mice. **(A)** Relative fluorescence of Alexa Fluor® 647(A647)-labelled dsDNA cargo injected subcutaneously and monitored over 56 days. **(B)** Relative fluorescence of Alexa Fluor® 647-labelled dsDNA cargo, releasing from an intratumoral injection site over 14 days. The fluorescent efficiency of each mouse was captured by IVIS imaging and was normalized to the respective initial (day 0) fluorescence. **(C)** Representative IVIS images of mice bearing subcutaneously administered particles containing fluorescent dsDNA (Red). **(D)** Representative IVIS images of the mice treated intratumorally with particles containing fluorescent dsDNA (Red).

In Vivo Nanoparticle Release from PLGA Microparticle Depots

To monitor NP release and retention *in vivo*, NPs were electrostatically complexed with a fluorescently-labeled double-stranded DNA (dsDNA/NP) and then loaded into PLGA MP depots (dsDNA/MP). Fluorescent dsDNA was used as representative cargo as it is a cost-effective analog to other nucleic acid sequences of similar length such as fluorescent siRNA. Free dsDNA/NP, nonporous dsDNA/MP, and porous dsDNA/MP were administered subcutaneously (s.c.) at a dose of 10 μg DNA (0.5 mg/kg) into BALB/c mice, and fluorescence was monitored with an *in vivo* imaging system (IVIS) to track the retention of dsDNA at the injection site (***Figures 5.3-A and 5.3-C***). Free dsDNA/NP rapidly cleared the injection site, with >50% clearance within 24 hours and undetectable levels present by 5 days. By contrast, both MP depots enhanced retention and sustained release of dsDNA/NP, with porous depots demonstrating faster release than analogous nonporous depots, particularly within the first week of administration. Gradual release from both depots was observed over the following month with significant fluorescence still evident at day 56.

We also evaluated NP retention in the context of intratumoral (i.t.) delivery, which is increasing in use both preclinically and clinically as an administration route for cancer immunotherapeutics, including several nucleic acid drugs[498-500]. Here, we administered free dsDNA/NP, nonporous dsDNA/MP, and porous dsDNA/MP into 50 mm^3 4T1 tumors growing in the inguinal mammary fat pad, fluorescence was monitored within the tumor over time with intravital fluorescence imaging via IVIS. Similar to the release profiles observed with s.c. administration, MP depots enabled sustained release of dsDNA/NP over a two-week period, the longest possible time-frame based on the endpoint tumor volume (~1500 mm^3). Again, the porous MP depots exhibited faster release with ~75% of cargo cleared within two weeks, whereas minimal

release from nonporous MPs was observed (***Figures 5.3-A and 5.3-B***). Notably, despite their cationic surface charge, free dsDNA/NP drained quickly with >60% of nucleic acid cleared from the tumor site within 24 hours. This rapid clearance may in part explain the need for multiple injections when using these or similar NPs for localized intratumoral delivery of siRNA or 5'ppp-RNA ligands of RIG-I[27, 28]. Moreover, these data add to a large body of evidence indicating that the fate of most intratumorally administered nanoparticles and/or macromolecular therapeutics is a short and often suboptimal intratumoral half-life followed by ultimate systemic clearance. This also further motivates the design of implantable or injectable depots for intratumoral administration[501, 502] or the incorporation of ligand to tether agents to local cells and/or extracellular matrix[503, 504].

In Vivo RNAi Luciferase Silencing

Based on their capacity to release ~50% of NP cargo into tumors within one week, we evaluated the ability of porous MP depots to sustain activity of a nucleic acid therapeutic, here, siRNA targeting luciferase. Inspired by several ongoing clinical trials exploring intratumoral immunotherapy[462, 498-500], intratumoral injections were employed for protein knockdown studies to demonstrate the utility of PLGA MP depots in a cancer setting. While subcutaneous injections are undoubtedly easier for physicians to perform, recent advances in surgical intervention have made intratumoral injections more practical, as almost every site in the human body can be biopsied and therefore injected[16]. Thus, both administration routes explored within the retention studies have potential for clinical translation. To evaluate luciferase knockdown, mice with 4T1-LUC tumors growing in the inguinal mammary fat pad were intratumorally administered a single 10 μg siRNA dose (0.5 mg/kg) of siLUC/NP either free or loaded into depots (siLUC/MP); siNC/NP and

siNC/MP were used as negative controls. IVIS imaging of both luminescence and fluorescence demonstrated a qualitatively high degree of co-localization between siLUC/NP and tumor cells (***Figure 5.4-B***), and MPs could also be identified within cyrosections of resected tumors (***Figure 5.4-A***). Using longitudinal IVIS imaging, we also quantified bioluminescence to determine the degree of luciferase knockdown from the anti-luciferase siRNA cargo 1-4 days post-intratumoral injection (***Figure 5.4-C***). We found that porous MP depots loaded with siLUC/NP resulted in ~50% reduction in luminescent signal relative to analogous depots loaded with siNC/NP control complexes. By contrast, at a 10 μg siRNA dose, no luciferase knockdown was observed using free siLUC/NP, potentially reflecting the relatively short half-life of NPs within the tumor after local administration. Collectively, these data demonstrate that increasing intratumoral residence time of nucleic acid therapeutics via sustained release can enhance and prolong biological activity.

In these studies, we utilized PLGA MPs as a depot for siRNA/NP owing to their favorable biocompatibility and tunable biodegradability. However, inefficient loading of hydrophilic cargo during the $W_1/O/W_2$ emulsion synthesis is a known limitation of PLGA depots, which we found to be the case as well for the loading of NPs (~1.8 μg oligonucleotide per mg PLGA). This necessitates delivery of a relatively high volume of MPs to obtain relevant doses of NPs in the context of RNAi, which may restrict the applications of this approach. While we achieved ~50% luciferase silencing over three days using a single dose of MPs, further enhancements may be achieved using doses higher than those employed herein, which were restrained by the volume of MPs that could be physically injected into 4T1 tumors. Therefore, for cancer therapy applications, PLGA MP depots for NP release may be better suited for localized delivery into tumor resection cavities that can be filled with a larger volume of MPs. To establish proof-of-concept, we used siRNA as a well-established model nucleic acid cargo throughout our investigations, but in

principle this approach can be used for local and sustained delivery of any cytosolically-active nucleic acid, including immunostimulatory agonists such as 5'ppp-RNA RIG-I ligands[28] or immunostimulatory DNA ligands of cGAS[204]. However, exploration of these promising immunotherapeutics is at a stage of relative infancy, and therefore much remains to be elucidated regarding dose and treatment regimens that result in optimal efficacy. Nonetheless, PLGA MP depots for release of endosomolytic NPs offer a promising strategy for enhancing the cytosolic delivery of such nucleic acids and locally sustaining their bioavailability and immunostimulatory activity *in vivo*.

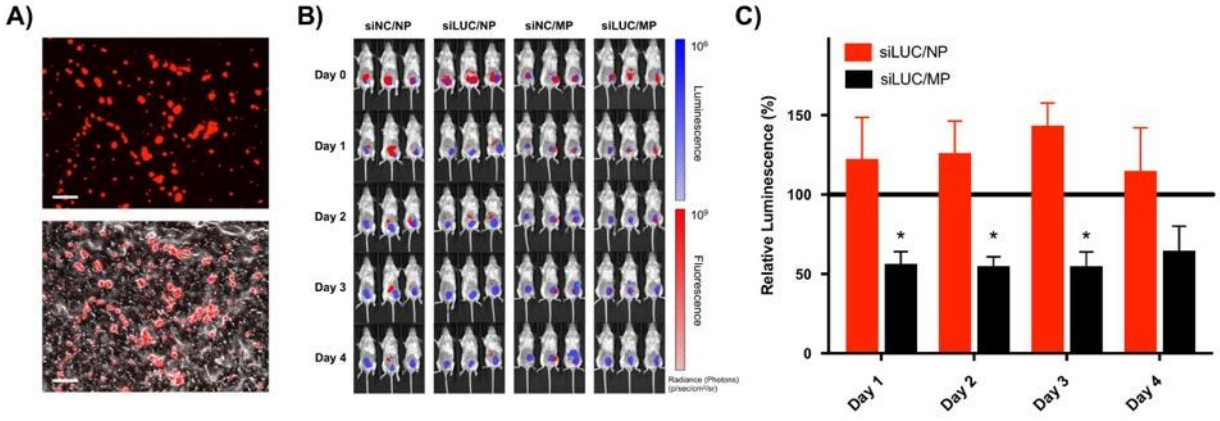

Figure 5.4. In vivo activity of PLGA microparticle depots for siRNA delivery. *In vivo* activity of free NP and porous MPs delivering Alexa Fluor® 647 siRNA cargo was investigated in an orthotopic 4T1-LUC breast cancer model. **(A)** Fluorescent (top) and overlaid fluorescent and bright field (bottom) images of cyrosections of tumor tissue following intratumoral injection of porous MPs. Scale: 75 µm. **(B)** Representative IVIS images of mice bearing luciferase-expressing 4T1-LUC cells (Blue), treated intratumorally with fluorescent RNA (Red). **(C)** Longitudinal analysis of luciferase silencing in a 4T1-LUC breast cancer tumor model treated with a single intratumoral injection of either free NPs or porous MPs. Luminescent signal for each treatment group was normalized to that of an analogous treatment containing scrambled negative control RNA substituted for luciferase siRNA.

In Vivo Therapy Study

To investigate potential therapeutic efficacy, PLGA MPs were loaded with previously described immunostimulatory 3pRNA / D-PDB nanoparticles[27, 28] and characterized for both *in vitro* and *in vivo* activity (***Figure 5.5***). In a longitudinal THP1-Dual reporter cell assay for IFN-I production, PLGA-3pRNA demonstrated peak activity 4 days after the initiation of a coculture treatment, while a pulse-chase administration of ITNP-3pRNA (*i.e.* cells washed 24 hours after treatment), which was intended to mimic the rapid clearance that such particles experience *in vivo*, resulted in peak activity at 24 hours post treatment (***Figure 5.5-A***). Moreover, at each timepoint from Day 4 post treatment to Day 10 post treatment, cells treated with PLGA-3pRNA exhibited greater activity than that of ITNP-3pRNA. Thus, PLGA-3pRNA can enable sustained high levels of IFN-I activity over time, while ITNP-3pRNA induces acute IFN-I production, lasting only 2–3 days.

4T1-LUC tumors were then employed to characterize PLGA-3pRNA as an intratumoral treatment. PLGA-3pRNA had no significant effect on tumor growth relative to both PBS and PLGA-NC as demonstrated by insignificant differences among the treatment groups for both tumor volume over time (***Figure 5.5-B***) and tumor luminescence over time (***Figure 5.5-C***). The treated mice can be visualized in the overlaid luminescence and fluorescence IVIS images that are indicative of 4T1-LUC tumor volume and fluorescently labelled 3pRNA colocalization, respectively (***Figure 5.5-D***). Notably, the IVIS images clearly demonstrate a major limitation for luminescence imaging tumors with injection site scabbing and ulcerations. The luminescent signal substantially dropped in the mice that developed such issues, despite their tumors continuing to increase in size. Indeed, injection site scabbing and ulcerations developed over time and were most pronounced on Day 8 post treatment. It should be noted that luminescent signal is weaker than the

fluorescent signal of many fluorophores (*e.g.* Alexa Fluor 647). Thus, while scabbing and ulcerations can block luminescent signal and limit the period of time that luminescence can be accurately quantified, a strong fluorescence signal can more easily penetrate such obstacles and thereby enable retention analysis for a longer period of time.

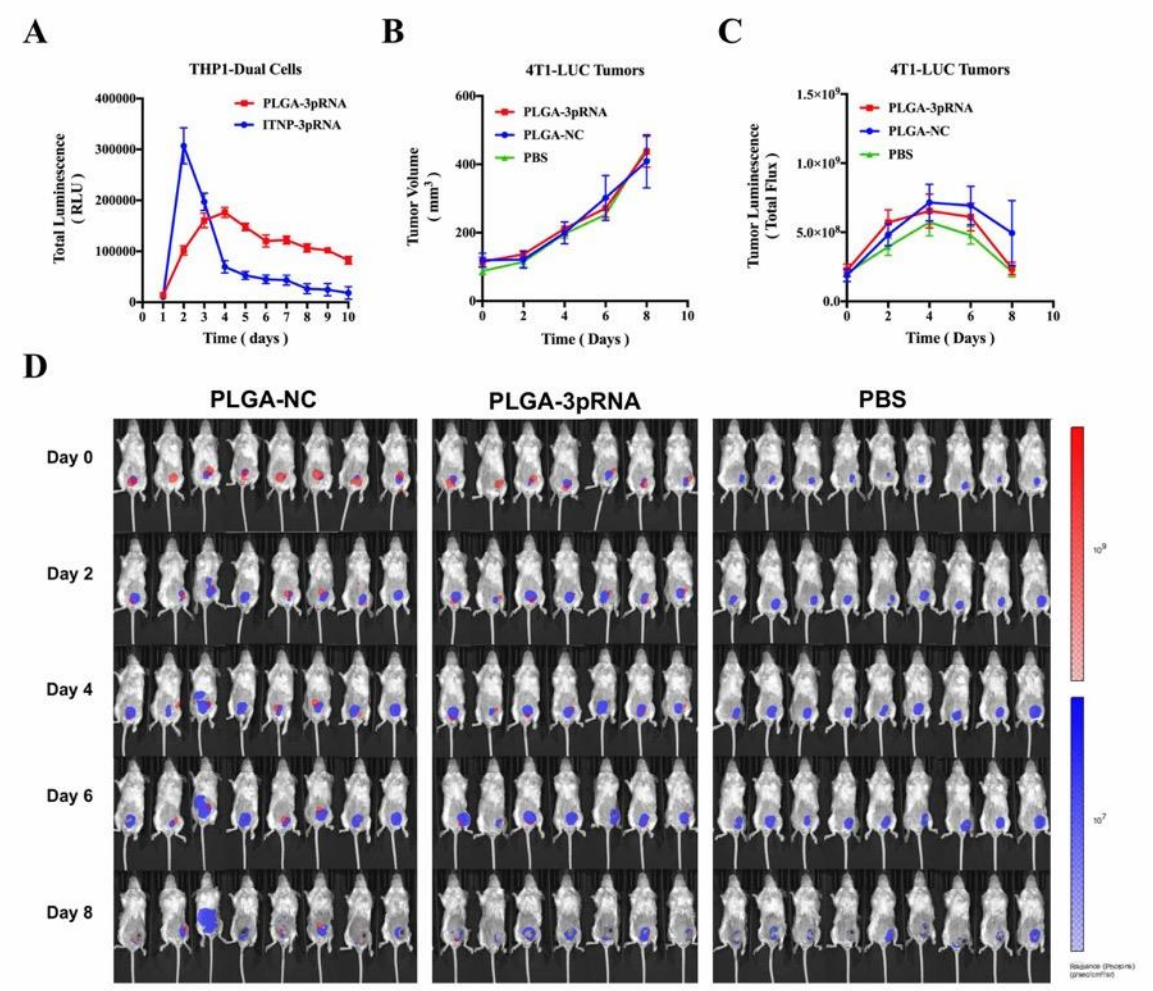

Figure 5.5. Immunostimulatory activity of PLGA microparticle depots loaded with 3pRNA / D-PDB. **(A)** Longitudinal THP1-Dual reporter cell assay of PLGA-3pRNA and ITNP-3pRNA. **(B)** Tumor growth plot for BALB/c mice bearing 4T1-LUC tumors following a single 100 µL intratumoral injection of PBS, PLGA-NC, or PLGA-3pRNA at a dose corresponding to 10 µg RNA. A two-way ANOVA with Tukey test was used for statistical analysis. **(C)** Longitudinal analysis of constitutive luciferase expression from the intratumorally treated 4T1-LUC tumors. **(D)** Overlaid luminescence (blue) and fluorescence (red) IVIS images evaluating 4T1-LUC tumor growth and 3pRNA colocalization in the BALB/c mice following intratumoral treatment.

While ITNP-3pRNA has demonstrated therapeutic efficacy in the 4T1 murine breast cancer model[27], PLGA-3pRNA did not exert detectable antitumor effects in the 4T1-LUC tumors, suggesting that this PLGA delivery platform may not be well-suited for this particular innate immune agonist and/or this tumor model. The lack of efficacy demonstrated by PLGA-3pRNA in the 4T1-LUC tumor model may possibly be attributable to dosing (*i.e.* too low of a dose for efficacy), which was limited by the drug loading capacity of the PLGA MPs coupled with the maximum possible intratumoral injection volume of ~ 100 µL. Accordingly, this delivery platform may be better suited for localized delivery into tumor resection cavities that can be filled with a larger volume of MPs and therefore a greater dose of NPs. Additionally, undesirable immunological effects may have arisen from altered RIG-I activation kinetics and/or changes to the cellular distribution of the 3pRNA, which could have occurred as a result of the PLGA-mediated delivery. Thus, PLGA MPs formulated to enable the sustained local release of other innate immune activators (*e.g.* NanoISD) that operate through distinctly different signaling pathways still have potential to demonstrate therapeutic efficacy in the 4T1-LUC tumor model.

Conclusion

Localized delivery of cytosolically-active nucleic acids offers a promising approach for spatiotemporal modulation of immune responses with broad potential applicability in the treatment of many diseases. However, efficacy in this setting is limited by inefficient cytosolic delivery as well as rapid clearance from the administration site. To address these challenges, we developed a nano-in-microparticle delivery platform using PLGA MPs as a depot for the controlled release of endosomolytic NPs that promote cytosolic delivery of electrostatically complexed nucleic acid cargo. Using siRNA as a model therapeutic, we demonstrated that the rate of release of siRNA/NP

complexes both *in vitro* and *in vivo* could be increased using ammonium bicarbonate as a porogen during the fabrication process. Importantly, we found that release of siRNA/NP complexes from PLGA MP depots resulted in sustained protein silencing *in vitro* as well as in an orthotopic murine breast cancer model via intratumoral administration. The observed 50% protein knockdown in breast cancer tumors may indeed be sufficient for delivery of an immunomodulatory agent where only a portion of cells within a tumor need to be stimulated in order to produce a more immunogenic tumor microenvironment. Accordingly, these studies demonstrate that controlled release of endosomolytic nanoparticles from porous MP depots may offer an enabling strategy for controlled and localized delivery of nucleic acid therapeutics that target cytosolic immunoregulatory machinery. Thus, while PLGA MPs designed to target the RIG-I pathway did not relay a therapeutic benefit in the 4T1-LUC tumor model, this technology still holds promise for the local administration of other immunotherapeutics. Additionally, improved performance could be achieved with a higher degree of drug loading and more tightly controlled kinetics of drug release that might enable sustained silencing and/or enhanced cytosolic delivery of siRNA or innate immune agonists. Lastly, co-administering chemotherapy or radiotherapy to ablate the majority of the tumor cells and allow for decreased tumor burden at the site of injection would likely synergize well with this platform.

Materials and Methods

Materials

All chemicals were supplied by Sigma Aldrich unless otherwise specified.

Synthesis of Endosomolytic Polymers

The amphiphilic diblock copolymer, poly(dimethylaminoethyl methacrylate)-*block*-[(propylacrylic acid)$_{0.3}$-*co*-(dimethylaminoethyl methacrylate)$_{0.3}$-*co*-(butyl methacrylate)$_{0.4}$] (p[DMAEMA]-*bl*-[PAA$_{0.3}$-*co*-DMAEMA$_{0.3}$-*co*-BMA$_{0.4}$]; D-PDB) was synthesized via reversible addition-fragmentation chain transfer (RAFT) polymerizations following a protocol adapted from Convertine *et al.*[454]. Briefly, 4-cyano-4-(ethylsulfanylthiocarbonyl)sulfanylpentanoic acid (ECT; Boron Molecular) was used as a chain transfer agent (CTA), and 2,2'-azobis(4-methoxy-2,4-dimethyl valeronitrile) (V-70; Wako Chemicals) was used as an initiator for RAFT polymerization. Mass measurements were performed using an analytical mass balance (XSE205DU DualRange; Mettler Toledo). Gravity filtration was employed in columns packed with aluminum oxide to remove inhibitors from monomer solutions. For the polymerization of the first block, DMAEMA, CTA, and initiator were dissolved in dioxane at a molar ratio of 100:1:0.05 at 40 wt% monomer, purged with nitrogen gas for 30 minutes on ice, and reacted at 30 ºC for 18 hours. The resultant polymer was then purified by precipitation (6x) in cold pentane followed by dialysis (3.5 kDa MWCO) in deionized water. Poly(DMAEMA) was then frozen at -80 ºC and then lyophilized for 3 days to obtain a dry powder.

For the polymerization of the second block, poly(DMAEMA) was used as a macroCTA (mCTA) and was added to DMAEMA, PAA, and BMA (30:30:40 mol %). PAA was synthesized as previously described using diethyl propylmalonate as the precursor[505]. Using N,N-dimethylacetamide (DMAC) as the reaction solvent, initiator was added to mCTA and monomers at a molar ratio of 450:1:0.4 representing total monomer, mCTA, and initiator, respectively at 40 wt% mCTA and monomer. The reaction vessel was purged with nitrogen gas for 30 minutes on ice followed by reaction for 24 hours at 30 ºC in an oil bath. The resultant polymer was then

purified by precipitation (6x) in pentane:ether (80:20) followed by dialysis in acetone (4 exchanges) and subsequent dialysis in deionized water. D-PDB was then frozen at -80 ºC and then lyophilized for 3 days. All lyophilized polymer was stored at -20 ºC until used.

The experimental degree of polymerization, polymer composition, and theoretical molecular weight were obtained by ^{1}H nuclear magnetic resonance (NMR) Spectroscopy ($CDCl_3$ with TMS, Bruker AV 400). Experimental molecular weight and polydispersity were determined via gel permeation chromatography (GPC) using HPLC-grade dimethylformamide (DMF) containing 0.1% LiBr as a mobile phase with inline light scattering (Wyatt Technology) and refractive index (Agilent) detectors. The ASTRA V Software (Wyatt Technology) was used for all GPC calculations. Hydrodynamic size of the polymer micelles at physiological pH 7.4 was measured via digital light scattering (DLS) using a Zetasizer Nano ZS Instrument (Malvern, USA). D-PDB used herein had a 1st block molecular weight of 10.3 kDa, a 2nd block molecular weight of 31.0 kDa, and a polydispersity index (PDI) of 1.24. The 2nd block composition was determined to be 28:33:39 for PAA, DMAEMA, and BMA, respectively. Additionally, the hydrodynamic diameter of the D-PDB micelles was ~100 nm by an intensity particle size distribution.

Formulation of Polymer and Nucleic Acid Complexes for In Vitro Experiments

Micellar nanoparticles (NPs) were formulated according to a protocol adapted from Wilson *et al.*[456]. Lyophilized D-PDB was dissolved in ethanol to 50 mg/mL and rapidly diluted in 100 mM phosphate buffer (pH 7.0) to a concentration of 10 mg/mL to induce self-assembly into micelles. Polymer micelles were subsequently diluted in phosphate buffer saline (PBS; pH 7.4, 155 mM NaCl, 1.05 mM KH_2PO_4, 3 mM Na_2HPO_4, Gibco) to a concentration to 1 mg/mL. The micelles were then added to nucleic acid solutions at concentrations corresponding to a charge ratio (*i.e.*

N/P ratio: molar charge from the polymer's tertiary amines relative to the molar charge of phosphate from the nucleic acid backbone) of 4:1. Note that the N:P ratio is based on the poly(DMAEMA) first block and assuming 50% protonation of DMAEMA groups at pH 7.4. D-PDB micelles and nucleic acid were incubated at room temperature for 20 minutes to ensure complete electrostatic complexation.

Formulation of Polymer and Nucleic Acid Complexes for In Vivo Experiments

D-PDB micelles were formulated as described above, followed by sterile filtration (0.2 µm polyethersulfone sterile filter) and subsequent concentration to 30-60 mg/mL in PBS via centrifugal filtration (Amicon® Ultra 0.5 mL Centrifugal Filter Units; Ultracel® - 3K, Regenerated Cellulose 3,000 NMWL, Millipore) following manufacturer's instructions. The final concentrated solution was collected, and an aliquot was used to determine the resultant polymer concentration using UV-vis spectroscopy (Synergy H1 Multi-Mode Microplate Reader, Biotek) based on an absorbance wavelength of 310 nm corresponding to ECT. The solution was added to nucleic acids at concentrations corresponding to a charge ratio (*i.e.* N/P ratio) of 4:1 as described above.

Cell Culture

All cell handling procedures were performed in accordance with published technical data sheets. Murine mammary epithelial 4T1-LUC tumor cells stably co-express destabilized copepod green fluorescent protein (cop-GFP) and firefly luciferase were generated using psuedotyped lentiviral particles. Briefly, a transfection mixture consisting of pGreenFire1-CMV (System Biosciences, Cat. No. TR011PA-1), psPAX2 (Addgene Plasmid #12260), and pCMV-VSV-G

(Addgene Plasmid #8454) in water at a quantity of 10, 10, and 1 µg, respectively, was added to a final volume of 558 µL in Opti-MEM media (Gibco, Cat. No. 31985062) in a polypropylene tube, followed by the addition of 42 µL FuGENE 6 (Promega, Cat. No. E2691). The tube was gently flicked to mix the plasmids before and after the addition of FuGENE 6. The transfection mixture was added dropwise to a T-75 tissue culture flask at approximately 50% confluency of HEK-293-T cells in 11 mL Dulbecco's modified eagle medium (DMEM, Gibco) supplemented to 10% heat-inactivated fetal bovine serum (HI-FBS) without antibiotics. Cells were incubated at 37 ºC for 18 hours, and then the media on the HEK-293-T cells was exchanged for DMEM supplemented with 10% HI-FBS and 1% penicillin/streptomycin (P/S). At 24 and 48 hours after this media change, the viral supernatant was removed, clarified by centrifugation (1000 × g, 5 minutes, room temperature) and syringe filtered (0.45 µm, nylon). To transduce 4T1 cells, viral supernatant was mixed 1:1 with fresh DMEM supplemented with 10% HI-FBS without antibiotics and applied to cells for 24 hours. Cells were selected with 5 µg/mL puromycin for two weeks then sorted into approximately equal populations of low, medium, and high expressing cop-GFP cells using fluorescence activated cell sorting of GFP (BD FACSARIA IIIu, BD Biosciences) in the Vanderbilt Flow Cytometry Shared Resource Facility. The high expressing cop-GFP 4T1-LUC cells were used for all luminescent experiments herein. 4T1 and 4T1-LUC cells were maintained in DMEM supplemented with 2 mM L-glutamine, 4.5 g/L glucose, 10% HI-FBS, and 1% P/S. Cells were kept in a humidified environment at 37 ºC with 5% CO_2. Puromycin was added to 4T1-LUC cells after every cell passage at a concentration of 1 µg/mL for the continually selection of cells.

Preparation of PLGA Microparticles Encapsulating Micellar Nanoparticles

PLGA MPs encapsulating pH-responsive NPs were formed using a water-in-oil-in-water

($W_1/O/W_2$) double emulsion synthesis method previously reported[490-493, 506]. A fluorescently labelled double-stranded DNA (5'-[6FAM]ATAGGCGTATTATACGCGATTAACG-3', negative control sequence) was used as representative cargo to determine the ideal conditions for the loading of NPs into PLGA MPs. Briefly, 100 mg of poly(D,L-lactide-*co*-glycolide) (PLGA, Resomer® RG 503, 50:50, ester-terminated, MW 24,000-38,000 Da) was dissolved in 750 µL of dichloromethane (DCM) for 30 minutes under continuous shaking at room temperature. 200 µL of NP solution (*i.e.* polyplexes prepared with D-PBD and various amounts of nucleic acid strands ranging in concentration from 1.9 nmol to 11.4 nmol) was added dropwise to the PLGA solution at a primary aqueous phase (W_1) to oil phase (O) volume ratio of 0.27. The primary emulsion (W_1/O) was prepared by sonicating the two phases for 30 seconds at 40% amplitude on ice using a Sonic Dismembrator (Fisher Scientific™ Model 120). The secondary emulsion ($W_1/O/W_2$) was formulated by homogenizing the primary emulsion into 15 mL of 1% polyvinyl alcohol solution (PVA) for 30 seconds at 20,000 rpm on ice using a T18 digital ULTRA-TURRAX®, equipped with a S18N-10G dispersing tool (IKA). The double emulsion was then transferred to a round bottom flask and rotary evaporated for 1 hour at 400 torr to allow complete evaporation of DCM. MPs were collected by centrifugation (10,000 x g, 10 minutes, 4 °C) and washed 3 times with sterile water. PLGA MPs were then frozen at -80 ºC for 5 hours and then lyophilized for 3 days. The effervescent salt, ammonium bicarbonate was employed as a porogen to create porous MPs. 20 wt% NH_4HCO_3 was incorporated into the W_1 aqueous phase along with the NPs and then emulsified with the oil phase as described. All PLGA MPs were stored at -20 °C until used.

The hydrodynamic diameter of the PLGA MPs was measured by laser-diffraction size analysis using a Mastersizer 2000 (Malvern, USA). Approximately, 10-20 mg of PLGA MPs were dissolved in deionized water and used for analysis. Measurements detected within the acceptable

range, between 10% and 15% obscuration, were deemed to be reproducible data points. Surface morphology and porosity of the PLGA MPs were analyzed using a Zeiss Merlin scanning electron microscope (SEM; Carl Zeiss Microscopy, LLC, ZEISS Group, Thornwood, NY) equipped with a GEMINI II column. SEM samples were prepared by reconstituting PLGA MPs in deionized water at a concentration of 2 mg/mL and then placing 20 µL of the solution on a strip of carbon tape (Ted Pella Inc.) adhered onto an aluminum SEM stub (Ø12.7 mm, Ted Pella Inc). After drying overnight, samples were sputter coated with gold-palladium for 120 seconds and immediately imaged via SEM.

Evaluation of Loading and Encapsulation Efficiency

To determine the nucleic acid loading and encapsulation efficiency, nucleic acids were extracted from PLGA MPs. In brief, 7.5 mg of PLGA MPs were dissolved in 400 µL DCM and continuously mixed for 45 min at room temperature. 400 µL of TE buffer supplemented with 100 mM NaCl was added to this mixture and vortexed vigorously for 5 minutes. The suspension was then centrifuged (15,000 x g, 10 minutes, 4 ºC). The aqueous layer was collected into a fresh tube, and the extraction was performed again. The two extracted layers were combined, incubated with 1% sodium dodecyl sulfate (SDS) for 10 minutes at room temperature to disassemble the any electrostatically associated nucleic acids, and nucleic acid concentration was determined via fluorescence spectroscopy (excitation/emission wavelengths of 495/525 nm for 6FAM-DNA or 650/685 nm for Alexa Fluor® 647 (A647)-siRNA). Nucleic acid loading and encapsulation efficiencies were determined based on the ratio of encapsulated nucleic acid to PLGA MPs (µg/mg) and percentage relative to the theoretical maximum loading (%), respectively.

In Vitro Release of Nanoparticles from PLGA Microparticles

To investigate the *in vitro* release profiles of NPs from porous and nonporous MPs, 20 mg of PLGA MPs was suspended 1 mL sterile PBS (pH 7.4, 0.02% sodium azide) in microcentrifuge tubes and maintained at 37 ºC with constant rotation. At pre-determined time intervals, tubes were centrifuged (15,000 rpm, 10 minutes, 4 ºC), and 900 µL of supernatant was removed for analysis, replaced by the same volume of fresh buffer, and frozen and lyophilized for further analysis. Each lyophilized sample was reconstituted in 220 µL TE buffer supplemented with 100 mM NaCl, pipetted into a UV-Star® microplate (100 µL/well), and quantified by a fluorescence plate reader (Synergy H1 Hybrid Multi-Mode Reader, BioTek) as described above. All samples were run in technical duplicates.

In Vivo Controlled Release of Nanoparticles from PLGA Microparticles

Female BALB/c mice were obtained from The Jackson Laboratory (Bar Harbor, ME) and maintained at the animal facilities of Vanderbilt University under conventional conditions. The mice were anesthetized with isoflurane gas and maintained at 37 ºC while their flanks or abdomens were depilated and sterilized for subcutaneous or intratumoral administration. NPs were prepared with A647-DNA (negative control sequence, IDT DNA) and loaded into PLGA MPs with or without porogen for subcutaneous and intratumoral *in vivo* release studies. 6-8 week old mice were anesthetized with isoflurane gas and given a single subcutaneous injection of porous MP (n=5), nonporous MP (n=5), or NP (n=3). For the murine tumor studies, 10^6 4T1-LUC cells were inoculated (50 µL injection volume) into the inguinal mammary fatpads of 6-8 week old mice anesthetized with isoflurane gas. Tumor volume was calculated using the equation: Volume=(Length x Width^2)/2. When tumor volumes reached 50-100 mm^3, mice were anesthetized

with isoflurane gas and administered a single intratumoral injection of porous MPs (n=3), nonporous MPs (n=3), or NPs (n=3). All treatments were administered at a 10 μg dose of nucleic acid in a 100 μL injection volume. Using constant image capture settings on an IVIS Spectrum (PerkinElmer), mice were imaged at predetermined time intervals to quantify A647 fluorescence. Relative release of NPs was determined by measuring the total fluorescent efficiency (cm^2) of A647 overtime and normalizing to the respective initial (day 0) values.

In Vitro Evaluation of Luciferase Knockdown

NPs were prepared with the siRNA oligos, siLUC (anti-luciferase sequence, 5'-CAAUUGCACUGAUAAUGAACUCCTC[3AlexF647N]-3'; IDT DNA) or siNC (negative control sequence, 5'-[5AlexF647N]AUACGCGUAUUAUACGCGAUUAACGAC-3'; IDT DNA) and encapsulated into porous MPs as described above. 4T1-LUC cells were seeded in five black 24-well plates (a separate plate for each day of imaging) with clear tissue culture treated bottoms (Sensoplate REF:662892; Greiner Bio-One) at 2000 cells per well (500 μL seeding volume). NPs were complexed with either siLUC (siLUC/NP) or siNC (siNC/NP) and embedded in porous MPs (siLUC/MP and siNC/MP). Cells were treated 24 hours later with free NPs or porous MPs at a final concentration of 50 nM nucleic acid per well. The supernatant in the free NP-treated wells was removed from all plates at 24 hours to mimic the NP clearance observed *in vivo*. Every 24 hours over the course of 5 days, Pierce D-luciferin (ThermoFisher Scientific) was administered to all the wells within the plate for the corresponding day to a final D-luciferin concentration of 0.15 mg/mL. 5 minutes after the addition of D-luciferin, plates were imaged for bioluminescent signal using an IVIS Lumina III (PerkinElmer). Images were captured at 24, 48, 72, 96, 120 hours post-treatment, and luciferase knockdown was quantified for each day based on

the percent decrease in bioluminescent signal (*i.e.* Total Flux, photons/second) relative to each respective negative control siRNA.

In Vivo Evaluation of Luciferase Knockdown

Female BALB/c mice were obtained from The Jackson Laboratory (Bar Harbor, ME) and maintained at the animal facilities of Vanderbilt University under conventional conditions. Orthotopic 4T1-LUC tumors were generated as described above. siLUC/NPs and siNC/NPs were prepared as described above and loaded into porous MPs (siLUC/MP and siNC/MP). When tumor volumes reached 50-100 mm^3, mice were anesthetized with isoflurane gas and administered a single intratumoral injection of free NPs or porous MPs (n=10 for all treatment groups). All treatments were administered at a 10 μg oligonucleotide dose (0.5 mg/kg) in a 100 μL injection volume. Using constant image capture settings on an IVIS Lumina III (PerkinElmer), mice were analyzed at predetermined time intervals for fluorescence and bioluminescence. Bioluminescence within the mice was measured 10 minutes after dorsal subcutaneous injection of 300 μL Pierce D-luciferin (15 mg/mL). After 14 days mice were euthanized and tumor samples were isolated postmortem for histological analysis.

Statistical Analysis

All data analysis was performed on Graphpad Prism (Version 7.0c). One-way analysis of variance (ANOVA) coupled with Tukey's post-test was used to compare statistical significance among multiple groups (>2). Differences between two groups were analyzed by unpaired t-tests. *In vivo* experiments were performed with at least 3 biological replicates, with ****P<0.0001, ***P<0.001, **P<0.01, *P<0.05 being considered statistically significant.

CHAPTER VI

PRELIMINARY INVESTIGATIONS INTO MODULATING STING SIGNALING

Introduction

Given the dynamic context-dependent nature of STING signaling, therapeutic strategies employed to direct downstream STING signaling represent a promising approach that may enable optimized application-specific treatments. Indeed, signaling kinetics and specific gene regulation can have a dramatic effect on disease outcome. Accordingly, molecules that can further shape the immune response from STING signaling, such as NF-κB modulators, manganese, ENPP1 inhibitors, and biomaterials with intrinsic immunostimulatory activity, are ideal candidates to be co-treatments administered with STING agonists. This chapter investigates several different avenues for modulating STING signaling by characterizing downstream immune effects.

NF-κB Modulation

As discussed in Chapter II, NF-κB modulation is one promising method of potentiation for innate immune activators. In this work, two strategies (*i.e.* NF-κB inhibitory peptides and Alu RNA with intrinsically low NF-κB activity) were employed to explore the effects of NF-κB modulation on innate immune activation. First, cGAS/STING pathway agonists were characterized with the established cell penetrating peptides (CPPs), SN50 and SN52, which can inhibit the downstream activity of NF-κB1 and NF-κB2, respectively. Recent reports in the literature suggest these cell penetrating peptides can tune the resultant immune profile of various adjuvants, which may be more beneficial than simply increasing the magnitude of PRR signaling.

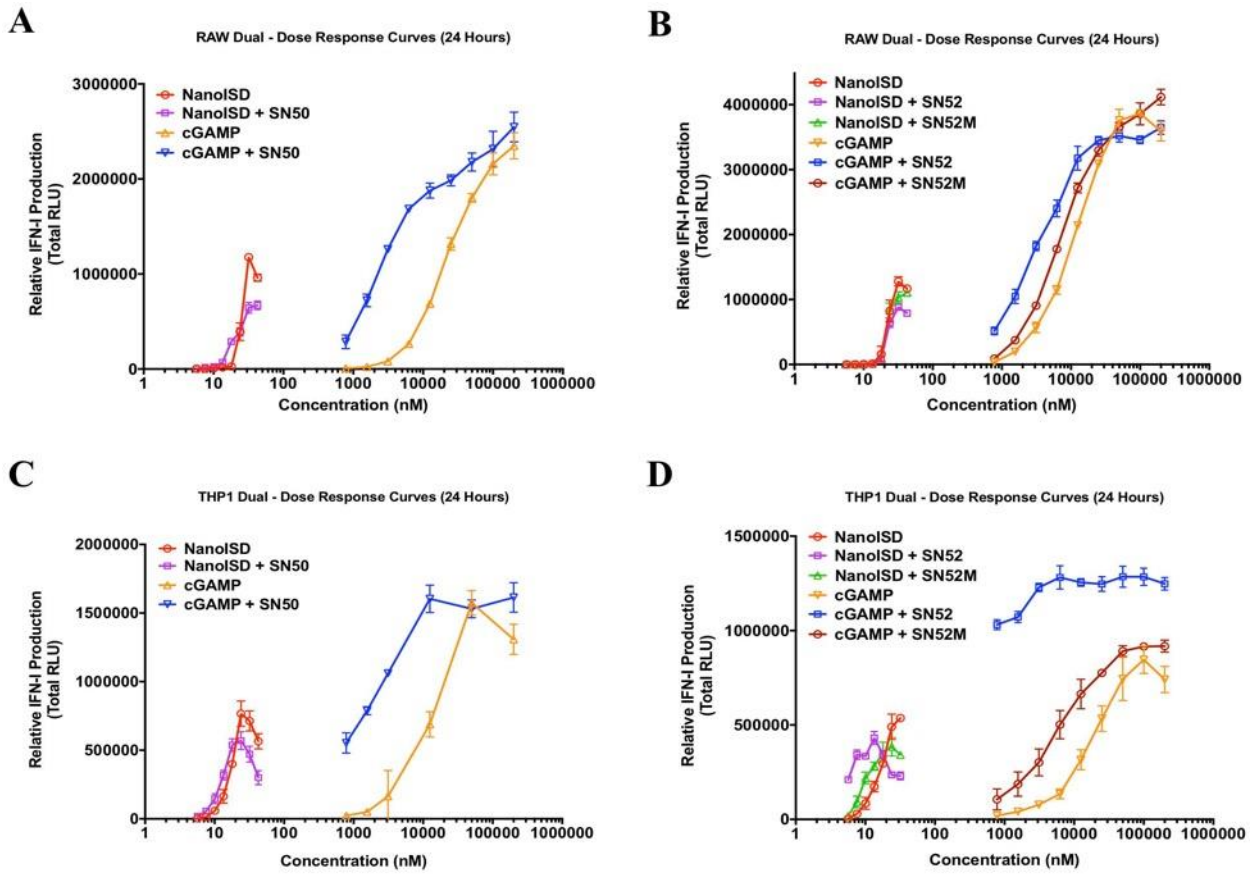

Figure 6.1. In vitro activity of NF-κB inhibitors and STING pathway agonists. **(A)** RAW-Dual reporter cell assay of SN50 with cGAS/STING pathway agonists. **(B)** RAW-Dual reporter cell assay of SN52 with cGAS/STING pathway agonists. SN52M is a negative control for the cell-penetrative peptide. **(C)** THP1-Dual reporter cell assay of SN50 with cGAS/STING pathway agonists. **(D)** THP1-Dual reporter cell assay of SN52 with cGAS/STING pathway agonists. SN52M is a negative control for the cell-penetrative peptide.

IFN-I reporter cells (*i.e.* murine RAW-Dual cells and human THP1-Dual cells) were used to quantify changes in the relative IFN-I production induced by cGAS/STING pathway agonists when the cells were pretreated with either SN50 or SN52 (***Figure 6.2***). SN50 and SN52 similarly increased the potency of cGAMP in both reporter cell lines, but only SN52 significantly increased the maximum efficacy of cGAMP in human THP1-Dual cells relative to the control treatments (*i.e.* free cGAMP and cGAMP plus the negative control CPP, SN52M). Notably, SN52 appeared to have less of an effect on the murine RAW-Dual cells compared to the human THP1-Dual cells.

Additionally, the effects of SN50 and SN52 on NanoISD treatment were less pronounced. Indeed, pretreatment with the CPPs slightly increased potency, but at the cost of reducing maximal efficacy, which was likely due to increased cellular toxicity from the combination treatment. Again, SN52 exhibited a noticeably reduced effects in the RAW-Dual cells.

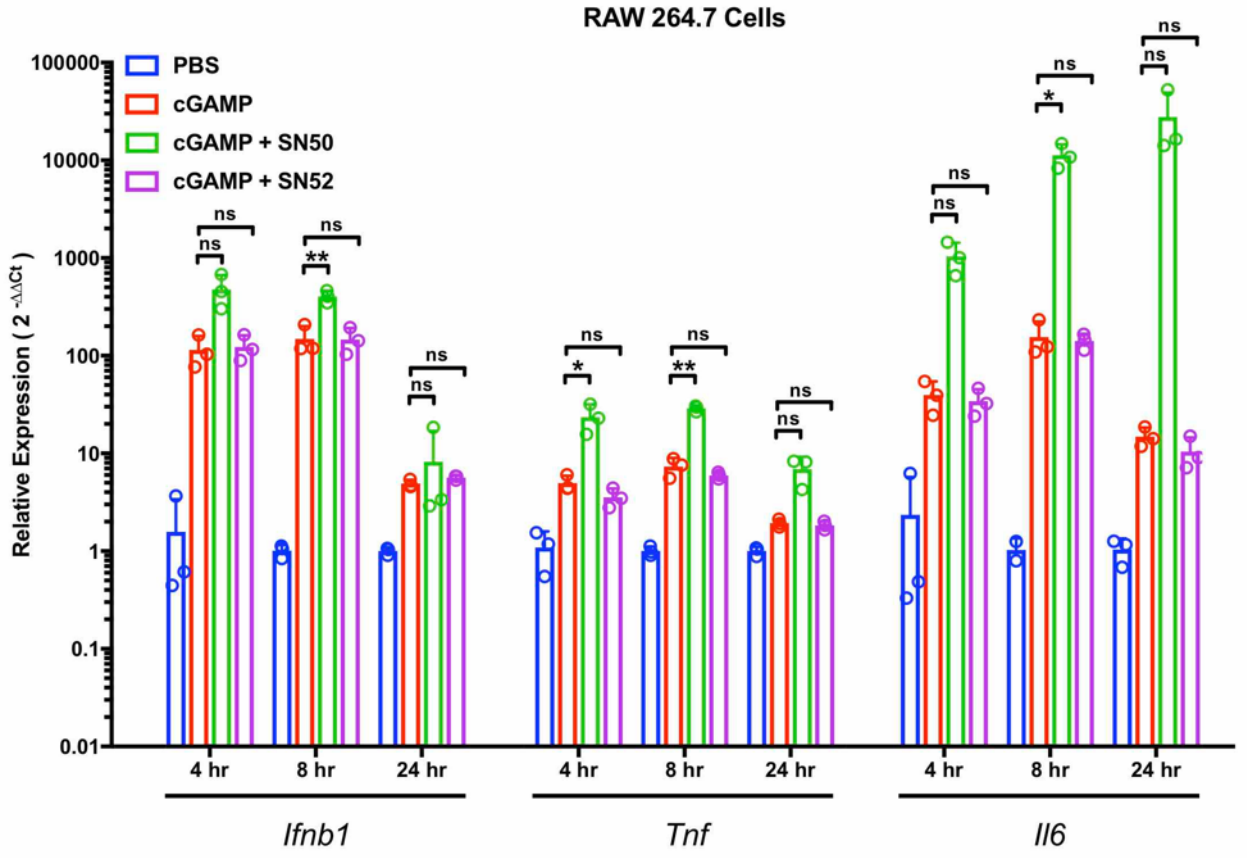

Figure 6.2. Longitudinal gene expression changes induced by cGAMP and NF-κB inhibitors.

To directly quantify changes in proinflammatory gene expression over time following treatment with cGAMP and the NF-κB inhibitors, qPCR was subsequently employed (***Figure 6.3***). In RAW 264.7 cells, SN50 significantly increase the expression of all 3 proinflammatory genes examined (*i.e. Ifnb1*, *Tnf*, and *Il6*) with the largest effects occurring at both 4 and 8 hours post cGAMP treatment, while SN52 had no effect. To explore possible cell-specific differences, a

similar study was conducted in THP1 cells for an 8 hour incubation (***Figure 6.4***). Consistent with the results in RAW 264.7 cells, SN50 also amplified the expression of all 3 proinflammatory genes in the THP1 cells. Interestingly, while SN52 clearly had no effect on the expression of *Tnf* and *Il6*, its increased expression of *Ifnb1* was approaching statistical significance (p = 0.20). It is possible that the treatment doses and/or data collection timepoint could be tweaked to further clarify the impact of SN52 on proinflammatory gene expression.

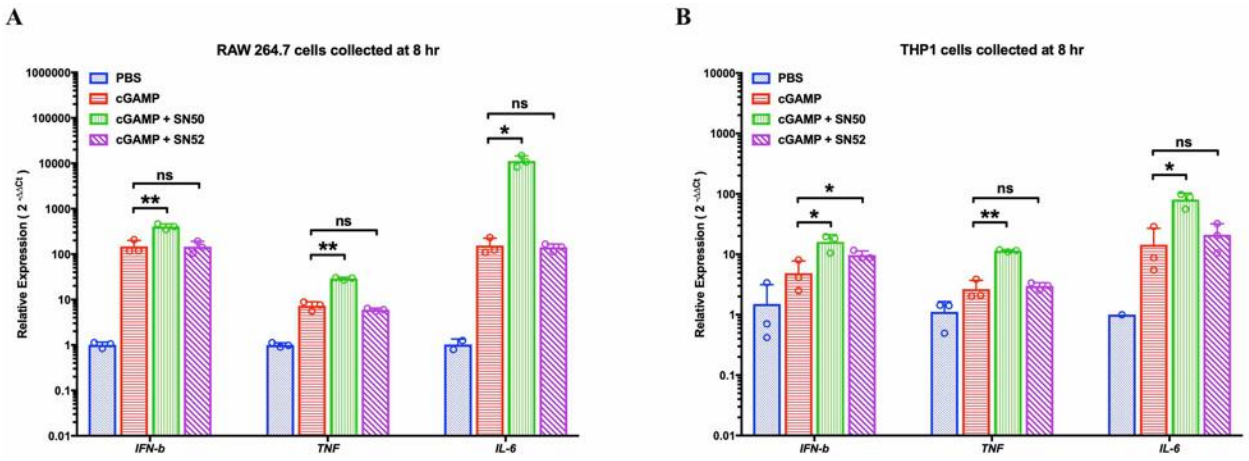

Figure 6.3. Gene expression changes induced by cGAMP and NF-κB inhibitors at 8 hours. **(A)** Gene expression changes in RAW 264.7 cells. **(B)** Gene expression changes in THP1 cells.

Since SN52 has previously been reported to enhance antitumor efficacy of radiation in the MC38 murine tumor model by potentiating cGAS/STING signaling, SN52 was explored as a cotreatment to NanoISD in the B16.F10 tumor model (***Figure 6.5***). SN52 displayed a rather marginal beneficial effect with slightly enhanced tumor attenuation and murine survival relative to NanoISD. While its antitumor effect with NanoISD is somewhat underwhelming, SN52 may have better efficacy when administered with STING agonist therapeutics.

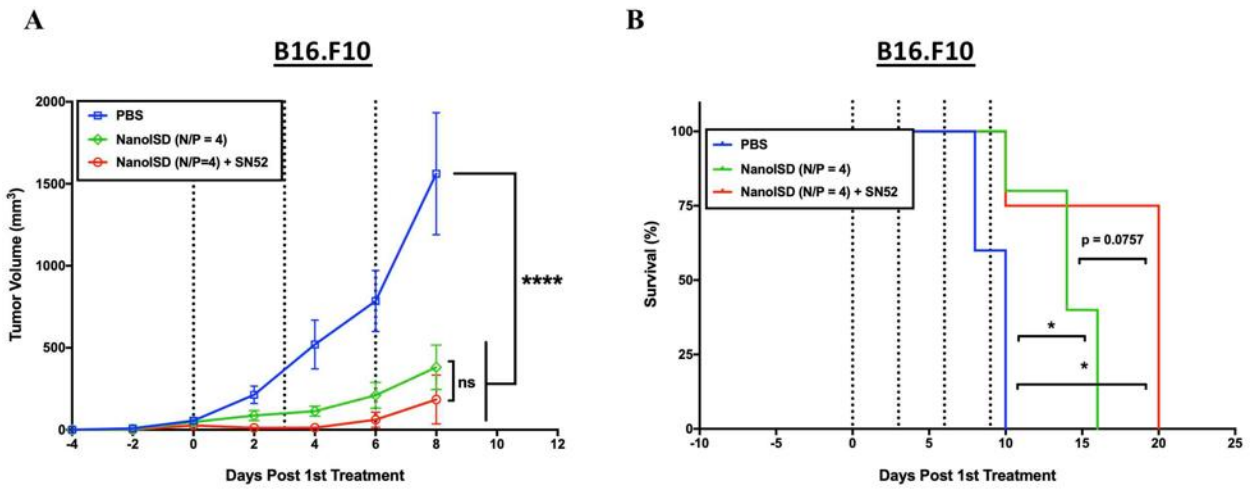

Figure 6.4. Therapeutic activity of NanoISD and SN52. **(A)** Tumor growth plot for B16.F10 tumors intratumorally treated with 100 µL of either PBS, NanoISD, or SN52 + NanoISD. The NanoISD dose corresponded to 2 µg DNA. The SN52 treatment corresponded to 40 µg protein. Treatments were administered four times *q3d* as indicated by the dotted lines. Tumor growth curves for each treatment were truncated when a mouse reached the study endpoint. A two-way ANOVA with Tukey test was used for statistical analysis. **(B)** Kaplan-Meier survival curve for B16.F10 tumors intratumorally treated with 100 µL of either PBS, NanoISD, or SN52 + NanoISD. Log rank (Mantel-Cox) test was used for statistical analysis relative to the PBS treatment group.

The second strategy pursued to investigate NF-κB modulation in the context of innate immune activation involved the use of alternative Alu RNA (*i.e.* Alu5 RNA). Our collaborators in the Aune Lab at Vanderbilt University have discovered that Alu5 RNA induces lower NF-κB activity relative to AluJb RNA when administered to cells with lipofectamine. In this work, it was first determined whether Alu5 RNA (Left Arm) could be packaged and delivered with D-PDB to simulate endogenous Alu RNA expression as in the case of AluJb RNA (Left Arm) / D-PDB. Alu5 RNA (Left Arm) was complexed to D-PDB at an N/P charge ratio of 4 and DLS was performed (***Figure 6.6-A***). Alu5 RNA (Left Arm) / D-PDB demonstrated a uniform particle size distribution, which was slightly larger than AluJb RNA (Left Arm) / D-PDB.

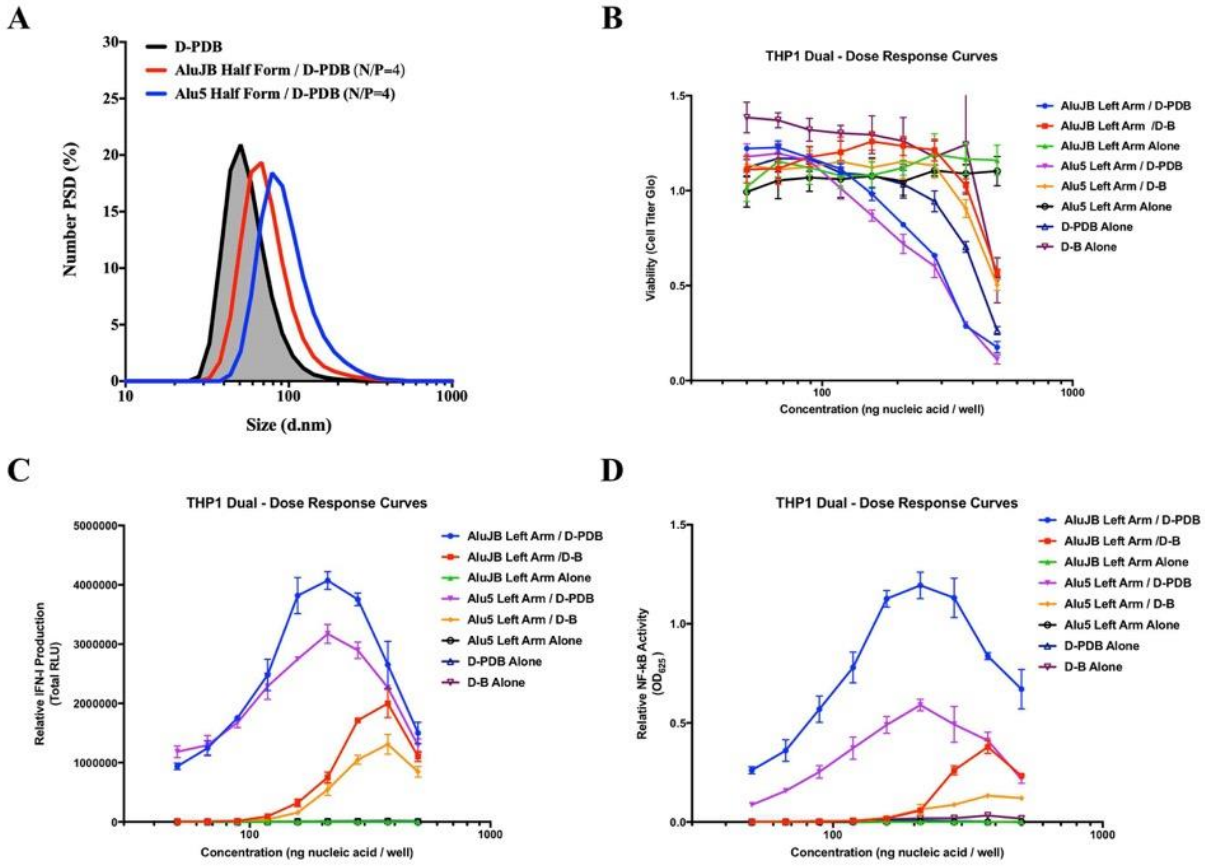

Figure 6.5. In vitro characterization of Alu5 RNA (Left Arm) / D-PDB. **(A)** DLS analysis of Alu5 RNA (Left Arm) / D-PDB relative to D-PDB and AluJb RNA (Left Arm) / D-PDB. **(B)** CellTiter-Glo assay at 24 hours post treatment for cellular viability of Alu5 RNA (Left Arm) alone or with D-PDB or D-B relative to that of AluJb RNA (Left Arm). **(C)** Quanti-Luc assay at 24 hours post treatment for relative IFN-I activity of Alu5 RNA (Left Arm) alone or with D-PDB or D-B relative to that of AluJb RNA (Left Arm). **(D)** Quanti-Blue assay at 24 hours post treatment for relative NF-κB activity of Alu5 RNA (Left Arm) alone or with D-PDB or D-B relative to that of AluJb RNA (Left Arm).

Subsequently, THP1-Dual reporter cells were employed to characterize the *in vitro* activity (*i.e.* relative IFN-I production and relative NF-κB signaling) of Alu5 RNA (Left Arm) / D-PDB, Alu5 RNA (Left Arm) / D-B (*i.e.* a non-endosomolytic analog), and free Alu5 RNA (Left Arm). The immunocellular toxicities of the Alu5 RNA (Left Arm) / polymer complexes were consistent with that of the AluJb RNA (Left Arm) / polymer complexes (***Figure 6.6-B***). Both free Alu5 RNA (Left Arm) and free AluJb RNA (Left Arm) demonstrated no efficacy, suggesting that some form

of cellular delivery is necessary for activity. In terms of relative IFN-I production, Alu5 RNA (Left Arm) / polymer complexes showed slightly lower maximal efficacy, but similar potency compared to AluJb RNA (Left Arm) / polymer complexes. Moreover, D-PDB evoked greater activity than D-B, which might suggest that cytosolic delivery (*i.e.* rather than endosomal delivery) is most important for efficacy. Notably, Alu5 RNA (Left Arm) did indeed exhibit significantly lower NF-κB activity with both the endosomolytic and non-endosomolytic carriers, as demonstrated by the Alu5 RNA (Left Arm) / AluJb RNA (Left Arm) ratios of maximum efficacy. When delivered with D-PDB, Alu5 RNA (Left Arm) had 78% the maximum efficacy of AluJb RNA (Left Arm) for relative IFN-I production versus 49% for NF-κB activity, and when delivered with D-B, Alu5 RNA (Left Arm) had 65% the maximum efficacy of AluJb RNA (Left Arm) for relative IFN-I production versus 35% for NF-κB activity.

Alu5 RNA (Left Arm) / D-PDB complexes were further characterized in B16.F10 melanoma models (***Figure 6.7***). Following a single intratumoral injection in the B16.F10 tumor model, Alu5 RNA (Left Arm) / D-PDB performed comparably to AluJb RNA (Left Arm) / D-PDB in terms of changes in the gene expression of various proinflammatory cytokines (***Figure 6.7-A***). B16.F10 IFN-LUC cells were subsequently employed to investigate the pharmacodynamics of the Alu RNA (Left Arm) / D-PDB NPs. The effects of Alu RNA (Left Arm) / D-PDB were first validated in the B16.F10 IFN-LUC cells *in vitro* following a 24 hour incubation. Consistent with the *in vitro* results from the THP1-Dual reporter cells, Alu5 RNA (Left Arm) / D-PDB exhibited a lower maximum efficacy than AluJb RNA (Left Arm) / D-PDB with similar potency, and free AluJb RNA (Left Arm) again showed no signs of immunostimulatory activity (***Figure 6.7-B and 6.7-C***). In the B16.F10 IFN-LUC tumor model, Alu5 RNA (Left Arm) / D-PDB evoked slightly higher IFN activity than AluJb RNA (Left Arm) / D-PDB with highest

expression for both treatments at 12–24 hours post intratumoral treatment (***Figure 6.7-D***). The increased IFN production from the two treatments, was accompanied by tumor attenuation (***Figure 6.7-E***) and prolonged survival (***Figure 6.7-F***). In this tumor model, the difference in therapeutic benefit between the two treatments was largely insignificant.

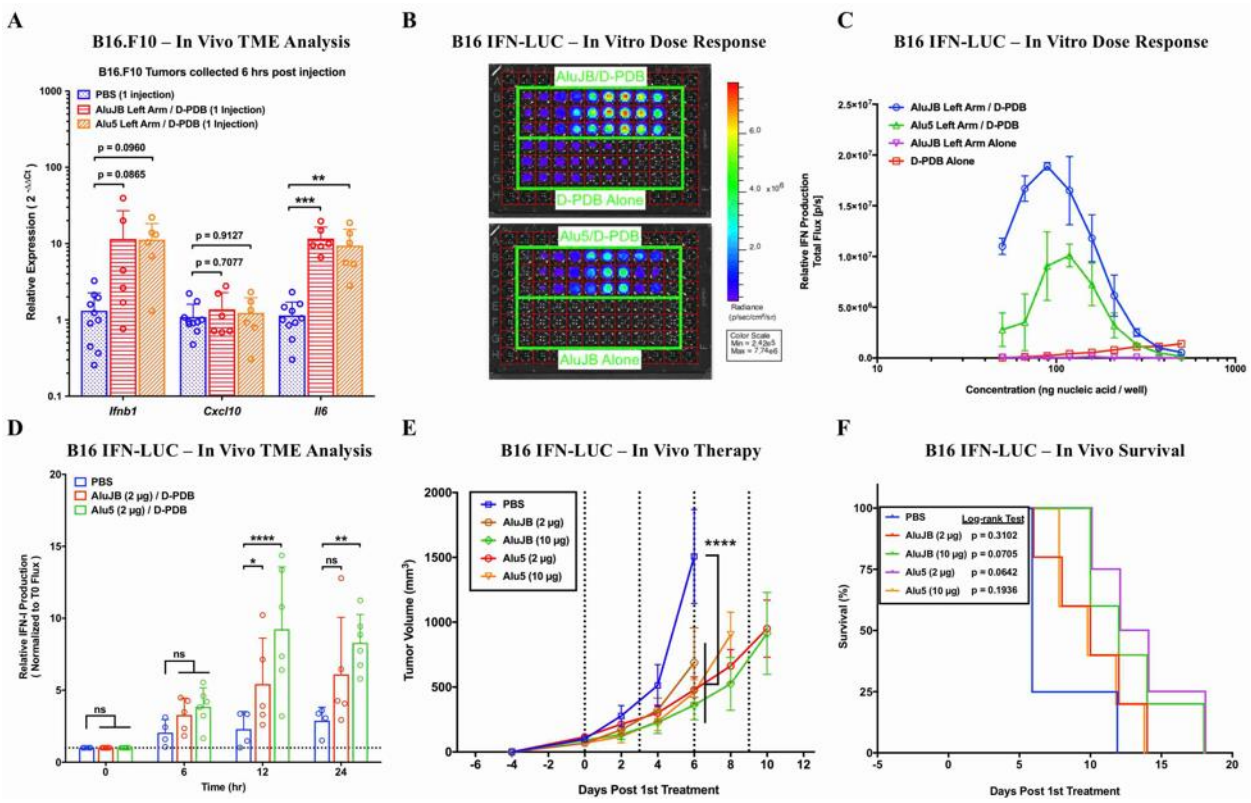

Figure 6.6. Anticancer effects of Alu5 RNA (Left Arm) / D-PDB. **(A)** B16.F10 IFN-LUC reporter cell assay of Alu5 RNA (Left Arm) / D-PDB relative to AluJb RNA (Left Arm), D-PDB, and AluJb RNA (Left Arm) / D-PDB. **(B)** Longitudinal analysis of intravital IFN activity in B16.F10 IFN-LUC tumors intratumorally treated with 100 µL of either PBS, AluJb RNA (Left Arm) / D-PDB (2 µg RNA), AluJb RNA (Left Arm) / D-PDB (10 µg RNA), Alu5 RNA (Left Arm) / D-PDB (2 µg RNA), or Alu5 RNA (Left Arm) / D-PDB (10 µg RNA) (n = 4 or greater per treatment group). **(C)** Tumor growth plot for B16.F10 IFN-LUC tumors intratumorally treated with 100 µL of either PBS, AluJb RNA (Left Arm) / D-PDB (2 µg RNA), AluJb RNA (Left Arm) / D-PDB (10 µg RNA), Alu5 RNA (Left Arm) / D-PDB (2 µg RNA), or Alu5 RNA (Left Arm) / D-PDB (10 µg RNA). Treatments were administered four times *q3d* as indicated by the dotted lines. Tumor growth curves for each treatment were truncated when a mouse reached the study endpoint. A two-way ANOVA with Tukey test was used for statistical analysis. **(D)** Kaplan-Meier survival curve for B16.F10 IFN-LUC tumors intratumorally treated with 100 µL of either PBS, AluJb RNA (Left

Arm) / D-PDB (2 μg RNA), AluJb RNA (Left Arm) / D-PDB (10 μg RNA), Alu5 RNA (Left Arm) / D-PDB (2 μg RNA), or Alu5 RNA (Left Arm) / D-PDB (10 μg RNA). Log rank (Mantel-Cox) test was used for statistical analysis relative to the PBS treatment group.

While the results from the alternative NF-κB activity of Alu5 RNA (Left Arm) did not manifest in changes to therapeutic benefit in this particular setting, it is possible that other less aggressive tumor models may indeed be impacted by such changes. Furthermore, the coadministration of immune checkpoint blockade might also improve responses and emphasize treatment specific differences, which could thereby help clarify implications that alternative NF-κB activity has on innate immune activation and antitumor immunity.

Manganese Potentiation

As discussed in Chapter II, manganese is now known to be a noteworthy potentiator of the cGAS/STING pathway. In this work, NanoISD was characterized with coadministration of manganese both *in vitro* and *in vivo* (***Figure 6.8***). THP1-Dual reporter cells were used to study the effect that Mn^{2+} pretreatment has on relative interferon production (***Figure 6.8-A***) and cellular viability (***Figure 6.8-B***). A fixed EC75 concentration of NanoISD was used with a dose response of $Mn2^{+}$ for one dose response of interest, and a fixed concentration of 1 mM $Mn2^{+}$ was used with a dose response of NanoISD for another dose response of interest. D-PDB, cGAMP, and Mn^{2+} were used as controls for the experiment. Notably, the effects of manganese pretreatment were surprisingly minimal. It should be noted that the previous reports that demonstrate the impact of manganese potentiation have not shown efficacy in such reporter cell models, which might suggest that another metric for efficacy (*e.g.* qPCR) could be more representative of the immunomodulatory effects of manganese ions.

Manganese was explored *in vivo* using the B16.F10 murine tumor model. $MnCl_2$ injected

intratumorally by itself did show some signs of therapeutic efficacy, as demonstrated by partial attenuation of tumor growth (***Figure 6.8-C***) and prolonged survival (***Figure 6.8-D***). However, combination with NanoISD showed no therapeutic advantage, which again could be a tumor-specific phenomenon or related to drug delivery. Indeed, co-packaging ISD and Mn^{2+} may result in a more therapeutically active treatment.

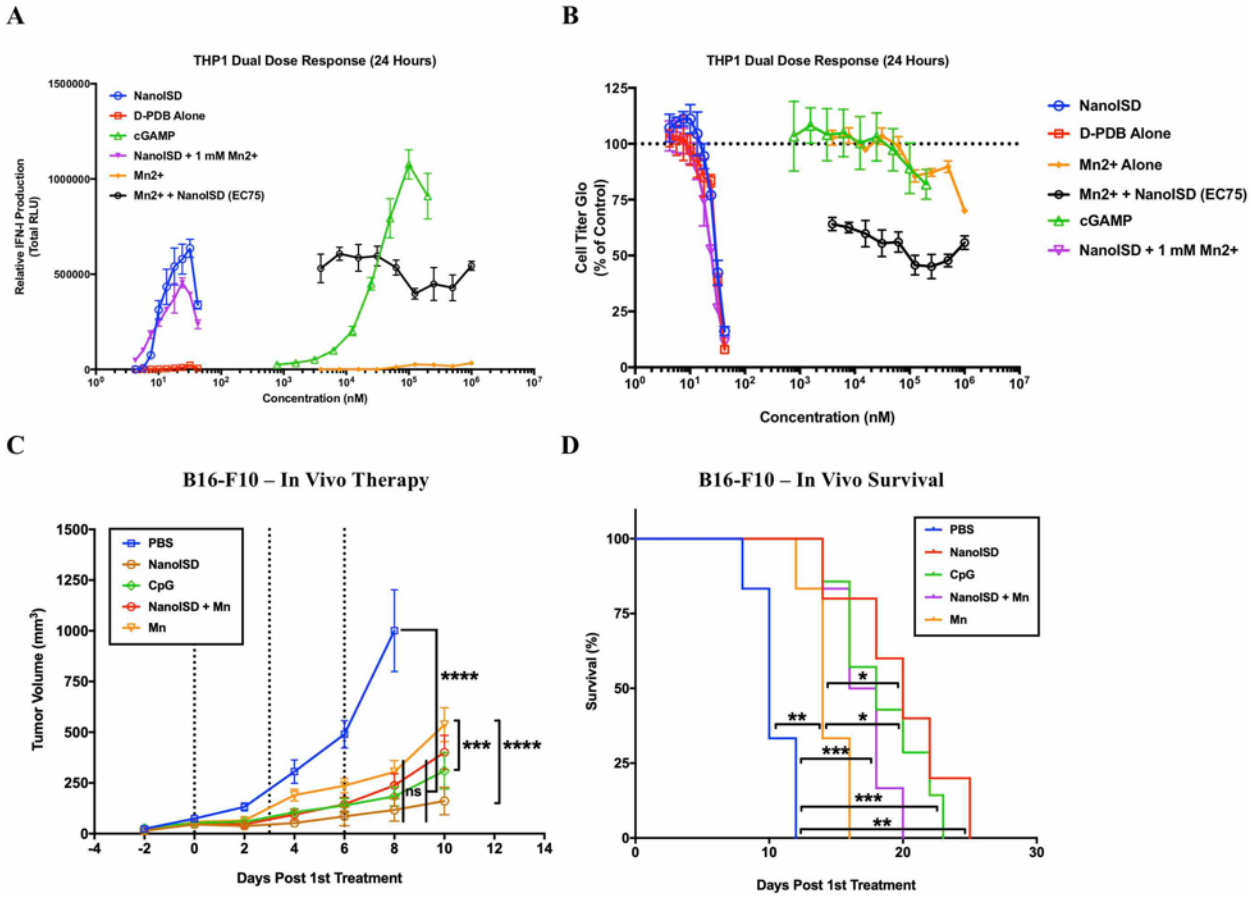

Figure 6.7. Manganese potentiation of STING signaling. **(A)** THP1-Dual reporter cell assay of $Mn2^{+}$ + NanoISD. **(B)** CellTiter-Glo assay at 24 hours post treatment for cellular viability of the treated THP1-Dual cells. **(C)** Tumor growth plot for B16.F10 tumors intratumorally treated with PBS, NanoISD, CpG DNA, NanoISD + $Mn2^{+}$, or $Mn2^{+}$.Treatments were administered four times *q3d* as indicated by the dotted lines. Tumor growth curves for each treatment were truncated when a mouse reached the study endpoint. A two-way ANOVA with Tukey test was used for statistical analysis. **(D)** Kaplan-Meier survival curve for B16.F10 tumors intratumorally treated with PBS, NanoISD, CpG DNA, NanoISD + $Mn2^{+}$, or $Mn2^{+}$. Log rank (Mantel-Cox) test was used for statistical analysis relative to the PBS treatment group.

ENPP1 Inhibition

ENPP1 inhibition, which was discussed in Chapter II along with manganese, is also a known potentiator of cGAS/STING signaling. To purse ENPP1 inhibition as a strategy to potentiate innate immune activation, a recently described small molecule inhibitor of ENPP1 (*i.e.* Compound C) was synthesized in-house and then coadministered with NanoISD in A549-Dual reporter cells to evaluate effects on relative IFN-I production (***Figure 6.9***). A fixed concentration of 30 µM Compound C was used with a dose response of NanoISD for one dose response of interest (***Figures 6.9-A and 6.9-C***), and a fixed EC75 concentration of NanoISD was used with a dose response of Compound C for another dose response of interest (***Figures 6.9-B and 6.9-D***).

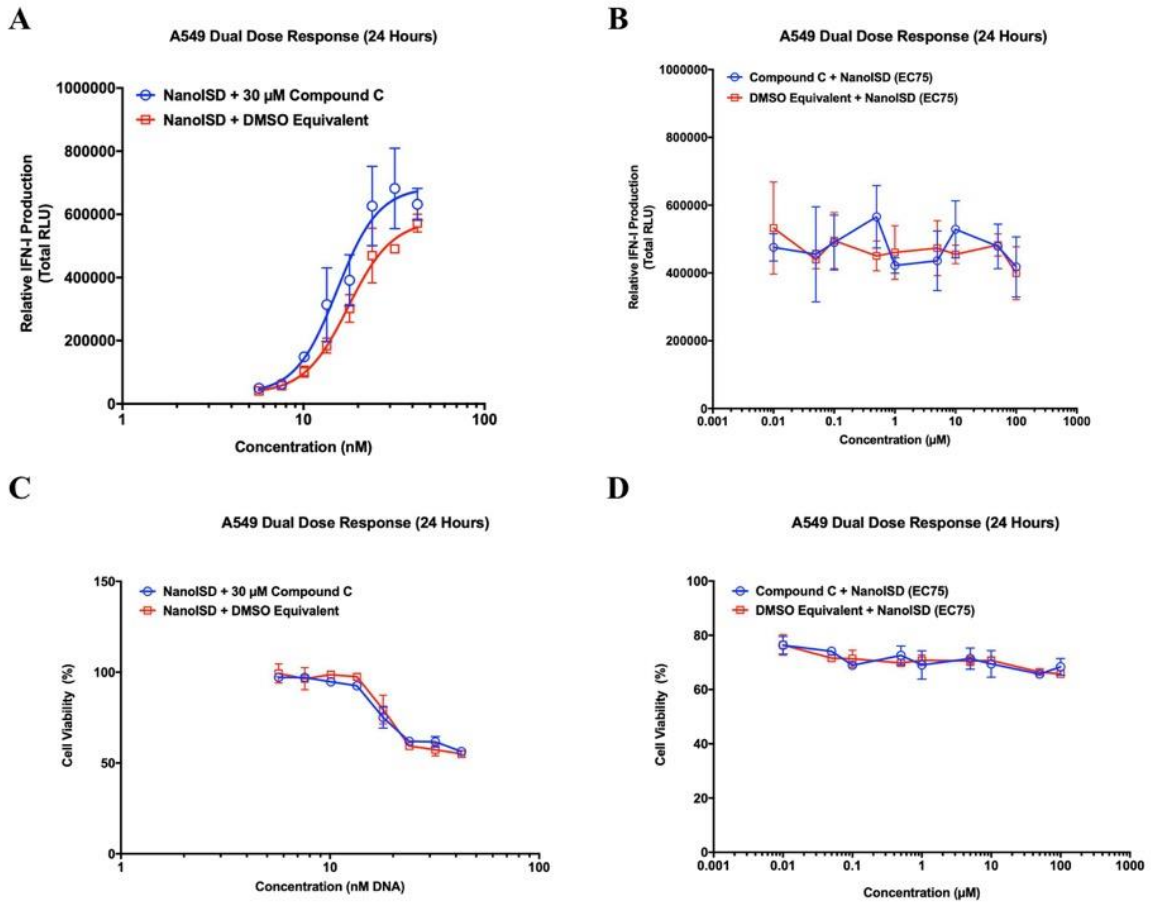

Figure 6.8. In vitro characterization of the ENPP1 inhibitor, Compound C. **(A)** A549-Dual reporter cell assay of a fixed 30 µM concentration of Compound C with a dose response of NanoISD. **(B)**

A549-Dual reporter cell assay of a dose response of Compound C with a fixed EC75 concentration of NanoISD. **(C)** CellTiter-Glo assay at 24 hours post treatment for cellular viability of the treated A549-Dual cells. **(D)** CellTiter-Glo assay at 24 hours post treatment for cellular viability of the treated A549-Dual cells.

In this particular experiment, Compound C had little to no effect on the relative IFN-I production. This lack of efficacy is likely attributable to the inability of the 2-D *in vitro* model to accurately recapitulate the context of ENPP1-regulated tumor microenvironments. Indeed, either the reporter cells do not produce enough ENPP1 to affect IFN-I production or the induction of IFN-I expression in this particular assay is not dependent on cell-to-cell transfer of cGAMP and therefore not appreciably regulated by ENPP1. Future *in vitro* experiments investigating the efficacy and potential utility of Compound C might involve spiking reporter cells with recombinant ENPP1 prior to treatment and/or utilizing cells that require cGAMP transfer for IFN-I induction. *In vivo* experiments (*e.g.* tumor therapy studies) also have potential to answer the outstanding questions and may be a more direct route of investigation, since they represent a more therapeutically relevant experimental setting.

Intrinsic Immunostimulatory Capacity of Nanocarriers

As determined in Aim 1 (Chapter 3), D-PDB elicits cGAS-dependent STING signaling, which is most likely due to mitochondrial DNA release into the cytosol. D-PDB is cationic, and therefore once in the cytosol, the polymer is likely to interact with and potentially destabilize the negatively charged mitochondrial membrane. Indeed, the charge density of cationic species (*e.g.* chitin-derived polymers) has been associated with mitochondrial DNA release and subsequent cGAS/STING signaling[507]. In addition to D-PDB, it is also shown in this work that several other nucleic acid carriers also exhibit cGAS-dependent STING signaling, as demonstrated by IFN-I

activity in RAW-Dual reporter cells (***Figure 6.12-A***) and a lack of IFN-I activity in RAW ISG KO cGAS reporter cells (***Figure 6.12-C***). For each treatment, similar toxicity profiles can be observed between the two cell lines (***Figures 6.12-B and 6.12-D***), indicating consistent delivery conditions.

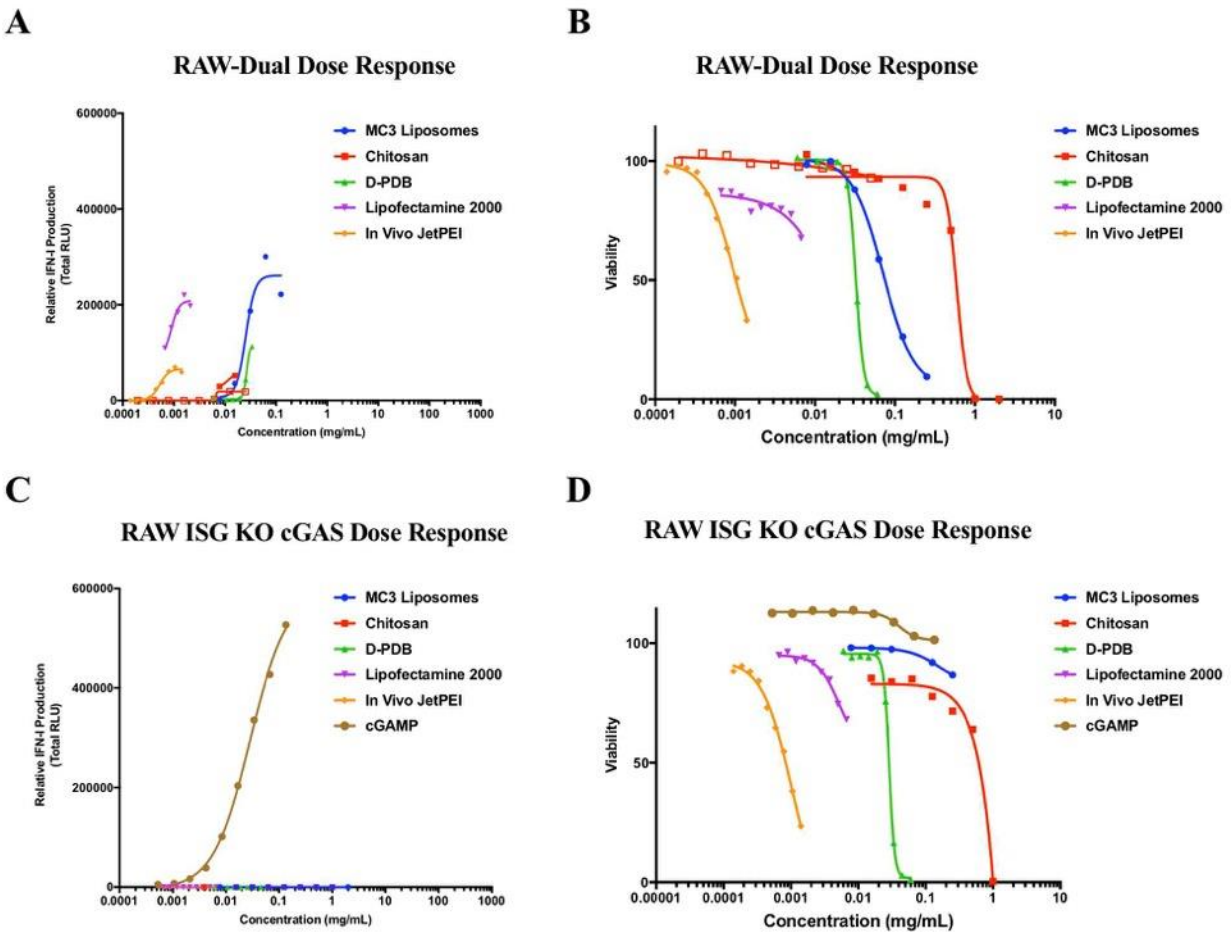

Figure 6.9. Several nanocarriers trigger cGAS-dependent IFN-I activity. **(A)** RAW-Dual reporter cell assay of various nanocarriers. **(B)** CellTiter-Glo assay at 24 hours post treatment for cellular viability of the treated RAW-Dual cells. **(C)** RAW ISG KO-cGAS reporter cell assay of various nanocarriers. **(D)** CellTiter-Glo assay at 24 hours post treatment for cellular viability of the treated RAW ISG KO-cGAS cells.

This discovery has important implications for nucleic acid delivery and particularly for gene delivery, as cGAS/STING signaling is quite likely counterproductive for successful gene

delivery / gene incorporation. Accordingly, one strategy to improve both *in vitro* and *in vivo* gene delivery might involve the use of cGAS and/or STING inhibitors. Data collected in our lab has demonstrated that the cGAS-dependent IFN-I activity from nanocarriers can indeed be inhibited through the use of either a cGAS inhibitor (*i.e.* RU.521) or a STING inhibitor (*i.e.* H-151) without effecting cellular viability (***Figure 6.13***). However, it remains to be seen whether such inhibition of proinflammatory gene expression can manifest in better gene delivery.

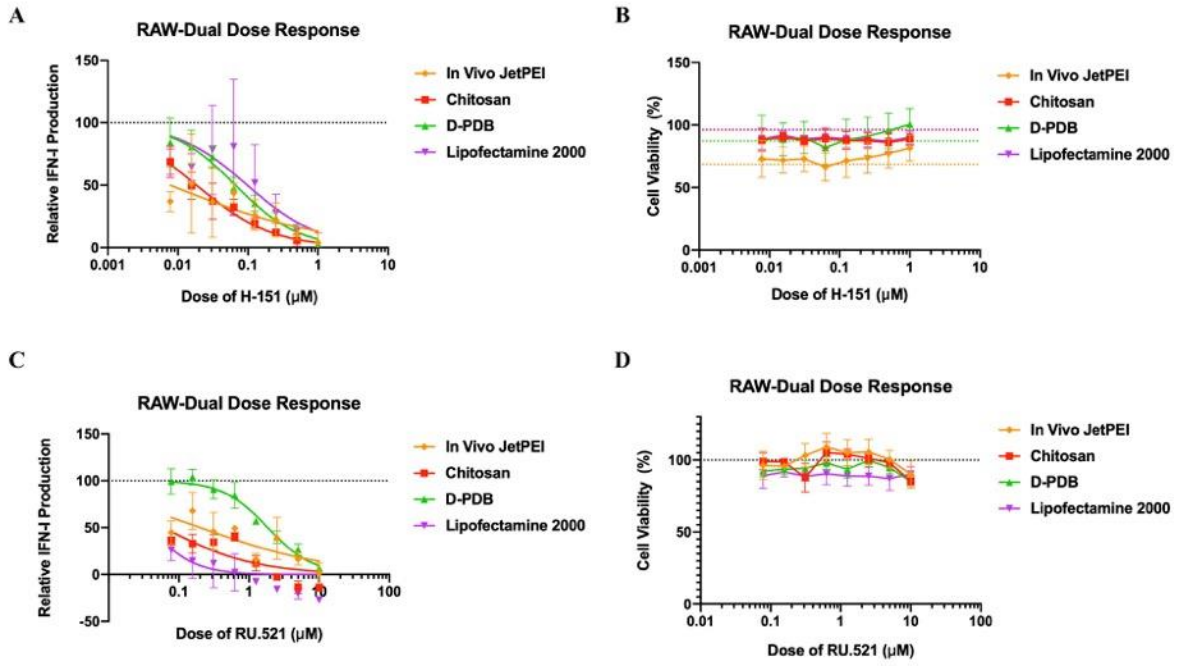

Figure 6.10. Inhibition of cGAS/STING signaling from various nanocarriers. Data courtesy of Lucinda Pastora (Wilson Lab). **(A)** RAW-Dual reporter cell assay of fixed EC75 concentrations of various nanocarriers with a dose response of the STING inhibitor, H-151. **(B)** CellTiter-Glo assay at 24 hours post treatment for cellular viability of the treated RAW-Dual cells. **(C)** RAW-Dual reporter cell assay of fixed EC75 concentrations of various nanocarriers with a dose response of the cGAS inhibitor, RU.521. **(D)** CellTiter-Glo assay at 24 hours post treatment for cellular viability of the treated RAW-Dual cells.

CHAPTER VII

CONCLUSIONS

Chapter Summaries, Limitations, and Future Directions

In Aim 1 of this dissertation (Chapter III), it was hypothesized that pharmacological activation of the cGAS enzyme can stimulate antitumor immunity. Accordingly, the objective of Aim 1 was to optimize cGAS ligands and develop cell-penetrating nanoparticles for their therapeutic delivery. A library of immunostimulatory DNA (ISD) was designed for optimal activation of the cGAS enzyme. Subsequently, the established nucleic acid carrier, D-PDB was employed for cytosolic delivery of the ISD, and formulation conditions were optimized. Utilizing several reporter cell assays, an iterative experimental screen of the various ISD / polymer complexes yielded NanoISD, a potent adjuvant that can trigger local cGAS/STING signaling via DNA-induced activation of the cGAS enzyme within the cytosol. NanoISD was found to evade major deoxyribonucleases, enhance cellular uptake, promote cytosolic delivery via endosomal escape, and efficiently trigger the cGAS/STING pathway in a cGAS-directed manner. Furthermore, NanoISD induced proinflammatory cytokine production, prompted the maturation of antigen presenting cells, promoted the tumor infiltration of NK cells and $CD8^+$ T cells, reduced tumor burden, and enhanced responses to ICB therapy. Thus, it was determined that pharmacologically targeting the cGAS protein can indeed stimulate antitumor immunity.

Regarding future work and applications, there are numerous strategies that may be pursued to enhance the therapeutic utility of NanoISD. While NanoISD does not require sustained retention like shorter nucleic acid / D-PDB complexes do, NanoISD-loaded depots (*e.g.* PLGA MPs, hydrogels, *etc.*) may enable prolonged activity through drug shielding. Indeed, the data in this

dissertation suggest that NanoISD likely becomes inactive over time when intratumorally administered by itself, and therefore longitudinal release from a drug delivery depot may result in the sustained release of NanoISD in an active form (as it did for siRNA / D-PDB complexes) and thereby improve its therapeutic efficacy. In addition to enhanced local delivery, systemic delivery may also improve therapeutic responses in metastatic tumor models. Accordingly, a second-generation version of NanoISD could potentially utilize an alternative carrier, such as a lipid nanoparticle (LNP) to accommodate systemic delivery of ISD. Combining NanoISD treatment with chemotherapies and/or other established cancer treatments may also result in improved therapeutic response by enabling enhanced tumor clearance. Lastly, as discussed in Chapter II, modulators of STING signaling have much promise for improving therapeutic responses, and NanoISD could therefore be engineered to co-deliver such modulators along with ISD.

In Aim 2 of this dissertation (Chapter IV), it was hypothesized that endogenous Alu RNA can be repurposed to stimulate antitumor immunity. Accordingly, the objective of Aim 2 was to develop cell-penetrating nanoparticles for the therapeutic delivery of immunostimulatory Alu RNA. Synthetic Alu RNA (*i.e.* immunostimulatory AluJb RNA) was *in vitro* transcribed, and D-PDB was again employed to facilitate local intracellular delivery. AluJb RNA (Left Arm) / D-PDB elicited potent induction of proinflammatory gene expression as determined *in vitro* by IFN-I reporter cell assays and *in vivo* by mRNA analysis of treated tumors as well as IVIS analysis of IFN-reporting tumors. Moreover, AluJb RNA (Left Arm) / D-PDB resulted in a significant therapeutic response as demonstrated by tumor attenuation and prolonged survival in the B16.F10 murine melanoma tumor model. Thus, it was determined that endogenous Alu RNAs can indeed be repurposed from multiple sclerosis to stimulate antitumor immunity.

Regarding future work and applications of AluJb RNA (Left Arm) / D-PDB, further

characterization of the pharmacokinetic properties of the nanoparticle may be necessary to fully understand the kinetics of signaling and its associated effects on innate immune activation. Other nanocarriers may also outperform D-PDB, which was primarily used in this work to demonstrate proof-of-concept. Lastly, Alu RNA could also be explored as a vaccine adjuvant in the context of infectious diseases, since vaccines often necessitate the use of adjuvants that enable the activation of innate immunity to provide long-lasting protection against pathogenic challenge.

In Aim 3 of this dissertation (Chapter V), it was hypothesized that drug delivery depots can enable sustained activity of cell-penetrating nanoparticles upon intratumoral administration and thereby limit the necessary number of injections required for efficacy. Accordingly, the objective of Aim 3 was to develop a drug delivery depot to sustain the activity of cell-penetrating nanoparticles in tumors. Biocompatible PLGA was used to encapsulate cell-penetrating nanoparticles in the form of microparticle depots. Successful nanoparticle loading was achieved, and subsequent nanoparticle release was demonstrated both *in vitro* and *in vivo* in both subcutaneous and intratumoral settings. Furthermore, the nanoparticles that were released from the PLGA microparticle depots preserved their functionality both *in vitro* and *in vivo*. Thus, it was determined that the PLGA depots could indeed promote sustained *in vivo* activity upon intratumoral administration using RNAi as a metric for cytosolic delivery and RNA functionality. Notably, the experimental model that was used for the *in vivo* study was so aggressive that freely administered cell-penetrating nanoparticles failed to register any *in vivo* activity from a single intratumoral treatment, which highlights the efficacy of the depot delivery strategy as the PLGA depots not only demonstrated significant activity, but also enabled sustained activity out to 3 days.

Notably, subsequent studies found that PLGA depots loaded with 5′ triphosphate RNA / D-PDB complexes (*i.e.* RIG-I adjuvant) failed to elicit a measurable therapeutic response to 4T1-

LUC tumors upon intratumoral administration, which suggests that there may be other immunological factors at play for RIG-I activity and that this drug delivery platform may be better suited for RNAi. Accordingly, future work might involve the use of the platform for the delivery of siRNA targeting immunosuppressive proteins that restrict the proper operation of the cancer-immunity-cycle or for the delivery of cell-penetrating nanoparticles in other therapeutic contexts (*e.g.* sustained delivery in lungs).

In the ancillary work of this dissertation (Chapter VI), several modulators of the STING pathway were characterized for their effects on downstream immune responses. NF-κB modulators demonstrated significant therapeutic effects, while manganese and ENPP1 inhibitors were not effective as applied in this work. Their lack of efficacy may be ascribed to the manner in which they were administered (*i.e.* separate treatments versus co-delivery in a single particle) and/or the experimental design. Indeed, reporter cells are an indirect readout for IFN-I production and they do not produce much ENPP1. Lastly, intrinsic cGAS-dependent activity of nanocarriers was confirmed and clearly implicates cGAS as a target for directed inhibition during DNA transfection. Each of the modulators that were investigated in this work have potential to shape immune responses when coadministered with STING pathway agonists and enable effective application-specific treatments. Thus, they warrant further investigation, especially in the context of cancer.

APPENDIX A

SUPPLEMENTARY MATERIAL FOR CHAPTER III

Sequence 1: **Phosphorothioate-capped 95-BP dsDNA**
A*C*A*CACACACACACACACACCATAA**AACAACAACAACAACAACAA**CACCA**ACACACACACACACACAC**CAACA**AACAACAACAACAACAA*C*A*A**

Secondary Structure Prediction Website: No Structures to Write

Complementary Sequence 1:
T*T*G*TTGTTGTTGTTGTTTGTTGGTGTGTGTGTGTGTGTGTTGGTGTTGTTGTTGTTGTTGTTTTATGGTGTGTGTGTGTGTG*T*G*T

Secondary Structure Prediction Website: Delta G = **+8.1** (unlikely to create any secondary structures)

Melting Temperature Prediction Website: GC content = 40 % ; T_M = **74 °C**
IDT OligoAnalyzer Tool Website: Maximum Delta G (*i.e.* free energy of the oligo sequence binding to its perfect complement) = **-163.94 kcal/mole**

Sequence 2: **Phosphorothioate-capped 70-BP dsDNA**
A*C*A*CACACACACACACACACCATAA**AACAACAACAACAACAACAA**CACCA**ACACACACACACACACA*C*A*C**

Secondary Structure Prediction Website: No Structures to Write

Complementary Sequence 2:
G*T*G*TGTGTGTGTGTGTTGGTGTTGTTGTTGTTGTTGTTTTATGGTGTGTGTGTGTGTG*T*G*T

Secondary Structure Prediction Website: Delta G = **+5.9** (unlikely to create any secondary structures)

Melting Temperature Prediction Website: GC content = 43 % ; T_M = **73 °C**
IDT OligoAnalyzer Tool Website: Maximum Delta G (*i.e.* free energy of the oligo sequence binding to its perfect complement) = **-118.35 kcal/mole**

Sequence 3: **Phosphorothioate-capped 45-BP dsDNA**
A*C*A*CACACACACACACACACACACA**AACAACAACAACAACAA*C*A*A**

Secondary Structure Prediction Website: No Structures to Write

Complementary Sequence 3:
T*T*G*TTGTTGTTGTTGTTTGTGTGTGTGTGTGTGTGTG*T*G*T

Secondary Structure Prediction Website: Delta G = **+3.8** (unlikely to create any secondary structures)

Melting Temperature Prediction Website: GC content = 40 % ; T_M = **66 °C**
IDT OligoAnalyzer Tool Website: Maximum Delta G (*i.e.* free energy of the oligo sequence binding to its perfect complement) = **-74.88 kcal/mole**

Sequence 4: **Phosphorothioate-capped 20-BP dsDNA**
A*C*A*CACACACACACACA*C*A*C

Secondary Structure Prediction Website: No Structures to Write

Complementary Sequence 4:
G*T*G*TGTGTGTGTGTG*T*G*T

Secondary Structure Prediction Website: Delta G = **+1.6** (unlikely to create any secondary structures)

Melting Temperature Prediction Website: GC content = 50 % ; T_M = **52 °C**
IDT OligoAnalyzer Tool Website: Maximum Delta G (*i.e.* free energy of the oligo sequence binding to its perfect complement) = **-31 kcal/mole**

Supplemental Figure A.S1- The starting ISD library of synthetic dsDNA from IDT. The star symbol (*i.e.* *) represents a phosphorothioate bond. Theoretical melting temperature values were obtained from the melting temperature prediction website, sciencelauncher.com/oligocalc.html. Theoretical maximum Delta G values were obtained from the IDT OligoAnalyzer Tool website, idtdna.com/calc/analyzer. Theoretical Delta G values for secondary structure formation were obtained from the secondary structure prediction website, rna.urmc.rochester.edu/RNAstructureWeb/Servers/Predict1/Predict1.html.

A

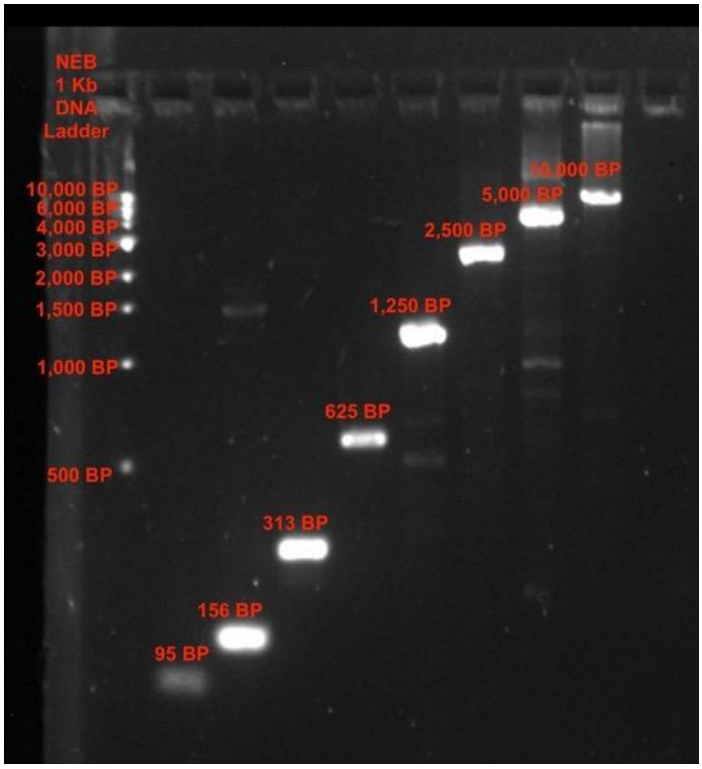

B

95BP TOP:
TGATAACACTGCGGCCAACTTACTTCTGACAACGATCGGAGGACCGAAGGAGCTAA
CCGCTTTTTTGCACAACATGGGGGATCATGTAACTCGCC

95BP BOT:
GGCGAGTTACATGATCCCCCATGTTGTGCAAAAAAGCGGTTAGCTCCTTCGGTCCTC
CGATCGTTGTCAGAAGTAAGTTGGCCGCAGTGTTATCA

156BP TOP:
TGATAACACTGCGGCCAACTTACTTCTGACAACGATCGGAGGACCGAAGGAGCTAA
CCGCTTTTTTGCACAACATGGGGGATCATGTAACTCGCCTTGATCGTTGGGAACCGG
AGCTGAATGAAGCCATACCAAACGACGAGCGTGACACCACGAT

156BP BOT:
ATCGTGGTGTCACGCTCGTCGTTTGGTATGGCTTCATTCAGCTCCGGTTCCCAACGAT
CAAGGCGAGTTACATGATCCCCCATGTTGTGCAAAAAAGCGGTTAGCTCCTTCGGTC
CTCCGATCGTTGTCAGAAGTAAGTTGGCCGCAGTGTTATCA

313BP TOP:
TGATAACACTGCGGCCAACTTACTTCTGACAACGATCGGAGGACCGAAGGAGCTAA
CCGCTTTTTTGCACAACATGGGGGATCATGTAACTCGCCTTGATCGTTGGGAACCGG
AGCTGAATGAAGCCATACCAAACGACGAGCGTGACACCACGATGCCTGTAGCAATG

GCAACAACGTTGCGCAAACTATTAACTGGCGAACTACTTACTCTAGCTTCCCGGCAA
CAATTAATAGACTGGATGGAGGCGGATAAAGTTGCAGGACCACTTCTGCGCTCGGC
CCTTCCGGCTGGCTGGTTTATTGCTGATAAA

313BP BOT:
TTTATCAGCAATAAACCAGCCAGCCGGAAGGGCCGAGCGCAGAAGTGGTCCTGCAA
CTTTATCCGCCTCCATCCAGTCTATTAATTGTTGCCGGGAAGCTAGAGTAAGTAGTTC
GCCAGTTAATAGTTTGCGCAACGTTGTTGCCATTGCTACAGGCATCGTGGTGTCACG
CTCGTCGTTTGGTATGGCTTCATTCAGCTCCGGTTCCCAACGATCAAGGCGAGTTAC
ATGATCCCCCATGTTGTGCAAAAAAGCGGTTAGCTCCTTCGGTCCTCCGATCGTTGT
CAGAAGTAAGTTGGCCGCAGTGTTATCA

625BP TOP:
TGATAACACTGCGGCCAACTTACTTCTGACAACGATCGGAGGACCGAAGGAGCTAA
CCGCTTTTTTGCACAACATGGGGGATCATGTAACTCGCCTTGATCGTTGGGAACCGG
AGCTGAATGAAGCCATACCAAACGACGAGCGTGACACCACGATGCCTGTAGCAATG
GCAACAACGTTGCGCAAACTATTAACTGGCGAACTACTTACTCTAGCTTCCCGGCAA
CAATTAATAGACTGGATGGAGGCGGATAAAGTTGCAGGACCACTTCTGCGCTCGGC
CCTTCCGGCTGGCTGGTTTATTGCTGATAAATCTGGAGCCGGTGAGCGTGGGTCTCG
CGGTATCATTGCAGCACTGGGGCCAGATGGTAAGCCCTCCCGTATCGTAGTTATCTA
CACGACGGGGAGTCAGGCAACTATGGATGAACGAAATAGACAGATCGCTGAGATAG
GTGCCTCACTGATTAAGCATTGGTAACTGTCAGACCAAGTTTACTCATATATACTTTA
GATTGATTTAAAACTTCATTTTTAATTTAAAAGGATCTAGGTGAAGATCCTTTTTGAT
AATCTCATGACCAAAATCCCTTAACGTGAGTTTTCGTTCCACTGAGCGTCAGACCCC

625BP BOT:
GGGGTCTGACGCTCAGTGGAACGAAAACTCACGTTAAGGGATTTTGGTCATGAGATT
ATCAAAAAGGATCTTCACCTAGATCCTTTTAAATTAAAAATGAAGTTTTAAATCAAT
CTAAAGTATATATGAGTAAACTTGGTCTGACAGTTACCAATGCTTAATCAGTGAGGC
ACCTATCTCAGCGATCTGTCTATTTCGTTCATCCATAGTTGCCTGACTCCCCGTCGTG
TAGATAACTACGATACGGGAGGGCTTACCATCTGGCCCCAGTGCTGCAATGATACCG
CGAGACCCACGCTCACCGGCTCCAGATTTATCAGCAATAAACCAGCCAGCCGGAAG
GGCCGAGCGCAGAAGTGGTCCTGCAACTTTATCCGCCTCCATCCAGTCTATTAATTG
TTGCCGGGAAGCTAGAGTAAGTAGTTCGCCAGTTAATAGTTTGCGCAACGTTGTTGC
CATTGCTACAGGCATCGTGGTGTCACGCTCGTCGTTTGGTATGGCTTCATTCAGCTCC
GGTTCCCAACGATCAAGGCGAGTTACATGATCCCCCATGTTGTGCAAAAAAGCGGTT
AGCTCCTTCGGTCCTCCGATCGTTGTCAGAAGTAAGTTGGCCGCAGTGTTATCA

1250BP TOP:
TGATAACACTGCGGCCAACTTACTTCTGACAACGATCGGAGGACCGAAGGAGCTAA
CCGCTTTTTTGCACAACATGGGGGATCATGTAACTCGCCTTGATCGTTGGGAACCGG
AGCTGAATGAAGCCATACCAAACGACGAGCGTGACACCACGATGCCTGTAGCAATG
GCAACAACGTTGCGCAAACTATTAACTGGCGAACTACTTACTCTAGCTTCCCGGCAA
CAATTAATAGACTGGATGGAGGCGGATAAAGTTGCAGGACCACTTCTGCGCTCGGC
CCTTCCGGCTGGCTGGTTTATTGCTGATAAATCTGGAGCCGGTGAGCGTGGGTCTCG
CGGTATCATTGCAGCACTGGGGCCAGATGGTAAGCCCTCCCGTATCGTAGTTATCTA

CACGACGGGGAGTCAGGCAACTATGGATGAACGAAATAGACAGATCGCTGAGATAG
GTGCCTCACTGATTAAGCATTGGTAACTGTCAGACCAAGTTTACTCATATATACTTTA
GATTGATTTAAAACTTCATTTTTAATTTAAAAGGATCTAGGTGAAGATCCTTTTTGAT
AATCTCATGACCAAAATCCCTTAACGTGAGTTTTCGTTCCACTGAGCGTCAGACCCC
GTAGAAAAGATCAAAGGATCTTCTTGAGATCCTTTTTTTCTGCGCGTAATCTGCTGCT
TGCAAACAAAAAAACCACCGCTACCAGCGGTGGTTTGTTTGCCGGATCAAGAGCTA
CCAACTCTTTTTCCGAAGGTAACTGGCTTCAGCAGAGCGCAGATACCAAATACTGTT
CTTCTAGTGTAGCCGTAGTTAGGCCACCACTTCAAGAACTCTGTAGCACCGCCTACA
TACCTCGCTCTGCTAATCCTGTTACCAGTGGCTGCTGCCAGTGGCGATAAGTCGTGT
CTTACCGGGTTGGACTCAAGACGATAGTTACCGGATAAGGCGCAGCGGTCGGGCTG
AACGGGGGGTTCGTGCACACAGCCCAGCTTGGAGCGAACGACCTACACCGAACTGA
GATACCTACAGCGTGAGCTATGAGAAAGCGCCACGCTTCCCGAAGGGAGAAAGGCG
GACAGGTATCCGGTAAGCGGCAGGGTCGGAACAGGAGAGCGCACGAGGGAGCTTC
CAGGGGGAAACGCCTGGTATCTTTATAGTCCTGTCGGGTTTCGCCACCTCTGACTTG
AGCGTCGATTTTTGTGATGCTCGTCAGGGGGGCGGAGCCTATGGAAAAACGCCAGC
AACG

1250BP BOT:

CGTTGCTGGCGTTTTTCCATAGGCTCCGCCCCCCTGACGAGCATCACAAAAATCGAC
GCTCAAGTCAGAGGTGGCGAAACCCGACAGGACTATAAAGATACCAGGCGTTTCCC
CCTGGAAGCTCCCTCGTGCGCTCTCCTGTTCCGACCCTGCCGCTTACCGGATACCTGT
CCGCCTTTCTCCCTTCGGGAAGCGTGGCGCTTTCTCATAGCTCACGCTGTAGGTATCT
CAGTTCGGTGTAGGTCGTTCGCTCCAAGCTGGGCTGTGTGCACGAACCCCCCGTTCA
GCCCGACCGCTGCGCCTTATCCGGTAACTATCGTCTTGAGTCCAACCCGGTAAGACA
CGACTTATCGCCACTGGCAGCAGCCACTGGTAACAGGATTAGCAGAGCGAGGTATG
TAGGCGGTGCTACAGAGTTCTTGAAGTGGTGGCCTAACTACGGCTACACTAGAAGA
ACAGTATTTGGTATCTGCGCTCTGCTGAAGCCAGTTACCTTCGGAAAAAGAGTTGGT
AGCTCTTGATCCGGCAAACAAACCACCGCTGGTAGCGGTGGTTTTTTTGTTTGCAAG
CAGCAGATTACGCGCAGAAAAAAAGGATCTCAAGAAGATCCTTTGATCTTTTCTACG
GGGTCTGACGCTCAGTGGAACGAAAACTCACGTTAAGGGATTTTGGTCATGAGATTA
TCAAAAAGGATCTTCACCTAGATCCTTTTAAATTAAAAATGAAGTTTTAAATCAATC
TAAAGTATATATGAGTAAACTTGGTCTGACAGTTACCAATGCTTAATCAGTGAGGCA
CCTATCTCAGCGATCTGTCTATTTCGTTCATCCATAGTTGCCTGACTCCCCGTCGTGT
AGATAACTACGATACGGGAGGGCTTACCATCTGGCCCCAGTGCTGCAATGATACCG
CGAGACCCACGCTCACCGGCTCCAGATTTATCAGCAATAAACCAGCCAGCCGGAAG
GGCCGAGCGCAGAAGTGGTCCTGCAACTTTATCCGCCTCCATCCAGTCTATTAATTG
TTGCCGGGAAGCTAGAGTAAGTAGTTCGCCAGTTAATAGTTTGCGCAACGTTGTTGC
CATTGCTACAGGCATCGTGGTGTCACGCTCGTCGTTTGGTATGGCTTCATTCAGCTCC
GGTTCCCAACGATCAAGGCGAGTTACATGATCCCCCATGTTGTGCAAAAAAGCGGTT
AGCTCCTTCGGTCCTCCGATCGTTGTCAGAAGTAAGTTGGCCGCAGTGTTATCA

2500BP TOP:

AGGGACAGCAGAGATCCACTTTGGCGCCGGCTCGAGGGGGCCCGGGTGCAAAGATG
GATAAAGTTTTAAACAGAGAGGAATCTTTGCAGCTAATGGACCTTCTAGGTCTTGAA
AGGAGTGGGAATTGGCTCCGGTGCCCGTCAGTGGGCAGAGCGCACATCGCCCACAG
TCCCCGAGAAGTTGGGGGGAGGGGTCGGCAATTGATCCGGTGCCTAGAGAAGGTGG

CGCGGGGTAAACTGGGAAAGTGATGTCGTGTACTGGCTCCGCCTTTTTCCCGAGGGT
GGGGGAGAACCGTATATAAGTGCAGTAGTCGCCGTGAACGTTCTTTTTCGCAACGGG
TTTGCCGCCAGAACACAGGTAAGTGCCGTGTGTGGTTCCCGCGGGCCTGGCCTCTTT
ACGGGTTATGGCCCTTGCGTGCCTTGAATTACTTCCACCTGGCTGCAGTACGTGATTC
TTGATCCCGAGCTTCGGGTTGGAAGTGGGTGGGAGAGTTCGAGGCCTTGCGCTTAAG
GAGCCCCTTCGCCTCGTGCTTGAGTTGAGGCCTGGCCTGGGCGCTGGGGCCGCCGCG
TGCGAATCTGGTGGCACCTTCGCGCCTGTCTCGCTGCTTTCGATAAGTCTCTAGCCAT
TTAAAATTTTTGATGACCTGCTGCGACGCTTTTTTTCTGGCAAGATAGTCTTGTAAAT
GCGGGCCAAGATCTGCACACTGGTATTTCGGTTTTTGGGGCCGCGGGCGGCGACGG
GGCCCGTGCGTCCCAGCGCACATGTTCGGCGAGGCGGGGCCTGCGAGCGCGGCCAC
CGAGAATCGGACGGGGGTAGTCTCAAGCTGGCCGGCCTGCTCTGGTGCCTGGCCTC
GCGCCGCCGTGTATCGCCCCGCCCTGGGCGGCAAGGCTGGCCCGGTCGGCACCAGT
TGCGTGAGCGGAAAGATGGCCGCTTCCCGGCCCTGCTGCAGGGAGCTCAAAATGGA
GGACGCGGCGCTCGGGAGAGCGGGCGGGTGAGTCACCCACACAAAGGAAAAGGGC
CTTTCCGTCCTCAGCCGTCGCTTCATGTGACTCCACGGAGTACCGGGCGCCGTCCAG
GCACCTCGATTAGTTCTCGAGCTTTTGGAGTACGTCGTCTTTAGGTTGGGGGGAGGG
GTTTTATGCGATGGAGTTTCCCCACACTGAGTGGGTGGAGACTGAAGTTAGGCCAGC
TTGGCACTTGATGTAATTCTCCTTGGAATTTGCCCTTTTTGAGTTTGGATCTTGGTTC
ATTCTCAAGCCTCAGACAGTGGTTCAAAGTTTTTTTCTTCCATTTCAGGTGTCGTGAC
GTACGGCCACCATGACCGAGTACAAGCCCACGGTGCGCCTCGCCACCCGCGACGAC
GTCCCCAGGGCCGTACGCACCCTCGCCGCCGCGTTCGCCGACTACCCCGCCACGCGC
CACACCGTCGATCCGGACCGCCACATCGAGCGGGTCACCGAGCTGCAAGAACTCTT
CCTCACGCGCGTCGGGCTCGACATCGGCAAGGTGTGGGTCGCGGACGACGGCGCCG
CCGTGGCGGTCTGGACCACGCCGGAGAGCGTCGAAGCGGGGGCGGTGTTCGCCGAG
ATCGGCCCGCGCATGGCCGAGTTGAGCGGTTCCCGGCTGGCCGCGCAGCAACAGAT
GGAAGGCCTCCTGGCGCCGCACCGGCCCAAGGAGCCCGCGTGGTTCCTGGCCACCG
TCGGAGTCTCGCCCGACCACCAGGGCAAGGGTCTGGGCAGCGCCGTCGTGCTCCCC
GGAGTGGAGGCGGCCGAGCGCGCCGGGGTGCCCGCCTTCCTGGAGACCTCCGCGCC
CCGCAACCTCCCCTTCTACGAGCGGCTCGGCTTCACCGTCACCGCCGACGTCGAGGT
GCCCGAAGGACCGCGCACCTGGTGCATGACCCGCAAGCCCGGTGCCTGAACGCGTT
AAGTCGACAATCAACCTCTGGATTACAAAATTTGTGAAAGATTGACTGGTATTCTTA
ACTATGTTGCTCCTTTTACGCTATGTGGATACGCTGCTTTAATGCCTTTGTATCATGC
TATTGCTTCCCGTATGGCTTTCATTTTCTCCTCCTTGTATAAATCCTGGTTGCTGTCTC
TTTATGAGGAGTTGTGGCCCGTTGTCAGGCAACGTGGCGTGGTGTGCACTGTGTTTG
CTGACGCAACCCCCACTGGTTGGGGCATTGCCACCACCTGTCAGCTCCTTTCCGGGA
CTTTCGCTTTCCCCCTCCCTATTGCCACGGCGGAACTCATCGCCGCCTGCCTTGCCCG
CTGCTGGACAGGGGCTCGGCTGTTGGGCACTGACAATTCCGTGGTGTTGTCGGGGAA
ATCATCGTCCTTTCCTTGGCTGCTCGCCTGTGTTGCCACCTGGATTCTGCGCGGGACG
TCCTTCTGCTACGTCCCTTCGGCCCTCAATCCAGCGGACCTTCCTTCCCGCGGCCTGC
TGCCGGCTCTGCGGCCTCTTCCGCGTCTTCGCCTTCGCCCTCAGACGAGTCGGATCT

2500BP BOT:

AGATCCGACTCGTCTGAGGGCGAAGGCGAAGACGCGGAAGAGGCCGCAGAGCCGG
CAGCAGGCCGCGGGAAGGAAGGTCCGCTGGATTGAGGGCCGAAGGGACGTAGCAG
AAGGACGTCCCGCGCAGAATCCAGGTGGCAACACAGGCGAGCAGCCAAGGAAAGG
ACGATGATTTCCCCGACAACACCACGGAATTGTCAGTGCCCAACAGCCGAGCCCCT

GTCCAGCAGCGGGCAAGGCAGGCGGCGATGAGTTCCGCCGTGGCAATAGGGAGGG
GGAAAGCGAAAGTCCCGGAAAGGAGCTGACAGGTGGTGGCAATGCCCCAACCAGT
GGGGGTTGCGTCAGCAAACACAGTGCACACCACGCCACGTTGCCTGACAACGGGCC
ACAACTCCTCATAAAGAGACAGCAACCAGGATTTATACAAGGAGGAGAAAATGAAA
GCCATACGGGAAGCAATAGCATGATACAAAGGCATTAAAGCAGCGTATCCACATAG
CGTAAAAGGAGCAACATAGTTAAGAATACCAGTCAATCTTTCACAAATTTTGTAATC
CAGAGGTTGATTGTCGACTTAACGCGTTCAGGCACCGGGCTTGCGGGTCATGCACCA
GGTGCGCGGTCCTTCGGGCACCTCGACGTCGGCGGTGACGGTGAAGCCGAGCCGCT
CGTAGAAGGGGAGGTTGCGGGGCGCGGAGGTCTCCAGGAAGGCGGGCACCCCGGC
GCGCTCGGCCGCCTCCACTCCGGGGAGCACGACGGCGCTGCCCAGACCCTTGCCCTG
GTGGTCGGGCGAGACTCCGACGGTGGCCAGGAACCACGCGGGCTCCTTGGGCCGGT
GCGGCGCCAGGAGGCCTTCCATCTGTTGCTGCGCGGCCAGCCGGGAACCGCTCAAC
TCGGCCATGCGCGGGCCGATCTCGGCGAACACCGCCCCCGCTTCGACGCTCTCCGGC
GTGGTCCAGACCGCCACGGCGGCGCCGTCGTCCGCGACCCACACCTTGCCGATGTCG
AGCCCGACGCGCGTGAGGAAGAGTTCTTGCAGCTCGGTGACCCGCTCGATGTGGCG
GTCCGGATCGACGGTGTGGCGCGTGGCGGGGTAGTCGGCGAACGCGGCGGCGAGGG
TGCGTACGGCCCTGGGGACGTCGTCGCGGGTGGCGAGGCGCACCGTGGGCTTGTAC
TCGGTCATGGTGGCCGTACGTCACGACACCTGAAATGGAAGAAAAAAACTTTGAAC
CACTGTCTGAGGCTTGAGAATGAACCAAGATCCAAACTCAAAAAGGGCAAATTCCA
AGGAGAATTACATCAAGTGCCAAGCTGGCCTAACTTCAGTCTCCACCCACTCAGTGT
GGGGAAACTCCATCGCATAAAACCCCTCCCCCCAACCTAAAGACGACGTACTCCAA
AAGCTCGAGAACTAATCGAGGTGCCTGGACGGCGCCCGGTACTCCGTGGAGTCACA
TGAAGCGACGGCTGAGGACGGAAAGGCCCTTTTCCTTTGTGTGGGTGACTCACCCGC
CCGCTCTCCCGAGCGCCGCGTCCTCCATTTTGAGCTCCCTGCAGCAGGGCCGGGAAG
CGGCCATCTTTCCGCTCACGCAACTGGTGCCGACCGGGCCAGCCTTGCCGCCCAGGG
CGGGGCGATACACGGCGGCGCGAGGCCAGGCACCAGAGCAGGCCGGCCAGCTTGA
GACTACCCCCGTCCGATTCTCGGTGGCCGCGCTCGCAGGCCCCGCCTCGCCGAACAT
GTGCGCTGGGACGCACGGGCCCCGTCGCCGCCCGCGGCCCCAAAAACCGAAATACC
AGTGTGCAGATCTTGGCCCGCATTTACAAGACTATCTTGCCAGAAAAAAAGCGTCGC
AGCAGGTCATCAAAAATTTTAAATGGCTAGAGACTTATCGAAAGCAGCGAGACAGG
CGCGAAGGTGCCACCAGATTCGCACGCGGCGGCCCCAGCGCCCAGGCCAGGCCTCA
ACTCAAGCACGAGGCGAAGGGGCTCCTTAAGCGCAAGGCCTCGAACTCTCCCACCC
ACTTCCAACCCGAAGCTCGGGATCAAGAATCACGTACTGCAGCCAGGTGGAAGTAA
TTCAAGGCACGCAAGGGCCATAACCCGTAAAGAGGCCAGGCCCGCGGGAACCACAC
ACGGCACTTACCTGTGTTCTGGCGGCAAACCCGTTGCGAAAAAGAACGTTCACGGC
GACTACTGCACTTATATACGGTTCTCCCCCACCCTCGGGAAAAAGGCGGAGCCAGTA
CACGACATCACTTTCCCAGTTTACCCCGCGCCACCTTCTCTAGGCACCGGATCAATT
GCCGACCCCTCCCCCCAACTTCTCGGGGACTGTGGGCGATGTGCGCTCTGCCCACTG
ACGGGCACCGGAGCCAATTCCCACTCCTTTCAAGACCTAGAAGGTCCATTAGCTGCA
AAGATTCCTCTCTGTTTAAAACTTTATCCATCTTTGCACCCGGGCCCCCTCGAGCCGG
CGCCAAAGTGGATCTCTGCTGTCCCT

5000BP TOP:

ATCCGGTGCCTAGAGAAGGTGGCGCGGGGTAAACTGGGAAAGTGATGTCGTGTACT
GGCTCCGCCTTTTTCCCGAGGGTGGGGGAGAACCGTATATAAGTGCAGTAGTCGCCG
TGAACGTTCTTTTTCGCAACGGGTTTGCCGCCAGAACACAGGTAAGTGCCGTGTGTG

GTTCCCGCGGGCCTGGCCTCTTTACGGGTTATGGCCCTTGCGTGCCTTGAATTACTTC
CACCTGGCTGCAGTACGTGATTCTTGATCCCGAGCTTCGGGTTGGAAGTGGGTGGGA
GAGTTCGAGGCCTTGCGCTTAAGGAGCCCCTTCGCCTCGTGCTTGAGTTGAGGCCTG
GCCTGGGCGCTGGGGCCGCCGCGTGCGAATCTGGTGGCACCTTCGCGCCTGTCTCGC
TGCTTTCGATAAGTCTCTAGCCATTTAAAATTTTTGATGACCTGCTGCGACGCTTTTT
TTCTGGCAAGATAGTCTTGTAAATGCGGGCCAAGATCTGCACACTGGTATTTCGGTT
TTTGGGGCCGCGGGCGGCGACGGGGCCCGTGCGTCCCAGCGCACATGTTCGGCGAG
GCGGGGCCTGCGAGCGCGGCCACCGAGAATCGGACGGGGGTAGTCTCAAGCTGGCC
GGCCTGCTCTGGTGCCTGGCCTCGCGCCGCCGTGTATCGCCCCGCCCTGGGCGGCAA
GGCTGGCCCGGTCGGCACCAGTTGCGTGAGCGGAAAGATGGCCGCTTCCCGGCCCT
GCTGCAGGGAGCTCAAAATGGAGGACGCGGCGCTCGGGAGAGCGGGCGGGTGAGT
CACCCACACAAAGGAAAAGGGCCTTTCCGTCCTCAGCCGTCGCTTCATGTGACTCCA
CGGAGTACCGGGCGCCGTCCAGGCACCTCGATTAGTTCTCGAGCTTTTGGAGTACGT
CGTCTTTAGGTTGGGGGGAGGGGTTTTATGCGATGGAGTTTCCCCACACTGAGTGGG
TGGAGACTGAAGTTAGGCCAGCTTGGCACTTGATGTAATTCTCCTTGGAATTTGCCC
TTTTTGAGTTTGGATCTTGGTTCATTCTCAAGCCTCAGACAGTGGTTCAAAGTTTTTT
TCTTCCATTTCAGGTGTCGTGACGTACGGCCACCATGACCGAGTACAAGCCCACGGT
GCGCCTCGCCACCCGCGACGACGTCCCCAGGGCCGTACGCACCCTCGCCGCCGCGTT
CGCCGACTACCCCGCCACGCGCCACACCGTCGATCCGGACCGCCACATCGAGCGGG
TCACCGAGCTGCAAGAACTCTTCCTCACGCGCGTCGGGCTCGACATCGGCAAGGTGT
GGGTCGCGGACGACGGCGCCGCCGTGGCGGTCTGGACCACGCCGGAGAGCGTCGAA
GCGGGGGCGGTGTTCGCCGAGATCGGCCCGCGCATGGCCGAGTTGAGCGGTTCCCG
GCTGGCCGCGCAGCAACAGATGGAAGGCCTCCTGGCGCCGCACCGGCCCAAGGAGC
CCGCGTGGTTCCTGGCCACCGTCGGAGTCTCGCCCGACCACCAGGGCAAGGGTCTG
GGCAGCGCCGTCGTGCTCCCCGGAGTGGAGGCGGCCGAGCGCGCCGGGGTGCCCGC
CTTCCTGGAGACCTCCGCGCCCCGCAACCTCCCCTTCTACGAGCGGCTCGGCTTCAC
CGTCACCGCCGACGTCGAGGTGCCCGAAGGACCGCGCACCTGGTGCATGACCCGCA
AGCCCGGTGCCTGAACGCGTTAAGTCGACAATCAACCTCTGGATTACAAAATTTGTG
AAAGATTGACTGGTATTCTTAACTATGTTGCTCCTTTTACGCTATGTGGATACGCTGC
TTTAATGCCTTTGTATCATGCTATTGCTTCCCGTATGGCTTTCATTTTCTCCTCCTTGT
ATAAATCCTGGTTGCTGTCTCTTTATGAGGAGTTGTGGCCCGTTGTCAGGCAACGTG
GCGTGGTGTGCACTGTGTTTGCTGACGCAACCCCCACTGGTTGGGGCATTGCCACCA
CCTGTCAGCTCCTTTCCGGGACTTTCGCTTTCCCCCTCCCTATTGCCACGGCGGAACT
CATCGCCGCCTGCCTTGCCCGCTGCTGGACAGGGGCTCGGCTGTTGGGCACTGACAA
TTCCGTGGTGTTGTCGGGGAAATCATCGTCCTTTCCTTGGCTGCTCGCCTGTGTTGCC
ACCTGGATTCTGCGCGGGACGTCCTTCTGCTACGTCCCTTCGGCCCTCAATCCAGCG
GACCTTCCTTCCCGCGGCCTGCTGCCGGCTCTGCGGCCTCTTCCGCGTCTTCGCCTTC
GCCCTCAGACGAGTCGGATCTCCCTTTGGGCCGCCTCCCCGCGTCGACTTTAAGACC
AATGACTTACAAGGCAGCTGTAGATCTTAGCCACTTTTTAAAAGAAAAGGGGGGAC
TGGAAGGGCTAATTCACTCCCAACGAAGACAAGATCTGCTTTTTGCTTGTACTGGGT
CTCTCTGGTTAGACCAGATCTGAGCCTGGGAGCTCTCTGGCTAACTAGGGAACCCAC
TGCTTAAGCCTCAATAAAGCTTGCCTTGAGTGCTTCAAGTAGTGTGTGCCCGTCTGTT
GTGTGACTCTGGTAACTAGAGATCCCTCAGACCCTTTTAGTCAGTGTGGAAAATCTC
TAGCAGTACGTATAGTAGTTCATGTCATCTTATTATTCAGTATTTATAACTTGCAAAG
AAATGAATATCAGAGAGTGAGAGGAACTTGTTTATTGCAGCTTATAATGGTTACAAA
TAAAGCAATAGCATCACAAATTTCACAAATAAAGCATTTTTTTCACTGCATTCTAGT

TGTGGTTTGTCCAAACTCATCAATGTATCTTATCATGTCTGGCTCTAGCTATCCCGCC
CCTAACTCCGCCCATCCCGCCCCTAACTCCGCCCAGTTCCGCCCATTCTCCGCCCCAT
GGCTGACTAATTTTTTTTATTTATGCAGAGGCCGAGGCCGCCTCGGCCTCTGAGCTAT
TCCAGAAGTAGTGAGGAGGCTTTTTTGGAGGCCTAGGGACGTACCCAATTCGCCCTA
TAGTGAGTCGTATTACGCGCGCTCACTGGCCGTCGTTTTACAACGTCGTGACTGGGA
AAACCCTGGCGTTACCCAACTTAATCGCCTTGCAGCACATCCCCCTTTCGCCAGCTG
GCGTAATAGCGAAGAGGCCCGCACCGATCGCCCTTCCCAACAGTTGCGCAGCCTGA
ATGGCGAATGGGACGCGCCCTGTAGCGGCGCATTAAGCGCGGCGGGTGTGGTGGTT
ACGCGCAGCGTGACCGCTACACTTGCCAGCGCCCTAGCGCCCGCTCCTTTCGCTTTC
TTCCCTTCCTTTCTCGCCACGTTCGCCGGCTTTCCCCGTCAAGCTCTAAATCGGGGGC
TCCCTTTAGGGTTCCGATTTAGTGCTTTACGGCACCTCGACCCCAAAAAACTTGATTA
GGGTGATGGTTCACGTAGTGGGCCATCGCCCTGATAGACGGTTTTTCGCCCTTTGAC
GTTGGAGTCCACGTTCTTTAATAGTGGACTCTTGTTCCAAACTGGAACAACACTCAA
CCCTATCTCGGTCTATTCTTTTGATTTATAAGGGATTTTGCCGATTTCGGCCTATTGG
TTAAAAAATGAGCTGATTTAACAAAAATTTAACGCGAATTTTAACAAAATATTAACG
CTTACAATTTAGGTGGCACTTTTCGGGGAAATGTGCGCGGAACCCCTATTTGTTTATT
TTTCTAAATACATTCAAATATGTATCCGCTCATGAGACAATAACCCTGATAAATGCT
TCAATAATATTGAAAAAGGAAGAGTATGAGTATTCAACATTTCCGTGTCGCCCTTAT
TCCCTTTTTTGCGGCATTTTGCCTTCCTGTTTTTGCTCACCCAGAAACGCTGGTGAAA
GTAAAAGATGCTGAAGATCAGTTGGGTGCACGAGTGGGTTACATCGAACTGGATCT
CAACAGCGGTAAGATCCTTGAGAGTTTTCGCCCCGAAGAACGTTTTCCAATGATGAG
CACTTTTAAAGTTCTGCTATGTGGCGCGGTATTATCCCGTATTGACGCCGGGCAAGA
GCAACTCGGTCGCCGCATACACTATTCTCAGAATGACTTGGTTGAGTACTCACCAGT
CACAGAAAAGCATCTTACGGATGGCATGACAGTAAGAGAATTATGCAGTGCTGCCA
TAACCATGAGTGATAACACTGCGGCCAACTTACTTCTGACAACGATCGGAGGACCG
AAGGAGCTAACCGCTTTTTTGCACAACATGGGGGATCATGTAACTCGCCTTGATCGT
TGGGAACCGGAGCTGAATGAAGCCATACCAAACGACGAGCGTGACACCACGATGCC
TGTAGCAATGGCAACAACGTTGCGCAAACTATTAACTGGCGAACTACTTACTCTAGC
TTCCCGGCAACAATTAATAGACTGGATGGAGGCGGATAAAGTTGCAGGACCACTTC
TGCGCTCGGCCCTTCCGGCTGGCTGGTTTATTGCTGATAAATCTGGAGCCGGTGAGC
GTGGGTCTCGCGGTATCATTGCAGCACTGGGGCCAGATGGTAAGCCCTCCCGTATCG
TAGTTATCTACACGACGGGGAGTCAGGCAACTATGGATGAACGAAATAGACAGATC
GCTGAGATAGGTGCCTCACTGATTAAGCATTGGTAACTGTCAGACCAAGTTTACTCA
TATATACTTTAGATTGATTTAAAACTTCATTTTTAATTTAAAAGGATCTAGGTGAAGA
TCCTTTTTGATAATCTCATGACCAAAATCCCTTAACGTGAGTTTTCGTTCCACTGAGC
GTCAGACCCCGTAGAAAAGATCAAAGGATCTTCTTGAGATCCTTTTTTTCTGCGCGT
AATCTGCTGCTTGCAAACAAAAAAACCACCGCTACCAGCGGTGGTTTGTTTGCCGGA
TCAAGAGCTACCAACTCTTTTTCCGAAGGTAACTGGCTTCAGCAGAGCGCAGATACC
AAATACTGTTCTTCTAGTGTAGCCGTAGTTAGGCCACCACTT

5000BP BOT:

AAGTGGTGGCCTAACTACGGCTACACTAGAAGAACAGTATTTGGTATCTGCGCTCTG
CTGAAGCCAGTTACCTTCGGAAAAAGAGTTGGTAGCTCTTGATCCGGCAAACAAAC
CACCGCTGGTAGCGGTGGTTTTTTTGTTTGCAAGCAGCAGATTACGCGCAGAAAAAA
AGGATCTCAAGAAGATCCTTTGATCTTTTCTACGGGGTCTGACGCTCAGTGGAACGA
AAACTCACGTTAAGGGATTTTGGTCATGAGATTATCAAAAAGGATCTTCACCTAGAT

CCTTTTAAATTAAAAATGAAGTTTTAAATCAATCTAAAGTATATATGAGTAAACTTG
GTCTGACAGTTACCAATGCTTAATCAGTGAGGCACCTATCTCAGCGATCTGTCTATTT
CGTTCATCCATAGTTGCCTGACTCCCCGTCGTGTAGATAACTACGATACGGGAGGGC
TTACCATCTGGCCCCAGTGCTGCAATGATACCGCGAGACCCACGCTCACCGGCTCCA
GATTTATCAGCAATAAACCAGCCAGCCGGAAGGGCCGAGCGCAGAAGTGGTCCTGC
AACTTTATCCGCCTCCATCCAGTCTATTAATTGTTGCCGGGAAGCTAGAGTAAGTAG
TTCGCCAGTTAATAGTTTGCGCAACGTTGTTGCCATTGCTACAGGCATCGTGGTGTC
ACGCTCGTCGTTTGGTATGGCTTCATTCAGCTCCGGTTCCCAACGATCAAGGCGAGT
TACATGATCCCCCATGTTGTGCAAAAAAGCGGTTAGCTCCTTCGGTCCTCCGATCGT
TGTCAGAAGTAAGTTGGCCGCAGTGTTATCACTCATGGTTATGGCAGCACTGCATAA
TTCTCTTACTGTCATGCCATCCGTAAGATGCTTTTCTGTGACTGGTGAGTACTCAACC
AAGTCATTCTGAGAATAGTGTATGCGGCGACCGAGTTGCTCTTGCCCGGCGTCAATA
CGGGATAATACCGCGCCACATAGCAGAACTTTAAAAGTGCTCATCATTGGAAAACG
TTCTTCGGGGCGAAAACTCTCAAGGATCTTACCGCTGTTGAGATCCAGTTCGATGTA
ACCCACTCGTGCACCCAACTGATCTTCAGCATCTTTTACTTTCACCAGCGTTTCTGGG
TGAGCAAAAACAGGAAGGCAAAATGCCGCAAAAAAGGGAATAAGGGCGACACGGA
AATGTTGAATACTCATACTCTTCCTTTTTCAATATTATTGAAGCATTTATCAGGGTTA
TTGTCTCATGAGCGGATACATATTTGAATGTATTTAGAAAAATAAACAAATAGGGGT
TCCGCGCACATTTCCCCGAAAAGTGCCACCTAAATTGTAAGCGTTAATATTTTGTTA
AAATTCGCGTTAAATTTTTGTTAAATCAGCTCATTTTTTAACCAATAGGCCGAAATCG
GCAAAATCCCTTATAAATCAAAAGAATAGACCGAGATAGGGTTGAGTGTTGTTCCA
GTTTGGAACAAGAGTCCACTATTAAAGAACGTGGACTCCAACGTCAAAGGGCGAAA
AACCGTCTATCAGGGCGATGGCCCACTACGTGAACCATCACCCTAATCAAGTTTTTT
GGGGTCGAGGTGCCGTAAAGCACTAAATCGGAACCCTAAAGGGAGCCCCCGATTTA
GAGCTTGACGGGGAAAGCCGGCGAACGTGGCGAGAAAGGAAGGGAAGAAAGCGAA
AGGAGCGGGCGCTAGGGCGCTGGCAAGTGTAGCGGTCACGCTGCGCGTAACCACCA
CACCCGCCGCGCTTAATGCGCCGCTACAGGGCGCGTCCCATTCGCCATTCAGGCTGC
GCAACTGTTGGGAAGGGCGATCGGTGCGGGCCTCTTCGCTATTACGCCAGCTGGCGA
AAGGGGGATGTGCTGCAAGGCGATTAAGTTGGGTAACGCCAGGGTTTTCCCAGTCA
CGACGTTGTAAAACGACGGCCAGTGAGCGCGCGTAATACGACTCACTATAGGGCGA
ATTGGGTACGTCCCTAGGCCTCCAAAAAAGCCTCCTCACTACTTCTGGAATAGCTCA
GAGGCCGAGGCGGCCTCGGCCTCTGCATAAATAAAAAAAATTAGTCAGCCATGGGG
CGGAGAATGGGCGGAACTGGGCGGAGTTAGGGGCGGGATGGGCGGAGTTAGGGGC
GGGATAGCTAGAGCCAGACATGATAAGATACATTGATGAGTTTGGACAAACCACAA
CTAGAATGCAGTGAAAAAAATGCTTTATTTGTGAAATTTGTGATGCTATTGCTTTATT
TGTAACCATTATAAGCTGCAATAAACAAGTTCCTCTCACTCTCTGATATTCATTTCTT
TGCAAGTTATAAATACTGAATAATAAGATGACATGAACTACTATACGTACTGCTAGA
GATTTTCCACACTGACTAAAAGGGTCTGAGGGATCTCTAGTTACCAGAGTCACACAA
CAGACGGGCACACACTACTTGAAGCACTCAAGGCAAGCTTTATTGAGGCTTAAGCA
GTGGGTTCCCTAGTTAGCCAGAGAGCTCCCAGGCTCAGATCTGGTCTAACCAGAGAG
ACCCAGTACAAGCAAAAAGCAGATCTTGTCTTCGTTGGGAGTGAATTAGCCCTTCCA
GTCCCCCCTTTTCTTTTAAAAAGTGGCTAAGATCTACAGCTGCCTTGTAAGTCATTGG
TCTTAAAGTCGACGCGGGGAGGCGGCCCAAAGGGAGATCCGACTCGTCTGAGGGCG
AAGGCGAAGACGCGGAAGAGGCCGCAGAGCCGGCAGCAGGCCGCGGGAAGGAAG
GTCCGCTGGATTGAGGGCCGAAGGGACGTAGCAGAAGGACGTCCCGCGCAGAATCC
AGGTGGCAACACAGGCGAGCAGCCAAGGAAAGGACGATGATTTCCCCGACAACAC

CACGGAATTGTCAGTGCCCAACAGCCGAGCCCCTGTCCAGCAGCGGGCAAGGCAGG
CGGCGATGAGTTCCGCCGTGGCAATAGGGAGGGGGAAAGCGAAAGTCCCGGAAAG
GAGCTGACAGGTGGTGGCAATGCCCCAACCAGTGGGGGTTGCGTCAGCAAACACAG
TGCACACCACGCCACGTTGCCTGACAACGGGCCACAACTCCTCATAAAGAGACAGC
AACCAGGATTTATACAAGGAGGAGAAAATGAAAGCCATACGGGAAGCAATAGCAT
GATACAAAGGCATTAAAGCAGCGTATCCACATAGCGTAAAAGGAGCAACATAGTTA
AGAATACCAGTCAATCTTTCACAAATTTTGTAATCCAGAGGTTGATTGTCGACTTAA
CGCGTTCAGGCACCGGGCTTGCGGGTCATGCACCAGGTGCGCGGTCCTTCGGGCACC
TCGACGTCGGCGGTGACGGTGAAGCCGAGCCGCTCGTAGAAGGGGAGGTTGCGGGG
CGCGGAGGTCTCCAGGAAGGCGGGCACCCCGGCGCGCTCGGCCGCCTCCACTCCGG
GGAGCACGACGGCGCTGCCCAGACCCTTGCCCTGGTGGTCGGGCGAGACTCCGACG
GTGGCCAGGAACCACGCGGGCTCCTTGGGCCGGTGCGGCGCCAGGAGGCCTTCCAT
CTGTTGCTGCGCGGCCAGCCGGGAACCGCTCAACTCGGCCATGCGCGGGCCGATCTC
GGCGAACACCGCCCCCGCTTCGACGCTCTCCGGCGTGGTCCAGACCGCCACGGCGG
CGCCGTCGTCCGCGACCCACACCTTGCCGATGTCGAGCCCGACGCGCGTGAGGAAG
AGTTCTTGCAGCTCGGTGACCCGCTCGATGTGGCGGTCCGGATCGACGGTGTGGCGC
GTGGCGGGGTAGTCGGCGAACGCGGCGGCGAGGGTGCGTACGGCCCTGGGGACGTC
GTCGCGGGTGGCGAGGCGCACCGTGGGCTTGTACTCGGTCATGGTGGCCGTACGTCA
CGACACCTGAAATGGAAGAAAAAAACTTTGAACCACTGTCTGAGGCTTGAGAATGA
ACCAAGATCCAAACTCAAAAAGGGCAAATTCCAAGGAGAATTACATCAAGTGCCAA
GCTGGCCTAACTTCAGTCTCCACCCACTCAGTGTGGGGAAACTCCATCGCATAAAAC
CCCTCCCCCCAACCTAAAGACGACGTACTCCAAAAGCTCGAGAACTAATCGAGGTG
CCTGGACGGCGCCCGGTACTCCGTGGAGTCACATGAAGCGACGGCTGAGGACGGAA
AGGCCCTTTTCCTTTGTGTGGGTGACTCACCCGCCCGCTCTCCCGAGCGCCGCGTCCT
CCATTTTGAGCTCCCTGCAGCAGGGCCGGGAAGCGGCCATCTTTCCGCTCACGCAAC
TGGTGCCGACCGGGCCAGCCTTGCCGCCCAGGGCGGGGCGATACACGGCGGCGCGA
GGCCAGGCACCAGAGCAGGCCGGCCAGCTTGAGACTACCCCCGTCCGATTCTCGGT
GGCCGCGCTCGCAGGCCCCGCCTCGCCGAACATGTGCGCTGGGACGCACGGGCCCC
GTCGCCGCCCGCGGCCCCAAAAACCGAAATACCAGTGTGCAGATCTTGGCCCGCAT
TTACAAGACTATCTTGCCAGAAAAAAAGCGTCGCAGCAGGTCATCAAAAATTTTAA
ATGGCTAGAGACTTATCGAAAGCAGCGAGACAGGCGCGAAGGTGCCACCAGATTCG
CACGCGGCGGCCCCAGCGCCCAGGCCAGGCCTCAACTCAAGCACGAGGCGAAGGG
GCTCCTTAAGCGCAAGGCCTCGAACTCTCCCACCCACTTCCAACCCGAAGCTCGGGA
TCAAGAATCACGTACTGCAGCCAGGTGGAAGTAATTCAAGGCACGCAAGGGCCATA
ACCCGTAAAGAGGCCAGGCCCGCGGGAACCACACACGGCACTTACCTGTGTTCTGG
CGGCAAACCCGTTGCGAAAAAGAACGTTCACGGCGACTACTGCACTTATATACGGTT
CTCCCCCACCCTCGGGAAAAAGGCGGAGCCAGTACACGACATCACTTTCCCAGTTTA
CCCCGCGCCACCTTCTCTAGGCACCGGAT

10000BP TOP:

ATCGTTTCAGACCCACCTCCCAACCCCGAGGGGACCCAGAGAGGGCCTATTTCCCAT
GATTCCTTCATATTTGCATATACGATACAAGGCTGTTAGAGAGATAATTAGAATTAA
TTTGACTGTAAACACAAAGATATTAGTACAAAATACGTGACGTAGAAAGTAATAAT
TTCTTGGGTAGTTTGCAGTTTTAAAATTATGTTTTAAAATGGACTATCATATGCTTAC
CGTAACTTGAAAGTATTTCGATTTCTTGGCTTTATATATCTTGTGGAAAGGACGAAA
CACCGGAGACGGTTGTAAATGAGCACACAAAATACACATGCTAAAATATTATATTCT

ATGACCTTTATAAAATCAACCAAAATCTTCTTTTTAATAACTTTAGTATCAATAATTA
GAATTTTTATGTTCCTTTTTGCAAACTTTTAATAAAAATGAGCAAAATAAAAAAACG
CTAGTTTTAGTAACTCGCGTTGTTTTCTTCACCTTTAATAATAGCTACTCCACCACTT
GTTCCTAAGCGGTCAGCTCCTGCTTCAATCATTTTTTGAGCATCTTCAAATGTTCTAA
CTCCACCAGCTGCTTTAACTAAAGCATTGTCTTTAACAACTGACTTCATTAGTTTAAC
ATCTTCAAATGTTGCACCTGATTTTGAAAATCCTGTTGATGTTTTAACAAATTCTAAT
CCAGCTTCAACAGCTATTTCACAAGCTTTCATGATTTCTTCTTTTGTTAATAAACAAT
TTTCCATAATACATTTAACAACATGTGATCCAGCTGCTTTTTTTACAGCTTTCATGTC
TTCTAAAACTAATTCATAATTTTTGTCTTTTAATGCACCAATATTTAATACCATATCA
ATTTCTGTTGCACCATCTTTAATTGCTTCAGAAACTTCGAATGCTTTTGTAGCTGTTG
TGCATGCACCTAGAGGAAAACCTACAACATTTGTTATTCCTACATTTGTGCCTTTTAA
TAATTCTTTACAATAGCTTGTTCAATATGAATTAACACAAACTGTTGCAAAATCAAA
TTCAATTGCTTCATCACATAATTGTTTAATTTCAGCTTTCGTAGCATCTTGTTTTAATA
ATGTGTGATCTATATATTTGTTTAGTTTCATTTTTTCTCCTATATATTCATTTTTAATTT
TAATTCTTTAATAATTTCGTCTACTTTAACTTTAGCGTTTTGAACAGATTCACCAACA
CCTATAAAATAAATTTTTAGTTTAGGTTCAGTTCCACTTGGGCGAACAGCAAATCAT
GACTTATCTTCTAAATAAAATTTTAGTAAGTCTTGTCCTGGCATATTATACATTCCAT
CGATGTAGTCTTCAACATTAACAACTTTAAGTCCAGCAATTTGAGTTAAGGGTGTTG
CTCTCAATGATTTCATTAATGGTTCAATTTTTAATTTCTTTTCTTCTGGTTTAAAATTC
AAGTTTAAAGTGAAAGTGTAATATGCACCCATTTCTTTAAATAAATCTTCTAAATAG
TCTACTAATGTTTTATTTTGTTTTTTATAAAATCAAGCAGCCTCTGCTATTAATATAG
AAGCTTGTATTCCATCTTTATCTCTAGCTGAGTCATCAATTACATATCCATAACTTTC
TTCATAAGCAAAAACAAAATTTAATCCGTTATCTTCTTCTTTAGCAATTTCTCTACCC
ATTCATTTAAATCCAGTTAAAGTTTTTACAATATTAACTCCATATTTTTCATGAGCGA
TTCTATCACCCAAATCACTTGTTACAAAACTTGAATATAGAGCCGGATTTTTTGGAA
TGCTATTTAAGCGTTTTAGATTTGATAATTTTCAATCAATTAAAATTGGTCCTGTTTG
ATTTCCATCTAATCTTACAAAATGACCATCATGTTTTATTGCCATTCCAAATCTGTCA
GCATCTGGGTCATTCATAATAATAATATCTGCATCATGTTTAATACCATATTCAAGC
GGTATTTTTCATGCAGGATCAAATTCTGGATTTGGATTTACAACATTTTTAAATGTTT
CATCTTCAAATGCATGCTCTTCAACCTCAATAACGTTATATCCTGATTCACGTAATAT
TTTTGGGGTAAATTTAGTTCCTGTTCCATTAACTGCGCTAAAAATAATTTTTAAATCT
TTTTTAGCTTCTTGCTCTTTTTTGTACGTCTCTGTTTTAGAGCTAGAAATAGCAAGTTA
AAATAAGGCTAGTCCGTTATCAACTTGAAAAAGTGGCACCGAGTCGGTGCTTTTTTA
AGCTTGGCGTAACTAGATCTTGAGACAAATGGCAGTATTCATCCACAATTTTAAAAG
AAAAGGGGGGATTGGGGGGTACAGTGCAGGGGAAAGAATAGTAGACATAATAGCA
ACAGACATACAAACTAAAGAATTACAAAAACAAATTACAAAAATTCAAAATTTTCG
GGTTTATTACAGGGACAGCAGAGATCCACTTTGGCGCCGGCTCGAGGGGGCCCGGG
TGCAAAGATGGATAAAGTTTTAAACAGAGAGGAATCTTTGCAGCTAATGGACCTTCT
AGGTCTTGAAAGGAGTGGGAATTGGCTCCGGTGCCCGTCAGTGGGCAGAGCGCACA
TCGCCCACAGTCCCCGAGAAGTTGGGGGGAGGGGTCGGCAATTGATCCGGTGCCTA
GAGAAGGTGGCGCGGGGTAAACTGGGAAAGTGATGTCGTGTACTGGCTCCGCCTTT
TTCCCGAGGGTGGGGGAGAACCGTATATAAGTGCAGTAGTCGCCGTGAACGTTCTTT
TTCGCAACGGGTTTGCCGCCAGAACACAGGTAAGTGCCGTGTGTGGTTCCCGCGGGC
CTGGCCTCTTTACGGGTTATGGCCCTTGCGTGCCTTGAATTACTTCCACCTGGCTGCA
GTACGTGATTCTTGATCCCGAGCTTCGGGTTGGAAGTGGGTGGGAGAGTTCGAGGCC
TTGCGCTTAAGGAGCCCCTTCGCCTCGTGCTTGAGTTGAGGCCTGGCCTGGGCGCTG

GGGCCGCCGCGTGCGAATCTGGTGGCACCTTCGCGCCTGTCTCGCTGCTTTCGATAA
GTCTCTAGCCATTTAAAATTTTTGATGACCTGCTGCGACGCTTTTTTTCTGGCAAGAT
AGTCTTGTAAATGCGGGCCAAGATCTGCACACTGGTATTTCGGTTTTTGGGGCCGCG
GGCGGCGACGGGGCCCGTGCGTCCCAGCGCACATGTTCGGCGAGGCGGGGCCTGCG
AGCGCGGCCACCGAGAATCGGACGGGGGTAGTCTCAAGCTGGCCGGCCTGCTCTGG
TGCCTGGCCTCGCGCCGCCGTGTATCGCCCCGCCCTGGGCGGCAAGGCTGGCCCGGT
CGGCACCAGTTGCGTGAGCGGAAAGATGGCCGCTTCCCGGCCCTGCTGCAGGGAGC
TCAAAATGGAGGACGCGGCGCTCGGGAGAGCGGGCGGGTGAGTCACCCACACAAA
GGAAAAGGGCCTTTCCGTCCTCAGCCGTCGCTTCATGTGACTCCACGGAGTACCGGG
CGCCGTCCAGGCACCTCGATTAGTTCTCGAGCTTTTGGAGTACGTCGTCTTTAGGTTG
GGGGGAGGGGTTTTATGCGATGGAGTTTCCCCACACTGAGTGGGTGGAGACTGAAG
TTAGGCCAGCTTGGCACTTGATGTAATTCTCCTTGGAATTTGCCCTTTTTGAGTTTGG
ATCTTGGTTCATTCTCAAGCCTCAGACAGTGGTTCAAAGTTTTTTTCTTCCATTTCAG
GTGTCGTGACGTACGGCCACCATGACCGAGTACAAGCCCACGGTGCGCCTCGCCAC
CCGCGACGACGTCCCCAGGGCCGTACGCACCCTCGCCGCCGCGTTCGCCGACTACCC
CGCCACGCGCCACACCGTCGATCCGGACCGCCACATCGAGCGGGTCACCGAGCTGC
AAGAACTCTTCCTCACGCGCGTCGGGCTCGACATCGGCAAGGTGTGGGTCGCGGAC
GACGGCGCCGCCGTGGCGGTCTGGACCACGCCGGAGAGCGTCGAAGCGGGGGCGGT
GTTCGCCGAGATCGGCCCGCGCATGGCCGAGTTGAGCGGTTCCCGGCTGGCCGCGC
AGCAACAGATGGAAGGCCTCCTGGCGCCGCACCGGCCCAAGGAGCCCGCGTGGTTC
CTGGCCACCGTCGGAGTCTCGCCCGACCACCAGGGCAAGGGTCTGGGCAGCGCCGT
CGTGCTCCCCGGAGTGGAGGCGGCCGAGCGCGCCGGGGTGCCCGCCTTCCTGGAGA
CCTCCGCGCCCCGCAACCTCCCCTTCTACGAGCGGCTCGGCTTCACCGTCACCGCCG
ACGTCGAGGTGCCCGAAGGACCGCGCACCTGGTGCATGACCCGCAAGCCCGGTGCC
TGAACGCGTTAAGTCGACAATCAACCTCTGGATTACAAAATTTGTGAAAGATTGACT
GGTATTCTTAACTATGTTGCTCCTTTTACGCTATGTGGATACGCTGCTTTAATGCCTT
TGTATCATGCTATTGCTTCCCGTATGGCTTTCATTTTCTCCTCCTTGTATAAATCCTGG
TTGCTGTCTCTTTATGAGGAGTTGTGGCCCGTTGTCAGGCAACGTGGCGTGGTGTGC
ACTGTGTTTGCTGACGCAACCCCCACTGGTTGGGGCATTGCCACCACCTGTCAGCTC
CTTTCCGGGACTTTCGCTTTCCCCCTCCCTATTGCCACGGCGGAACTCATCGCCGCCT
GCCTTGCCCGCTGCTGGACAGGGGCTCGGCTGTTGGGCACTGACAATTCCGTGGTGT
TGTCGGGGAAATCATCGTCCTTTCCTTGGCTGCTCGCCTGTGTTGCCACCTGGATTCT
GCGCGGGACGTCCTTCTGCTACGTCCCTTCGGCCCTCAATCCAGCGGACCTTCCTTCC
CGCGGCCTGCTGCCGGCTCTGCGGCCTCTTCCGCGTCTTCGCCTTCGCCCTCAGACG
AGTCGGATCTCCCTTTGGGCCGCCTCCCCGCGTCGACTTTAAGACCAATGACTTACA
AGGCAGCTGTAGATCTTAGCCACTTTTTAAAAGAAAAGGGGGGACTGGAAGGGCTA
ATTCACTCCCAACGAAGACAAGATCTGCTTTTTGCTTGTACTGGGTCTCTCTGGTTAG
ACCAGATCTGAGCCTGGGAGCTCTCTGGCTAACTAGGGAACCCACTGCTTAAGCCTC
AATAAAGCTTGCCTTGAGTGCTTCAAGTAGTGTGTGCCCGTCTGTTGTGTGACTCTG
GTAACTAGAGATCCCTCAGACCCTTTTAGTCAGTGTGGAAAATCTCTAGCAGTACGT
ATAGTAGTTCATGTCATCTTATTATTCAGTATTTATAACTTGCAAAGAAATGAATATC
AGAGAGTGAGAGGAACTTGTTTATTGCAGCTTATAATGGTTACAAATAAAGCAATA
GCATCACAAATTTCACAAATAAAGCATTTTTTTCACTGCATTCTAGTTGTGGTTTGTC
CAAACTCATCAATGTATCTTATCATGTCTGGCTCTAGCTATCCCGCCCCTAACTCCGC
CCATCCCGCCCCTAACTCCGCCCAGTTCCGCCCATTCTCCGCCCCATGGCTGACTAAT
TTTTTTTATTTATGCAGAGGCCGAGGCCGCCTCGGCCTCTGAGCTATTCCAGAAGTA

GTGAGGAGGCTTTTTTGGAGGCCTAGGGACGTACCCAATTCGCCCTATAGTGAGTCG
TATTACGCGCGCTCACTGGCCGTCGTTTTACAACGTCGTGACTGGGAAAACCCTGGC
GTTACCCAACTTAATCGCCTTGCAGCACATCCCCCTTTCGCCAGCTGGCGTAATAGC
GAAGAGGCCCGCACCGATCGCCCTTCCCAACAGTTGCGCAGCCTGAATGGCGAATG
GGACGCGCCCTGTAGCGGCGCATTAAGCGCGGCGGGTGTGGTGGTTACGCGCAGCG
TGACCGCTACACTTGCCAGCGCCCTAGCGCCCGCTCCTTTCGCTTTCTTCCCTTCCTT
TCTCGCCACGTTCGCCGGCTTTCCCCGTCAAGCTCTAAATCGGGGGCTCCCTTTAGG
GTTCCGATTTAGTGCTTTACGGCACCTCGACCCCAAAAAACTTGATTAGGGTGATGG
TTCACGTAGTGGGCCATCGCCCTGATAGACGGTTTTTCGCCCTTTGACGTTGGAGTCC
ACGTTCTTTAATAGTGGACTCTTGTTCCAAACTGGAACAACACTCAACCCTATCTCG
GTCTATTCTTTTGATTTATAAGGGATTTTGCCGATTTCGGCCTATTGGTTAAAAAATG
AGCTGATTTAACAAAAATTTAACGCGAATTTTAACAAAATATTAACGCTTACAATTT
AGGTGGCACTTTTCGGGGAAATGTGCGCGGAACCCCTATTTGTTTATTTTTCTAAATA
CATTCAAATATGTATCCGCTCATGAGACAATAACCCTGATAAATGCTTCAATAATAT
TGAAAAAGGAAGAGTATGAGTATTCAACATTTCCGTGTCGCCCTTATTCCCTTTTTTG
CGGCATTTTGCCTTCCTGTTTTTGCTCACCCAGAAACGCTGGTGAAAGTAAAAGATG
CTGAAGATCAGTTGGGTGCACGAGTGGGTTACATCGAACTGGATCTCAACAGCGGT
AAGATCCTTGAGAGTTTTCGCCCCGAAGAACGTTTTCCAATGATGAGCACTTTTAAA
GTTCTGCTATGTGGCGCGGTATTATCCCGTATTGACGCCGGGCAAGAGCAACTCGGT
CGCCGCATACACTATTCTCAGAATGACTTGGTTGAGTACTCACCAGTCACAGAAAAG
CATCTTACGGATGGCATGACAGTAAGAGAATTATGCAGTGCTGCCATAACCATGAGT
GATAACACTGCGGCCAACTTACTTCTGACAACGATCGGAGGACCGAAGGAGCTAAC
CGCTTTTTTGCACAACATGGGGGATCATGTAACTCGCCTTGATCGTTGGGAACCGGA
GCTGAATGAAGCCATACCAAACGACGAGCGTGACACCACGATGCCTGTAGCAATGG
CAACAACGTTGCGCAAACTATTAACTGGCGAACTACTTACTCTAGCTTCCCGGCAAC
AATTAATAGACTGGATGGAGGCGGATAAAGTTGCAGGACCACTTCTGCGCTCGGCC
CTTCCGGCTGGCTGGTTTATTGCTGATAAATCTGGAGCCGGTGAGCGTGGGTCTCGC
GGTATCATTGCAGCACTGGGGCCAGATGGTAAGCCCTCCCGTATCGTAGTTATCTAC
ACGACGGGGAGTCAGGCAACTATGGATGAACGAAATAGACAGATCGCTGAGATAG
GTGCCTCACTGATTAAGCATTGGTAACTGTCAGACCAAGTTTACTCATATATACTTTA
GATTGATTTAAAACTTCATTTTTAATTTAAAAGGATCTAGGTGAAGATCCTTTTTGAT
AATCTCATGACCAAAATCCCTTAACGTGAGTTTTCGTTCCACTGAGCGTCAGACCCC
GTAGAAAAGATCAAAGGATCTTCTTGAGATCCTTTTTTTCTGCGCGTAATCTGCTGCT
TGCAAACAAAAAAACCACCGCTACCAGCGGTGGTTTGTTTGCCGGATCAAGAGCTA
CCAACTCTTTTTCCGAAGGTAACTGGCTTCAGCAGAGCGCAGATACCAAATACTGTT
CTTCTAGTGTAGCCGTAGTTAGGCCACCACTTCAAGAACTCTGTAGCACCGCCTACA
TACCTCGCTCTGCTAATCCTGTTACCAGTGGCTGCTGCCAGTGGCGATAAGTCGTGT
CTTACCGGGTTGGACTCAAGACGATAGTTACCGGATAAGGCGCAGCGGTCGGGCTG
AACGGGGGGTTCGTGCACACAGCCCAGCTTGGAGCGAACGACCTACACCGAACTGA
GATACCTACAGCGTGAGCTATGAGAAAGCGCCACGCTTCCCGAAGGGAGAAAGGCG
GACAGGTATCCGGTAAGCGGCAGGGTCGGAACAGGAGAGCGCACGAGGGAGCTTC
CAGGGGGAAACGCCTGGTATCTTTATAGTCCTGTCGGGTTTCGCCACCTCTGACTTG
AGCGTCGATTTTTGTGATGCTCGTCAGGGGGGCGGAGCCTATGGAAAAACGCCAGC
AACGCGGCCTTTTTACGGTTCCTGGCCTTTTGCTGGCCTTTTGCTCACATGTTCTTTCC
TGCGTTATCCCCTGATTCTGTGGATAACCGTATTACCGCCTTTGAGTGAGCTGATACC
GCTCGCCGCAGCCGAACGACCGAGCGCAGCGAGTCAGTGAGCGAGGAAGCGGAAG

AGCGCCCAATACGCAAACCGCCTCTCCCCGCGCGTTGGCCGATTCATTAATGCAGCT
GGCACGACAGGTTTCCCGACTGGAAAGCGGGCAGTGAGCGCAACGCAATTAATGTG
AGTTAGCTCACTCATTAGGCACCCCAGGCTTTACACTTTATGCTTCCGGCTCGTATGT
TGTGTGGAATTGTGAGCGGATAACAATTTCACACAGGAAACAGCTATGACCATGATT
ACGCCAAGCGCGCAATTAACCCTCACTAAAGGGAACAAAAGCTGGAGCTGCAAGCT
TAATGTAGTCTTATGCAATACTCTTGTAGTCTTGCAACATGGTAACGATGAGTTAGC
AACATGCCTTACAAGGAGAGAAAAAGCACCGTGCATGCCGATTGGTGGAAGTAAGG
TGGTACGATCGTGCCTTATTAGGAAGGCAACAGACGGGTCTGACATGGATTGGACG
AACCACTGAATTGCCGCATTGCAGAGATATTGTATTTAAGTGCCTAGCTCGATACAT
AAACGGGTCTCTCTGGTTAGACCAGATCTGAGCCTGGGAGCTCTCTGGCTAACTAGG
GAACCCACTGCTTAAGCCTCAATAAAGCTTGCCTTGAGTGCTTCAAGTAGTGTGTGC
CCGTCTGTTGTGTGACTCTGGTAACTAGAGATCCCTCAGACCCTTTTAGTCAGTGTGG
AAAATCTCTAGCAGTGGCGCCCGAACAGGGACTTGAAAGCGAAAGGGAAACCAGA
GGAGCTCTCTCGACGCAGGACTCGGCTTGCTGAAGCGCGCACGGCAAGAGGCGAGG
GGCGGCGACTGGTGAGTACGCCAAAAATTTTGACTAGCGGAGGCTAGAAGGAGAGA
GATGGGTGCGAGAGCGTCAGTATTAAGCGGGGGAGAATTAGATCGCGATGGGAAAA
AATTCGGTTAAGGCCAGGGGGAAAGAAAAAATATAAATTAAAACATATAGTATGGG
CAAGCAGGGAGCTAGAACGATTCGCAGTTAATCCTGGCCTGTTAGAAACATCAGAA
GGCTGTAGACAAATACTGGGACAGCTACAACCATCCCTTCAGACAGGATCAGAAGA
ACTTAGATCATTATATAATACAGTAGCAACCCTCTATTGTGTGCATCAAAGGATAGA
GATAAAAGACACCAAGGAAGCTTTAGACAAGATAGAGGAAGAGCAAAACAAAAGT
AAGACCACCGCACAGCAAGCGGCCGCTGATCTTCAGACCTGGAGGAGGAGATATGA
GGGACAATTGGAGAAGTGAATTATATAAATATAAAGTAGTAAAAATTGAACCATTA
GGAGTAGCACCCACCAAGGCAAAGAGAAGAGTGGTGCAGAGAGAAAAAAGAGCAG
TGGGAATAGGAGCTTTGTTCCTTGGGTTCTTGGGAGCAGCAGGAAGCACTATGGGCG
CAGCGTCAATGACGCTGACGGTACAGGCCAGACAATTATTGTCTGGTATAGTGCAGC
AGCAGAACAATTTGCTGAGGGCTATTGAGGCGCAACAGCATCTGTTGCAACTCACA
GTCTGGGGCATCAAGCAGCTCCAGGCAAGAATCCTGGCTGTGGAAAGATACCTAAA
GGATCAACAGCTCCTGGGGATTTGGGGTTGCTCTGGAAAACTCATTTGCACCACTGC
TGTGCCTTGGAATGCTAGTTGGAGTAATAAATCTCTGGAACAGATTTGGAATCACAC
GACCTGGATGGAGTGGGACAGAGAAATTAACAATTACACAAGCTTAATACACTCCT
TAATTGAAGAATCGCAAAACCAGCAAGA

10000BP BOT:

TCTTGCTGGTTTTGCGATTCTTCAATTAAGGAGTGTATTAAGCTTGTGTAATTGTTAA
TTTCTCTGTCCCACTCCATCCAGGTCGTGTGATTCCAAATCTGTTCCAGAGATTTATT
ACTCCAACTAGCATTCCAAGGCACAGCAGTGGTGCAAATGAGTTTTCCAGAGCAAC
CCCAAATCCCCAGGAGCTGTTGATCCTTTAGGTATCTTTCCACAGCCAGGATTCTTGC
CTGGAGCTGCTTGATGCCCCAGACTGTGAGTTGCAACAGATGCTGTTGCGCCTCAAT
AGCCCTCAGCAAATTGTTCTGCTGCTGCACTATACCAGACAATAATTGTCTGGCCTG
TACCGTCAGCGTCATTGACGCTGCGCCCATAGTGCTTCCTGCTGCTCCCAAGAACCC
AAGGAACAAAGCTCCTATTCCCACTGCTCTTTTTTCTCTCTGCACCACTCTTCTCTTT
GCCTTGGTGGGTGCTACTCCTAATGGTTCAATTTTTACTACTTTATATTTATATAATT
CACTTCTCCAATTGTCCCTCATATCTCCTCCTCCAGGTCTGAAGATCAGCGGCCGCTT
GCTGTGCGGTGGTCTTACTTTTGTTTTGCTCTTCCTCTATCTTGTCTAAAGCTTCCTTG
GTGTCTTTTATCTCTATCCTTTGATGCACACAATAGAGGGTTGCTACTGTATTATATA

ATGATCTAAGTTCTTCTGATCCTGTCTGAAGGGATGGTTGTAGCTGTCCCAGTATTTG
TCTACAGCCTTCTGATGTTTCTAACAGGCCAGGATTAACTGCGAATCGTTCTAGCTCC
CTGCTTGCCCATACTATATGTTTTAATTTATATTTTTTCTTTCCCCCTGGCCTTAACCG
AATTTTTTCCCATCGCGATCTAATTCTCCCCCGCTTAATACTGACGCTCTCGCACCCA
TCTCTCTCCTTCTAGCCTCCGCTAGTCAAAATTTTTGGCGTACTCACCAGTCGCCGCC
CCTCGCCTCTTGCCGTGCGCGCTTCAGCAAGCCGAGTCCTGCGTCGAGAGAGCTCCT
CTGGTTTCCCTTTCGCTTTCAAGTCCCTGTTCGGGCGCCACTGCTAGAGATTTTCCAC
ACTGACTAAAAGGGTCTGAGGGATCTCTAGTTACCAGAGTCACACAACAGACGGGC
ACACACTACTTGAAGCACTCAAGGCAAGCTTTATTGAGGCTTAAGCAGTGGGTTCCC
TAGTTAGCCAGAGAGCTCCCAGGCTCAGATCTGGTCTAACCAGAGAGACCCGTTTAT
GTATCGAGCTAGGCACTTAAATACAATATCTCTGCAATGCGGCAATTCAGTGGTTCG
TCCAATCCATGTCAGACCCGTCTGTTGCCTTCCTAATAAGGCACGATCGTACCACCT
TACTTCCACCAATCGGCATGCACGGTGCTTTTTCTCTCCTTGTAAGGCATGTTGCTAA
CTCATCGTTACCATGTTGCAAGACTACAAGAGTATTGCATAAGACTACATTAAGCTT
GCAGCTCCAGCTTTTGTTCCCTTTAGTGAGGGTTAATTGCGCGCTTGGCGTAATCATG
GTCATAGCTGTTTCCTGTGTGAAATTGTTATCCGCTCACAATTCCACACAACATACG
AGCCGGAAGCATAAAGTGTAAAGCCTGGGGTGCCTAATGAGTGAGCTAACTCACAT
TAATTGCGTTGCGCTCACTGCCCGCTTTCCAGTCGGGAAACCTGTCGTGCCAGCTGC
ATTAATGAATCGGCCAACGCGCGGGGAGAGGCGGTTTGCGTATTGGGCGCTCTTCCG
CTTCCTCGCTCACTGACTCGCTGCGCTCGGTCGTTCGGCTGCGGCGAGCGGTATCAG
CTCACTCAAAGGCGGTAATACGGTTATCCACAGAATCAGGGGATAACGCAGGAAAG
AACATGTGAGCAAAAGGCCAGCAAAAGGCCAGGAACCGTAAAAAGGCCGCGTTGC
TGGCGTTTTTCCATAGGCTCCGCCCCCCTGACGAGCATCACAAAAATCGACGCTCAA
GTCAGAGGTGGCGAAACCCGACAGGACTATAAAGATACCAGGCGTTTCCCCCTGGA
AGCTCCCTCGTGCGCTCTCCTGTTCCGACCCTGCCGCTTACCGGATACCTGTCCGCCT
TTCTCCCTTCGGGAAGCGTGGCGCTTTCTCATAGCTCACGCTGTAGGTATCTCAGTTC
GGTGTAGGTCGTTCGCTCCAAGCTGGGCTGTGTGCACGAACCCCCCGTTCAGCCCGA
CCGCTGCGCCTTATCCGGTAACTATCGTCTTGAGTCCAACCCGGTAAGACACGACTT
ATCGCCACTGGCAGCAGCCACTGGTAACAGGATTAGCAGAGCGAGGTATGTAGGCG
GTGCTACAGAGTTCTTGAAGTGGTGGCCTAACTACGGCTACACTAGAAGAACAGTAT
TTGGTATCTGCGCTCTGCTGAAGCCAGTTACCTTCGGAAAAAGAGTTGGTAGCTCTT
GATCCGGCAAACAAACCACCGCTGGTAGCGGTGGTTTTTTTGTTTGCAAGCAGCAGA
TTACGCGCAGAAAAAAAGGATCTCAAGAAGATCCTTTGATCTTTTCTACGGGGTCTG
ACGCTCAGTGGAACGAAAACTCACGTTAAGGGATTTTGGTCATGAGATTATCAAAA
AGGATCTTCACCTAGATCCTTTTAAATTAAAAATGAAGTTTTAAATCAATCTAAAGT
ATATATGAGTAAACTTGGTCTGACAGTTACCAATGCTTAATCAGTGAGGCACCTATC
TCAGCGATCTGTCTATTTCGTTCATCCATAGTTGCCTGACTCCCCGTCGTGTAGATAA
CTACGATACGGGAGGGCTTACCATCTGGCCCCAGTGCTGCAATGATACCGCGAGAC
CCACGCTCACCGGCTCCAGATTTATCAGCAATAAACCAGCCAGCCGGAAGGGCCGA
GCGCAGAAGTGGTCCTGCAACTTTATCCGCCTCCATCCAGTCTATTAATTGTTGCCG
GGAAGCTAGAGTAAGTAGTTCGCCAGTTAATAGTTTGCGCAACGTTGTTGCCATTGC
TACAGGCATCGTGGTGTCACGCTCGTCGTTTGGTATGGCTTCATTCAGCTCCGGTTCC
CAACGATCAAGGCGAGTTACATGATCCCCCATGTTGTGCAAAAAAGCGGTTAGCTCC
TTCGGTCCTCCGATCGTTGTCAGAAGTAAGTTGGCCGCAGTGTTATCACTCATGGTT
ATGGCAGCACTGCATAATTCTCTTACTGTCATGCCATCCGTAAGATGCTTTTCTGTGA
CTGGTGAGTACTCAACCAAGTCATTCTGAGAATAGTGTATGCGGCGACCGAGTTGCT

CTTGCCCGGCGTCAATACGGGATAATACCGCGCCACATAGCAGAACTTTAAAAGTG
CTCATCATTGGAAAACGTTCTTCGGGGCGAAAACTCTCAAGGATCTTACCGCTGTTG
AGATCCAGTTCGATGTAACCCACTCGTGCACCCAACTGATCTTCAGCATCTTTTACTT
TCACCAGCGTTTCTGGGTGAGCAAAAACAGGAAGGCAAAATGCCGCAAAAAAGGG
AATAAGGGCGACACGGAAATGTTGAATACTCATACTCTTCCTTTTTCAATATTATTG
AAGCATTTATCAGGGTTATTGTCTCATGAGCGGATACATATTTGAATGTATTTAGAA
AAATAAACAAATAGGGGTTCCGCGCACATTTCCCCGAAAAGTGCCACCTAAATTGT
AAGCGTTAATATTTTGTTAAAATTCGCGTTAAATTTTTGTTAAATCAGCTCATTTTTT
AACCAATAGGCCGAAATCGGCAAAATCCCTTATAAATCAAAAGAATAGACCGAGAT
AGGGTTGAGTGTTGTTCCAGTTTGGAACAAGAGTCCACTATTAAAGAACGTGGACTC
CAACGTCAAAGGGCGAAAAACCGTCTATCAGGGCGATGGCCCACTACGTGAACCAT
CACCCTAATCAAGTTTTTTGGGGTCGAGGTGCCGTAAAGCACTAAATCGGAACCCTA
AAGGGAGCCCCCGATTTAGAGCTTGACGGGGAAAGCCGGCGAACGTGGCGAGAAA
GGAAGGGAAGAAAGCGAAAGGAGCGGGCGCTAGGGCGCTGGCAAGTGTAGCGGTC
ACGCTGCGCGTAACCACCACACCCGCCGCGCTTAATGCGCCGCTACAGGGCGCGTC
CCATTCGCCATTCAGGCTGCGCAACTGTTGGGAAGGGCGATCGGTGCGGGCCTCTTC
GCTATTACGCCAGCTGGCGAAAGGGGGATGTGCTGCAAGGCGATTAAGTTGGGTAA
CGCCAGGGTTTTCCCAGTCACGACGTTGTAAAACGACGGCCAGTGAGCGCGCGTAA
TACGACTCACTATAGGGCGAATTGGGTACGTCCCTAGGCCTCCAAAAAAGCCTCCTC
ACTACTTCTGGAATAGCTCAGAGGCCGAGGCGGCCTCGGCCTCTGCATAAATAAAA
AAAATTAGTCAGCCATGGGGCGGAGAATGGGCGGAACTGGGCGGAGTTAGGGGCG
GGATGGGCGGAGTTAGGGGCGGGATAGCTAGAGCCAGACATGATAAGATACATTGA
TGAGTTTGGACAAACCACAACTAGAATGCAGTGAAAAAAATGCTTTATTTGTGAAAT
TTGTGATGCTATTGCTTTATTTGTAACCATTATAAGCTGCAATAAACAAGTTCCTCTC
ACTCTCTGATATTCATTTCTTTGCAAGTTATAAATACTGAATAATAAGATGACATGA
ACTACTATACGTACTGCTAGAGATTTTCCACACTGACTAAAAGGGTCTGAGGGATCT
CTAGTTACCAGAGTCACACAACAGACGGGCACACACTACTTGAAGCACTCAAGGCA
AGCTTTATTGAGGCTTAAGCAGTGGGTTCCCTAGTTAGCCAGAGAGCTCCCAGGCTC
AGATCTGGTCTAACCAGAGAGACCCAGTACAAGCAAAAAGCAGATCTTGTCTTCGTT
GGGAGTGAATTAGCCCTTCCAGTCCCCCCTTTTCTTTTAAAAAGTGGCTAAGATCTA
CAGCTGCCTTGTAAGTCATTGGTCTTAAAGTCGACGCGGGGAGGCGGCCCAAAGGG
AGATCCGACTCGTCTGAGGGCGAAGGCGAAGACGCGGAAGAGGCCGCAGAGCCGG
CAGCAGGCCGCGGGAAGGAAGGTCCGCTGGATTGAGGGCCGAAGGGACGTAGCAG
AAGGACGTCCCGCGCAGAATCCAGGTGGCAACACAGGCGAGCAGCCAAGGAAAGG
ACGATGATTTCCCCGACAACACCACGGAATTGTCAGTGCCCAACAGCCGAGCCCCT
GTCCAGCAGCGGGCAAGGCAGGCGGCGATGAGTTCCGCCGTGGCAATAGGGAGGG
GGAAAGCGAAAGTCCCGGAAAGGAGCTGACAGGTGGTGGCAATGCCCCAACCAGT
GGGGGTTGCGTCAGCAAACACAGTGCACACCACGCCACGTTGCCTGACAACGGGCC
ACAACTCCTCATAAAGAGACAGCAACCAGGATTTATACAAGGAGGAGAAAATGAAA
GCCATACGGGAAGCAATAGCATGATACAAAGGCATTAAAGCAGCGTATCCACATAG
CGTAAAAGGAGCAACATAGTTAAGAATACCAGTCAATCTTTCACAAATTTTGTAATC
CAGAGGTTGATTGTCGACTTAACGCGTTCAGGCACCGGGCTTGCGGGTCATGCACCA
GGTGCGCGGTCCTTCGGGCACCTCGACGTCGGCGGTGACGGTGAAGCCGAGCCGCT
CGTAGAAGGGGAGGTTGCGGGGCGCGGAGGTCTCCAGGAAGGCGGGCACCCCGGC
GCGCTCGGCCGCCTCCACTCCGGGGAGCACGACGGCGCTGCCCAGACCCTTGCCCTG
GTGGTCGGGCGAGACTCCGACGGTGGCCAGGAACCACGCGGGCTCCTTGGGCCGGT

GCGGCGCCAGGAGGCCTTCCATCTGTTGCTGCGCGGCCAGCCGGGAACCGCTCAAC
TCGGCCATGCGCGGGCCGATCTCGGCGAACACCGCCCCCGCTTCGACGCTCTCCGGC
GTGGTCCAGACCGCCACGGCGGCGCCGTCGTCCGCGACCCACACCTTGCCGATGTCG
AGCCCGACGCGCGTGAGGAAGAGTTCTTGCAGCTCGGTGACCCGCTCGATGTGGCG
GTCCGGATCGACGGTGTGGCGCGTGGCGGGGTAGTCGGCGAACGCGGCGGCGAGGG
TGCGTACGGCCCTGGGGACGTCGTCGCGGGTGGCGAGGCGCACCGTGGGCTTGTAC
TCGGTCATGGTGGCCGTACGTCACGACACCTGAAATGGAAGAAAAAAACTTTGAAC
CACTGTCTGAGGCTTGAGAATGAACCAAGATCCAAACTCAAAAAGGGCAAATTCCA
AGGAGAATTACATCAAGTGCCAAGCTGGCCTAACTTCAGTCTCCACCCACTCAGTGT
GGGGAAACTCCATCGCATAAAACCCCTCCCCCCAACCTAAAGACGACGTACTCCAA
AAGCTCGAGAACTAATCGAGGTGCCTGGACGGCGCCCGGTACTCCGTGGAGTCACA
TGAAGCGACGGCTGAGGACGGAAAGGCCCTTTTCCTTTGTGTGGGTGACTCACCCGC
CCGCTCTCCCGAGCGCCGCGTCCTCCATTTTGAGCTCCCTGCAGCAGGGCCGGGAAG
CGGCCATCTTTCCGCTCACGCAACTGGTGCCGACCGGGCCAGCCTTGCCGCCCAGGG
CGGGGCGATACACGGCGGCGCGAGGCCAGGCACCAGAGCAGGCCGGCCAGCTTGA
GACTACCCCCGTCCGATTCTCGGTGGCCGCGCTCGCAGGCCCCGCCTCGCCGAACAT
GTGCGCTGGGACGCACGGGCCCCGTCGCCGCCCGCGGCCCCAAAAACCGAAATACC
AGTGTGCAGATCTTGGCCCGCATTTACAAGACTATCTTGCCAGAAAAAAAGCGTCGC
AGCAGGTCATCAAAAATTTTAAATGGCTAGAGACTTATCGAAAGCAGCGAGACAGG
CGCGAAGGTGCCACCAGATTCGCACGCGGCGGCCCCAGCGCCCAGGCCAGGCCTCA
ACTCAAGCACGAGGCGAAGGGGCTCCTTAAGCGCAAGGCCTCGAACTCTCCCACCC
ACTTCCAACCCGAAGCTCGGGATCAAGAATCACGTACTGCAGCCAGGTGGAAGTAA
TTCAAGGCACGCAAGGGCCATAACCCGTAAAGAGGCCAGGCCCGCGGGAACCACAC
ACGGCACTTACCTGTGTTCTGGCGGCAAACCCGTTGCGAAAAAGAACGTTCACGGC
GACTACTGCACTTATATACGGTTCTCCCCCACCCTCGGGAAAAAGGCGGAGCCAGTA
CACGACATCACTTTCCCAGTTTACCCCGCGCCACCTTCTCTAGGCACCGGATCAATT
GCCGACCCCTCCCCCCAACTTCTCGGGGACTGTGGGCGATGTGCGCTCTGCCCACTG
ACGGGCACCGGAGCCAATTCCCACTCCTTTCAAGACCTAGAAGGTCCATTAGCTGCA
AAGATTCCTCTCTGTTTAAAACTTTATCCATCTTTGCACCCGGGCCCCCTCGAGCCGG
CGCCAAAGTGGATCTCTGCTGTCCCTGTAATAAACCCGAAAATTTTGAATTTTTGTA
ATTTGTTTTTGTAATTCTTTAGTTTGTATGTCTGTTGCTATTATGTCTACTATTCTTTCC
CCTGCACTGTACCCCCCAATCCCCCCTTTTCTTTTAAAATTGTGGATGAATACTGCCA
TTTGTCTCAAGATCTAGTTACGCCAAGCTTAAAAAAGCACCGACTCGGTGCCACTTT
TTCAAGTTGATAACGGACTAGCCTTATTTTAACTTGCTATTTCTAGCTCTAAAACAGA
GACGTACAAAAAAGAGCAAGAAGCTAAAAAAGATTTAAAAATTATTTTTAGCGCAG
TTAATGGAACAGGAACTAAATTTACCCCAAAAATATTACGTGAATCAGGATATAAC
GTTATTGAGGTTGAAGAGCATGCATTTGAAGATGAAACATTTAAAAATGTTGTAAAT
CCAAATCCAGAATTTGATCCTGCATGAAAAATACCGCTTGAATATGGTATTAAACAT
GATGCAGATATTATTATTATGAATGACCCAGATGCTGACAGATTTGGAATGGCAATA
AAACATGATGGTCATTTTGTAAGATTAGATGGAAATCAAACAGGACCAATTTTAATT
GATTGAAAATTATCAAATCTAAAACGCTTAAATAGCATTCCAAAAAATCCGGCTCTA
TATTCAAGTTTTGTAACAAGTGATTTGGGTGATAGAATCGCTCATGAAAAATATGGA
GTTAATATTGTAAAAACTTTAACTGGATTTAAATGAATGGGTAGAGAAATTGCTAAA
GAAGAAGATAACGGATTAAATTTTGTTTTTGCTTATGAAGAAAGTTATGGATATGTA
ATTGATGACTCAGCTAGAGATAAAGATGGAATACAAGCTTCTATATTAATAGCAGA
GGCTGCTTGATTTTATAAAAAACAAAATAAAACATTAGTAGACTATTTAGAAGATTT

ATTTAAAGAAATGGGTGCATATTACACTTTCACTTTAAACTTGAATTTTAAACCAGA
AGAAAAGAAATTAAAAATTGAACCATTAATGAAATCATTGAGAGCAACACCCTTAA
CTCAAATTGCTGGACTTAAAGTTGTTAATGTTGAAGACTACATCGATGGAATGTATA
ATATGCCAGGACAAGACTTACTAAAATTTTATTTAGAAGATAAGTCATGATTTGCTG
TTCGCCCAAGTGGAACTGAACCTAAACTAAAAATTTATTTTATAGGTGTTGGTGAAT
CTGTTCAAAACGCTAAAGTTAAAGTAGACGAAATTATTAAAGAATTAAAATTAAAA
ATGAATATATAGGAGAAAAAATGAAACTAAACAAATATATAGATCACACATTATTA
AAACAAGATGCTACGAAAGCTGAAATTAAACAATTATGTGATGAAGCAATTGAATT
TGATTTTGCAACAGTTTGTGTTAATTCATATTGAACAAGCTATTGTAAAGAATTATTA
AAAGGCACAAATGTAGGAATAACAAATGTTGTAGGTTTTCCTCTAGGTGCATGCACA
ACAGCTACAAAAGCATTCGAAGTTTCTGAAGCAATTAAAGATGGTGCAACAGAAAT
TGATATGGTATTAAATATTGGTGCATTAAAAGACAAAAATTATGAATTAGTTTTAGA
AGACATGAAAGCTGTAAAAAAAGCAGCTGGATCACATGTTGTTAAATGTATTATGG
AAAATTGTTTATTAACAAAAGAAGAAATCATGAAAGCTTGTGAAATAGCTGTTGAA
GCTGGATTAGAATTTGTTAAAACATCAACAGGATTTTCAAAATCAGGTGCAACATTT
GAAGATGTTAAACTAATGAAGTCAGTTGTTAAAGACAATGCTTTAGTTAAAGCAGCT
GGTGGAGTTAGAACATTTGAAGATGCTCAAAAAATGATTGAAGCAGGAGCTGACCG
CTTAGGAACAAGTGGTGGAGTAGCTATTATTAAAGGTGAAGAAAACAACGCGAGTT
ACTAAAACTAGCGTTTTTTTATTTTGCTCATTTTTATTAAAAGTTTGCAAAAAGGAAC
ATAAAAATTCTAATTATTGATACTAAAGTTATTAAAAAGAAGATTTTGGTTGATTTT
ATAAAGGTCATAGAATATAATATTTTAGCATGTGTATTTTGTGTGCTCATTTACAACC
GTCTCCGGTGTTTCGTCCTTTCCACAAGATATATAAAGCCAAGAAATCGAAATACTT
TCAAGTTACGGTAAGCATATGATAGTCCATTTTAAAACATAATTTTAAAACTGCAAA
CTACCCAAGAAATTATTACTTTCTACGTCACGTATTTTGTACTAATATCTTTGTGTTT
ACAGTCAAATTAATTCTAATTATCTCTCTAACAGCCTTGTATCGTATATGCAAATATG
AAGGAATCATGGGAAATAGGCCCTCTCTGGGTCCCCTCGGGGTTGGGAGGTGGGTC
TGAAACGAT

Supplemental Figure A.S2- The second ISD library of larger PCR-amplified dsDNA. **(A)** Gel Electrophoresis of PCR-amplified dsDNA. The NEB 1 kb DNA Ladder was used for reference. **(B)** Sequences for each PCR-amplified dsDNA molecules. Primers used for each PCR-amplification were determined using the NCBI Primer Blast tool website, ncbi.nlm.nih.gov/tools/primer-blast/ and are highlighted in yellow for the forward primers and in red for the reverse primers.

A

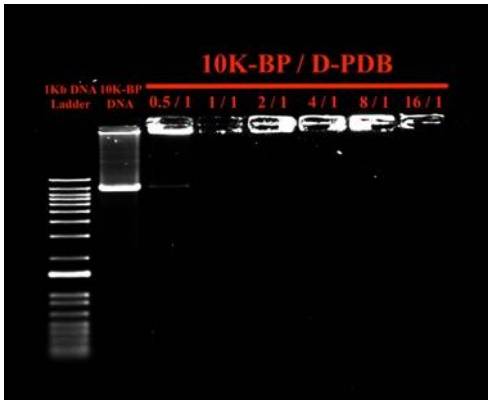

B

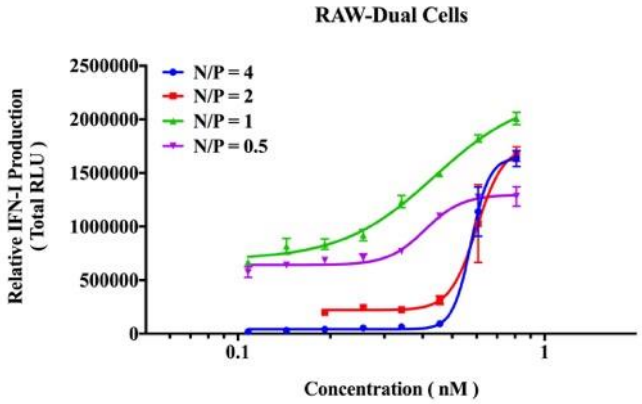

C

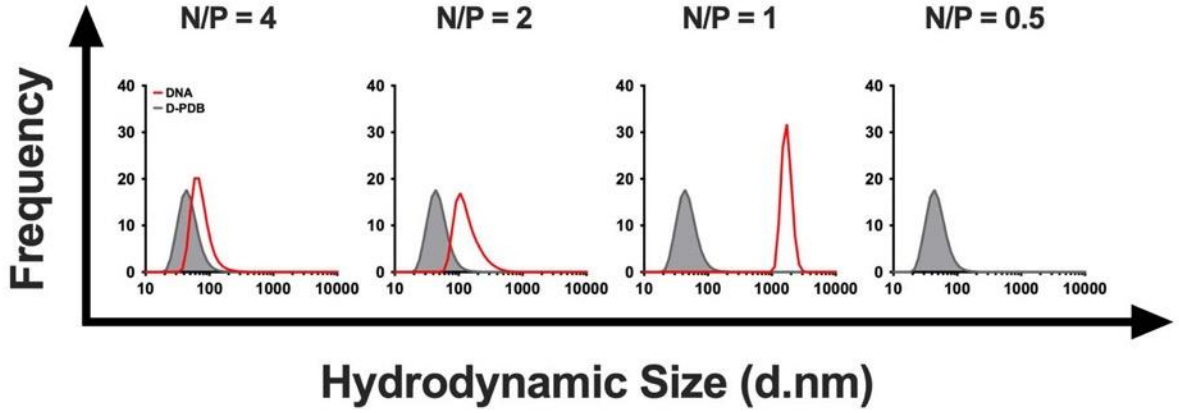

Supplemental Figure A.S3- Effects of N/P Charge Ratio. **(A)** Agarose gel image. Lanes comprise 1 µg DNA mixed with the indicated amount of D-PDB. The TrackIt™ 1 Kb Plus DNA Ladder was used for reference. PCR-amplified 10,000-BP dsDNA / D-PDB at varying N/P charge ratios was tested for DNA loading. **(B)** RAW-Dual reporter cell assay of PCR-amplified 5000-BP dsDNA / D-PDB at varying N/P charge ratios. **(C)** DLS analysis of PCR-amplified 5000-BP dsDNA / D-PDB at varying N/P charge ratios. Frequency indicates the number-based particle size distribution. Hydrodynamic size indicates the particle diameter in nm. N/P = 0.5 was not colloidally stable to collect an accurate size measurement.

A

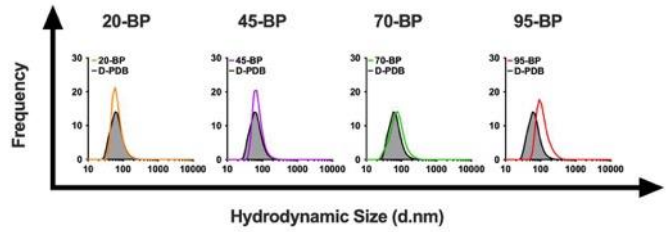

Malvern Zetasizer	Number PSD Peak (Mode)
D-PDB	59 nm
20-BP / D-PDB	59 nm
45-BP / D-PDB	68 nm
70-BP / D-PDB	79 nm
95-BP / D-PDB (NanoISD)	91 nm

B

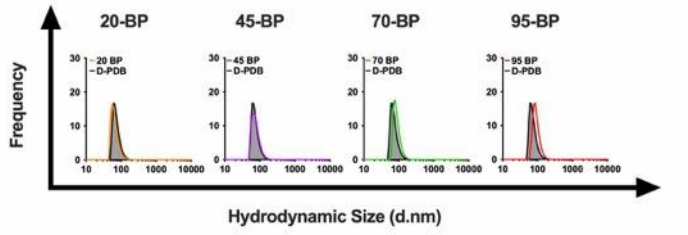

Anton Paar Litesizer	Number PSD Peak (Mode)
D-PDB	61 nm
20-BP / D-PDB	56 nm
45-BP / D-PDB	66 nm
70-BP / D-PDB	77 nm
95-BP / D-PDB (NanoISD)	84 nm

Supplemental Figure A.S4- DLS analysis of the synthetic, phosphorothioate-capped dsDNA library. **(A)** Synthetic, phosphorothioate-capped dsDNA library complexed to D-PDB at an N/P charge ratio of 4. Data presented as number-based particle size distribution. Malvern Zetasizer used for quantification. **(B)** Synthetic, phosphorothioate-capped ISD library complexed to D-PDB at an N/P charge ratio of 4. Data presented as number-based particle size distribution. DLS using an Anton Paar Litesizer was used as a second form of particle size analysis.

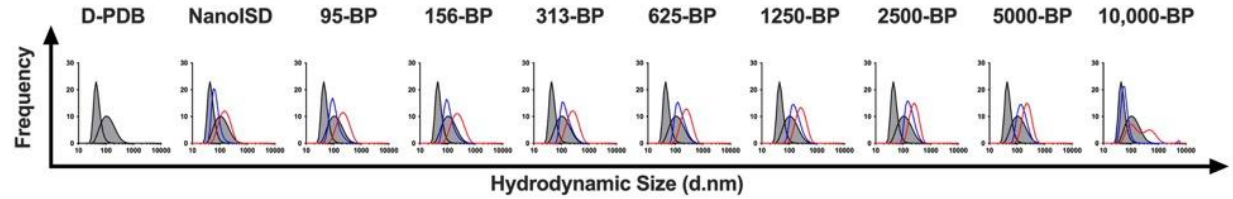

Malvern Zetasizer	Number PSD Peak (Mode)
D-PDB	44 nm
NanoISD	59 nm
95-BP / D-PDB	91 nm
156-BP / D-PDB	91 nm
313-BP / D-PDB	106 nm
625-BP / D-PDB	122 nm
1250-BP / D-PDB	142 nm
2500-BP / D-PDB	142 nm
5000-BP / D-PDB	142 nm
10,000-BP / D-PDB	N/A

Supplemental Figure A.S5- DLS analysis of the PCR-amplified dsDNA library. PCR-amplified dsDNA library complexed to D-PDB at an N/P charge ratio of 4. Data presented as both number-based particle size distribution (blue) and intensity-based particle size distribution (red).

A

RAW-Dual Dose Response:

Treatment	Maximum Efficacy (RLU)	EC_{50} Values (nM)
95-BP / D-PDB	396,233	22.4
70-BP / D-PDB	385,838	31.3
45-BP / D-PDB	240,839	43.5
20-BP / D-PDB	84,923	112.9
95-BP	449	N/A
D-PDB	20,651	442.3
cGAMP	522,049	31,579.1

B

THP1-Dual Dose Response:

Treatment	Maximum Efficacy (RLU)	EC_{50} Values (nM)
95-BP / D-PDB	1,648,495	14.1
70-BP / D-PDB	1,089,124	21.8
45-BP / D-PDB	684,302	37.2
20-BP / D-PDB	493,610	115.1
95-BP	1,197	N/A
D-PDB	208,907	537.8
cGAMP	2,514,642	27,759.1

C

A549-Dual Dose Response:

Treatment	Maximum Efficacy (RLU)	EC_{50} Values (nM)
95-BP / D-PDB	1,983,308	19.1
70-BP / D-PDB	1,424,241	24.7
45-BP / D-PDB	749,267	45.0
20-BP / D-PDB	698,816	113.4
95-BP	0	N/A
D-PDB	652,675	535.6
cGAMP	1,695,993	38,503.3

Supplemental Figure A.S6- Maximum efficacy and EC50 values.

A

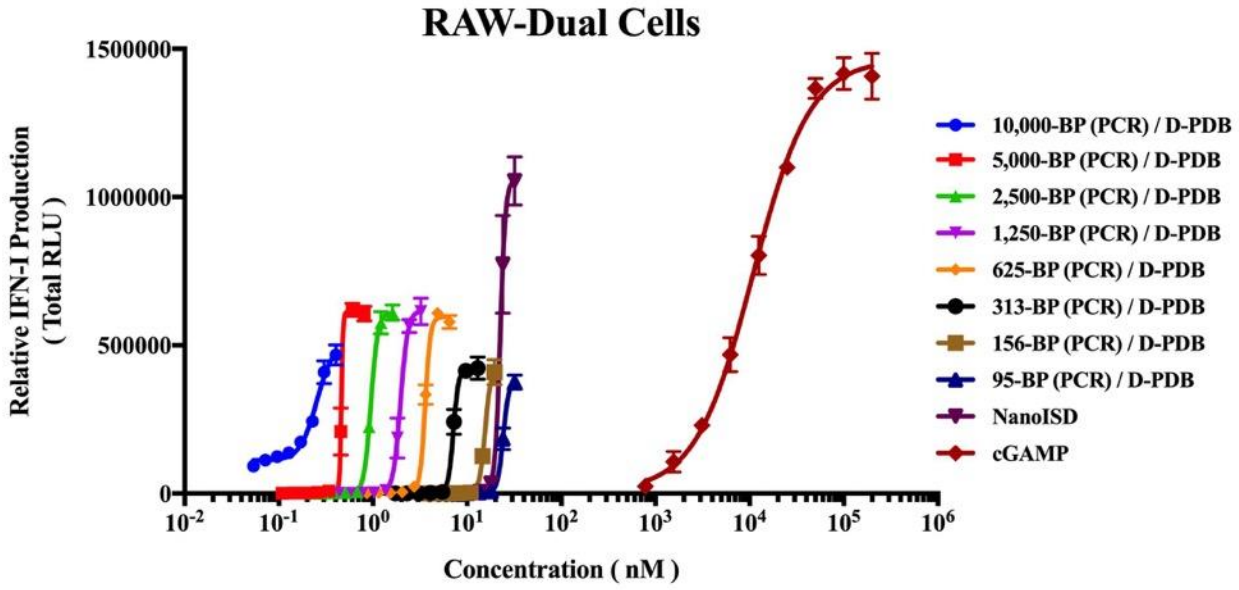

B

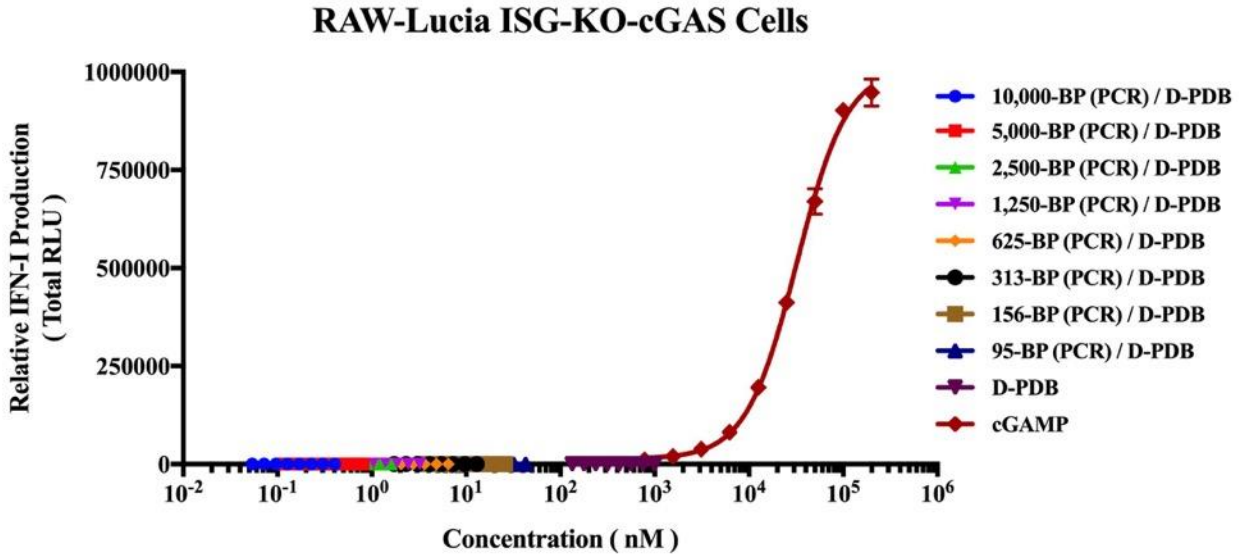

Supplemental Figure A.S7- Activity of the PCR-amplified dsDNA library with D-PDB. **(A)** RAW-Dual IFN-I reporter cell assay of PCR-amplified dsDNA library complexed to D-PDB at an N/P charge ratio of 4. **(B)** RAW-Lucia ISG-KO-cGAS IFN-I reporter cell assay of PCR-amplified dsDNA library complexed to D-PDB at an N/P charge ratio of 4. The dose response curve for free D-PDB is positioned along the x-axis in terms of the molar amount of polymer chains rather than molar amount of loaded dsDNA, and each dose response that utilized the polymer was administered using equivalent D-PDB concentrations.

A

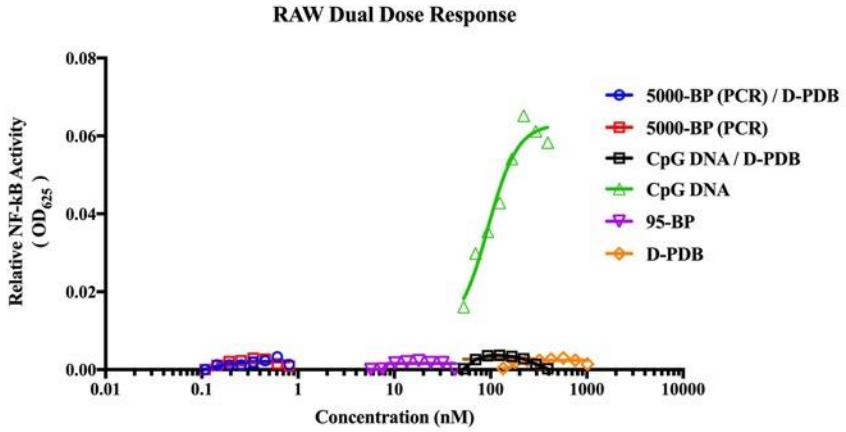

B

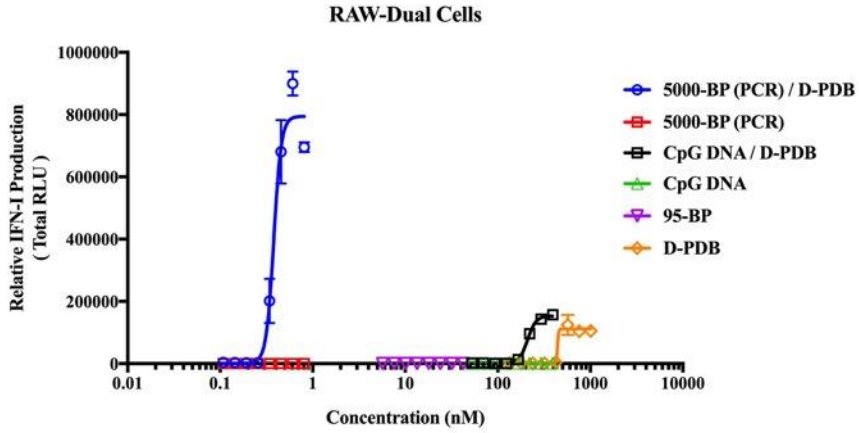

C

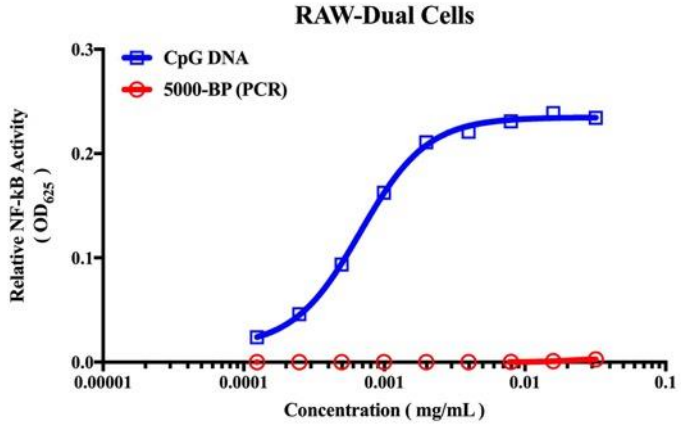

Supplementary Figure A.S8- Analysis of NF-κB pathway activity. **(A)** RAW-Dual reporter cell assay for relative NF-κB activity of various indicated DNA molecules with or without D-PDB as indicated. **(B)** RAW-Dual reporter cell assay for relative IFN-I activity of various indicated DNA molecules with or without D-PDB as indicated. **(C)** RAW-Dual reporter cell assay for relative NF-κB activity of PCR-amplified 5000-BP dsDNA and CpG DNA (*i.e.* ODN 1826) over a larger concentration range.

A

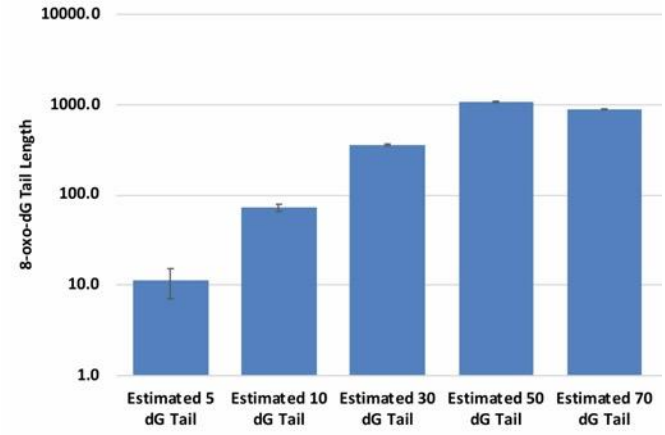

B

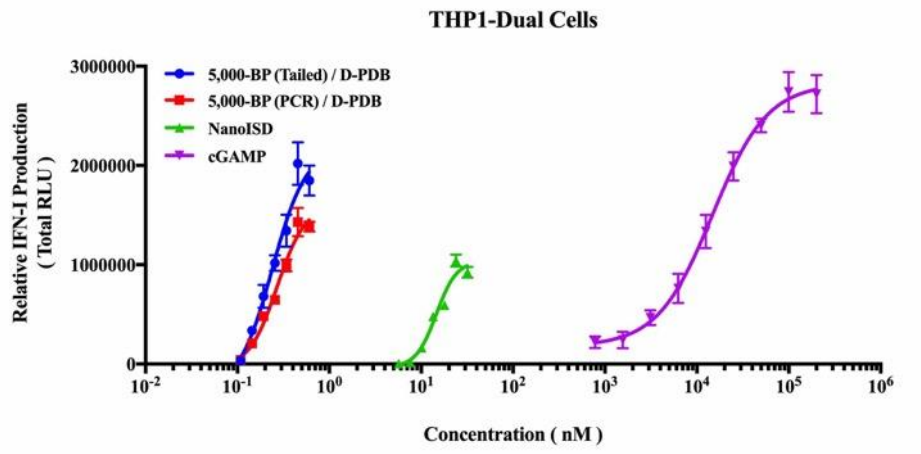

C

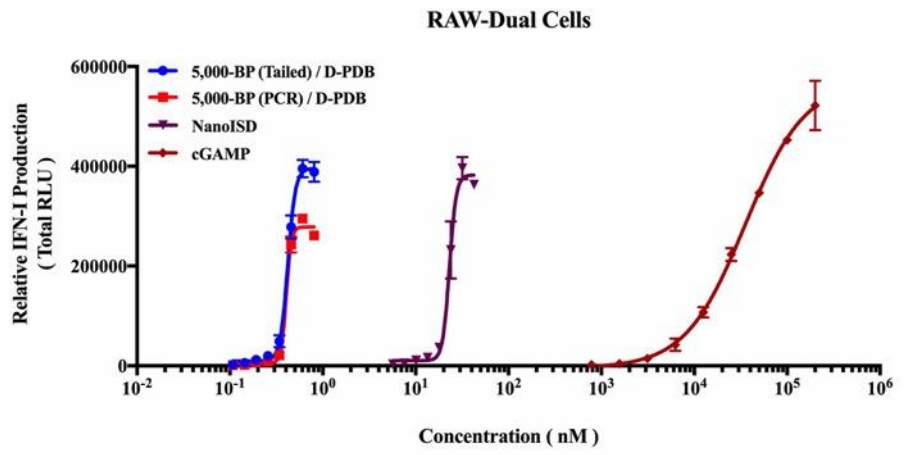

Supplementary Figure A.S9- Characterization of Large ISD Tailed with Oxidized Guanine. **(A)** ELISA for oxidized guanine was used to confirm successful addition of oxidized guanine. **(B)** THP1-Dual reporter cell assay for relative IFN-I activity of various compounds as indicated. **(C)** RAW-Dual reporter cell assay for relative IFN-I activity of various compounds as indicated.

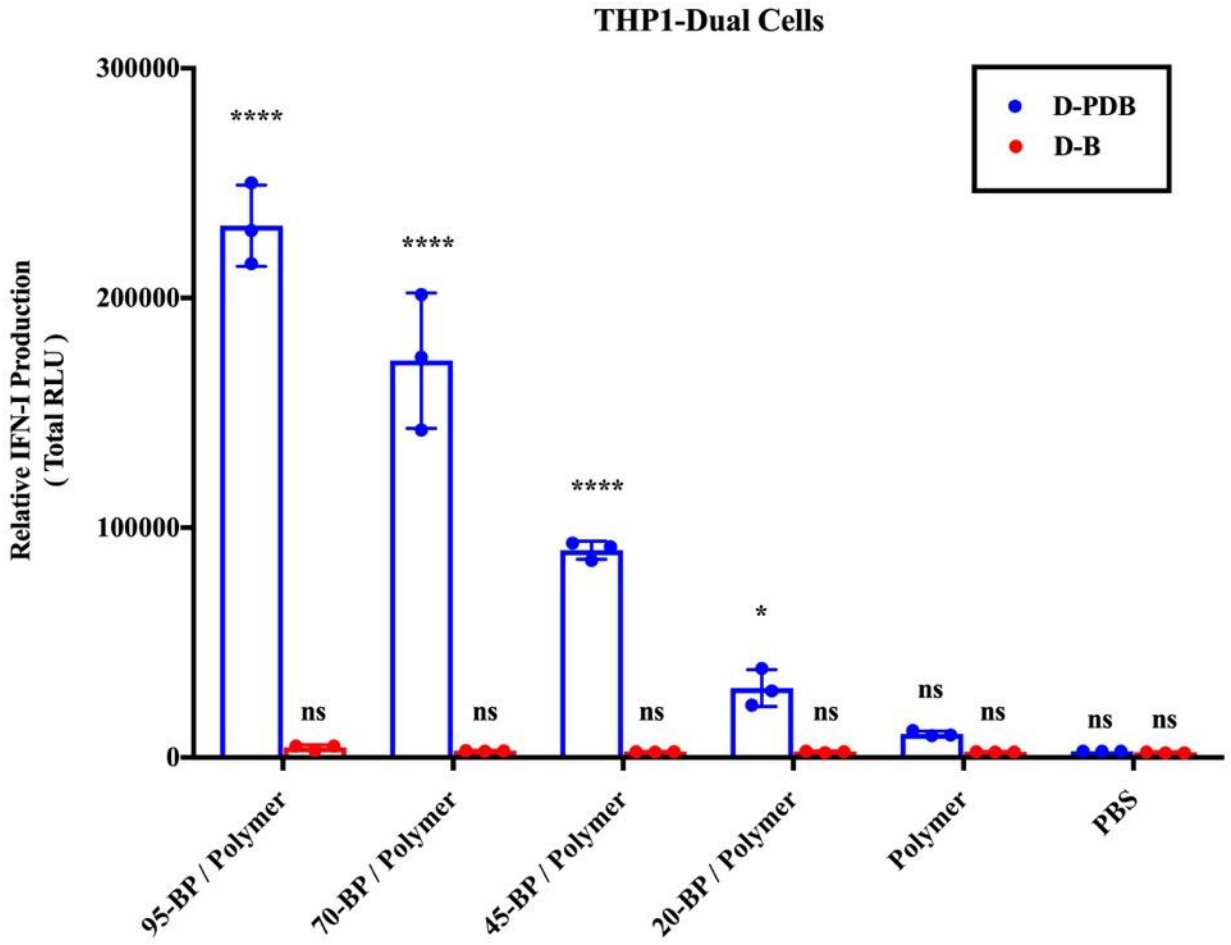

Supplemental Figure A.S10- Activity of the synthetic ISD library with D-PDB or D-B as carriers. THP1-Dual IFN-I reporter cells were treated with 1.5 µg/mL DNA using an N/P charge ratio of 5. A two-way ANOVA with Sidak test was used for statistical analysis.

Nanoparticle	Zeta Potential (mV)
D-PDB	+ 16.27
20-BP / D-PDB	+ 9.49
45-BP / D-PDB	+ 15.50
70-BP / D-PDB	+ 13.10
95-BP / D-PDB	+ 14.87

Supplemental Figure A.S11- Zeta potential of D-PDB and the synthetic ISD library with D-PDB.

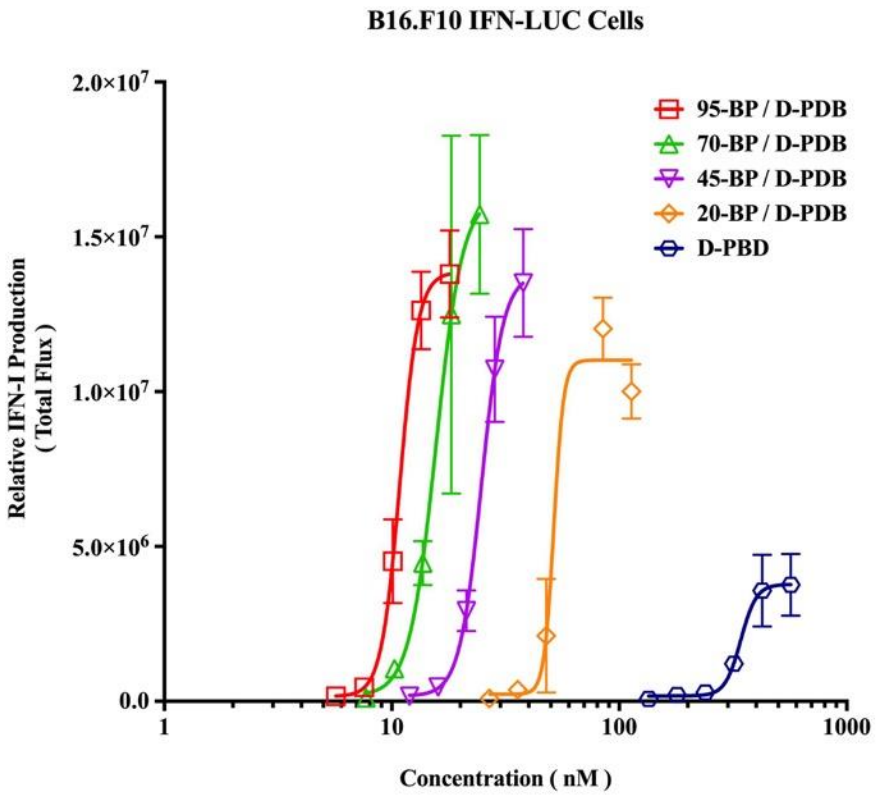

Supplemental Figure A.S12- Activity of the synthetic ISD library with D-PDB in B16.F10 IFN-LUC cells. B16.F10 IFN-LUC reporter cell assay of synthetic, variable-length ISD library complexed to D-PDB at an N/P charge ratio of 4. EC_{50} values for 95-BP / D-PDB, 70-BP / D-PDB, 45-BP / D-PDB, 20-BP / D-PDB, and D-PDB are 11 nM, 15 nM, 25 nM, 52 nM, and 339 nM, respectively. The dose response curve for free D-PDB is positioned along the x-axis in terms of the molar amount of polymer chains rather than molar amount of loaded dsDNA, and each dose response that utilized the polymer was administered using equivalent D-PDB concentrations.

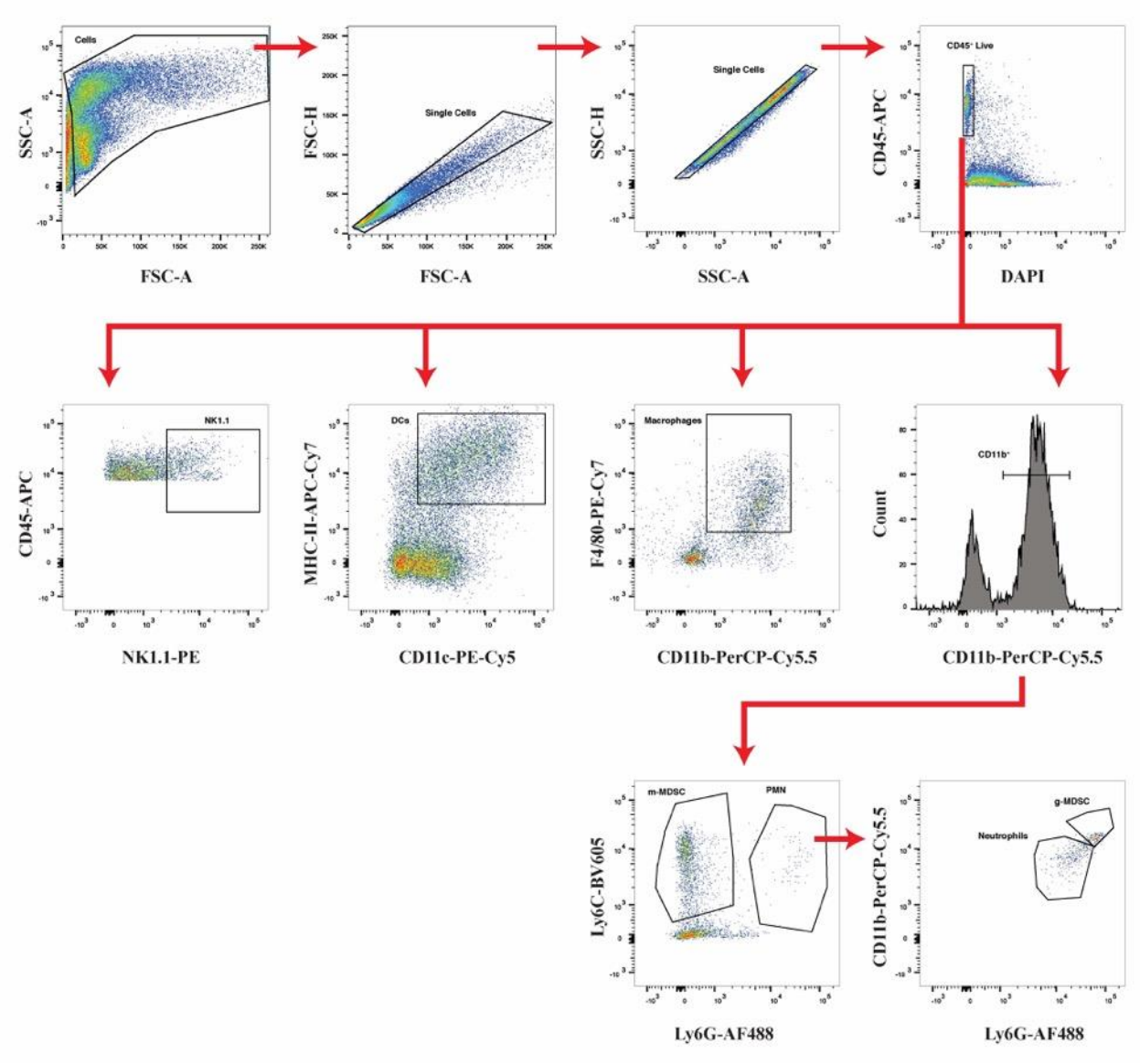

Supplemental Figure A.S13- Flow cytometry gating strategy for myeloid cell panel.

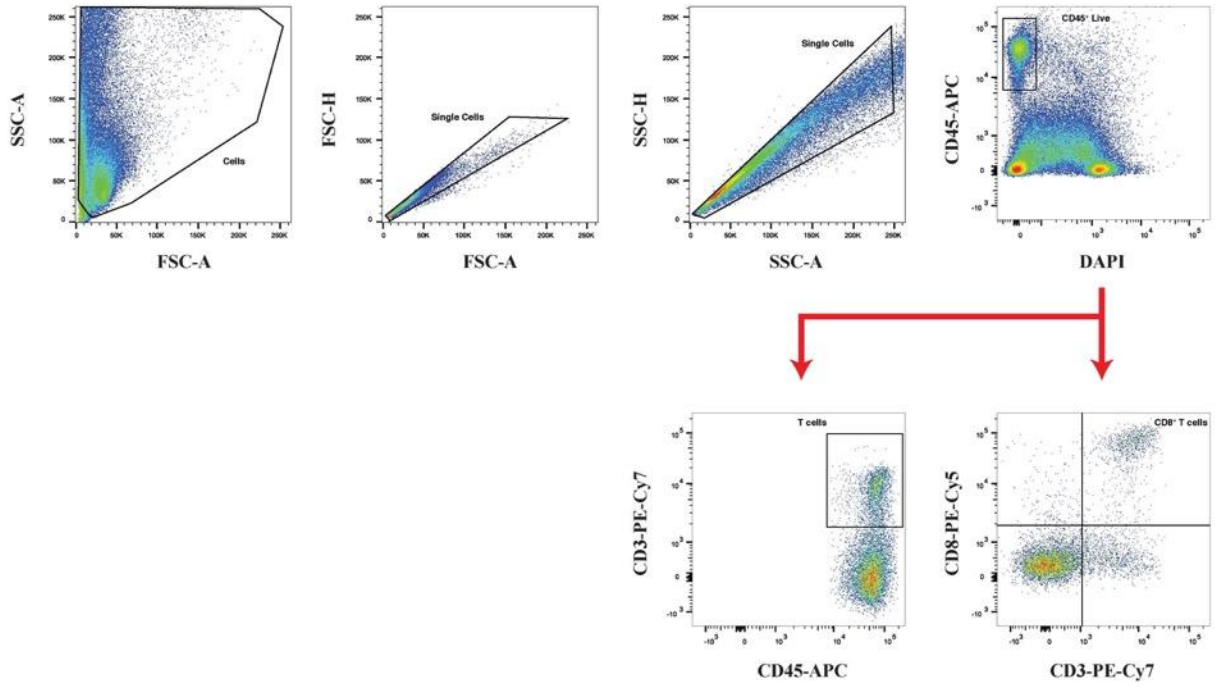

Supplemental Figure A.S14- Flow cytometry gating strategy for T cell panel.

A

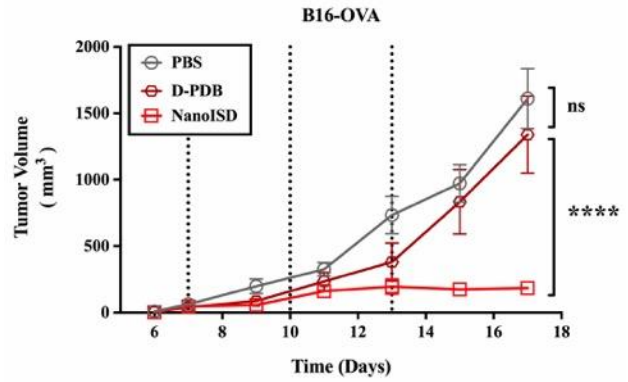

B

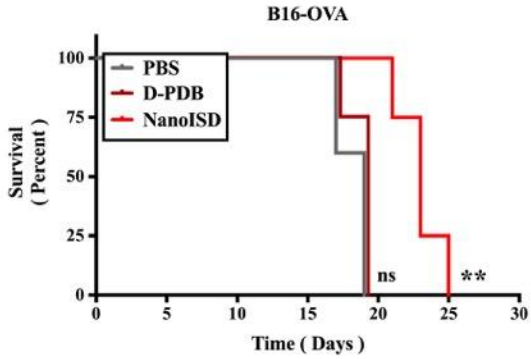

Supplemental Figure A.S15- Therapeutic effect of NanoISD in the B16-OVA tumor model. **(A)** Tumor growth plot for B16-OVA tumors intratumorally treated with 100 µL of either PBS or NanoISD at a dose corresponding to 20 µg DNA (n = 4 or greater per treatment group). Treatments were administered 3 times q3d as indicated by the dotted lines. Tumor growth curves were truncated to the day that mice began to reach the study endpoint. A two-way ANOVA with Tukey test was used for statistical analysis. Statistics on the graph represent the analysis for the final day shown (*i.e.* day 17). **(B)** Kaplan-Meier Survival Curve for B16-OVA tumors intratumorally treated with 100 µL of either PBS, D-PDB, or NanoISD. Log rank (Mantel-Cox) test was used for statistical analysis.

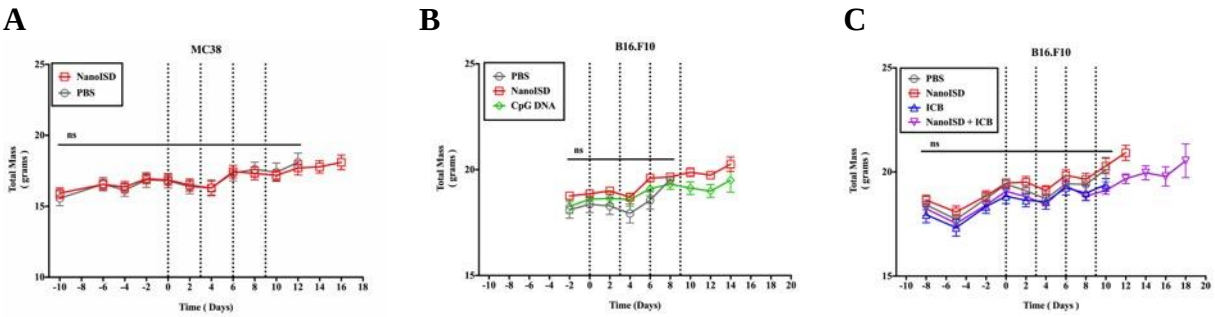

Supplemental Figure A.S16- Intratumorally injected NanoISD is well-tolerated. **(A)** Total mouse weight over time for the mice with MC38 tumors corresponding to studies described in ***Figures 7a and 7b***. Intratumoral treatments were administered 4 times q3d as indicated by the dotted lines. A two-way ANOVA with Sidak test was used for statistical analysis. Statistics on the graph represent the analysis for each of the treatment groups relative to PBS. **(B)** Total mouse weight over time for the mice with B16-F10 tumors corresponding to studies described in ***Figures 7c and 7d***. Intratumoral treatments were administered 4 times q3d as indicated by the dotted lines. A two-way ANOVA with Tukey test was used for statistical analysis. Statistics on the graph represent the analysis for each of the treatment groups relative to PBS. **(C)** Total mouse weight over time for the mice with B16-F10 tumors corresponding to studies described in ***Figures 7e and 7f***. Intratumoral treatments were administered 4 times q3d as indicated by the dotted lines. A two-way ANOVA with Tukey test was used for statistical analysis. Statistics on the graph represent the analysis for each of the treatment groups relative to PBS.

Polymer	PAA (%)	DMAEMA (%)	BMA (%)	Molecular Weight (kDa)
1st Block	0	100	0	9.40
2nd Block	28	35	37	38.69

Supplemental Figure A.S17- D-PDB composition as determined by ^{1}H NMR analysis.

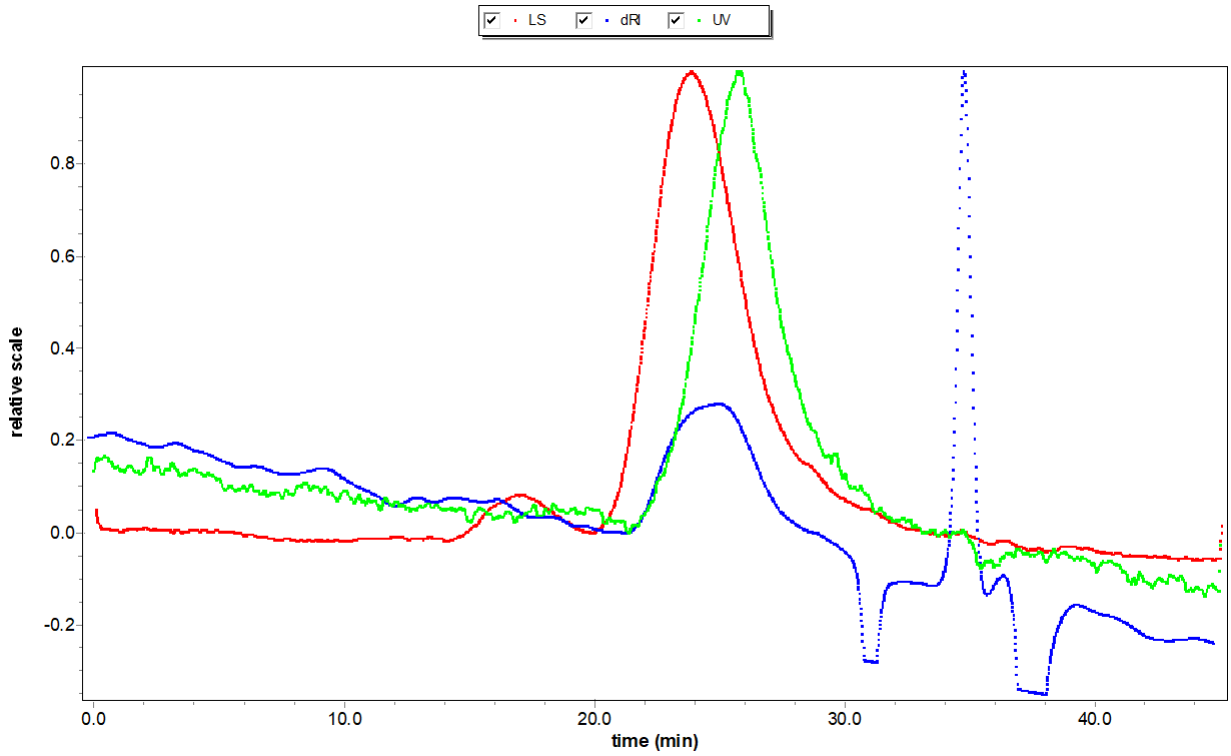

Supplemental Figure A.S18- GPC spectrum of D-PDB. GPC analysis indicated that the total molecular weight of polymer was 41.56 kDa and the PDI was 1.136. Since ^{1}H NMR indicated the total molecular weight of D-PDB was 48.09 kDa, an average molecular weight of 44.8 kDa was used for all calculations regarding polymer concentration.

REFERENCES

1. Sung, H.; Ferlay, J.; Siegel, R. L.; Laversanne, M.; Soerjomataram, I.; Jemal, A.; Bray, F., Global Cancer Statistics 2020: GLOBOCAN Estimates of Incidence and Mortality Worldwide for 36 Cancers in 185 Countries. *CA Cancer J Clin* **2021,** *71* (3), 209-249.
2. Siegel, R. L.; Miller, K. D.; Fuchs, H. E.; Jemal, A., Cancer Statistics, 2021. *CA Cancer J Clin* **2021,** *71* (1), 7-33.
3. Ayers, M.; Lunceford, J.; Nebozhyn, M.; Murphy, E.; Loboda, A.; Kaufman, D. R.; Albright, A.; Cheng, J. D.; Kang, S. P.; Shankaran, V.; Piha-Paul, S. A.; Yearley, J.; Seiwert, T. Y.; Ribas, A.; McClanahan, T. K., IFN-gamma-related mRNA profile predicts clinical response to PD-1 blockade. *J Clin Invest* **2017,** *127* (8), 2930-2940.
4. Broz, P.; Monack, D. M., Newly described pattern recognition receptors team up against intracellular pathogens. *Nature Reviews Immunology* **2013,** *13* (8), 551-565.
5. Vanpouille-Box, C.; Hoffmann, J. A.; Galluzzi, L., Pharmacological modulation of nucleic acid sensors - therapeutic potential and persisting obstacles. *Nat Rev Drug Discov* **2019,** *18* (11), 845-867.
6. Whitehead, K. A.; Langer, R.; Anderson, D. G., Knocking down barriers: advances in siRNA delivery. *Nat Rev Drug Discov* **2009,** *8* (2), 129-38.
7. Convertine, A. J.; Benoit, D. S.; Duvall, C. L.; Hoffman, A. S.; Stayton, P. S., Development of a novel endosomolytic diblock copolymer for siRNA delivery. *J Control Release* **2009,** *133* (3), 221-9.
8. Convertine, A. J.; Diab, C.; Prieve, M.; Paschal, A.; Hoffman, A. S.; Johnson, P. H.; Stayton, P. S., pH-responsive polymeric micelle carriers for siRNA drugs. *Biomacromolecules* **2010,** *11* (11), 2904-11.
9. Devarajan, P. V.; Jain, S., *Targeted drug delivery: concepts and design*. Springer: 2015.
10. Kunath, K.; von Harpe, A.; Petersen, H.; Fischer, D.; Voigt, K.; Kissel, T.; Bickel, U., The structure of PEG-modified poly(ethylene imines) influences biodistribution and pharmacokinetics of their complexes with NF-kappaB decoy in mice. *Pharm Res* **2002,** *19* (6), 810-7.
11. Lv, H.; Zhang, S.; Wang, B.; Cui, S.; Yan, J., Toxicity of cationic lipids and cationic polymers in gene delivery. *J Control Release* **2006,** *114* (1), 100-9.
12. Park, W.; Heo, Y. J.; Han, D. K., New opportunities for nanoparticles in cancer immunotherapy. *Biomater Res* **2018,** *22*, 24.
13. Jiang, W.; von Roemeling, C. A.; Chen, Y.; Qie, Y.; Liu, X.; Chen, J.; Kim, B. Y. S., Designing nanomedicine for immuno-oncology. *Nature Biomedical Engineering* **2017,** *1* (2), 0029.
14. Rothschilds, A. M.; Wittrup, K. D., What, Why, Where, and When: Bringing Timing to Immuno-Oncology. *Trends Immunol* **2019,** *40* (1), 12-21.
15. Amos, S. M.; Duong, C. P.; Westwood, J. A.; Ritchie, D. S.; Junghans, R. P.; Darcy, P. K.; Kershaw, M. H., Autoimmunity associated with immunotherapy of cancer. *Blood* **2011,** *118* (3), 499-509.
16. Marabelle, A.; Tselikas, L.; de Baere, T.; Houot, R., Intratumoral immunotherapy: using the tumor as the remedy. *Ann Oncol* **2017,** *28* (suppl_12), xii33-xii43.
17. Singh, M.; Overwijk, W. W., Intratumoral immunotherapy for melanoma. *Cancer Immunol Immunother* **2015,** *64* (7), 911-21.

18. Zaharoff, D. A.; Hance, K. W.; Rogers, C. J.; Schlom, J.; Greiner, J. W., Intratumoral immunotherapy of established solid tumors with chitosan/IL-12. *J Immunother* **2010,** *33* (7), 697-705.
19. Sanchez-Paulete, A. R.; Teijeira, A.; Quetglas, J. I.; Rodriguez-Ruiz, M. E.; Sanchez-Arraez, A.; Labiano, S.; Etxeberria, I.; Azpilikueta, A.; Bolanos, E.; Ballesteros-Briones, M. C.; Casares, N.; Quezada, S. A.; Berraondo, P.; Sancho, D.; Smerdou, C.; Melero, I., Intratumoral Immunotherapy with XCL1 and sFlt3L Encoded in Recombinant Semliki Forest Virus-Derived Vectors Fosters Dendritic Cell-Mediated T-cell Cross-Priming. *Cancer Res* **2018,** *78* (23), 6643-6654.
20. Raj, S.; Miller, L. D.; Triozzi, P. L., Addressing the Adult Soft Tissue Sarcoma Microenvironment with Intratumoral Immunotherapy. *Sarcoma* **2018,** *2018*, 9305294.
21. Decout, A.; Katz, J. D.; Venkatraman, S.; Ablasser, A., The cGAS–STING pathway as a therapeutic target in inflammatory diseases. *Nature Reviews Immunology* **2021**.
22. Hemphill, W. O.; Simpson, S. R.; Liu, M.; Salsbury, F. R., Jr.; Hollis, T.; Grayson, J. M.; Perrino, F. W., TREX1 as a Novel Immunotherapeutic Target. *Front Immunol* **2021,** *12*, 660184.
23. Luecke, S.; Holleufer, A.; Christensen, M. H.; Jonsson, K. L.; Boni, G. A.; Sorensen, L. K.; Johannsen, M.; Jakobsen, M. R.; Hartmann, R.; Paludan, S. R., cGAS is activated by DNA in a length-dependent manner. *EMBO Rep* **2017,** *18* (10), 1707-1715.
24. Hasler, J.; Strub, K., Alu elements as regulators of gene expression. *Nucleic Acids Res* **2006,** *34* (19), 5491-7.
25. Heinrich, M. J.; Purcell, C. A.; Pruijssers, A. J.; Zhao, Y.; Spurlock, C. F., 3rd; Sriram, S.; Ogden, K. M.; Dermody, T. S.; Scholz, M. B.; Crooke, P. S., 3rd; Karijolich, J.; Aune, T. M., Endogenous double-stranded Alu RNA elements stimulate IFN-responses in relapsing remitting multiple sclerosis. *J Autoimmun* **2019,** *100*, 40-51.
26. Tossberg, J. T.; Heinrich, R. M.; Farley, V. M.; Crooke, P. S., 3rd; Aune, T. M., Adenosine-to-Inosine RNA Editing of Alu Double-Stranded (ds)RNAs Is Markedly Decreased in Multiple Sclerosis and Unedited Alu dsRNAs Are Potent Activators of Proinflammatory Transcriptional Responses. *J Immunol* **2020,** *205* (10), 2606-2617.
27. Elion, D. L.; Jacobson, M. E.; Hicks, D. J.; Rahman, B.; Sanchez, V.; Gonzales-Ericsson, P. I.; Fedorova, O.; Pyle, A. M.; Wilson, J. T.; Cook, R. S., Therapeutically Active RIG-I Agonist Induces Immunogenic Tumor Cell Killing in Breast Cancers. *Cancer Res* **2018,** *78* (21), 6183-6195.
28. Jacobson, M. E.; Wang-Bishop, L.; Becker, K. W.; Wilson, J. T., Delivery of 5'-triphosphate RNA with endosomolytic nanoparticles potently activates RIG-I to improve cancer immunotherapy. *Biomater Sci* **2019,** *7* (2), 547-559.
29. Johnson, L. R.; Lee, D. Y.; Eacret, J. S.; Ye, D.; June, C. H.; Minn, A. J., The immunostimulatory RNA RN7SL1 enables CAR-T cells to enhance autonomous and endogenous immune function. *Cell* **2021,** *184* (19), 4981-4995 e14.
30. Hammerich, L.; Marron, T. U.; Upadhyay, R.; Svensson-Arvelund, J.; Dhainaut, M.; Hussein, S.; Zhan, Y.; Ostrowski, D.; Yellin, M.; Marsh, H.; Salazar, A. M.; Rahman, A. H.; Brown, B. D.; Merad, M.; Brody, J. D., Systemic clinical tumor regressions and potentiation of PD1 blockade with in situ vaccination. *Nat Med* **2019,** *25* (5), 814-824.
31. Barber, G. N., STING: infection, inflammation and cancer. *Nat Rev Immunol* **2015,** *15* (12), 760-70.
32. Ahn, J.; Barber, G. N., STING signaling and host defense against microbial infection.

Exp Mol Med **2019,** *51* (12), 1-10.
33. Wu, X.; Wu, F. H.; Wang, X.; Wang, L.; Siedow, J. N.; Zhang, W.; Pei, Z. M., Molecular evolutionary and structural analysis of the cytosolic DNA sensor cGAS and STING. *Nucleic Acids Res* **2014,** *42* (13), 8243-57.
34. Margolis, S. R.; Wilson, S. C.; Vance, R. E., Evolutionary Origins of cGAS-STING Signaling. *Trends Immunol* **2017,** *38* (10), 733-743.
35. Kranzusch, P. J.; Wilson, S. C.; Lee, A. S.; Berger, J. M.; Doudna, J. A.; Vance, R. E., Ancient Origin of cGAS-STING Reveals Mechanism of Universal 2',3' cGAMP Signaling. *Mol Cell* **2015,** *59* (6), 891-903.
36. Xia, T.; Konno, H.; Ahn, J.; Barber, G. N., Deregulation of STING Signaling in Colorectal Carcinoma Constrains DNA Damage Responses and Correlates With Tumorigenesis. *Cell Rep* **2016,** *14* (2), 282-97.
37. Xia, T.; Konno, H.; Barber, G. N., Recurrent Loss of STING Signaling in Melanoma Correlates with Susceptibility to Viral Oncolysis. *Cancer Res* **2016,** *76* (22), 6747-6759.
38. Xiao, N.; Wei, J.; Xu, S.; Du, H.; Huang, M.; Zhang, S.; Ye, W.; Sun, L.; Chen, Q., cGAS activation causes lupus-like autoimmune disorders in a TREX1 mutant mouse model. *J Autoimmun* **2019,** *100*, 84-94.
39. Yu, Y.; Liu, Y.; An, W.; Song, J.; Zhang, Y.; Zhao, X., STING-mediated inflammation in Kupffer cells contributes to progression of nonalcoholic steatohepatitis. *J Clin Invest* **2019,** *129* (2), 546-555.
40. Ablasser, A.; Chen, Z. J., cGAS in action: Expanding roles in immunity and inflammation. *Science* **2019,** *363* (6431).
41. Chen, Q.; Sun, L.; Chen, Z. J., Regulation and function of the cGAS-STING pathway of cytosolic DNA sensing. *Nat Immunol* **2016,** *17* (10), 1142-9.
42. Motwani, M.; Pesiridis, S.; Fitzgerald, K. A., DNA sensing by the cGAS-STING pathway in health and disease. *Nat Rev Genet* **2019,** *20* (11), 657-674.
43. Hooy, R. M.; Sohn, J., The allosteric activation of cGAS underpins its dynamic signaling landscape. *Elife* **2018,** *7*.
44. Wu, J.; Chen, Z. J., Innate immune sensing and signaling of cytosolic nucleic acids. *Annu Rev Immunol* **2014,** *32*, 461-88.
45. Corrales, L.; Glickman, L. H.; McWhirter, S. M.; Kanne, D. B.; Sivick, K. E.; Katibah, G. E.; Woo, S. R.; Lemmens, E.; Banda, T.; Leong, J. J.; Metchette, K.; Dubensky, T. W., Jr.; Gajewski, T. F., Direct Activation of STING in the Tumor Microenvironment Leads to Potent and Systemic Tumor Regression and Immunity. *Cell Rep* **2015,** *11* (7), 1018-30.
46. Honda, K.; Takaoka, A.; Taniguchi, T., Type I interferon [corrected] gene induction by the interferon regulatory factor family of transcription factors. *Immunity* **2006,** *25* (3), 349-60.
47. Borden, E. C., Interferons alpha and beta in cancer: therapeutic opportunities from new insights. *Nat Rev Drug Discov* **2019,** *18* (3), 219-234.
48. Gajewski, T. F.; Corrales, L., New perspectives on type I IFNs in cancer. *Cytokine Growth Factor Rev* **2015,** *26* (2), 175-8.
49. Benci, J. L.; Johnson, L. R.; Choa, R.; Xu, Y.; Qiu, J.; Zhou, Z.; Xu, B.; Ye, D.; Nathanson, K. L.; June, C. H.; Wherry, E. J.; Zhang, N. R.; Ishwaran, H.; Hellmann, M. D.; Wolchok, J. D.; Kambayashi, T.; Minn, A. J., Opposing Functions of Interferon Coordinate Adaptive and Innate Immune Responses to Cancer Immune Checkpoint Blockade. *Cell* **2019,** *178* (4), 933-948 e14.
50. Marcus, A.; Mao, A. J.; Lensink-Vasan, M.; Wang, L.; Vance, R. E.; Raulet, D. H.,

Tumor-Derived cGAMP Triggers a STING-Mediated Interferon Response in Non-tumor Cells to Activate the NK Cell Response. *Immunity* **2018,** *49* (4), 754-763 e4.
51. Paludan, S. R.; Reinert, L. S.; Hornung, V., DNA-stimulated cell death: implications for host defence, inflammatory diseases and cancer. *Nat Rev Immunol* **2019,** *19* (3), 141-153.
52. Murthy, A. M. V.; Robinson, N.; Kumar, S., Crosstalk between cGAS-STING signaling and cell death. *Cell Death Differ* **2020,** *27* (11), 2989-3003.
53. Demaria, O.; De Gassart, A.; Coso, S.; Gestermann, N.; Di Domizio, J.; Flatz, L.; Gaide, O.; Michielin, O.; Hwu, P.; Petrova, T. V.; Martinon, F.; Modlin, R. L.; Speiser, D. E.; Gilliet, M., STING activation of tumor endothelial cells initiates spontaneous and therapeutic antitumor immunity. *Proc Natl Acad Sci U S A* **2015,** *112* (50), 15408-13.
54. Li, T.; Cheng, H.; Yuan, H.; Xu, Q.; Shu, C.; Zhang, Y.; Xu, P.; Tan, J.; Rui, Y.; Li, P.; Tan, X., Antitumor Activity of cGAMP via Stimulation of cGAS-cGAMP-STING-IRF3 Mediated Innate Immune Response. *Sci Rep* **2016,** *6*, 19049.
55. Prantner, D.; Perkins, D. J.; Lai, W.; Williams, M. S.; Sharma, S.; Fitzgerald, K. A.; Vogel, S. N., 5,6-Dimethylxanthenone-4-acetic acid (DMXAA) activates stimulator of interferon gene (STING)-dependent innate immune pathways and is regulated by mitochondrial membrane potential. *J Biol Chem* **2012,** *287* (47), 39776-88.
56. Woo, S. R.; Fuertes, M. B.; Corrales, L.; Spranger, S.; Furdyna, M. J.; Leung, M. Y.; Duggan, R.; Wang, Y.; Barber, G. N.; Fitzgerald, K. A.; Alegre, M. L.; Gajewski, T. F., STING-dependent cytosolic DNA sensing mediates innate immune recognition of immunogenic tumors. *Immunity* **2014,** *41* (5), 830-42.
57. Yum, S.; Li, M.; Chen, Z. J., Old dogs, new trick: classic cancer therapies activate cGAS. *Cell Res* **2020**.
58. Storozynsky, Q.; Hitt, M. M., The Impact of Radiation-Induced DNA Damage on cGAS-STING-Mediated Immune Responses to Cancer. *Int J Mol Sci* **2020,** *21* (22).
59. Le Naour, J.; Zitvogel, L.; Galluzzi, L.; Vacchelli, E.; Kroemer, G., Trial watch: STING agonists in cancer therapy. *Oncoimmunology* **2020,** *9* (1), 1777624.
60. Su, T.; Zhang, Y.; Valerie, K.; Wang, X. Y.; Lin, S.; Zhu, G., STING activation in cancer immunotherapy. *Theranostics* **2019,** *9* (25), 7759-7771.
61. Wu, J. J.; Zhao, L.; Hu, H. G.; Li, W. H.; Li, Y. M., Agonists and inhibitors of the STING pathway: Potential agents for immunotherapy. *Med Res Rev* **2019**.
62. Dobbs, N.; Burnaevskiy, N.; Chen, D.; Gonugunta, V. K.; Alto, N. M.; Yan, N., STING Activation by Translocation from the ER Is Associated with Infection and Autoinflammatory Disease. *Cell Host Microbe* **2015,** *18* (2), 157-68.
63. Lepelley, A.; Martin-Niclos, M. J.; Le Bihan, M.; Marsh, J. A.; Uggenti, C.; Rice, G. I.; Bondet, V.; Duffy, D.; Hertzog, J.; Rehwinkel, J.; Amselem, S.; Boulisfane-El Khalifi, S.; Brennan, M.; Carter, E.; Chatenoud, L.; Chhun, S.; Coulomb l'Hermine, A.; Depp, M.; Legendre, M.; Mackenzie, K. J.; Marey, J.; McDougall, C.; McKenzie, K. J.; Molina, T. J.; Neven, B.; Seabra, L.; Thumerelle, C.; Wislez, M.; Nathan, N.; Manel, N.; Crow, Y. J.; Fremond, M. L., Mutations in COPA lead to abnormal trafficking of STING to the Golgi and interferon signaling. *J Exp Med* **2020,** *217* (11).
64. Deng, Z.; Chong, Z.; Law, C. S.; Mukai, K.; Ho, F. O.; Martinu, T.; Backes, B. J.; Eckalbar, W. L.; Taguchi, T.; Shum, A. K., A defect in COPI-mediated transport of STING causes immune dysregulation in COPA syndrome. *J Exp Med* **2020,** *217* (11).
65. Mukai, K.; Ogawa, E.; Uematsu, R.; Kuchitsu, Y.; Kiku, F.; Uemura, T.; Waguri, S.; Suzuki, T.; Dohmae, N.; Arai, H.; Shum, A. K.; Taguchi, T., Homeostatic regulation of STING

by retrograde membrane traffic to the ER. *Nat Commun* **2021,** *12* (1), 61.
66. Ishikawa, H.; Barber, G. N., STING is an endoplasmic reticulum adaptor that facilitates innate immune signalling. *Nature* **2008,** *455* (7213), 674-8.
67. Burdette, D. L.; Monroe, K. M.; Sotelo-Troha, K.; Iwig, J. S.; Eckert, B.; Hyodo, M.; Hayakawa, Y.; Vance, R. E., STING is a direct innate immune sensor of cyclic di-GMP. *Nature* **2011,** *478* (7370), 515-8.
68. Sun, L.; Wu, J.; Du, F.; Chen, X.; Chen, Z. J., Cyclic GMP-AMP synthase is a cytosolic DNA sensor that activates the type I interferon pathway. *Science* **2013,** *339* (6121), 786-91.
69. Wu, J.; Sun, L.; Chen, X.; Du, F.; Shi, H.; Chen, C.; Chen, Z. J., Cyclic GMP-AMP is an endogenous second messenger in innate immune signaling by cytosolic DNA. *Science* **2013,** *339* (6121), 826-30.
70. Cai, X.; Chiu, Y. H.; Chen, Z. J., The cGAS-cGAMP-STING pathway of cytosolic DNA sensing and signaling. *Mol Cell* **2014,** *54* (2), 289-96.
71. Cavlar, T.; Ablasser, A.; Hornung, V., Induction of type I IFNs by intracellular DNA-sensing pathways. *Immunol Cell Biol* **2012,** *90* (5), 474-82.
72. Ahn, J.; Ruiz, P.; Barber, G. N., Intrinsic self-DNA triggers inflammatory disease dependent on STING. *J Immunol* **2014,** *193* (9), 4634-42.
73. Ahn, J.; Barber, G. N., Self-DNA, STING-dependent signaling and the origins of autoinflammatory disease. *Curr Opin Immunol* **2014,** *31*, 121-6.
74. Pandey, S.; Kawai, T., Chapter 5 - Host DNA Induced Inflammation and Autoimmune Diseases. In *Biological DNA Sensor*, Ishii, K. J.; Tang, C. K., Eds. Academic Press: Amsterdam, 2014; pp 103-132.
75. Zierhut, C.; Funabiki, H., Regulation and Consequences of cGAS Activation by Self-DNA. *Trends Cell Biol* **2020,** *30* (8), 594-605.
76. Ho, S. S.; Zhang, W. Y.; Tan, N. Y.; Khatoo, M.; Suter, M. A.; Tripathi, S.; Cheung, F. S.; Lim, W. K.; Tan, P. H.; Ngeow, J.; Gasser, S., The DNA Structure-Specific Endonuclease MUS81 Mediates DNA Sensor STING-Dependent Host Rejection of Prostate Cancer Cells. *Immunity* **2016,** *44* (5), 1177-89.
77. Chen, Q.; Boire, A.; Jin, X.; Valiente, M.; Er, E. E.; Lopez-Soto, A.; Jacob, L.; Patwa, R.; Shah, H.; Xu, K.; Cross, J. R.; Massague, J., Carcinoma-astrocyte gap junctions promote brain metastasis by cGAMP transfer. *Nature* **2016,** *533* (7604), 493-498.
78. Vanpouille-Box, C.; Demaria, S.; Formenti, S. C.; Galluzzi, L., Cytosolic DNA Sensing in Organismal Tumor Control. *Cancer Cell* **2018,** *34* (3), 361-378.
79. Bhat, N.; Fitzgerald, K. A., Recognition of cytosolic DNA by cGAS and other STING-dependent sensors. *Eur J Immunol* **2014,** *44* (3), 634-40.
80. Benmerzoug, S.; Rose, S.; Bounab, B.; Gosset, D.; Duneau, L.; Chenuet, P.; Mollet, L.; Le Bert, M.; Lambers, C.; Geleff, S.; Roth, M.; Fauconnier, L.; Sedda, D.; Carvalho, C.; Perche, O.; Laurenceau, D.; Ryffel, B.; Apetoh, L.; Kiziltunc, A.; Uslu, H.; Albez, F. S.; Akgun, M.; Togbe, D.; Quesniaux, V. F. J., STING-dependent sensing of self-DNA drives silica-induced lung inflammation. *Nat Commun* **2018,** *9* (1), 5226.
81. Ma, F.; Li, B.; Liu, S. Y.; Iyer, S. S.; Yu, Y.; Wu, A.; Cheng, G., Positive feedback regulation of type I IFN production by the IFN-inducible DNA sensor cGAS. *J Immunol* **2015,** *194* (4), 1545-54.
82. Civril, F.; Deimling, T.; de Oliveira Mann, C. C.; Ablasser, A.; Moldt, M.; Witte, G.; Hornung, V.; Hopfner, K. P., Structural mechanism of cytosolic DNA sensing by cGAS. *Nature*

2013, *498* (7454), 332-7.
83. Kranzusch, P. J.; Lee, A. S.; Berger, J. M.; Doudna, J. A., Structure of human cGAS reveals a conserved family of second-messenger enzymes in innate immunity. *Cell Rep* **2013,** *3* (5), 1362-8.
84. Li, X.; Shu, C.; Yi, G.; Chaton, C. T.; Shelton, C. L.; Diao, J.; Zuo, X.; Kao, C. C.; Herr, A. B.; Li, P., Cyclic GMP-AMP synthase is activated by double-stranded DNA-induced oligomerization. *Immunity* **2013,** *39* (6), 1019-31.
85. Zhang, X.; Wu, J.; Du, F.; Xu, H.; Sun, L.; Chen, Z.; Brautigam, C. A.; Zhang, X.; Chen, Z. J., The cytosolic DNA sensor cGAS forms an oligomeric complex with DNA and undergoes switch-like conformational changes in the activation loop. *Cell Rep* **2014,** *6* (3), 421-30.
86. Xie, W.; Lama, L.; Adura, C.; Tomita, D.; Glickman, J. F.; Tuschl, T.; Patel, D. J., Human cGAS catalytic domain has an additional DNA-binding interface that enhances enzymatic activity and liquid-phase condensation. *Proc Natl Acad Sci U S A* **2019,** *116* (24), 11946-11955.
87. Gao, P.; Ascano, M.; Wu, Y.; Barchet, W.; Gaffney, B. L.; Zillinger, T.; Serganov, A. A.; Liu, Y.; Jones, R. A.; Hartmann, G.; Tuschl, T.; Patel, D. J., Cyclic [G(2',5')pA(3',5')p] is the metazoan second messenger produced by DNA-activated cyclic GMP-AMP synthase. *Cell* **2013,** *153* (5), 1094-107.
88. Du, M.; Chen, Z. J., DNA-induced liquid phase condensation of cGAS activates innate immune signaling. *Science* **2018,** *361* (6403), 704-709.
89. Zhang, X.; Shi, H.; Wu, J.; Zhang, X.; Sun, L.; Chen, C.; Chen, Z. J., Cyclic GMP-AMP containing mixed phosphodiester linkages is an endogenous high-affinity ligand for STING. *Mol Cell* **2013,** *51* (2), 226-35.
90. Danilchanka, O.; Mekalanos, J. J., Cyclic dinucleotides and the innate immune response. *Cell* **2013,** *154* (5), 962-970.
91. Zhou, W.; Whiteley, A. T.; de Oliveira Mann, C. C.; Morehouse, B. R.; Nowak, R. P.; Fischer, E. S.; Gray, N. S.; Mekalanos, J. J.; Kranzusch, P. J., Structure of the Human cGAS-DNA Complex Reveals Enhanced Control of Immune Surveillance. *Cell* **2018,** *174* (2), 300-311 e11.
92. Karayel, E.; Burckstummer, T.; Bilban, M.; Durnberger, G.; Weitzer, S.; Martinez, J.; Superti-Furga, G., The TLR-independent DNA recognition pathway in murine macrophages: Ligand features and molecular signature. *Eur J Immunol* **2009,** *39* (7), 1929-36.
93. Herzner, A. M.; Hagmann, C. A.; Goldeck, M.; Wolter, S.; Kubler, K.; Wittmann, S.; Gramberg, T.; Andreeva, L.; Hopfner, K. P.; Mertens, C.; Zillinger, T.; Jin, T.; Xiao, T. S.; Bartok, E.; Coch, C.; Ackermann, D.; Hornung, V.; Ludwig, J.; Barchet, W.; Hartmann, G.; Schlee, M., Sequence-specific activation of the DNA sensor cGAS by Y-form DNA structures as found in primary HIV-1 cDNA. *Nat Immunol* **2015,** *16* (10), 1025-33.
94. Zhou, W.; Mohr, L.; Maciejowski, J.; Kranzusch, P. J., cGAS phase separation inhibits TREX1-mediated DNA degradation and enhances cytosolic DNA sensing. *Mol Cell* **2021,** *81* (4), 739-755 e7.
95. Hooy, R. M.; Massaccesi, G.; Rousseau, K. E.; Chattergoon, M. A.; Sohn, J., Allosteric coupling between Mn2+ and dsDNA controls the catalytic efficiency and fidelity of cGAS. *Nucleic Acids Res* **2020,** *48* (8), 4435-4447.
96. Andreeva, L.; Hiller, B.; Kostrewa, D.; Lassig, C.; de Oliveira Mann, C. C.; Jan Drexler, D.; Maiser, A.; Gaidt, M.; Leonhardt, H.; Hornung, V.; Hopfner, K. P., cGAS senses

long and HMGB/TFAM-bound U-turn DNA by forming protein-DNA ladders. *Nature* **2017,** *549* (7672), 394-398.
97. Lugrin, J.; Martinon, F., The AIM2 inflammasome: Sensor of pathogens and cellular perturbations. *Immunol Rev* **2018,** *281* (1), 99-114.
98. Hornung, V.; Ablasser, A.; Charrel-Dennis, M.; Bauernfeind, F.; Horvath, G.; Caffrey, D. R.; Latz, E.; Fitzgerald, K. A., AIM2 recognizes cytosolic dsDNA and forms a caspase-1-activating inflammasome with ASC. *Nature* **2009,** *458* (7237), 514-8.
99. Corrales, L.; Woo, S. R.; Williams, J. B.; McWhirter, S. M.; Dubensky, T. W., Jr.; Gajewski, T. F., Antagonism of the STING Pathway via Activation of the AIM2 Inflammasome by Intracellular DNA. *J Immunol* **2016,** *196* (7), 3191-8.
100. Liu, C.; Yue, R.; Yang, Y.; Cui, Y.; Yang, L.; Zhao, D.; Zhou, X., AIM2 inhibits autophagy and IFN-beta production during M. bovis infection. *Oncotarget* **2016,** *7* (30), 46972-46987.
101. Yan, S.; Shen, H.; Lian, Q.; Jin, W.; Zhang, R.; Lin, X.; Gu, W.; Sun, X.; Meng, G.; Tian, Z.; Chen, Z. W.; Sun, B., Deficiency of the AIM2-ASC Signal Uncovers the STING-Driven Overreactive Response of Type I IFN and Reciprocal Depression of Protective IFN-gamma Immunity in Mycobacterial Infection. *J Immunol* **2018,** *200* (3), 1016-1026.
102. Nakaya, Y.; Lilue, J.; Stavrou, S.; Moran, E. A.; Ross, S. R., AIM2-Like Receptors Positively and Negatively Regulate the Interferon Response Induced by Cytosolic DNA. *mBio* **2017,** *8* (4).
103. Banerjee, I.; Behl, B.; Mendonca, M.; Shrivastava, G.; Russo, A. J.; Menoret, A.; Ghosh, A.; Vella, A. T.; Vanaja, S. K.; Sarkar, S. N.; Fitzgerald, K. A.; Rathinam, V. A. K., Gasdermin D Restrains Type I Interferon Response to Cytosolic DNA by Disrupting Ionic Homeostasis. *Immunity* **2018,** *49* (3), 413-426 e5.
104. Cridland, J. A.; Curley, E. Z.; Wykes, M. N.; Schroder, K.; Sweet, M. J.; Roberts, T. L.; Ragan, M. A.; Kassahn, K. S.; Stacey, K. J., The mammalian PYHIN gene family: phylogeny, evolution and expression. *BMC Evol Biol* **2012,** *12*, 140.
105. Gaidt, M. M.; Ebert, T. S.; Chauhan, D.; Ramshorn, K.; Pinci, F.; Zuber, S.; O'Duill, F.; Schmid-Burgk, J. L.; Hoss, F.; Buhmann, R.; Wittmann, G.; Latz, E.; Subklewe, M.; Hornung, V., The DNA Inflammasome in Human Myeloid Cells Is Initiated by a STING-Cell Death Program Upstream of NLRP3. *Cell* **2017,** *171* (5), 1110-1124 e18.
106. Jin, T.; Perry, A.; Jiang, J.; Smith, P.; Curry, J. A.; Unterholzner, L.; Jiang, Z.; Horvath, G.; Rathinam, V. A.; Johnstone, R. W.; Hornung, V.; Latz, E.; Bowie, A. G.; Fitzgerald, K. A.; Xiao, T. S., Structures of the HIN domain:DNA complexes reveal ligand binding and activation mechanisms of the AIM2 inflammasome and IFI16 receptor. *Immunity* **2012,** *36* (4), 561-71.
107. Li, H.; Wang, J.; Wang, J.; Cao, L. S.; Wang, Z. X.; Wu, J. W., Structural mechanism of DNA recognition by the p202 HINa domain: insights into the inhibition of Aim2-mediated inflammatory signalling. *Acta Crystallogr F Struct Biol Commun* **2014,** *70* (Pt 1), 21-9.
108. Emming, S.; Schroder, K., Tiered DNA sensors for escalating responses. *Science* **2019,** *365* (6460), 1375-1376.
109. Muruve, D. A.; Petrilli, V.; Zaiss, A. K.; White, L. R.; Clark, S. A.; Ross, P. J.; Parks, R. J.; Tschopp, J., The inflammasome recognizes cytosolic microbial and host DNA and triggers an innate immune response. *Nature* **2008,** *452* (7183), 103-7.
110. Morrone, S. R.; Matyszewski, M.; Yu, X.; Delannoy, M.; Egelman, E. H.; Sohn, J., Assembly-driven activation of the AIM2 foreign-dsDNA sensor provides a polymerization

template for downstream ASC. *Nat Commun* **2015,** *6*, 7827.
111. Morrone, S. R.; Wang, T.; Constantoulakis, L. M.; Hooy, R. M.; Delannoy, M. J.; Sohn, J., Cooperative assembly of IFI16 filaments on dsDNA provides insights into host defense strategy. *Proc Natl Acad Sci U S A* **2014,** *111* (1), E62-71.
112. Matyszewski, M.; Morrone, S. R.; Sohn, J., Digital signaling network drives the assembly of the AIM2-ASC inflammasome. *Proc Natl Acad Sci U S A* **2018,** *115* (9), E1963-E1972.
113. Liu, T.; Yamaguchi, Y.; Shirasaki, Y.; Shikada, K.; Yamagishi, M.; Hoshino, K.; Kaisho, T.; Takemoto, K.; Suzuki, T.; Kuranaga, E.; Ohara, O.; Miura, M., Single-cell imaging of caspase-1 dynamics reveals an all-or-none inflammasome signaling response. *Cell Rep* **2014,** *8* (4), 974-82.
114. Roberts, T. L.; Idris, A.; Dunn, J. A.; Kelly, G. M.; Burnton, C. M.; Hodgson, S.; Hardy, L. L.; Garceau, V.; Sweet, M. J.; Ross, I. L.; Hume, D. A.; Stacey, K. J., HIN-200 proteins regulate caspase activation in response to foreign cytoplasmic DNA. *Science* **2009,** *323* (5917), 1057-60.
115. Gulen, M. F.; Koch, U.; Haag, S. M.; Schuler, F.; Apetoh, L.; Villunger, A.; Radtke, F.; Ablasser, A., Signalling strength determines proapoptotic functions of STING. *Nat Commun* **2017,** *8* (1), 427.
116. Aliru, M. L.; Schoenhals, J. E.; Venkatesulu, B. P.; Anderson, C. C.; Barsoumian, H. B.; Younes, A. I.; LS, K. M.; Soeung, M.; Aziz, K. E.; Welsh, J. W.; Krishnan, S., Radiation therapy and immunotherapy: what is the optimal timing or sequencing? *Immunotherapy* **2018,** *10* (4), 299-316.
117. Liu, S.; Guan, W., STING Signaling Promotes Apoptosis, Necrosis, and Cell Death: An Overview and Update. *Mediators Inflamm* **2018,** *2018*, 1202797.
118. Sokolowska, O.; Nowis, D., STING Signaling in Cancer Cells: Important or Not? *Arch Immunol Ther Exp (Warsz)* **2018,** *66* (2), 125-132.
119. Hu, Q.; Wu, J.; Ren, Y.; Wu, X.; Gao, L.; Wang, G.; Gu, G.; Ren, H.; Hong, Z.; Slade, D. A.; Ren, J., Degree of STING activation is associated with disease outcomes. *Gut* **2020,** *69* (4), 792-794.
120. Roers, A.; Hiller, B.; Hornung, V., Recognition of Endogenous Nucleic Acids by the Innate Immune System. *Immunity* **2016,** *44* (4), 739-54.
121. Miyake, K.; Shibata, T.; Ohto, U.; Shimizu, T., Emerging roles of the processing of nucleic acids and Toll-like receptors in innate immune responses to nucleic acids. *J Leukoc Biol* **2017,** *101* (1), 135-142.
122. Gao, D.; Li, T.; Li, X. D.; Chen, X.; Li, Q. Z.; Wight-Carter, M.; Chen, Z. J., Activation of cyclic GMP-AMP synthase by self-DNA causes autoimmune diseases. *Proc Natl Acad Sci U S A* **2015,** *112* (42), E5699-705.
123. Baranovskii, A. G.; Buneva, V. N.; Nevinsky, G. A., Human deoxyribonucleases. *Biochemistry (Mosc)* **2004,** *69* (6), 587-601.
124. Benmerzoug, S.; Ryffel, B.; Togbe, D.; Quesniaux, V. F. J., Self-DNA Sensing in Lung Inflammatory Diseases. *Trends Immunol* **2019,** *40* (8), 719-734.
125. Wang, Q.; Liu, X.; Zhou, Q.; Wang, C., Cytosolic sensing of aberrant DNA: arming STING on the endoplasmic reticulum. *Expert Opin Ther Targets* **2015,** *19* (10), 1397-409.
126. Stetson, D. B.; Ko, J. S.; Heidmann, T.; Medzhitov, R., Trex1 prevents cell-intrinsic initiation of autoimmunity. *Cell* **2008,** *134* (4), 587-98.
127. Gray, E. E.; Treuting, P. M.; Woodward, J. J.; Stetson, D. B., Cutting Edge: cGAS Is

Required for Lethal Autoimmune Disease in the Trex1-Deficient Mouse Model of Aicardi-Goutieres Syndrome. *J Immunol* **2015,** *195* (5), 1939-43.
128. Ablasser, A.; Hemmerling, I.; Schmid-Burgk, J. L.; Behrendt, R.; Roers, A.; Hornung, V., TREX1 deficiency triggers cell-autonomous immunity in a cGAS-dependent manner. *J Immunol* **2014,** *192* (12), 5993-7.
129. Orebaugh, C. D.; Fye, J. M.; Harvey, S.; Hollis, T.; Perrino, F. W., The TREX1 exonuclease R114H mutation in Aicardi-Goutieres syndrome and lupus reveals dimeric structure requirements for DNA degradation activity. *J Biol Chem* **2011,** *286* (46), 40246-54.
130. Xu, J.; Zoltick, P. W.; Gamero, A. M.; Gallucci, S., TLR ligands up-regulate Trex1 expression in murine conventional dendritic cells through type I Interferon and NF-kappaB-dependent signaling pathways. *J Leukoc Biol* **2014,** *96* (1), 93-103.
131. Vanpouille-Box, C.; Alard, A.; Aryankalayil, M. J.; Sarfraz, Y.; Diamond, J. M.; Schneider, R. J.; Inghirami, G.; Coleman, C. N.; Formenti, S. C.; Demaria, S., DNA exonuclease Trex1 regulates radiotherapy-induced tumour immunogenicity. *Nat Commun* **2017,** *8*, 15618.
132. Diamond, J. M.; Vanpouille-Box, C.; Spada, S.; Rudqvist, N. P.; Chapman, J. R.; Ueberheide, B. M.; Pilones, K. A.; Sarfraz, Y.; Formenti, S. C.; Demaria, S., Exosomes Shuttle TREX1-Sensitive IFN-Stimulatory dsDNA from Irradiated Cancer Cells to DCs. *Cancer Immunol Res* **2018,** *6* (8), 910-920.
133. Azzam, E. I.; Jay-Gerin, J. P.; Pain, D., Ionizing radiation-induced metabolic oxidative stress and prolonged cell injury. *Cancer Lett* **2012,** *327* (1-2), 48-60.
134. Yoshida, T.; Goto, S.; Kawakatsu, M.; Urata, Y.; Li, T. S., Mitochondrial dysfunction, a probable cause of persistent oxidative stress after exposure to ionizing radiation. *Free Radic Res* **2012,** *46* (2), 147-53.
135. Gehrke, N.; Mertens, C.; Zillinger, T.; Wenzel, J.; Bald, T.; Zahn, S.; Tuting, T.; Hartmann, G.; Barchet, W., Oxidative damage of DNA confers resistance to cytosolic nuclease TREX1 degradation and potentiates STING-dependent immune sensing. *Immunity* **2013,** *39* (3), 482-95.
136. Fang, C.; Mo, F.; Liu, L.; Du, J.; Luo, M.; Men, K.; Na, F.; Wang, W.; Yang, H.; Wei, X., Oxidized mitochondrial DNA sensing by STING signaling promotes the antitumor effect of an irradiated immunogenic cancer cell vaccine. *Cell Mol Immunol* **2020**.
137. Huang, K. W.; Liu, T. C.; Liang, R. Y.; Chu, L. Y.; Cheng, H. L.; Chu, J. W.; Hsiao, Y. Y., Structural basis for overhang excision and terminal unwinding of DNA duplexes by TREX1. *PLoS Biol* **2018,** *16* (5), e2005653.
138. Dai, J.; Huang, Y. J.; He, X.; Zhao, M.; Wang, X.; Liu, Z. S.; Xue, W.; Cai, H.; Zhan, X. Y.; Huang, S. Y.; He, K.; Wang, H.; Wang, N.; Sang, Z.; Li, T.; Han, Q. Y.; Mao, J.; Diao, X.; Song, N.; Chen, Y.; Li, W. H.; Man, J. H.; Li, A. L.; Zhou, T.; Liu, Z. G.; Zhang, X. M.; Li, T., Acetylation Blocks cGAS Activity and Inhibits Self-DNA-Induced Autoimmunity. *Cell* **2019,** *176* (6), 1447-1460 e14.
139. Xia, P.; Ye, B.; Wang, S.; Zhu, X.; Du, Y.; Xiong, Z.; Tian, Y.; Fan, Z., Glutamylation of the DNA sensor cGAS regulates its binding and synthase activity in antiviral immunity. *Nat Immunol* **2016,** *17* (4), 369-78.
140. Seo, G. J.; Yang, A.; Tan, B.; Kim, S.; Liang, Q.; Choi, Y.; Yuan, W.; Feng, P.; Park, H. S.; Jung, J. U., Akt Kinase-Mediated Checkpoint of cGAS DNA Sensing Pathway. *Cell Rep* **2015,** *13* (2), 440-9.
141. Hu, M. M.; Yang, Q.; Xie, X. Q.; Liao, C. Y.; Lin, H.; Liu, T. T.; Yin, L.; Shu, H. B.,

Sumoylation Promotes the Stability of the DNA Sensor cGAS and the Adaptor STING to Regulate the Kinetics of Response to DNA Virus. *Immunity* **2016,** *45* (3), 555-569.
142. Wang, Q.; Huang, L.; Hong, Z.; Lv, Z.; Mao, Z.; Tang, Y.; Kong, X.; Li, S.; Cui, Y.; Liu, H.; Zhang, L.; Zhang, X.; Jiang, L.; Wang, C.; Zhou, Q., The E3 ubiquitin ligase RNF185 facilitates the cGAS-mediated innate immune response. *PLoS Pathog* **2017,** *13* (3), e1006264.
143. Chen, X.; Chen, Y., Ubiquitination of cGAS by TRAF6 regulates anti-DNA viral innate immune responses. *Biochem Biophys Res Commun* **2019,** *514* (3), 659-664.
144. Gekara, N. O.; Jiang, H., The innate immune DNA sensor cGAS: A membrane, cytosolic, or nuclear protein? *Sci Signal* **2019,** *12* (581).
145. Barnett, K. C.; Coronas-Serna, J. M.; Zhou, W.; Ernandes, M. J.; Cao, A.; Kranzusch, P. J.; Kagan, J. C., Phosphoinositide Interactions Position cGAS at the Plasma Membrane to Ensure Efficient Distinction between Self- and Viral DNA. *Cell* **2019,** *176* (6), 1432-1446 e11.
146. Xia, P.; Wang, S.; Ye, B.; Du, Y.; Li, C.; Xiong, Z.; Qu, Y.; Fan, Z., A Circular RNA Protects Dormant Hematopoietic Stem Cells from DNA Sensor cGAS-Mediated Exhaustion. *Immunity* **2018,** *48* (4), 688-701 e7.
147. Yang, H.; Wang, H.; Ren, J.; Chen, Q.; Chen, Z. J., cGAS is essential for cellular senescence. *Proc Natl Acad Sci U S A* **2017,** *114* (23), E4612-E4620.
148. Orzalli, M. H.; Broekema, N. M.; Diner, B. A.; Hancks, D. C.; Elde, N. C.; Cristea, I. M.; Knipe, D. M., cGAS-mediated stabilization of IFI16 promotes innate signaling during herpes simplex virus infection. *Proc Natl Acad Sci U S A* **2015,** *112* (14), E1773-81.
149. Liu, H.; Zhang, H.; Wu, X.; Ma, D.; Wu, J.; Wang, L.; Jiang, Y.; Fei, Y.; Zhu, C.; Tan, R.; Jungblut, P.; Pei, G.; Dorhoi, A.; Yan, Q.; Zhang, F.; Zheng, R.; Liu, S.; Liang, H.; Liu, Z.; Yang, H.; Chen, J.; Wang, P.; Tang, T.; Peng, W.; Hu, Z.; Xu, Z.; Huang, X.; Wang, J.; Li, H.; Zhou, Y.; Liu, F.; Yan, D.; Kaufmann, S. H. E.; Chen, C.; Mao, Z.; Ge, B., Nuclear cGAS suppresses DNA repair and promotes tumorigenesis. *Nature* **2018,** *563* (7729), 131-136.
150. Jiang, H.; Xue, X.; Panda, S.; Kawale, A.; Hooy, R. M.; Liang, F.; Sohn, J.; Sung, P.; Gekara, N. O., Chromatin-bound cGAS is an inhibitor of DNA repair and hence accelerates genome destabilization and cell death. *EMBO J* **2019,** *38* (21), e102718.
151. Gentili, M.; Lahaye, X.; Nadalin, F.; Nader, G. P. F.; Puig Lombardi, E.; Herve, S.; De Silva, N. S.; Rookhuizen, D. C.; Zueva, E.; Goudot, C.; Maurin, M.; Bochnakian, A.; Amigorena, S.; Piel, M.; Fachinetti, D.; Londono-Vallejo, A.; Manel, N., The N-Terminal Domain of cGAS Determines Preferential Association with Centromeric DNA and Innate Immune Activation in the Nucleus. *Cell Rep* **2019,** *26* (9), 2377-2393 e13.
152. Volkman, H. E.; Cambier, S.; Gray, E. E.; Stetson, D. B., Tight nuclear tethering of cGAS is essential for preventing autoreactivity. *Elife* **2019,** *8*.
153. Guey, B.; Wischnewski, M.; Decout, A.; Makasheva, K.; Kaynak, M.; Sakar, M. S.; Fierz, B.; Ablasser, A., BAF restricts cGAS on nuclear DNA to prevent innate immune activation. *Science* **2020,** *369* (6505), 823-828.
154. Li, T.; Huang, T.; Du, M.; Chen, X.; Du, F.; Ren, J.; Chen, Z. J., Phosphorylation and chromatin tethering prevent cGAS activation during mitosis. *Science* **2021,** *371* (6535).
155. Zierhut, C.; Yamaguchi, N.; Paredes, M.; Luo, J. D.; Carroll, T.; Funabiki, H., The Cytoplasmic DNA Sensor cGAS Promotes Mitotic Cell Death. *Cell* **2019,** *178* (2), 302-315 e23.
156. Shang, G.; Zhu, D.; Li, N.; Zhang, J.; Zhu, C.; Lu, D.; Liu, C.; Yu, Q.; Zhao, Y.; Xu, S.; Gu, L., Crystal structures of STING protein reveal basis for recognition of cyclic di-GMP. *Nat Struct Mol Biol* **2012,** *19* (7), 725-7.

157. Shang, G.; Zhang, C.; Chen, Z. J.; Bai, X. C.; Zhang, X., Cryo-EM structures of STING reveal its mechanism of activation by cyclic GMP-AMP. *Nature* **2019,** *567* (7748), 389-393.
158. Huang, Y. H.; Liu, X. Y.; Du, X. X.; Jiang, Z. F.; Su, X. D., The structural basis for the sensing and binding of cyclic di-GMP by STING. *Nat Struct Mol Biol* **2012,** *19* (7), 728-30.
159. Yin, Q.; Tian, Y.; Kabaleeswaran, V.; Jiang, X.; Tu, D.; Eck, M. J.; Chen, Z. J.; Wu, H., Cyclic di-GMP sensing via the innate immune signaling protein STING. *Mol Cell* **2012,** *46* (6), 735-45.
160. Ramanjulu, J. M.; Pesiridis, G. S.; Yang, J.; Concha, N.; Singhaus, R.; Zhang, S. Y.; Tran, J. L.; Moore, P.; Lehmann, S.; Eberl, H. C.; Muelbaier, M.; Schneck, J. L.; Clemens, J.; Adam, M.; Mehlmann, J.; Romano, J.; Morales, A.; Kang, J.; Leister, L.; Graybill, T. L.; Charnley, A. K.; Ye, G.; Nevins, N.; Behnia, K.; Wolf, A. I.; Kasparcova, V.; Nurse, K.; Wang, L.; Puhl, A. C.; Li, Y.; Klein, M.; Hopson, C. B.; Guss, J.; Bantscheff, M.; Bergamini, G.; Reilly, M. A.; Lian, Y.; Duffy, K. J.; Adams, J.; Foley, K. P.; Gough, P. J.; Marquis, R. W.; Smothers, J.; Hoos, A.; Bertin, J., Design of amidobenzimidazole STING receptor agonists with systemic activity. *Nature* **2018,** *564* (7736), 439-443.
161. Ergun, S. L.; Fernandez, D.; Weiss, T. M.; Li, L., STING Polymer Structure Reveals Mechanisms for Activation, Hyperactivation, and Inhibition. *Cell* **2019,** *178* (2), 290-301 e10.
162. Ni, G.; Konno, H.; Barber, G. N., Ubiquitination of STING at lysine 224 controls IRF3 activation. *Sci Immunol* **2017,** *2* (11).
163. Mukai, K.; Konno, H.; Akiba, T.; Uemura, T.; Waguri, S.; Kobayashi, T.; Barber, G. N.; Arai, H.; Taguchi, T., Activation of STING requires palmitoylation at the Golgi. *Nat Commun* **2016,** *7*, 11932.
164. Ishikawa, H.; Ma, Z.; Barber, G. N., STING regulates intracellular DNA-mediated, type I interferon-dependent innate immunity. *Nature* **2009,** *461* (7265), 788-92.
165. Saitoh, T.; Fujita, N.; Hayashi, T.; Takahara, K.; Satoh, T.; Lee, H.; Matsunaga, K.; Kageyama, S.; Omori, H.; Noda, T.; Yamamoto, N.; Kawai, T.; Ishii, K.; Takeuchi, O.; Yoshimori, T.; Akira, S., Atg9a controls dsDNA-driven dynamic translocation of STING and the innate immune response. *Proc Natl Acad Sci U S A* **2009,** *106* (49), 20842-6.
166. Luo, W. W.; Li, S.; Li, C.; Lian, H.; Yang, Q.; Zhong, B.; Shu, H. B., iRhom2 is essential for innate immunity to DNA viruses by mediating trafficking and stability of the adaptor STING. *Nat Immunol* **2016,** *17* (9), 1057-66.
167. Liu, S.; Cai, X.; Wu, J.; Cong, Q.; Chen, X.; Li, T.; Du, F.; Ren, J.; Wu, Y. T.; Grishin, N. V.; Chen, Z. J., Phosphorylation of innate immune adaptor proteins MAVS, STING, and TRIF induces IRF3 activation. *Science* **2015,** *347* (6227), aaa2630.
168. Ogawa, E.; Mukai, K.; Saito, K.; Arai, H.; Taguchi, T., The binding of TBK1 to STING requires exocytic membrane traffic from the ER. *Biochem Biophys Res Commun* **2018,** *503* (1), 138-145.
169. Yum, S.; Li, M.; Fang, Y.; Chen, Z. J., TBK1 recruitment to STING activates both IRF3 and NF-kappaB that mediate immune defense against tumors and viral infections. *Proc Natl Acad Sci U S A* **2021,** *118* (14).
170. Tanaka, Y.; Chen, Z. J., STING specifies IRF3 phosphorylation by TBK1 in the cytosolic DNA signaling pathway. *Sci Signal* **2012,** *5* (214), ra20.
171. Abe, T.; Harashima, A.; Xia, T.; Konno, H.; Konno, K.; Morales, A.; Ahn, J.; Gutman, D.; Barber, G. N., STING recognition of cytoplasmic DNA instigates cellular defense. *Mol Cell* **2013,** *50* (1), 5-15.
172. Stetson, D. B.; Medzhitov, R., Recognition of cytosolic DNA activates an IRF3-

dependent innate immune response. *Immunity* **2006,** *24* (1), 93-103.
173. Chin, E. N.; Yu, C.; Vartabedian, V. F.; Jia, Y.; Kumar, M.; Gamo, A. M.; Vernier, W.; Ali, S. H.; Kissai, M.; Lazar, D. C.; Nguyen, N.; Pereira, L. E.; Benish, B.; Woods, A. K.; Joseph, S. B.; Chu, A.; Johnson, K. A.; Sander, P. N.; Martinez-Pena, F.; Hampton, E. N.; Young, T. S.; Wolan, D. W.; Chatterjee, A. K.; Schultz, P. G.; Petrassi, H. M.; Teijaro, J. R.; Lairson, L. L., Antitumor activity of a systemic STING-activating non-nucleotide cGAMP mimetic. *Science* **2020,** *369* (6506), 993-999.
174. Yu, X.; Zhang, L.; Shen, J.; Zhai, Y.; Jiang, Q.; Yi, M.; Deng, X.; Ruan, Z.; Fang, R.; Chen, Z.; Ning, X.; Jiang, Z., The STING phase-separator suppresses innate immune signalling. *Nat Cell Biol* **2021,** *23* (4), 330-340.
175. Xiao, Q.; McAtee, C. K.; Su, X., Phase separation in immune signalling. *Nat Rev Immunol* **2021**.
176. Peran, I.; Mittag, T., Molecular structure in biomolecular condensates. *Curr Opin Struct Biol* **2020,** *60*, 17-26.
177. Kato, M.; Han, T. W.; Xie, S.; Shi, K.; Du, X.; Wu, L. C.; Mirzaei, H.; Goldsmith, E. J.; Longgood, J.; Pei, J.; Grishin, N. V.; Frantz, D. E.; Schneider, J. W.; Chen, S.; Li, L.; Sawaya, M. R.; Eisenberg, D.; Tycko, R.; McKnight, S. L., Cell-free formation of RNA granules: low complexity sequence domains form dynamic fibers within hydrogels. *Cell* **2012,** *149* (4), 753-67.
178. Balka, K. R.; Louis, C.; Saunders, T. L.; Smith, A. M.; Calleja, D. J.; D'Silva, D. B.; Moghaddas, F.; Tailler, M.; Lawlor, K. E.; Zhan, Y.; Burns, C. J.; Wicks, I. P.; Miner, J. J.; Kile, B. T.; Masters, S. L.; De Nardo, D., TBK1 and IKKepsilon Act Redundantly to Mediate STING-Induced NF-kappaB Responses in Myeloid Cells. *Cell Rep* **2020,** *31* (1), 107492.
179. Abe, T.; Barber, G. N., Cytosolic-DNA-mediated, STING-dependent proinflammatory gene induction necessitates canonical NF-kappaB activation through TBK1. *J Virol* **2014,** *88* (10), 5328-41.
180. Bakhoum, S. F.; Ngo, B.; Laughney, A. M.; Cavallo, J. A.; Murphy, C. J.; Ly, P.; Shah, P.; Sriram, R. K.; Watkins, T. B. K.; Taunk, N. K.; Duran, M.; Pauli, C.; Shaw, C.; Chadalavada, K.; Rajasekhar, V. K.; Genovese, G.; Venkatesan, S.; Birkbak, N. J.; McGranahan, N.; Lundquist, M.; LaPlant, Q.; Healey, J. H.; Elemento, O.; Chung, C. H.; Lee, N. Y.; Imielenski, M.; Nanjangud, G.; Pe'er, D.; Cleveland, D. W.; Powell, S. N.; Lammerding, J.; Swanton, C.; Cantley, L. C., Chromosomal instability drives metastasis through a cytosolic DNA response. *Nature* **2018,** *553* (7689), 467-472.
181. McWhirter, S. M.; Barbalat, R.; Monroe, K. M.; Fontana, M. F.; Hyodo, M.; Joncker, N. T.; Ishii, K. J.; Akira, S.; Colonna, M.; Chen, Z. J.; Fitzgerald, K. A.; Hayakawa, Y.; Vance, R. E., A host type I interferon response is induced by cytosolic sensing of the bacterial second messenger cyclic-di-GMP. *J Exp Med* **2009,** *206* (9), 1899-911.
182. Chen, H.; Sun, H.; You, F.; Sun, W.; Zhou, X.; Chen, L.; Yang, J.; Wang, Y.; Tang, H.; Guan, Y.; Xia, W.; Gu, J.; Ishikawa, H.; Gutman, D.; Barber, G.; Qin, Z.; Jiang, Z., Activation of STAT6 by STING is critical for antiviral innate immunity. *Cell* **2011,** *147* (2), 436-46.
183. Flood, B. A.; Higgs, E. F.; Li, S.; Luke, J. J.; Gajewski, T. F., STING pathway agonism as a cancer therapeutic. *Immunol Rev* **2019,** *290* (1), 24-38.
184. Thanos, D.; Maniatis, T., Virus induction of human IFN beta gene expression requires the assembly of an enhanceosome. *Cell* **1995,** *83* (7), 1091-100.
185. Maniatis, T.; Falvo, J. V.; Kim, T. H.; Kim, T. K.; Lin, C. H.; Parekh, B. S.; Wathelet,

M. G., Structure and function of the interferon-beta enhanceosome. *Cold Spring Harb Symp Quant Biol* **1998,** *63*, 609-20.
186. Panne, D.; Maniatis, T.; Harrison, S. C., An atomic model of the interferon-beta enhanceosome. *Cell* **2007,** *129* (6), 1111-23.
187. Smale, S. T., Selective transcription in response to an inflammatory stimulus. *Cell* **2010,** *140* (6), 833-44.
188. Diner, E. J.; Burdette, D. L.; Wilson, S. C.; Monroe, K. M.; Kellenberger, C. A.; Hyodo, M.; Hayakawa, Y.; Hammond, M. C.; Vance, R. E., The innate immune DNA sensor cGAS produces a noncanonical cyclic dinucleotide that activates human STING. *Cell Rep* **2013,** *3* (5), 1355-61.
189. Yi, G.; Brendel, V. P.; Shu, C.; Li, P.; Palanathan, S.; Cheng Kao, C., Single nucleotide polymorphisms of human STING can affect innate immune response to cyclic dinucleotides. *PLoS One* **2013,** *8* (10), e77846.
190. Jin, L.; Xu, L. G.; Yang, I. V.; Davidson, E. J.; Schwartz, D. A.; Wurfel, M. M.; Cambier, J. C., Identification and characterization of a loss-of-function human MPYS variant. *Genes Immun* **2011,** *12* (4), 263-9.
191. Patel, S.; Jin, L., TMEM173 variants and potential importance to human biology and disease. *Genes Immun* **2019,** *20* (1), 82-89.
192. Li, S.; Luo, M.; Wang, Z.; Feng, Q.; Wilhelm, J.; Wang, X.; Li, W.; Wang, J.; Cholka, A.; Fu, Y. X.; Sumer, B. D.; Yu, H.; Gao, J., Prolonged activation of innate immune pathways by a polyvalent STING agonist. *Nat Biomed Eng* **2021**.
193. Shih, A. Y.; Damm-Ganamet, K. L.; Mirzadegan, T., Dynamic Structural Differences between Human and Mouse STING Lead to Differing Sensitivity to DMXAA. *Biophys J* **2018,** *114* (1), 32-39.
194. Carozza, J. A.; Böhnert, V.; Nguyen, K. C.; Skariah, G.; Shaw, K. E.; Brown, J. A.; Rafat, M.; von Eyben, R.; Graves, E. E.; Glenn, J. S.; Smith, M.; Li, L., Extracellular cGAMP is a cancer-cell-produced immunotransmitter involved in radiation-induced anticancer immunity. *Nature Cancer* **2020,** *1* (2), 184-196.
195. Ritchie, C.; Cordova, A. F.; Hess, G. T.; Bassik, M. C.; Li, L., SLC19A1 Is an Importer of the Immunotransmitter cGAMP. *Mol Cell* **2019,** *75* (2), 372-381 e5.
196. Zhou, C.; Chen, X.; Planells-Cases, R.; Chu, J.; Wang, L.; Cao, L.; Li, Z.; Lopez-Cayuqueo, K. I.; Xie, Y.; Ye, S.; Wang, X.; Ullrich, F.; Ma, S.; Fang, Y.; Zhang, X.; Qian, Z.; Liang, X.; Cai, S. Q.; Jiang, Z.; Zhou, D.; Leng, Q.; Xiao, T. S.; Lan, K.; Yang, J.; Li, H.; Peng, C.; Qiu, Z.; Jentsch, T. J.; Xiao, H., Transfer of cGAMP into Bystander Cells via LRRC8 Volume-Regulated Anion Channels Augments STING-Mediated Interferon Responses and Anti-viral Immunity. *Immunity* **2020**.
197. Lahey, L. J.; Wen, X.; Mardjuki, R. E.; Böhnert, V.; Hess, G. T.; Ritchie, C.; Carozza, J. A.; Maduke, M.; Bassik, M. C.; Li, L., The LRRC8A:C Heteromeric Channel Is a cGAMP Transporter and the Dominant cGAMP Importer in Human Vasculature Cells. *bioRxiv* **2020**, 2020.02.13.948273.
198. Ablasser, A.; Schmid-Burgk, J. L.; Hemmerling, I.; Horvath, G. L.; Schmidt, T.; Latz, E.; Hornung, V., Cell intrinsic immunity spreads to bystander cells via the intercellular transfer of cGAMP. *Nature* **2013,** *503* (7477), 530-4.
199. Schadt, L.; Sparano, C.; Schweiger, N. A.; Silina, K.; Cecconi, V.; Lucchiari, G.; Yagita, H.; Guggisberg, E.; Saba, S.; Nascakova, Z.; Barchet, W.; van den Broek, M., Cancer-Cell-Intrinsic cGAS Expression Mediates Tumor Immunogenicity. *Cell Rep* **2019,** *29* (5), 1236-

1248 e7.
200. Pepin, G.; De Nardo, D.; Rootes, C. L.; Ullah, T. R.; Al-Asmari, S. S.; Balka, K. R.; Li, H. M.; Quinn, K. M.; Moghaddas, F.; Chappaz, S.; Kile, B. T.; Morand, E. F.; Masters, S. L.; Stewart, C. R.; Williams, B. R. G.; Gantier, M. P., Connexin-Dependent Transfer of cGAMP to Phagocytes Modulates Antiviral Responses. *mBio* **2020,** *11* (1).
201. Wang, J.; Li, P.; Yu, Y.; Fu, Y.; Jiang, H.; Lu, M.; Sun, Z.; Jiang, S.; Lu, L.; Wu, M. X., Pulmonary surfactant-biomimetic nanoparticles potentiate heterosubtypic influenza immunity. *Science* **2020,** *367* (6480).
202. Luther, J.; Khan, S.; Gala, M. K.; Kedrin, D.; Sridharan, G.; Goodman, R. P.; Garber, J. J.; Masia, R.; Diagacomo, E.; Adams, D.; King, K. R.; Piaker, S.; Reinecker, H. C.; Yarmush, M. L.; Argemi, J.; Bataller, R.; Dienstag, J. L.; Chung, R. T.; Patel, S. J., Hepatic gap junctions amplify alcohol liver injury by propagating cGAS-mediated IRF3 activation. *Proc Natl Acad Sci U S A* **2020**.
203. Xu, S.; Ducroux, A.; Ponnurangam, A.; Vieyres, G.; Franz, S.; Musken, M.; Zillinger, T.; Malassa, A.; Ewald, E.; Hornung, V.; Barchet, W.; Haussler, S.; Pietschmann, T.; Goffinet, C., cGAS-Mediated Innate Immunity Spreads Intercellularly through HIV-1 Env-Induced Membrane Fusion Sites. *Cell Host Microbe* **2016,** *20* (4), 443-457.
204. Ahn, J.; Xia, T.; Rabasa Capote, A.; Betancourt, D.; Barber, G. N., Extrinsic Phagocyte-Dependent STING Signaling Dictates the Immunogenicity of Dying Cells. *Cancer Cell* **2018,** *33* (5), 862-873 e5.
205. Naser Al Deen, N.; AbouHaidar, M.; Talhouk, R., Connexin43 as a Tumor Suppressor: Proposed Connexin43 mRNA-circularRNAs-microRNAs Axis Towards Prevention and Early Detection in Breast Cancer. *Front Med (Lausanne)* **2019,** *6*, 192.
206. Sirnes, S.; Bruun, J.; Kolberg, M.; Kjenseth, A.; Lind, G. E.; Svindland, A.; Brech, A.; Nesbakken, A.; Lothe, R. A.; Leithe, E.; Rivedal, E., Connexin43 acts as a colorectal cancer tumor suppressor and predicts disease outcome. *Int J Cancer* **2012,** *131* (3), 570-81.
207. Bonacquisti, E. E.; Nguyen, J., Connexin 43 (Cx43) in cancer: Implications for therapeutic approaches via gap junctions. *Cancer Lett* **2019,** *442*, 439-444.
208. Zhou, Y.; Fei, M.; Zhang, G.; Liang, W. C.; Lin, W.; Wu, Y.; Piskol, R.; Ridgway, J.; McNamara, E.; Huang, H.; Zhang, J.; Oh, J.; Patel, J. M.; Jakubiak, D.; Lau, J.; Blackwood, B.; Bravo, D. D.; Shi, Y.; Wang, J.; Hu, H. M.; Lee, W. P.; Jesudason, R.; Sangaraju, D.; Modrusan, Z.; Anderson, K. R.; Warming, S.; Roose-Girma, M.; Yan, M., Blockade of the Phagocytic Receptor MerTK on Tumor-Associated Macrophages Enhances P2X7R-Dependent STING Activation by Tumor-Derived cGAMP. *Immunity* **2020,** *52* (2), 357-373 e9.
209. Luteijn, R. D.; Zaver, S. A.; Gowen, B. G.; Wyman, S. K.; Garelis, N. E.; Onia, L.; McWhirter, S. M.; Katibah, G. E.; Corn, J. E.; Woodward, J. J.; Raulet, D. H., SLC19A1 transports immunoreactive cyclic dinucleotides. *Nature* **2019,** *573* (7774), 434-438.
210. Gentili, M.; Kowal, J.; Tkach, M.; Satoh, T.; Lahaye, X.; Conrad, C.; Boyron, M.; Lombard, B.; Durand, S.; Kroemer, G.; Loew, D.; Dalod, M.; Thery, C.; Manel, N., Transmission of innate immune signaling by packaging of cGAMP in viral particles. *Science* **2015,** *349* (6253), 1232-6.
211. Bridgeman, A.; Maelfait, J.; Davenne, T.; Partridge, T.; Peng, Y.; Mayer, A.; Dong, T.; Kaever, V.; Borrow, P.; Rehwinkel, J., Viruses transfer the antiviral second messenger cGAMP between cells. *Science* **2015,** *349* (6253), 1228-32.
212. Kalamvoki, M.; Du, T.; Roizman, B., Cells infected with herpes simplex virus 1 export

to uninfected cells exosomes containing STING, viral mRNAs, and microRNAs. *Proc Natl Acad Sci U S A* **2014,** *111* (46), E4991-6.
213. Torralba, D.; Baixauli, F.; Villarroya-Beltri, C.; Fernandez-Delgado, I.; Latorre-Pellicer, A.; Acin-Perez, R.; Martin-Cofreces, N. B.; Jaso-Tamame, A. L.; Iborra, S.; Jorge, I.; Gonzalez-Aseguinolaza, G.; Garaude, J.; Vicente-Manzanares, M.; Enriquez, J. A.; Mittelbrunn, M.; Sanchez-Madrid, F., Priming of dendritic cells by DNA-containing extracellular vesicles from activated T cells through antigen-driven contacts. *Nat Commun* **2018,** *9* (1), 2658.
214. Kato, Y.; Park, J.; Takamatsu, H.; Konaka, H.; Aoki, W.; Aburaya, S.; Ueda, M.; Nishide, M.; Koyama, S.; Hayama, Y.; Kinehara, Y.; Hirano, T.; Shima, Y.; Narazaki, M.; Kumanogoh, A., Apoptosis-derived membrane vesicles drive the cGAS-STING pathway and enhance type I IFN production in systemic lupus erythematosus. *Ann Rheum Dis* **2018,** *77* (10), 1507-1515.
215. Cordova, A. F.; Ritchie, C.; Bohnert, V.; Li, L., Human SLC46A2 Is the Dominant cGAMP Importer in Extracellular cGAMP-Sensing Macrophages and Monocytes. *ACS Cent Sci* **2021,** *7* (6), 1073-1088.
216. Oyamada, M.; Oyamada, Y.; Takamatsu, T., Regulation of connexin expression. *Biochim Biophys Acta* **2005,** *1719* (1-2), 6-23.
217. Strange, K.; Yamada, T.; Denton, J. S., A 30-year journey from volume-regulated anion currents to molecular structure of the LRRC8 channel. *J Gen Physiol* **2019,** *151* (2), 100-117.
218. Chen, L.; Konig, B.; Liu, T.; Pervaiz, S.; Razzaque, Y. S.; Stauber, T., More than just a pressure relief valve: physiological roles of volume-regulated LRRC8 anion channels. *Biol Chem* **2019,** *400* (11), 1481-1496.
219. Jentsch, T. J., VRACs and other ion channels and transporters in the regulation of cell volume and beyond. *Nat Rev Mol Cell Biol* **2016,** *17* (5), 293-307.
220. Osei-Owusu, J.; Yang, J.; Vitery, M. D. C.; Qiu, Z., Molecular Biology and Physiology of Volume-Regulated Anion Channel (VRAC). *Curr Top Membr* **2018,** *81*, 177-203.
221. Liu, T.; Stauber, T., The Volume-Regulated Anion Channel LRRC8/VRAC Is Dispensable for Cell Proliferation and Migration. *Int J Mol Sci* **2019,** *20* (11).
222. Hubbell, J. A.; Swartz, M. A., Trojan horses for immunotherapy. *Nature Nanotechnology* **2019,** *14* (3), 196-197.
223. Li, L.; Yin, Q.; Kuss, P.; Maliga, Z.; Millan, J. L.; Wu, H.; Mitchison, T. J., Hydrolysis of 2'3'-cGAMP by ENPP1 and design of nonhydrolyzable analogs. *Nat Chem Biol* **2014,** *10* (12), 1043-8.
224. Namasivayam, V.; Lee, S. Y.; Muller, C. E., The promiscuous ectonucleotidase NPP1: molecular insights into substrate binding and hydrolysis. *Biochim Biophys Acta Gen Subj* **2017,** *1861* (3), 603-614.
225. Lau, W. M.; Doucet, M.; Stadel, R.; Huang, D.; Weber, K. L.; Kominsky, S. L., Enpp1: a potential facilitator of breast cancer bone metastasis. *PLoS One* **2013,** *8* (7), e66752.
226. Li, J.; Duran, M. A.; Dhanota, N.; Chatila, W. K.; Bettigole, S. E.; Kwon, J.; Sriram, R. K.; Humphries, M. P.; Salto-Tellez, M.; James, J. A.; Hanna, M. G.; Melms, J. C.; Vallabhaneni, S.; Litchfield, K.; Usaite, I.; Biswas, D.; Bareja, R.; Li, H. W.; Martin, M. L.; Dorsaint, P.; Cavallo, J. A.; Li, P.; Pauli, C.; Gottesdiener, L.; DiPardo, B. J.; Hollmann, T. J.; Merghoub, T.; Wen, H. Y.; Reis-Filho, J. S.; Riaz, N.; Su, S. M.; Kalbasi, A.; Vasan, N.; Powell, S. N.; Wolchok, J. D.; Elemento, O.; Swanton, C.; Shoushtari, A. N.; Parkes, E. E.; Izar, B.; Bakhoum, S. F., Metastasis and immune evasion from extracellular cGAMP hydrolysis.

Cancer Discov **2020**.
227. Kawaguchi, M.; Han, X.; Hisada, T.; Nishikawa, S.; Kano, K.; Ieda, N.; Aoki, J.; Toyama, T.; Nakagawa, H., Development of an ENPP1 Fluorescence Probe for Inhibitor Screening, Cellular Imaging, and Prognostic Assessment of Malignant Breast Cancer. *J Med Chem* **2019,** *62* (20), 9254-9269.
228. Yan, H.; Wang, X.; KuoLee, R.; Chen, W., Synthesis and immunostimulatory properties of the phosphorothioate analogues of cdiGMP. *Bioorg Med Chem Lett* **2008,** *18* (20), 5631-4.
229. Eckstein, F., Phosphorothioates, essential components of therapeutic oligonucleotides. *Nucleic Acid Ther* **2014,** *24* (6), 374-87.
230. Liu, H.; Moura-Alves, P.; Pei, G.; Mollenkopf, H. J.; Hurwitz, R.; Wu, X.; Wang, F.; Liu, S.; Ma, M.; Fei, Y.; Zhu, C.; Koehler, A. B.; Oberbeck-Mueller, D.; Hahnke, K.; Klemm, M.; Guhlich-Bornhof, U.; Ge, B.; Tuukkanen, A.; Kolbe, M.; Dorhoi, A.; Kaufmann, S. H., cGAS facilitates sensing of extracellular cyclic dinucleotides to activate innate immunity. *EMBO Rep* **2019,** *20* (4).
231. Shae, D.; Becker, K. W.; Christov, P.; Yun, D. S.; Lytton-Jean, A. K. R.; Sevimli, S.; Ascano, M.; Kelley, M.; Johnson, D. B.; Balko, J. M.; Wilson, J. T., Endosomolytic polymersomes increase the activity of cyclic dinucleotide STING agonists to enhance cancer immunotherapy. *Nat Nanotechnol* **2019,** *14* (3), 269-278.
232. Ahn, J.; Xia, T.; Konno, H.; Konno, K.; Ruiz, P.; Barber, G. N., Inflammation-driven carcinogenesis is mediated through STING. *Nat Commun* **2014,** *5*, 5166.
233. Kwon, J.; Bakhoum, S. F., The Cytosolic DNA-Sensing cGAS-STING Pathway in Cancer. *Cancer Discov* **2020,** *10* (1), 26-39.
234. Zheng, J.; Mo, J.; Zhu, T.; Zhuo, W.; Yi, Y.; Hu, S.; Yin, J.; Zhang, W.; Zhou, H.; Liu, Z., Comprehensive elaboration of the cGAS-STING signaling axis in cancer development and immunotherapy. *Mol Cancer* **2020,** *19* (1), 133.
235. Chen, D. S.; Mellman, I., Oncology meets immunology: the cancer-immunity cycle. *Immunity* **2013,** *39* (1), 1-10.
236. Lian, Y.; Duffy, K. J.; Yang, J., STING Activation and its Application in Immuno-Oncology. *Curr Top Med Chem* **2019,** *19* (24), 2205-2227.
237. Khoo, L. T.; Chen, L. Y., Role of the cGAS-STING pathway in cancer development and oncotherapeutic approaches. *EMBO Rep* **2018,** *19* (12).
238. Woo, S. R.; Corrales, L.; Gajewski, T. F., The STING pathway and the T cell-inflamed tumor microenvironment. *Trends Immunol* **2015,** *36* (4), 250-6.
239. Li, W.; Lu, L.; Lu, J.; Wang, X.; Yang, C.; Jin, J.; Wu, L.; Hong, X.; Li, F.; Cao, D.; Yang, Y.; Wu, M.; Su, B.; Cheng, J.; Yang, X.; Di, W.; Deng, L., cGAS-STING-mediated DNA sensing maintains CD8(+) T cell stemness and promotes antitumor T cell therapy. *Sci Transl Med* **2020,** *12* (549).
240. Huang, L.; Wang, Z.; Liu, C.; Xu, C.; Mbofung, R. M.; McKenzie, J. A.; Khong, H.; Hwu, P.; Peng, W., CpG-based immunotherapy impairs antitumor activity of BRAF inhibitors in a B-cell-dependent manner. *Oncogene* **2017,** *36* (28), 4081-4086.
241. Liu, X.; Pu, Y.; Cron, K.; Deng, L.; Kline, J.; Frazier, W. A.; Xu, H.; Peng, H.; Fu, Y. X.; Xu, M. M., CD47 blockade triggers T cell-mediated destruction of immunogenic tumors. *Nat Med* **2015,** *21* (10), 1209-15.
242. Konno, H.; Yamauchi, S.; Berglund, A.; Putney, R. M.; Mule, J. J.; Barber, G. N., Suppression of STING signaling through epigenetic silencing and missense mutation impedes DNA damage mediated cytokine production. *Oncogene* **2018,** *37* (15), 2037-2051.

243. Bakhoum, S. F.; Cantley, L. C., The Multifaceted Role of Chromosomal Instability in Cancer and Its Microenvironment. *Cell* **2018,** *174* (6), 1347-1360.
244. Lemos, H.; Huang, L.; McGaha, T. L.; Mellor, A. L., Cytosolic DNA sensing via the stimulator of interferon genes adaptor: Yin and Yang of immune responses to DNA. *Eur J Immunol* **2014,** *44* (10), 2847-53.
245. Lemos, H.; Mohamed, E.; Huang, L.; Ou, R.; Pacholczyk, G.; Arbab, A. S.; Munn, D.; Mellor, A. L., STING Promotes the Growth of Tumors Characterized by Low Antigenicity via IDO Activation. *Cancer Res* **2016,** *76* (8), 2076-81.
246. Corrales, L.; Woo, S.-R.; Gajewski, T. F., Extremely potent immunotherapeutic activity of a STING agonist in the B16 melanoma model in vivo. *Journal for ImmunoTherapy of Cancer* **2013,** *1* (1), O15.
247. Qin, X. Q.; Tao, N.; Dergay, A.; Moy, P.; Fawell, S.; Davis, A.; Wilson, J. M.; Barsoum, J., Interferon-beta gene therapy inhibits tumor formation and causes regression of established tumors in immune-deficient mice. *Proc Natl Acad Sci U S A* **1998,** *95* (24), 14411-6.
248. Kim, H. S.; Lee, M. S., STAT1 as a key modulator of cell death. *Cell Signal* **2007,** *19* (3), 454-65.
249. Ryuke, Y.; Mizuno, M.; Natsume, A.; Suzuki, O.; Nobayashi, M.; Kageshita, T.; Matsumoto, K.; Saida, T.; Yoshida, J., Growth inhibition of subcutaneous mouse melanoma and induction of natural killer cells by liposome-mediated interferon-beta gene therapy. *Melanoma Res* **2003,** *13* (4), 349-56.
250. Spaapen, R. M.; Leung, M. Y.; Fuertes, M. B.; Kline, J. P.; Zhang, L.; Zheng, Y.; Fu, Y. X.; Luo, X.; Cohen, K. S.; Gajewski, T. F., Therapeutic activity of high-dose intratumoral IFN-beta requires direct effect on the tumor vasculature. *J Immunol* **2014,** *193* (8), 4254-60.
251. Indraccolo, S., Interferon-alpha as angiogenesis inhibitor: learning from tumor models. *Autoimmunity* **2010,** *43* (3), 244-7.
252. Luft, T.; Pang, K. C.; Thomas, E.; Hertzog, P.; Hart, D. N.; Trapani, J.; Cebon, J., Type I IFNs enhance the terminal differentiation of dendritic cells. *J Immunol* **1998,** *161* (4), 1947-53.
253. Paquette, R. L.; Hsu, N. C.; Kiertscher, S. M.; Park, A. N.; Tran, L.; Roth, M. D.; Glaspy, J. A., Interferon-alpha and granulocyte-macrophage colony-stimulating factor differentiate peripheral blood monocytes into potent antigen-presenting cells. *J Leukoc Biol* **1998,** *64* (3), 358-67.
254. Radvanyi, L. G.; Banerjee, A.; Weir, M.; Messner, H., Low levels of interferon-alpha induce CD86 (B7.2) expression and accelerates dendritic cell maturation from human peripheral blood mononuclear cells. *Scand J Immunol* **1999,** *50* (5), 499-509.
255. Yang, X.; Zhang, X.; Fu, M. L.; Weichselbaum, R. R.; Gajewski, T. F.; Guo, Y.; Fu, Y. X., Targeting the tumor microenvironment with interferon-beta bridges innate and adaptive immune responses. *Cancer Cell* **2014,** *25* (1), 37-48.
256. Fuertes, M. B.; Kacha, A. K.; Kline, J.; Woo, S. R.; Kranz, D. M.; Murphy, K. M.; Gajewski, T. F., Host type I IFN signals are required for antitumor CD8+ T cell responses through CD8{alpha}+ dendritic cells. *J Exp Med* **2011,** *208* (10), 2005-16.
257. Qin, X. Q.; Beckham, C.; Brown, J. L.; Lukashev, M.; Barsoum, J., Human and mouse IFN-beta gene therapy exhibits different anti-tumor mechanisms in mouse models. *Mol Ther* **2001,** *4* (4), 356-64.
258. Gidlund, M.; Orn, A.; Wigzell, H.; Senik, A.; Gresser, I., Enhanced NK cell activity in mice injected with interferon and interferon inducers. *Nature* **1978,** *273* (5665), 759-61.

259. Snell, L. M.; McGaha, T. L.; Brooks, D. G., Type I Interferon in Chronic Virus Infection and Cancer. *Trends Immunol* **2017,** *38* (8), 542-557.
260. Sivick, K. E.; Desbien, A. L.; Glickman, L. H.; Reiner, G. L.; Corrales, L.; Surh, N. H.; Hudson, T. E.; Vu, U. T.; Francica, B. J.; Banda, T.; Katibah, G. E.; Kanne, D. B.; Leong, J. J.; Metchette, K.; Bruml, J. R.; Ndubaku, C. O.; McKenna, J. M.; Feng, Y.; Zheng, L.; Bender, S. L.; Cho, C. Y.; Leong, M. L.; van Elsas, A.; Dubensky, T. W., Jr.; McWhirter, S. M., Magnitude of Therapeutic STING Activation Determines CD8(+) T Cell-Mediated Anti-tumor Immunity. *Cell Rep* **2018,** *25* (11), 3074-3085 e5.
261. Wilson, N. S.; Behrens, G. M.; Lundie, R. J.; Smith, C. M.; Waithman, J.; Young, L.; Forehan, S. P.; Mount, A.; Steptoe, R. J.; Shortman, K. D.; de Koning-Ward, T. F.; Belz, G. T.; Carbone, F. R.; Crabb, B. S.; Heath, W. R.; Villadangos, J. A., Systemic activation of dendritic cells by Toll-like receptor ligands or malaria infection impairs cross-presentation and antiviral immunity. *Nat Immunol* **2006,** *7* (2), 165-72.
262. Tzeng, A.; Kauke, M. J.; Zhu, E. F.; Moynihan, K. D.; Opel, C. F.; Yang, N. J.; Mehta, N.; Kelly, R. L.; Szeto, G. L.; Overwijk, W. W.; Irvine, D. J.; Wittrup, K. D., Temporally Programmed CD8alpha(+) DC Activation Enhances Combination Cancer Immunotherapy. *Cell Rep* **2016,** *17* (10), 2503-2511.
263. Borden, E. C.; Parkinson, D., A perspective on the clinical effectiveness and tolerance of interferon-alpha. *Semin Oncol* **1998,** *25* (1 Suppl 1), 3-8.
264. Weber, J. S.; Yang, J. C.; Atkins, M. B.; Disis, M. L., Toxicities of Immunotherapy for the Practitioner. *J Clin Oncol* **2015,** *33* (18), 2092-9.
265. Wu, J.; Dobbs, N.; Yang, K.; Yan, N., Interferon-Independent Activities of Mammalian STING Mediate Antiviral Response and Tumor Immune Evasion. *Immunity* **2020,** *53* (1), 115-126 e5.
266. Hou, Y.; Liang, H.; Rao, E.; Zheng, W.; Huang, X.; Deng, L.; Zhang, Y.; Yu, X.; Xu, M.; Mauceri, H.; Arina, A.; Weichselbaum, R. R.; Fu, Y. X., Non-canonical NF-kappaB Antagonizes STING Sensor-Mediated DNA Sensing in Radiotherapy. *Immunity* **2018,** *49* (3), 490-503 e4.
267. Zhu, Y.; An, X.; Zhang, X.; Qiao, Y.; Zheng, T.; Li, X., STING: a master regulator in the cancer-immunity cycle. *Mol Cancer* **2019,** *18* (1), 152.
268. Coffelt, S. B.; de Visser, K. E., Immune-mediated mechanisms influencing the efficacy of anticancer therapies. *Trends Immunol* **2015,** *36* (4), 198-216.
269. Skrnjug, I.; Guzman, C. A.; Rueckert, C., Cyclic GMP-AMP displays mucosal adjuvant activity in mice. *PLoS One* **2014,** *9* (10), e110150.
270. Gutjahr, A.; Papagno, L.; Nicoli, F.; Kanuma, T.; Kuse, N.; Cabral-Piccin, M. P.; Rochereau, N.; Gostick, E.; Lioux, T.; Perouzel, E.; Price, D. A.; Takiguchi, M.; Verrier, B.; Yamamoto, T.; Paul, S.; Appay, V., The STING ligand cGAMP potentiates the efficacy of vaccine-induced CD8+ T cells. *JCI Insight* **2019,** *4* (7).
271. Corrales, L.; Matson, V.; Flood, B.; Spranger, S.; Gajewski, T. F., Innate immune signaling and regulation in cancer immunotherapy. *Cell Res* **2017,** *27* (1), 96-108.
272. Spranger, S.; Dai, D.; Horton, B.; Gajewski, T. F., Tumor-Residing Batf3 Dendritic Cells Are Required for Effector T Cell Trafficking and Adoptive T Cell Therapy. *Cancer Cell* **2017,** *31* (5), 711-723 e4.
273. Diamond, M. S.; Kinder, M.; Matsushita, H.; Mashayekhi, M.; Dunn, G. P.; Archambault, J. M.; Lee, H.; Arthur, C. D.; White, J. M.; Kalinke, U.; Murphy, K. M.; Schreiber, R. D., Type I interferon is selectively required by dendritic cells for immune rejection

of tumors. *J Exp Med* **2011,** *208* (10), 1989-2003.
274. Worbs, T.; Hammerschmidt, S. I.; Forster, R., Dendritic cell migration in health and disease. *Nat Rev Immunol* **2017,** *17* (1), 30-48.
275. Hampton, H. R.; Chtanova, T., Lymphatic Migration of Immune Cells. *Front Immunol* **2019,** *10*, 1168.
276. Thompson, E. D.; Enriquez, H. L.; Fu, Y. X.; Engelhard, V. H., Tumor masses support naive T cell infiltration, activation, and differentiation into effectors. *J Exp Med* **2010,** *207* (8), 1791-804.
277. Ma, Y.; Adjemian, S.; Mattarollo, S. R.; Yamazaki, T.; Aymeric, L.; Yang, H.; Portela Catani, J. P.; Hannani, D.; Duret, H.; Steegh, K.; Martins, I.; Schlemmer, F.; Michaud, M.; Kepp, O.; Sukkurwala, A. Q.; Menger, L.; Vacchelli, E.; Droin, N.; Galluzzi, L.; Krzysiek, R.; Gordon, S.; Taylor, P. R.; Van Endert, P.; Solary, E.; Smyth, M. J.; Zitvogel, L.; Kroemer, G., Anticancer chemotherapy-induced intratumoral recruitment and differentiation of antigen-presenting cells. *Immunity* **2013,** *38* (4), 729-41.
278. Chelvanambi, M.; Fecek, R. J.; Taylor, J. L.; Storkus, W. J., STING agonist-based treatment promotes vascular normalization and tertiary lymphoid structure formation in the therapeutic melanoma microenvironment. *J Immunother Cancer* **2021,** *9* (2).
279. Wang, N.; Liang, H.; Zen, K., Molecular mechanisms that influence the macrophage m1-m2 polarization balance. *Front Immunol* **2014,** *5*, 614.
280. Cheng, N.; Watkins-Schulz, R.; Junkins, R. D.; David, C. N.; Johnson, B. M.; Montgomery, S. A.; Peine, K. J.; Darr, D. B.; Yuan, H.; McKinnon, K. P.; Liu, Q.; Miao, L.; Huang, L.; Bachelder, E. M.; Ainslie, K. M.; Ting, J. P. Y., A nanoparticle-incorporated STING activator enhances antitumor immunity in PD-L1–insensitive models of triple-negative breast cancer. *JCI Insight* **2018,** *3* (22).
281. Downey, C. M.; Aghaei, M.; Schwendener, R. A.; Jirik, F. R., DMXAA causes tumor site-specific vascular disruption in murine non-small cell lung cancer, and like the endogenous non-canonical cyclic dinucleotide STING agonist, 2'3'-cGAMP, induces M2 macrophage repolarization. *PLoS One* **2014,** *9* (6), e99988.
282. Pan, X. Q., The mechanism of the anticancer function of M1 macrophages and their use in the clinic. *Chin J Cancer* **2012,** *31* (12), 557-63.
283. Chen, Y.; Song, Y.; Du, W.; Gong, L.; Chang, H.; Zou, Z., Tumor-associated macrophages: an accomplice in solid tumor progression. *J Biomed Sci* **2019,** *26* (1), 78.
284. Wong, P.; Pamer, E. G., CD8 T cell responses to infectious pathogens. *Annu Rev Immunol* **2003,** *21*, 29-70.
285. Zhu, J.; Yamane, H.; Paul, W. E., Differentiation of effector CD4 T cell populations (*). *Annu Rev Immunol* **2010,** *28*, 445-89.
286. Wang, J.; Li, P.; Wu, M. X., Natural STING Agonist as an "Ideal" Adjuvant for Cutaneous Vaccination. *J Invest Dermatol* **2016,** *136* (11), 2183-2191.
287. Shakya, A. K.; Lee, C. H.; Uddin, M. J.; Gill, H. S., Assessment of Th1/Th2 Bias of STING Agonists Coated on Microneedles for Possible Use in Skin Allergen Immunotherapy. *Mol Pharm* **2018,** *15* (11), 5437-5443.
288. Heusinkveld, M.; de Vos van Steenwijk, P. J.; Goedemans, R.; Ramwadhdoebe, T. H.; Gorter, A.; Welters, M. J.; van Hall, T.; van der Burg, S. H., M2 macrophages induced by prostaglandin E2 and IL-6 from cervical carcinoma are switched to activated M1 macrophages by CD4+ Th1 cells. *J Immunol* **2011,** *187* (3), 1157-65.
289. Eisel, D.; Das, K.; Dickes, E.; Konig, R.; Osen, W.; Eichmuller, S. B., Cognate

Interaction With CD4(+) T Cells Instructs Tumor-Associated Macrophages to Acquire M1-Like Phenotype. *Front Immunol* **2019,** *10*, 219.
290. Cerboni, S.; Jeremiah, N.; Gentili, M.; Gehrmann, U.; Conrad, C.; Stolzenberg, M. C.; Picard, C.; Neven, B.; Fischer, A.; Amigorena, S.; Rieux-Laucat, F.; Manel, N., Intrinsic antiproliferative activity of the innate sensor STING in T lymphocytes. *J Exp Med* **2017,** *214* (6), 1769-1785.
291. Larkin, B.; Ilyukha, V.; Sorokin, M.; Buzdin, A.; Vannier, E.; Poltorak, A., Cutting Edge: Activation of STING in T Cells Induces Type I IFN Responses and Cell Death. *J Immunol* **2017,** *199* (2), 397-402.
292. Hunter, M. C.; Teijeira, A.; Halin, C., T Cell Trafficking through Lymphatic Vessels. *Front Immunol* **2016,** *7*, 613.
293. Pham, T. H.; Okada, T.; Matloubian, M.; Lo, C. G.; Cyster, J. G., S1P1 receptor signaling overrides retention mediated by G alpha i-coupled receptors to promote T cell egress. *Immunity* **2008,** *28* (1), 122-33.
294. Schwab, S. R.; Pereira, J. P.; Matloubian, M.; Xu, Y.; Huang, Y.; Cyster, J. G., Lymphocyte sequestration through S1P lyase inhibition and disruption of S1P gradients. *Science* **2005,** *309* (5741), 1735-9.
295. Lo, C. G.; Xu, Y.; Proia, R. L.; Cyster, J. G., Cyclical modulation of sphingosine-1-phosphate receptor 1 surface expression during lymphocyte recirculation and relationship to lymphoid organ transit. *J Exp Med* **2005,** *201* (2), 291-301.
296. Harlin, H.; Meng, Y.; Peterson, A. C.; Zha, Y.; Tretiakova, M.; Slingluff, C.; McKee, M.; Gajewski, T. F., Chemokine expression in melanoma metastases associated with CD8+ T-cell recruitment. *Cancer Res* **2009,** *69* (7), 3077-85.
297. Pak-Wittel, M. A.; Yang, L.; Sojka, D. K.; Rivenbark, J. G.; Yokoyama, W. M., Interferon-gamma mediates chemokine-dependent recruitment of natural killer cells during viral infection. *Proc Natl Acad Sci U S A* **2013,** *110* (1), E50-9.
298. Barry, K. C.; Hsu, J.; Broz, M. L.; Cueto, F. J.; Binnewies, M.; Combes, A. J.; Nelson, A. E.; Loo, K.; Kumar, R.; Rosenblum, M. D.; Alvarado, M. D.; Wolf, D. M.; Bogunovic, D.; Bhardwaj, N.; Daud, A. I.; Ha, P. K.; Ryan, W. R.; Pollack, J. L.; Samad, B.; Asthana, S.; Chan, V.; Krummel, M. F., A natural killer-dendritic cell axis defines checkpoint therapy-responsive tumor microenvironments. *Nat Med* **2018,** *24* (8), 1178-1191.
299. Munn, L. L.; Jain, R. K., Vascular regulation of antitumor immunity. *Science* **2019,** *365* (6453), 544-545.
300. Yang, H.; Lee, W. S.; Kong, S. J.; Kim, C. G.; Kim, J. H.; Chang, S. K.; Kim, S.; Kim, G.; Chon, H. J.; Kim, C., STING activation reprograms tumor vasculatures and synergizes with VEGFR2 blockade. *J Clin Invest* **2019,** *129* (10), 4350-4364.
301. Tang, C. H.; Zundell, J. A.; Ranatunga, S.; Lin, C.; Nefedova, Y.; Del Valle, J. R.; Hu, C. C., Agonist-Mediated Activation of STING Induces Apoptosis in Malignant B Cells. *Cancer Res* **2016,** *76* (8), 2137-52.
302. Takashima, K.; Takeda, Y.; Oshiumi, H.; Shime, H.; Okabe, M.; Ikawa, M.; Matsumoto, M.; Seya, T., STING in tumor and host cells cooperatively work for NK cell-mediated tumor growth retardation. *Biochem Biophys Res Commun* **2016,** *478* (4), 1764-71.
303. Grabosch, S.; Bulatovic, M.; Zeng, F.; Ma, T.; Zhang, L.; Ross, M.; Brozick, J.; Fang, Y.; Tseng, G.; Kim, E.; Gambotto, A.; Elishaev, E.; R, P. E.; Vlad, A. M., Cisplatin-induced immune modulation in ovarian cancer mouse models with distinct inflammation profiles. *Oncogene* **2019,** *38* (13), 2380-2393.

304. Roemer, M. G.; Advani, R. H.; Redd, R. A.; Pinkus, G. S.; Natkunam, Y.; Ligon, A. H.; Connelly, C. F.; Pak, C. J.; Carey, C. D.; Daadi, S. E.; Chapuy, B.; de Jong, D.; Hoppe, R. T.; Neuberg, D. S.; Shipp, M. A.; Rodig, S. J., Classical Hodgkin Lymphoma with Reduced beta2M/MHC Class I Expression Is Associated with Inferior Outcome Independent of 9p24.1 Status. *Cancer Immunol Res* **2016,** *4* (11), 910-916.
305. Garrido, F.; Aptsiauri, N.; Doorduijn, E. M.; Garcia Lora, A. M.; van Hall, T., The urgent need to recover MHC class I in cancers for effective immunotherapy. *Curr Opin Immunol* **2016,** *39*, 44-51.
306. Alexandrov, L. B.; Stratton, M. R., Mutational signatures: the patterns of somatic mutations hidden in cancer genomes. *Curr Opin Genet Dev* **2014,** *24*, 52-60.
307. Nicolai, C. J.; Wolf, N.; Chang, I. C.; Kirn, G.; Marcus, A.; Ndubaku, C. O.; McWhirter, S. M.; Raulet, D. H., NK cells mediate clearance of CD8(+) T cell-resistant tumors in response to STING agonists. *Sci Immunol* **2020,** *5* (45).
308. Lam, A. R.; Bert, N. L.; Ho, S. S.; Shen, Y. J.; Tang, L. F.; Xiong, G. M.; Croxford, J. L.; Koo, C. X.; Ishii, K. J.; Akira, S.; Raulet, D. H.; Gasser, S., RAE1 ligands for the NKG2D receptor are regulated by STING-dependent DNA sensor pathways in lymphoma. *Cancer Res* **2014,** *74* (8), 2193-2203.
309. Parkes, E. E.; Walker, S. M.; Taggart, L. E.; McCabe, N.; Knight, L. A.; Wilkinson, R.; McCloskey, K. D.; Buckley, N. E.; Savage, K. I.; Salto-Tellez, M.; McQuaid, S.; Harte, M. T.; Mullan, P. B.; Harkin, D. P.; Kennedy, R. D., Activation of STING-Dependent Innate Immune Signaling By S-Phase-Specific DNA Damage in Breast Cancer. *J Natl Cancer Inst* **2017,** *109* (1).
310. Pepin, G.; Nejad, C.; Ferrand, J.; Thomas, B. J.; Stunden, H. J.; Sanij, E.; Foo, C. H.; Stewart, C. R.; Cain, J. E.; Bardin, P. G.; Williams, B. R. G.; Gantier, M. P., Topoisomerase 1 Inhibition Promotes Cyclic GMP-AMP Synthase-Dependent Antiviral Responses. *mBio* **2017,** *8* (5).
311. Luthra, P.; Aguirre, S.; Yen, B. C.; Pietzsch, C. A.; Sanchez-Aparicio, M. T.; Tigabu, B.; Morlock, L. K.; Garcia-Sastre, A.; Leung, D. W.; Williams, N. S.; Fernandez-Sesma, A.; Bukreyev, A.; Basler, C. F., Topoisomerase II Inhibitors Induce DNA Damage-Dependent Interferon Responses Circumventing Ebola Virus Immune Evasion. *mBio* **2017,** *8* (2).
312. Lohard, S.; Bourgeois, N.; Maillet, L.; Gautier, F.; Fetiveau, A.; Lasla, H.; Nguyen, F.; Vuillier, C.; Dumont, A.; Moreau-Aubry, A.; Frapin, M.; David, L.; Loussouarn, D.; Kerdraon, O.; Campone, M.; Jezequel, P.; Juin, P. P.; Barille-Nion, S., STING-dependent paracriny shapes apoptotic priming of breast tumors in response to anti-mitotic treatment. *Nat Commun* **2020,** *11* (1), 259.
313. Wilkinson, R. D.; Johnston, D. I.; Parkes, E. E.; McCabe, N.; Kennedy, R. D., Abstract 3787: Exploring the effect of chemotherapies on STING-dependent cytokine release. *Cancer Research* **2018,** *78* (13 Supplement), 3787.
314. Maekawa, H.; Inoue, T.; Ouchi, H.; Jao, T. M.; Inoue, R.; Nishi, H.; Fujii, R.; Ishidate, F.; Tanaka, T.; Tanaka, Y.; Hirokawa, N.; Nangaku, M.; Inagi, R., Mitochondrial Damage Causes Inflammation via cGAS-STING Signaling in Acute Kidney Injury. *Cell Rep* **2019,** *29* (5), 1261-1273 e6.
315. Unterholzner, L.; Dunphy, G., cGAS-independent STING activation in response to DNA damage. *Mol Cell Oncol* **2019,** *6* (4), 1558682.
316. Wang, Z.; Chen, J.; Hu, J.; Zhang, H.; Xu, F.; He, W.; Wang, X.; Li, M.; Lu, W.; Zeng, G.; Zhou, P.; Huang, P.; Chen, S.; Li, W.; Xia, L. P.; Xia, X., cGAS/STING axis

mediates a topoisomerase II inhibitor-induced tumor immunogenicity. *J Clin Invest* **2019,** *129* (11), 4850-4862.
317. Deng, L.; Liang, H.; Xu, M.; Yang, X.; Burnette, B.; Arina, A.; Li, X. D.; Mauceri, H.; Beckett, M.; Darga, T.; Huang, X.; Gajewski, T. F.; Chen, Z. J.; Fu, Y. X.; Weichselbaum, R. R., STING-Dependent Cytosolic DNA Sensing Promotes Radiation-Induced Type I Interferon-Dependent Antitumor Immunity in Immunogenic Tumors. *Immunity* **2014,** *41* (5), 843-52.
318. Chabanon, R. M.; Muirhead, G.; Krastev, D. B.; Adam, J.; Morel, D.; Garrido, M.; Lamb, A.; Henon, C.; Dorvault, N.; Rouanne, M.; Marlow, R.; Bajrami, I.; Cardenosa, M. L.; Konde, A.; Besse, B.; Ashworth, A.; Pettitt, S. J.; Haider, S.; Marabelle, A.; Tutt, A. N.; Soria, J. C.; Lord, C. J.; Postel-Vinay, S., PARP inhibition enhances tumor cell-intrinsic immunity in ERCC1-deficient non-small cell lung cancer. *J Clin Invest* **2019,** *129* (3), 1211-1228.
319. Ding, L.; Kim, H. J.; Wang, Q.; Kearns, M.; Jiang, T.; Ohlson, C. E.; Li, B. B.; Xie, S.; Liu, J. F.; Stover, E. H.; Howitt, B. E.; Bronson, R. T.; Lazo, S.; Roberts, T. M.; Freeman, G. J.; Konstantinopoulos, P. A.; Matulonis, U. A.; Zhao, J. J., PARP Inhibition Elicits STING-Dependent Antitumor Immunity in Brca1-Deficient Ovarian Cancer. *Cell Rep* **2018,** *25* (11), 2972-2980 e5.
320. Pantelidou, C.; Sonzogni, O.; De Oliveria Taveira, M.; Mehta, A. K.; Kothari, A.; Wang, D.; Visal, T.; Li, M. K.; Pinto, J.; Castrillon, J. A.; Cheney, E. M.; Bouwman, P.; Jonkers, J.; Rottenberg, S.; Guerriero, J. L.; Wulf, G. M.; Shapiro, G. I., PARP Inhibitor Efficacy Depends on CD8(+) T-cell Recruitment via Intratumoral STING Pathway Activation in BRCA-Deficient Models of Triple-Negative Breast Cancer. *Cancer Discov* **2019,** *9* (6), 722-737.
321. Reislander, T.; Lombardi, E. P.; Groelly, F. J.; Miar, A.; Porru, M.; Di Vito, S.; Wright, B.; Lockstone, H.; Biroccio, A.; Harris, A.; Londono-Vallejo, A.; Tarsounas, M., BRCA2 abrogation triggers innate immune responses potentiated by treatment with PARP inhibitors. *Nat Commun* **2019,** *10* (1), 3143.
322. Shen, J.; Zhao, W.; Ju, Z.; Wang, L.; Peng, Y.; Labrie, M.; Yap, T. A.; Mills, G. B.; Peng, G., PARPi Triggers the STING-Dependent Immune Response and Enhances the Therapeutic Efficacy of Immune Checkpoint Blockade Independent of BRCAness. *Cancer Res* **2019,** *79* (2), 311-319.
323. Dillon, M. T.; Bergerhoff, K. F.; Pedersen, M.; Whittock, H.; Crespo-Rodriguez, E.; Patin, E. C.; Pearson, A.; Smith, H. G.; Paget, J. T. E.; Patel, R. R.; Foo, S.; Bozhanova, G.; Ragulan, C.; Fontana, E.; Desai, K.; Wilkins, A. C.; Sadanandam, A.; Melcher, A.; McLaughlin, M.; Harrington, K. J., ATR Inhibition Potentiates the Radiation-induced Inflammatory Tumor Microenvironment. *Clin Cancer Res* **2019,** *25* (11), 3392-3403.
324. Dan, H.; Zhang, S.; Zhou, Y.; Guan, Q., DNA Methyltransferase Inhibitors: Catalysts For Antitumour Immune Responses. *Onco Targets Ther* **2019,** *12*, 10903-10916.
325. Gravina, G. L.; Festuccia, C.; Marampon, F.; Popov, V. M.; Pestell, R. G.; Zani, B. M.; Tombolini, V., Biological rationale for the use of DNA methyltransferase inhibitors as new strategy for modulation of tumor response to chemotherapy and radiation. *Mol Cancer* **2010,** *9*, 305.
326. Falahat, R.; Berglund, A.; Putney, R. M.; Perez-Villarroel, P.; Aoyama, S.; Pilon-Thomas, S.; Barber, G. N.; Mule, J. J., Epigenetic reprogramming of tumor cell-intrinsic STING function sculpts antigenicity and T cell recognition of melanoma. *Proc Natl Acad Sci U S A* **2021,** *118* (15).

327. Kitai, Y.; Kawasaki, T.; Sueyoshi, T.; Kobiyama, K.; Ishii, K. J.; Zou, J.; Akira, S.; Matsuda, T.; Kawai, T., DNA-Containing Exosomes Derived from Cancer Cells Treated with Topotecan Activate a STING-Dependent Pathway and Reinforce Antitumor Immunity. *J Immunol* **2017,** *198* (4), 1649-1659.
328. Sen, T.; Rodriguez, B. L.; Chen, L.; Corte, C. M. D.; Morikawa, N.; Fujimoto, J.; Cristea, S.; Nguyen, T.; Diao, L.; Li, L.; Fan, Y.; Yang, Y.; Wang, J.; Glisson, B. S.; Wistuba, II; Sage, J.; Heymach, J. V.; Gibbons, D. L.; Byers, L. A., Targeting DNA Damage Response Promotes Antitumor Immunity through STING-Mediated T-cell Activation in Small Cell Lung Cancer. *Cancer Discov* **2019,** *9* (5), 646-661.
329. Baird, J. R.; Friedman, D.; Cottam, B.; Dubensky, T. W., Jr.; Kanne, D. B.; Bambina, S.; Bahjat, K.; Crittenden, M. R.; Gough, M. J., Radiotherapy Combined with Novel STING-Targeting Oligonucleotides Results in Regression of Established Tumors. *Cancer Res* **2016,** *76* (1), 50-61.
330. Gui, X.; Yang, H.; Li, T.; Tan, X.; Shi, P.; Li, M.; Du, F.; Chen, Z. J., Autophagy induction via STING trafficking is a primordial function of the cGAS pathway. *Nature* **2019,** *567* (7747), 262-266.
331. Michaud, M.; Martins, I.; Sukkurwala, A. Q.; Adjemian, S.; Ma, Y.; Pellegatti, P.; Shen, S.; Kepp, O.; Scoazec, M.; Mignot, G.; Rello-Varona, S.; Tailler, M.; Menger, L.; Vacchelli, E.; Galluzzi, L.; Ghiringhelli, F.; di Virgilio, F.; Zitvogel, L.; Kroemer, G., Autophagy-dependent anticancer immune responses induced by chemotherapeutic agents in mice. *Science* **2011,** *334* (6062), 1573-7.
332. Landman, S. L.; Ressing, M. E.; van der Veen, A. G., Balancing STING in antimicrobial defense and autoinflammation. *Cytokine Growth Factor Rev* **2020,** *55*, 1-14.
333. Zhao, J.; Ma, S.; Xu, Y.; Si, X.; Yao, H.; Huang, Z.; Zhang, Y.; Yu, H.; Tang, Z.; Song, W.; Chen, X., In situ activation of STING pathway with polymeric SN38 for cancer chemoimmunotherapy. *Biomaterials* **2021,** *268*, 120542.
334. Ding, C.; Song, Z.; Shen, A.; Chen, T.; Zhang, A., Small molecules targeting the innate immune cGAS–STING–TBK1 signaling pathway. *Acta Pharmaceutica Sinica B* **2020**.
335. Hall, J.; Ralph, E. C.; Shanker, S.; Wang, H.; Byrnes, L. J.; Horst, R.; Wong, J.; Brault, A.; Dumlao, D.; Smith, J. F.; Dakin, L. A.; Schmitt, D. C.; Trujillo, J.; Vincent, F.; Griffor, M.; Aulabaugh, A. E., The catalytic mechanism of cyclic GMP-AMP synthase (cGAS) and implications for innate immunity and inhibition. *Protein Sci* **2017,** *26* (12), 2367-2380.
336. Hyman, A. A.; Simons, K., Cell biology. Beyond oil and water--phase transitions in cells. *Science* **2012,** *337* (6098), 1047-9.
337. Vincent, J.; Adura, C.; Gao, P.; Luz, A.; Lama, L.; Asano, Y.; Okamoto, R.; Imaeda, T.; Aida, J.; Rothamel, K.; Gogakos, T.; Steinberg, J.; Reasoner, S.; Aso, K.; Tuschl, T.; Patel, D. J.; Glickman, J. F.; Ascano, M., Small molecule inhibition of cGAS reduces interferon expression in primary macrophages from autoimmune mice. *Nat Commun* **2017,** *8* (1), 750.
338. Lama, L.; Adura, C.; Xie, W.; Tomita, D.; Kamei, T.; Kuryavyi, V.; Gogakos, T.; Steinberg, J. I.; Miller, M.; Ramos-Espiritu, L.; Asano, Y.; Hashizume, S.; Aida, J.; Imaeda, T.; Okamoto, R.; Jennings, A. J.; Michino, M.; Kuroita, T.; Stamford, A.; Gao, P.; Meinke, P.; Glickman, J. F.; Patel, D. J.; Tuschl, T., Development of human cGAS-specific small-molecule inhibitors for repression of dsDNA-triggered interferon expression. *Nat Commun* **2019,** *10* (1), 2261.
339. Zhao, Z.; Ma, Z.; Wang, B.; Guan, Y.; Su, X. D.; Jiang, Z., Mn(2+) Directly Activates cGAS and Structural Analysis Suggests Mn(2+) Induces a Noncanonical Catalytic Synthesis of

2'3'-cGAMP. *Cell Rep* **2020,** *32* (7), 108053.
340. Lv, M.; Chen, M.; Zhang, R.; Zhang, W.; Wang, C.; Zhang, Y.; Wei, X.; Guan, Y.; Liu, J.; Feng, K.; Jing, M.; Wang, X.; Liu, Y.-C.; Mei, Q.; Han, W.; Jiang, Z., Manganese is critical for antitumor immune responses via cGAS-STING and improves the efficacy of clinical immunotherapy. *Cell Research* **2020,** *30* (11), 966-979.
341. Laursen, M. F.; Christensen, E.; Degn, L. L. T.; Jonsson, K.; Jakobsen, M. R.; Agger, R.; Kofod-Olsen, E., CD11c-targeted Delivery of DNA to Dendritic Cells Leads to cGAS- and STING-dependent Maturation. *J Immunother* **2018,** *41* (1), 9-18.
342. Huang, L.; Li, L.; Lemos, H.; Chandler, P. R.; Pacholczyk, G.; Baban, B.; Barber, G. N.; Hayakawa, Y.; McGaha, T. L.; Ravishankar, B.; Munn, D. H.; Mellor, A. L., Cutting edge: DNA sensing via the STING adaptor in myeloid dendritic cells induces potent tolerogenic responses. *J Immunol* **2013,** *191* (7), 3509-13.
343. Zhou, M.; Wang, X.; Lin, S.; Cheng, Y.; Zhao, S.; Lin, J.; Fang, Z.; Lou, Z.; Qin, L.; Wei, H., Multifunctional STING-Activating Mn3 O4 @Au-dsDNA/DOX Nanoparticle for Antitumor Immunotherapy. *Adv Healthc Mater* **2020,** *9* (13), e2000064.
344. Zheng, M.; Xie, L.; Liang, Y.; Wu, S.; Xu, H.; Zhang, Y.; Liu, H.; Lin, D.; Han, J.; Lu, K., Recognition of cytosolic DNA attenuates glucose metabolism and induces AMPK mediated energy stress response. *Int J Biol Sci* **2015,** *11* (5), 587-94.
345. Goldberg, M. S., Improving cancer immunotherapy through nanotechnology. *Nat Rev Cancer* **2019,** *19* (10), 587-602.
346. Riley, R. S.; June, C. H.; Langer, R.; Mitchell, M. J., Delivery technologies for cancer immunotherapy. *Nat Rev Drug Discov* **2019,** *18* (3), 175-196.
347. Waldron, K. J.; Rutherford, J. C.; Ford, D.; Robinson, N. J., Metalloproteins and metal sensing. *Nature* **2009,** *460* (7257), 823-30.
348. Wang, C.; Zhang, R.; Wei, X.; Lv, M.; Jiang, Z., Metalloimmunology: The metal ion-controlled immunity. *Adv Immunol* **2020,** *145*, 187-241.
349. Wang, C.; Guan, Y.; Lv, M.; Zhang, R.; Guo, Z.; Wei, X.; Du, X.; Yang, J.; Li, T.; Wan, Y.; Su, X.; Huang, X.; Jiang, Z., Manganese Increases the Sensitivity of the cGAS-STING Pathway for Double-Stranded DNA and Is Required for the Host Defense against DNA Viruses. *Immunity* **2018,** *48* (4), 675-687 e7.
350. Wang, C.; Sun, Z.; Zhao, C.; Zhang, Z.; Wang, H.; Liu, Y.; Guo, Y.; Zhang, B.; Gu, L.; Yu, Y.; Hu, Y.; Wu, J., Maintaining manganese in tumor to activate cGAS-STING pathway evokes a robust abscopal anti-tumor effect. *J Control Release* **2021,** *331*, 480-490.
351. Hou, L.; Tian, C.; Yan, Y.; Zhang, L.; Zhang, H.; Zhang, Z., Manganese-Based Nanoactivator Optimizes Cancer Immunotherapy via Enhancing Innate Immunity. *ACS Nano* **2020,** *14* (4), 3927-3940.
352. Chen, C.; Tong, Y.; Zheng, Y.; Shi, Y.; Chen, Z.; Li, J.; Liu, X.; Zhang, D.; Yang, H., Cytosolic Delivery of Thiolated Mn-cGAMP Nanovaccine to Enhance the Antitumor Immune Responses. *Small* **2021**, e2006970.
353. Yang, X.; Yang, Y.; Bian, J.; Wei, J.; Wang, Z.; Zhou, Z.; Li, Z.; Sun, M., Converting primary tumor towards an in situ STING-activating vaccine via a biomimetic nanoplatform against recurrent and metastatic tumors. *Nano Today* **2021,** *38*, 101109.
354. Gao, M.; Xie, Y.-Q.; Lei, K.; Zhao, Y.; Kurum, A.; Van Herck, S.; Guo, Y.; Hu, X.; Tang, L., A Manganese Phosphate Nanocluster Activates the cGAS-STING Pathway for Enhanced Cancer Immunotherapy. *Advanced Therapeutics* **2021,** *n/a* (n/a), 2100065.
355. Yoh, S. M.; Schneider, M.; Seifried, J.; Soonthornvacharin, S.; Akleh, R. E.; Olivieri,

K. C.; De Jesus, P. D.; Ruan, C.; de Castro, E.; Ruiz, P. A.; Germanaud, D.; des Portes, V.; Garcia-Sastre, A.; Konig, R.; Chanda, S. K., PQBP1 Is a Proximal Sensor of the cGAS-Dependent Innate Response to HIV-1. *Cell* **2015,** *161* (6), 1293-1305.
356. Lian, H.; Wei, J.; Zang, R.; Ye, W.; Yang, Q.; Zhang, X. N.; Chen, Y. D.; Fu, Y. Z.; Hu, M. M.; Lei, C. Q.; Luo, W. W.; Li, S.; Shu, H. B., ZCCHC3 is a co-sensor of cGAS for dsDNA recognition in innate immune response. *Nat Commun* **2018,** *9* (1), 3349.
357. Liu, Z. S.; Cai, H.; Xue, W.; Wang, M.; Xia, T.; Li, W. J.; Xing, J. Q.; Zhao, M.; Huang, Y. J.; Chen, S.; Wu, S. M.; Wang, X.; Liu, X.; Pang, X.; Zhang, Z. Y.; Li, T.; Dai, J.; Dong, F.; Xia, Q.; Li, A. L.; Zhou, T.; Liu, Z. G.; Zhang, X. M.; Li, T., G3BP1 promotes DNA binding and activation of cGAS. *Nat Immunol* **2019,** *20* (1), 18-28.
358. Zhang, Y.; Ma, Z.; Wang, Y.; Boyer, J.; Ni, G.; Cheng, L.; Su, S.; Zhang, Z.; Zhu, Z.; Qian, J.; Su, L.; Zhang, Q.; Damania, B.; Liu, P., Streptavidin Promotes DNA Binding and Activation of cGAS to Enhance Innate Immunity. *iScience* **2020,** *23* (9), 101463.
359. Moser, B. A.; Escalante-Buendia, Y.; Steinhardt, R. C.; Rosenberger, M. G.; Cassaidy, B. J.; Naorem, N.; Chon, A. C.; Nguyen, M. H.; Tran, N. T.; Esser-Kahn, A. P., Small Molecule NF-kappaB Inhibitors as Immune Potentiators for Enhancement of Vaccine Adjuvants. *Front Immunol* **2020,** *11*, 511513.
360. Onyedibe, K. I.; Wang, M.; Sintim, H. O., ENPP1, an Old Enzyme with New Functions, and Small Molecule Inhibitors-A STING in the Tale of ENPP1. *Molecules* **2019,** *24* (22).
361. Schlee, M.; Hartmann, G., Discriminating self from non-self in nucleic acid sensing. *Nat Rev Immunol* **2016,** *16* (9), 566-80.
362. Iurescia, S.; Fioretti, D.; Rinaldi, M., Nucleic Acid Sensing Machinery: Targeting Innate Immune System for Cancer Therapy. *Recent Pat Anticancer Drug Discov* **2018,** *13* (1), 2-17.
363. Dubensky, T. W., Jr.; Kanne, D. B.; Leong, M. L., Rationale, progress and development of vaccines utilizing STING-activating cyclic dinucleotide adjuvants. *Ther Adv Vaccines* **2013,** *1* (4), 131-43.
364. An, X.; Zhu, Y.; Zheng, T.; Wang, G.; Zhang, M.; Li, J.; Ji, H.; Li, S.; Yang, S.; Xu, D.; Li, Z.; Wang, T.; He, Y.; Zhang, L.; Yang, W.; Zhao, R.; Hao, D.; Li, X., An Analysis of the Expression and Association with Immune Cell Infiltration of the cGAS/STING Pathway in Pan-Cancer. *Mol Ther Nucleic Acids* **2019,** *14*, 80-89.
365. Bruni, D.; Angell, H. K.; Galon, J., The immune contexture and Immunoscore in cancer prognosis and therapeutic efficacy. *Nat Rev Cancer* **2020,** *20* (11), 662-680.
366. Petitprez, F.; Meylan, M.; de Reynies, A.; Sautes-Fridman, C.; Fridman, W. H., The Tumor Microenvironment in the Response to Immune Checkpoint Blockade Therapies. *Front Immunol* **2020,** *11*, 784.
367. Liu, R.; Yang, F.; Yin, J. Y.; Liu, Y. Z.; Zhang, W.; Zhou, H. H., Influence of Tumor Immune Infiltration on Immune Checkpoint Inhibitor Therapeutic Efficacy: A Computational Retrospective Study. *Front Immunol* **2021,** *12*, 685370.
368. Wang-Bishop, L.; Wehbe, M.; Shae, D.; James, J.; Hacker, B. C.; Garland, K.; Chistov, P. P.; Rafat, M.; Balko, J. M.; Wilson, J. T., Potent STING activation stimulates immunogenic cell death to enhance antitumor immunity in neuroblastoma. *J Immunother Cancer* **2020,** *8* (1).
369. Yum, S.; Li, M.; Chen, Z. J., Old dogs, new trick: classic cancer therapies activate cGAS. *Cell Res* **2020,** *30* (8), 639-648.
370. Marloye, M.; Lawler, S. E.; Berger, G., Current patent and clinical status of stimulator of interferon genes (STING) agonists for cancer immunotherapy. *Pharm Pat Anal* **2019,** *8* (4), 87-

90.
371. Ding, C.; Song, Z.; Shen, A.; Chen, T.; Zhang, A., Small molecules targeting the innate immune cGASSTINGTBK1 signaling pathway. *Acta Pharm Sin B* **2020,** *10* (12), 2272-2298.
372. Palanca-Wessels, M. C.; Convertine, A. J.; Cutler-Strom, R.; Booth, G. C.; Lee, F.; Berguig, G. Y.; Stayton, P. S.; Press, O. W., Anti-CD22 antibody targeting of pH-responsive micelles enhances small interfering RNA delivery and gene silencing in lymphoma cells. *Mol Ther* **2011,** *19* (8), 1529-37.
373. Nelson, C. E.; Gupta, M. K.; Adolph, E. J.; Shannon, J. M.; Guelcher, S. A.; Duvall, C. L., Sustained local delivery of siRNA from an injectable scaffold. *Biomaterials* **2012,** *33* (4), 1154-61.
374. Arany, S.; Xu, Q.; Hernady, E.; Benoit, D. S.; Dewhurst, S.; Ovitt, C. E., Pro-apoptotic gene knockdown mediated by nanocomplexed siRNA reduces radiation damage in primary salivary gland cultures. *J Cell Biochem* **2012,** *113* (6), 1955-65.
375. Arany, S.; Benoit, D. S.; Dewhurst, S.; Ovitt, C. E., Nanoparticle-mediated gene silencing confers radioprotection to salivary glands in vivo. *Mol Ther* **2013,** *21* (6), 1182-94.
376. Li, H.; Yu, S. S.; Miteva, M.; Nelson, C. E.; Werfel, T.; Giorgio, T. D.; Duvall, C. L., Matrix Metalloproteinase Responsive, Proximity-activated Polymeric Nanoparticles for siRNA Delivery. *Adv Funct Mater* **2013,** *23* (24), 3040-3052.
377. Nelson, C. E.; Kim, A. J.; Adolph, E. J.; Gupta, M. K.; Yu, F.; Hocking, K. M.; Davidson, J. M.; Guelcher, S. A.; Duvall, C. L., Tunable delivery of siRNA from a biodegradable scaffold to promote angiogenesis in vivo. *Adv Mater* **2014,** *26* (4), 607-14, 506.
378. Li, H.; Miteva, M.; Kirkbride, K. C.; Cheng, M. J.; Nelson, C. E.; Simpson, E. M.; Gupta, M. K.; Duvall, C. L.; Giorgio, T. D., Dual MMP7-proximity-activated and folate receptor-targeted nanoparticles for siRNA delivery. *Biomacromolecules* **2015,** *16* (1), 192-201.
379. Horev, B.; Klein, M. I.; Hwang, G.; Li, Y.; Kim, D.; Koo, H.; Benoit, D. S., pH-activated nanoparticles for controlled topical delivery of farnesol to disrupt oral biofilm virulence. *ACS Nano* **2015,** *9* (3), 2390-404.
380. Martin, J. R.; Nelson, C. E.; Gupta, M. K.; Yu, F.; Sarett, S. M.; Hocking, K. M.; Pollins, A. C.; Nanney, L. B.; Davidson, J. M.; Guelcher, S. A.; Duvall, C. L., Local Delivery of PHD2 siRNA from ROS-Degradable Scaffolds to Promote Diabetic Wound Healing. *Adv Healthc Mater* **2016,** *5* (21), 2751-2757.
381. Zhou, J.; Horev, B.; Hwang, G.; Klein, M. I.; Koo, H.; Benoit, D. S., Characterization and optimization of pH-responsive polymer nanoparticles for drug delivery to oral biofilms. *J Mater Chem B* **2016,** *4* (18), 3075-3085.
382. Wang, Y.; Malcolm, D. W.; Benoit, D. S. W., Controlled and sustained delivery of siRNA/NPs from hydrogels expedites bone fracture healing. *Biomaterials* **2017,** *139*, 127-138.
383. Wang, Y.; Zhang, S.; Benoit, D. S. W., Degradable poly(ethylene glycol) (PEG)-based hydrogels for spatiotemporal control of siRNA/nanoparticle delivery. *J Control Release* **2018,** *287*, 58-66.
384. Garland, K. M.; Sevimli, S.; Kilchrist, K. V.; Duvall, C. L.; Cook, R. S.; Wilson, J. T., Microparticle Depots for Controlled and Sustained Release of Endosomolytic Nanoparticles. *Cell Mol Bioeng* **2019,** *12* (5), 429-442.
385. Putney, S. D.; Benkovic, S. J.; Schimmel, P. R., A DNA fragment with an alpha-phosphorothioate nucleotide at one end is asymmetrically blocked from digestion by exonuclease III and can be replicated in vivo. *Proc Natl Acad Sci U S A* **1981,** *78* (12), 7350-4.
386. Cabral, H.; Matsumoto, Y.; Mizuno, K.; Chen, Q.; Murakami, M.; Kimura, M.;

Terada, Y.; Kano, M. R.; Miyazono, K.; Uesaka, M.; Nishiyama, N.; Kataoka, K., Accumulation of sub-100 nm polymeric micelles in poorly permeable tumours depends on size. *Nat Nanotechnol* **2011,** *6* (12), 815-23.
387. Pezzoli, D.; Giupponi, E.; Mantovani, D.; Candiani, G., Size matters for in vitro gene delivery: investigating the relationships among complexation protocol, transfection medium, size and sedimentation. *Sci Rep* **2017,** *7*, 44134.
388. Kreiss, P.; Cameron, B.; Rangara, R.; Mailhe, P.; Aguerre-Charriol, O.; Airiau, M.; Scherman, D.; Crouzet, J.; Pitard, B., Plasmid DNA size does not affect the physicochemical properties of lipoplexes but modulates gene transfer efficiency. *Nucleic Acids Res* **1999,** *27* (19), 3792-8.
389. Wiser, C.; Kim, B.; Vincent, J.; Ascano, M., Small molecule inhibition of human cGAS reduces total cGAMP output and cytokine expression in cells. *Sci Rep* **2020,** *10* (1), 7604.
390. Wei, X.; Shao, B.; He, Z.; Ye, T.; Luo, M.; Sang, Y.; Liang, X.; Wang, W.; Luo, S.; Yang, S.; Zhang, S.; Gong, C.; Gou, M.; Deng, H.; Zhao, Y.; Yang, H.; Deng, S.; Zhao, C.; Yang, L.; Qian, Z.; Li, J.; Sun, X.; Han, J.; Jiang, C.; Wu, M.; Zhang, Z., Cationic nanocarriers induce cell necrosis through impairment of Na(+)/K(+)-ATPase and cause subsequent inflammatory response. *Cell Res* **2015,** *25* (2), 237-53.
391. Liu, L.; Liu, Y.; Xu, B.; Liu, C.; Jia, Y.; Liu, T.; Fang, C.; Wang, W.; Ren, J.; He, Z.; Men, K.; Liang, X.; Luo, M.; Shao, B.; Mao, Y.; Xiao, H.; Qian, Z.; Geng, J.; Dong, B.; Mi, P.; Jiang, Y.; Wei, Y.; Wei, X., Negative regulation of cationic nanoparticle-induced inflammatory toxicity through the increased production of prostaglandin E2 via mitochondrial DNA-activated Ly6C(+) monocytes. *Theranostics* **2018,** *8* (11), 3138-3152.
392. Balka, K. R.; De Nardo, D., Molecular and spatial mechanisms governing STING signalling. *FEBS J* **2020**.
393. de Oliveira Mann, C. C.; Orzalli, M. H.; King, D. S.; Kagan, J. C.; Lee, A. S. Y.; Kranzusch, P. J., Modular Architecture of the STING C-Terminal Tail Allows Interferon and NF-kappaB Signaling Adaptation. *Cell Rep* **2019,** *27* (4), 1165-1175 e5.
394. Krieg, A. M., CpG motifs in bacterial DNA and their immune effects. *Annu Rev Immunol* **2002,** *20*, 709-60.
395. Krieg, A. M.; Wu, T.; Weeratna, R.; Efler, S. M.; Love-Homan, L.; Yang, L.; Yi, A. K.; Short, D.; Davis, H. L., Sequence motifs in adenoviral DNA block immune activation by stimulatory CpG motifs. *Proc Natl Acad Sci U S A* **1998,** *95* (21), 12631-6.
396. Lee, J.; Sohn, J. W.; Zhang, Y.; Leong, K. W.; Pisetsky, D.; Sullenger, B. A., Nucleic acid-binding polymers as anti-inflammatory agents. *Proc Natl Acad Sci U S A* **2011,** *108* (34), 14055-60.
397. Jackman, J. G.; Juwarker, H.; Poveromo, L. P.; Levinson, H.; Leong, K. W.; Sullenger, B. A., Polycationic Nanofibers for Nucleic Acid Scavenging. *Biomacromolecules* **2016,** *17* (11), 3706-3713.
398. Kawai, T.; Akira, S., Signaling to NF-kappaB by Toll-like receptors. *Trends Mol Med* **2007,** *13* (11), 460-9.
399. Hacker, H.; Mischak, H.; Miethke, T.; Liptay, S.; Schmid, R.; Sparwasser, T.; Heeg, K.; Lipford, G. B.; Wagner, H., CpG-DNA-specific activation of antigen-presenting cells requires stress kinase activity and is preceded by non-specific endocytosis and endosomal maturation. *EMBO J* **1998,** *17* (21), 6230-40.
400. Wilson, J. T.; Keller, S.; Manganiello, M. J.; Cheng, C.; Lee, C. C.; Opara, C.; Convertine, A.; Stayton, P. S., pH-Responsive nanoparticle vaccines for dual-delivery of

antigens and immunostimulatory oligonucleotides. *ACS Nano* **2013,** *7* (5), 3912-25.
401. Kosuri, S.; Church, G. M., Large-scale de novo DNA synthesis: technologies and applications. *Nat Methods* **2014,** *11* (5), 499-507.
402. Shivalingam, A.; Brown, T., Synthesis of chemically modified DNA. *Biochem Soc Trans* **2016,** *44* (3), 709-15.
403. Napirei, M.; Karsunky, H.; Zevnik, B.; Stephan, H.; Mannherz, H. G.; Moroy, T., Features of systemic lupus erythematosus in Dnase1-deficient mice. *Nat Genet* **2000,** *25* (2), 177-81.
404. Prince, W. S.; Baker, D. L.; Dodge, A. H.; Ahmed, A. E.; Chestnut, R. W.; Sinicropi, D. V., Pharmacodynamics of recombinant human DNase I in serum. *Clin Exp Immunol* **1998,** *113* (2), 289-96.
405. Steinhagen, F.; Zillinger, T.; Peukert, K.; Fox, M.; Thudium, M.; Barchet, W.; Putensen, C.; Klinman, D.; Latz, E.; Bode, C., Suppressive oligodeoxynucleotides containing TTAGGG motifs inhibit cGAS activation in human monocytes. *Eur J Immunol* **2018,** *48* (4), 605-611.
406. Counis, M. F.; Torriglia, A., Acid DNases and their interest among apoptotic endonucleases. *Biochimie* **2006,** *88* (12), 1851-8.
407. Roberts, T. C.; Langer, R.; Wood, M. J. A., Advances in oligonucleotide drug delivery. *Nat Rev Drug Discov* **2020,** *19* (10), 673-694.
408. de la Harpe, K. M.; Kondiah, P. P. D.; Choonara, Y. E.; Marimuthu, T.; du Toit, L. C.; Pillay, V., The Hemocompatibility of Nanoparticles: A Review of Cell-Nanoparticle Interactions and Hemostasis. *Cells* **2019,** *8* (10).
409. Melero, I.; Castanon, E.; Alvarez, M.; Champiat, S.; Marabelle, A., Intratumoural administration and tumour tissue targeting of cancer immunotherapies. *Nat Rev Clin Oncol* **2021**.
410. Peynshaert, K.; Manshian, B. B.; Joris, F.; Braeckmans, K.; De Smedt, S. C.; Demeester, J.; Soenen, S. J., Exploiting intrinsic nanoparticle toxicity: the pros and cons of nanoparticle-induced autophagy in biomedical research. *Chem Rev* **2014,** *114* (15), 7581-609.
411. Waldman, A. D.; Fritz, J. M.; Lenardo, M. J., A guide to cancer immunotherapy: from T cell basic science to clinical practice. *Nat Rev Immunol* **2020,** *20* (11), 651-668.
412. Bourquin, C.; Anz, D.; Zwiorek, K.; Lanz, A. L.; Fuchs, S.; Weigel, S.; Wurzenberger, C.; von der Borch, P.; Golic, M.; Moder, S.; Winter, G.; Coester, C.; Endres, S., Targeting CpG oligonucleotides to the lymph node by nanoparticles elicits efficient antitumoral immunity. *J Immunol* **2008,** *181* (5), 2990-8.
413. Liu, H.; Moynihan, K. D.; Zheng, Y.; Szeto, G. L.; Li, A. V.; Huang, B.; Van Egeren, D. S.; Park, C.; Irvine, D. J., Structure-based programming of lymph-node targeting in molecular vaccines. *Nature* **2014,** *507* (7493), 519-22.
414. Li, S.; Luo, M.; Wang, Z.; Feng, Q.; Wilhelm, J.; Wang, X.; Li, W.; Wang, J.; Cholka, A.; Fu, Y. X.; Sumer, B. D.; Yu, H.; Gao, J., Prolonged activation of innate immune pathways by a polyvalent STING agonist. *Nat Biomed Eng* **2021,** *5* (5), 455-466.
415. Franklin, D. A.; Sharick, J. T.; Ericsson-Gonzalez, P. I.; Sanchez, V.; Dean, P. T.; Opalenik, S. R.; Cairo, S.; Judde, J. G.; Lewis, M. T.; Chang, J. C.; Sanders, M. E.; Cook, R. S.; Skala, M. C.; Bordeaux, J.; Orozco Bender, J.; Vaupel, C.; Geiss, G.; Hinerfeld, D.; Balko, J. M., MEK activation modulates glycolysis and supports suppressive myeloid cells in TNBC. *JCI Insight* **2020,** *5* (15).
416. Liu, C.; Lou, Y.; Lizee, G.; Qin, H.; Liu, S.; Rabinovich, B.; Kim, G. J.; Wang, Y. H.; Ye, Y.; Sikora, A. G.; Overwijk, W. W.; Liu, Y. J.; Wang, G.; Hwu, P., Plasmacytoid

dendritic cells induce NK cell-dependent, tumor antigen-specific T cell cross-priming and tumor regression in mice. *J Clin Invest* **2008,** *118* (3), 1165-75.
417. Ribas, A.; Medina, T.; Kirkwood, J. M.; Zakharia, Y.; Gonzalez, R.; Davar, D.; Chmielowski, B.; Campbell, K. M.; Bao, R.; Kelley, H.; Morris, A.; Mauro, D.; Wooldridge, J. E.; Luke, J. J.; Weiner, G. J.; Krieg, A. M.; Milhem, M. M., Overcoming PD-1 Blockade Resistance With CpG-A Toll-Like Receptor 9 Agonist Vidutolimod in Patients With Metastatic Melanoma. *Cancer Discovery* **2021**, candisc.0425.2021.
418. Hornung, V.; Rothenfusser, S.; Britsch, S.; Krug, A.; Jahrsdorfer, B.; Giese, T.; Endres, S.; Hartmann, G., Quantitative expression of toll-like receptor 1-10 mRNA in cellular subsets of human peripheral blood mononuclear cells and sensitivity to CpG oligodeoxynucleotides. *J Immunol* **2002,** *168* (9), 4531-7.
419. Uhlen, M.; Fagerberg, L.; Hallstrom, B. M.; Lindskog, C.; Oksvold, P.; Mardinoglu, A.; Sivertsson, A.; Kampf, C.; Sjostedt, E.; Asplund, A.; Olsson, I.; Edlund, K.; Lundberg, E.; Navani, S.; Szigyarto, C. A.; Odeberg, J.; Djureinovic, D.; Takanen, J. O.; Hober, S.; Alm, T.; Edqvist, P. H.; Berling, H.; Tegel, H.; Mulder, J.; Rockberg, J.; Nilsson, P.; Schwenk, J. M.; Hamsten, M.; von Feilitzen, K.; Forsberg, M.; Persson, L.; Johansson, F.; Zwahlen, M.; von Heijne, G.; Nielsen, J.; Ponten, F., Proteomics. Tissue-based map of the human proteome. *Science* **2015,** *347* (6220), 1260419.
420. Uhlen, M.; Zhang, C.; Lee, S.; Sjostedt, E.; Fagerberg, L.; Bidkhori, G.; Benfeitas, R.; Arif, M.; Liu, Z.; Edfors, F.; Sanli, K.; von Feilitzen, K.; Oksvold, P.; Lundberg, E.; Hober, S.; Nilsson, P.; Mattsson, J.; Schwenk, J. M.; Brunnstrom, H.; Glimelius, B.; Sjoblom, T.; Edqvist, P. H.; Djureinovic, D.; Micke, P.; Lindskog, C.; Mardinoglu, A.; Ponten, F., A pathology atlas of the human cancer transcriptome. *Science* **2017,** *357* (6352).
421. Verrier, E. R.; Langevin, C., Cyclic Guanosine Monophosphate-Adenosine Monophosphate Synthase (cGAS), a Multifaceted Platform of Intracellular DNA Sensing. *Front Immunol* **2021,** *12*, 637399.
422. Zhou, C.; Chen, X.; Planells-Cases, R.; Chu, J.; Wang, L.; Cao, L.; Li, Z.; Lopez-Cayuqueo, K. I.; Xie, Y.; Ye, S.; Wang, X.; Ullrich, F.; Ma, S.; Fang, Y.; Zhang, X.; Qian, Z.; Liang, X.; Cai, S. Q.; Jiang, Z.; Zhou, D.; Leng, Q.; Xiao, T. S.; Lan, K.; Yang, J.; Li, H.; Peng, C.; Qiu, Z.; Jentsch, T. J.; Xiao, H., Transfer of cGAMP into Bystander Cells via LRRC8 Volume-Regulated Anion Channels Augments STING-Mediated Interferon Responses and Anti-viral Immunity. *Immunity* **2020,** *52* (5), 767-781 e6.
423. Lahey, L. J.; Mardjuki, R. E.; Wen, X.; Hess, G. T.; Ritchie, C.; Carozza, J. A.; Bohnert, V.; Maduke, M.; Bassik, M. C.; Li, L., LRRC8A:C/E Heteromeric Channels Are Ubiquitous Transporters of cGAMP. *Mol Cell* **2020,** *80* (4), 578-591 e5.
424. Chipurupalli, S.; Ganesan, R.; Dhanabal, S. P.; Kumar, M. S.; Robinson, N., Pharmacological STING Activation Is a Potential Alternative to Overcome Drug-Resistance in Melanoma. *Front Oncol* **2020,** *10*, 758.
425. Knight, F. C.; Gilchuk, P.; Kumar, A.; Becker, K. W.; Sevimli, S.; Jacobson, M. E.; Suryadevara, N.; Wang-Bishop, L.; Boyd, K. L.; Crowe, J. E., Jr.; Joyce, S.; Wilson, J. T., Mucosal Immunization with a pH-Responsive Nanoparticle Vaccine Induces Protective CD8(+) Lung-Resident Memory T Cells. *ACS Nano* **2019,** *13* (10), 10939-10960.
426. Liang, H.; Deng, L.; Hou, Y.; Meng, X.; Huang, X.; Rao, E.; Zheng, W.; Mauceri, H.; Mack, M.; Xu, M.; Fu, Y. X.; Weichselbaum, R. R., Host STING-dependent MDSC mobilization drives extrinsic radiation resistance. *Nat Commun* **2017,** *8* (1), 1736.
427. Overberger, C. G., Macromolecular syntheses. In *Poly(2-Ethylacrylic Acid)*, Ferritto, M.

T., D.A., Ed. Wiley.: New York,, p 13 volumes.
428. Hartmann, G., Nucleic Acid Immunity. *Adv Immunol* **2017,** *133*, 121-169.
429. Chen, N.; Xia, P.; Li, S.; Zhang, T.; Wang, T. T.; Zhu, J., RNA sensors of the innate immune system and their detection of pathogens. *IUBMB Life* **2017,** *69* (5), 297-304.
430. Chow, K. T.; Gale, M., Jr.; Loo, Y. M., RIG-I and Other RNA Sensors in Antiviral Immunity. *Annu Rev Immunol* **2018,** *36*, 667-694.
431. Uehata, T.; Takeuchi, O., RNA Recognition and Immunity-Innate Immune Sensing and Its Posttranscriptional Regulation Mechanisms. *Cells* **2020,** *9* (7).
432. McWhirter, S. M.; Jefferies, C. A., Nucleic Acid Sensors as Therapeutic Targets for Human Disease. *Immunity* **2020,** *53* (1), 78-97.
433. Samuel, C. E., Adenosine deaminase acting on RNA (ADAR1), a suppressor of double-stranded RNA-triggered innate immune responses. *J Biol Chem* **2019,** *294* (5), 1710-1720.
434. Garland, K. M.; Rosch, J. C.; Carson, C. S.; Wang-Bishop, L.; Hanna, A.; Sevimli, S.; Van Kaer, C.; Balko, J. M.; Ascano, M.; Wilson, J. T., Pharmacological Activation of cGAS for Cancer Immunotherapy. *Frontiers in Immunology* **2021,** *12* (4843).
435. Wu, S. Y.; Lopez-Berestein, G.; Calin, G. A.; Sood, A. K., RNAi therapies: drugging the undruggable. *Sci Transl Med* **2014,** *6* (240), 240ps7.
436. Ozcan, G.; Ozpolat, B.; Coleman, R. L.; Sood, A. K.; Lopez-Berestein, G., Preclinical and clinical development of siRNA-based therapeutics. *Adv Drug Deliv Rev* **2015,** *87*, 108-19.
437. Zhu, X.; Nishimura, F.; Sasaki, K.; Fujita, M.; Dusak, J. E.; Eguchi, J.; Fellows-Mayle, W.; Storkus, W. J.; Walker, P. R.; Salazar, A. M.; Okada, H., Toll like receptor-3 ligand poly-ICLC promotes the efficacy of peripheral vaccinations with tumor antigen-derived peptide epitopes in murine CNS tumor models. *J Transl Med* **2007,** *5*, 10.
438. Cooper, C.; Mackie, D., Hepatitis B surface antigen-1018 ISS adjuvant-containing vaccine: a review of HEPLISAV safety and efficacy. *Expert Rev Vaccines* **2011,** *10* (4), 417-27.
439. Jiang, W.; Zhu, F. G.; Bhagat, L.; Yu, D.; Tang, J. X.; Kandimalla, E. R.; La Monica, N.; Agrawal, S., A Toll-like receptor 7, 8, and 9 antagonist inhibits Th1 and Th17 responses and inflammasome activation in a model of IL-23-induced psoriasis. *J Invest Dermatol* **2013,** *133* (7), 1777-84.
440. Iurescia, S.; Fioretti, D.; Rinaldi, M., Targeting Cytosolic Nucleic Acid-Sensing Pathways for Cancer Immunotherapies. *Front Immunol* **2018,** *9*, 711.
441. Fire, A.; Xu, S.; Montgomery, M. K.; Kostas, S. A.; Driver, S. E.; Mello, C. C., Potent and specific genetic interference by double-stranded RNA in Caenorhabditis elegans. *Nature* **1998,** *391* (6669), 806-11.
442. Sioud, M., RNA interference: mechanisms, technical challenges, and therapeutic opportunities. *Methods Mol Biol* **2015,** *1218*, 1-15.
443. Zhu, F. G.; Jiang, W.; Bhagat, L.; Wang, D.; Yu, D.; Tang, J. X.; Kandimalla, E. R.; La Monica, N.; Agrawal, S., A novel antagonist of Toll-like receptors 7, 8 and 9 suppresses lupus disease-associated parameters in NZBW/F1 mice. *Autoimmunity* **2013,** *46* (7), 419-28.
444. van den Boorn, J. G.; Barchet, W.; Hartmann, G., Nucleic acid adjuvants: toward an educated vaccine. *Advances in immunology* **2012,** *114*, 1-32.
445. Poeck, H.; Besch, R.; Maihoefer, C.; Renn, M.; Tormo, D.; Morskaya, S. S.; Kirschnek, S.; Gaffal, E.; Landsberg, J.; Hellmuth, J.; Schmidt, A.; Anz, D.; Bscheider, M.; Schwerd, T.; Berking, C.; Bourquin, C.; Kalinke, U.; Kremmer, E.; Kato, H.; Akira, S.; Meyers, R.; Häcker, G.; Neuenhahn, M.; Busch, D.; Ruland, J.; Rothenfusser, S.; Prinz, M.; Hornung, V.; Endres, S.; Tüting, T.; Hartmann, G., 5′-triphosphate-siRNA: turning gene

silencing and RIG-I activation against melanoma. *Nature Medicine* **2008,** *14* (11), 1256-1263.
446. Radovic-Moreno, A. F.; Chernyak, N.; Mader, C. C.; Nallagatla, S.; Kang, R. S.; Hao, L.; Walker, D. A.; Halo, T. L.; Merkel, T. J.; Rische, C. H.; Anantatmula, S.; Burkhart, M.; Mirkin, C. A.; Gryaznov, S. M., Immunomodulatory spherical nucleic acids. *Proc Natl Acad Sci U S A* **2015,** *112* (13), 3892-7.
447. Bobbin, M. L.; Rossi, J. J., RNA Interference (RNAi)-Based Therapeutics: Delivering on the Promise? *Annu Rev Pharmacol Toxicol* **2016,** *56*, 103-22.
448. Wang, L. L.; Burdick, J. A., Engineered Hydrogels for Local and Sustained Delivery of RNA-Interference Therapies. *Adv Healthc Mater* **2017,** *6* (1).
449. Johannes, L.; Lucchino, M., Current Challenges in Delivery and Cytosolic Translocation of Therapeutic RNAs. *Nucleic Acid Ther* **2018,** *28* (3), 178-193.
450. Smith, S. A.; Selby, L. I.; Johnston, A. P. R.; Such, G. K., The Endosomal Escape of Nanoparticles: Towards More Efficient Cellular Delivery. *Bioconjug Chem* **2018**.
451. Aliabadi, H. M., 3 - Natural polymers in nucleic acid delivery. In *Polymers and Nanomaterials for Gene Therapy*, Narain, R., Ed. Woodhead Publishing: 2016; pp 55-80.
452. Krhac Levacic, A.; Morys, S.; Wagner, E., Solid-phase supported design of carriers for therapeutic nucleic acid delivery. *Biosci Rep* **2017,** *37* (5).
453. Sarett, S. M.; Nelson, C. E.; Duvall, C. L., Technologies for controlled, local delivery of siRNA. *J Control Release* **2015,** *218*, 94-113.
454. Convertine, A. J.; Diab, C.; Prieve, M.; Paschal, A.; Hoffman, A. S.; Johnson, P. H.; Stayton, P. S., pH-Responsive Polymeric Micelle Carriers for siRNA Drugs. *Biomacromolecules* **2010,** *11* (11), 2904-2910.
455. Malcolm, D. W.; Freeberg, M. A. T.; Wang, Y.; Sims, K. R., Jr.; Awad, H. A.; Benoit, D. S. W., Diblock Copolymer Hydrophobicity Facilitates Efficient Gene Silencing and Cytocompatible Nanoparticle-Mediated siRNA Delivery to Musculoskeletal Cell Types. *Biomacromolecules* **2017,** *18* (11), 3753-3765.
456. Wilson, J. T.; Keller, S.; Manganiello, M. J.; Cheng, C.; Lee, C.-C.; Opara, C.; Convertine, A.; Stayton, P. S., pH-Responsive Nanoparticle Vaccines for Dual-Delivery of Antigens and Immunostimulatory Oligonucleotides. *ACS Nano* **2013,** *7* (5), 3912-3925.
457. Milling, L.; Zhang, Y.; Irvine, D. J., Delivering safer immunotherapies for cancer. *Adv Drug Deliv Rev* **2017,** *114*, 79-101.
458. National Center for, I.; Respiratory, D., General recommendations on immunization --- recommendations of the Advisory Committee on Immunization Practices (ACIP). *MMWR Recomm Rep* **2011,** *60* (2), 1-64.
459. Zhang, L.; Wang, W.; Wang, S., Effect of vaccine administration modality on immunogenicity and efficacy. *Expert Rev Vaccines* **2015,** *14* (11), 1509-23.
460. Senti, G.; Freiburghaus, A. U.; Larenas-Linnemann, D.; Hoffmann, H. J.; Patterson, A. M.; Klimek, L.; Di Bona, D.; Pfaar, O.; Ahlbeck, L.; Akdis, M.; Weinfeld, D.; Contreras-Verduzco, F. A.; Pedroza-Melendez, A.; Skaarup, S. H.; Lee, S. M.; Cardell, L. O.; Schmid, J. M.; Westin, U.; Dollner, R.; Kundig, T. M., Intralymphatic Immunotherapy: Update and Unmet Needs. *Int Arch Allergy Immunol* **2019,** *178* (2), 141-149.
461. van den Boorn, J. G.; Hartmann, G., Turning Tumors into Vaccines: Co-opting the Innate Immune System. *Immunity* **2013,** *39* (1), 27-37.
462. Marabelle, A.; Kohrt, H.; Caux, C.; Levy, R., Intratumoral immunization: a new paradigm for cancer therapy. *Clin Cancer Res* **2014,** *20* (7), 1747-56.
463. Langer, R., Drug delivery and targeting. *Nature* **1998,** *392* (6679 Suppl), 5-10.

464. Wu-Pong, S.; Rojanasakul, Y., *Biopharmaceutical drug design and development*. 2nd ed.; Humana Press: Totowa, NJ, 2008; p x, 375 p.
465. Bartlett, D. W.; Davis, M. E., Insights into the kinetics of siRNA-mediated gene silencing from live-cell and live-animal bioluminescent imaging. *Nucleic Acids Res* **2006,** *34* (1), 322-33.
466. Beyranvand Nejad, E.; Welters, M. J.; Arens, R.; van der Burg, S. H., The importance of correctly timing cancer immunotherapy. *Expert Opin Biol Ther* **2017,** *17* (1), 87-103.
467. Young, K. H.; Baird, J. R.; Savage, T.; Cottam, B.; Friedman, D.; Bambina, S.; Messenheimer, D. J.; Fox, B.; Newell, P.; Bahjat, K. S.; Gough, M. J.; Crittenden, M. R., Optimizing Timing of Immunotherapy Improves Control of Tumors by Hypofractionated Radiation Therapy. *PLoS One* **2016,** *11* (6), e0157164.
468. Yan, J.; Wang, Z.-Y.; Yang, H.-Z.; Liu, H.-Z.; Mi, S.; Lv, X.-X.; Fu, X.-M.; Yan, H.-M.; Zhang, X.-W.; Zhan, Q.-M.; Hu, Z.-W., Timing Is Critical for an Effective Anti-Metastatic Immunotherapy: The Decisive Role of IFNγ/STAT1-Mediated Activation of Autophagy. *PLOS ONE* **2011,** *6* (9), e24705.
469. Kwong, B.; Gai, S. A.; Elkhader, J.; Wittrup, K. D.; Irvine, D. J., Localized immunotherapy via liposome-anchored Anti-CD137 + IL-2 prevents lethal toxicity and elicits local and systemic antitumor immunity. *Cancer Research* **2013,** *73* (5), 1547-1558.
470. Jewell, C. M.; López, S. C. B.; Irvine, D. J., In situ engineering of the lymph node microenvironment via intranodal injection of adjuvant-releasing polymer particles. *Proceedings of the National Academy of Sciences* **2011,** *108* (38), 15745-15750.
471. Ali, O. A.; Huebsch, N.; Cao, L.; Dranoff, G.; Mooney, D. J., Infection-mimicking materials to program dendritic cells in situ. *Nature Materials* **2009,** *8* (2), 151-158.
472. Wang, C.; Sun, W.; Wright, G.; Wang, A. Z.; Gu, Z., Inflammation-Triggered Cancer Immunotherapy by Programmed Delivery of CpG and Anti-PD1 Antibody. *Adv Mater* **2016,** *28* (40), 8912-8920.
473. Nishikawa, M.; Mizuno, Y.; Mohri, K.; Matsuoka, N.; Rattanakiat, S.; Takahashi, Y.; Funabashi, H.; Luo, D.; Takakura, Y., Biodegradable CpG DNA hydrogels for sustained delivery of doxorubicin and immunostimulatory signals in tumor-bearing mice. *Biomaterials* **2011,** *32* (2), 488-94.
474. Ali, O. A.; Verbeke, C.; Johnson, C.; Sands, R. W.; Lewin, S. A.; White, D.; Doherty, E.; Dranoff, G.; Mooney, D. J., Identification of immune factors regulating antitumor immunity using polymeric vaccines with multiple adjuvants. *Cancer Res* **2014,** *74* (6), 1670-81.
475. Pannier, A. K.; Shea, L. D., Controlled release systems for DNA delivery. *Mol Ther* **2004,** *10* (1), 19-26.
476. Rathbone, M. J.; Hadgraft, J.; Roberts, M. S., *Modified-Release Drug Delivery Technology*. Taylor & Francis: 2002.
477. Brudno, Y.; Mooney, D. J., On-demand drug delivery from local depots. *J Control Release* **2015,** *219*, 8-17.
478. Nelson, C. E.; Gupta, M. K.; Adolph, E. J.; Shannon, J. M.; Guelcher, S. A.; Duvall, C. L., Sustained local delivery of siRNA from an injectable scaffold. *Biomaterials* **2012,** *33* (4), 1154-1161.
479. Danhier, F.; Ansorena, E.; Silva, J. M.; Coco, R.; Le Breton, A.; Preat, V., PLGA-based nanoparticles: an overview of biomedical applications. *J Control Release* **2012,** *161* (2), 505-22.
480. Makadia, H. K.; Siegel, S. J., Poly Lactic-co-Glycolic Acid (PLGA) as Biodegradable Controlled Drug Delivery Carrier. *Polymers (Basel)* **2011,** *3* (3), 1377-1397.

481. Han, F. Y.; Thurecht, K. J.; Whittaker, A. K.; Smith, M. T., Bioerodable PLGA-Based Microparticles for Producing Sustained-Release Drug Formulations and Strategies for Improving Drug Loading. *Front Pharmacol* **2016,** *7*, 185.
482. Cohen, H.; Levy, R. J.; Gao, J.; Fishbein, I.; Kousaev, V.; Sosnowski, S.; Slomkowski, S.; Golomb, G., Sustained delivery and expression of DNA encapsulated in polymeric nanoparticles. *Gene Ther* **2000,** *7* (22), 1896-905.
483. Cun, D.; Foged, C.; Yang, M.; Frokjaer, S.; Nielsen, H. M., Preparation and characterization of poly(DL-lactide-co-glycolide) nanoparticles for siRNA delivery. *Int J Pharm* **2010,** *390* (1), 70-5.
484. Cun, D.; Jensen, D. K.; Maltesen, M. J.; Bunker, M.; Whiteside, P.; Scurr, D.; Foged, C.; Nielsen, H. M., High loading efficiency and sustained release of siRNA encapsulated in PLGA nanoparticles: quality by design optimization and characterization. *Eur J Pharm Biopharm* **2011,** *77* (1), 26-35.
485. Khan, A.; Benboubetra, M.; Sayyed, P. Z.; Ng, K. W.; Fox, S.; Beck, G.; Benter, I. F.; Akhtar, S., Sustained polymeric delivery of gene silencing antisense ODNs, siRNA, DNAzymes and ribozymes: in vitro and in vivo studies. *J Drug Target* **2004,** *12* (6), 393-404.
486. Langer, R.; Tirrell, D. A., Designing materials for biology and medicine. *Nature* **2004,** *428* (6982), 487-92.
487. Luby, T. M.; Cole, G.; Baker, L.; Kornher, J. S.; Ramstedt, U.; Hedley, M. L., Repeated immunization with plasmid DNA formulated in poly(lactide-co-glycolide) microparticles is well tolerated and stimulates durable T cell responses to the tumor-associated antigen cytochrome P450 1B1. *Clin Immunol* **2004,** *112* (1), 45-53.
488. Luten, J.; van Nostrum, C. F.; De Smedt, S. C.; Hennink, W. E., Biodegradable polymers as non-viral carriers for plasmid DNA delivery. *J Control Release* **2008,** *126* (2), 97-110.
489. Wang, D.; Robinson, D. R.; Kwon, G. S.; Samuel, J., Encapsulation of plasmid DNA in biodegradable poly(D, L-lactic-co-glycolic acid) microspheres as a novel approach for immunogene delivery. *J Control Release* **1999,** *57* (1), 9-18.
490. Chang, E.; McClellan, A. J.; Farley, W. J.; Li, D. Q.; Pflugfelder, S. C.; De Paiva, C. S., Biodegradable PLGA-Based Drug Delivery Systems for Modulating Ocular Surface Disease under Experimental Murine Dry Eye. *J Clin Exp Ophthalmol* **2011,** *2* (11).
491. Frauke Pistel, K.; Breitenbach, A.; Zange-Volland, R.; Kissel, T., Brush-like branched biodegradable polyesters, part III. Protein release from microspheres of poly(vinyl alcohol)-graft-poly(D,L-lactic-co-glycolic acid). *J Control Release* **2001,** *73* (1), 7-20.
492. Ogawa, Y.; Yamamoto, M.; Okada, H.; Yashiki, T.; Shimamoto, T., A new technique to efficiently entrap leuprolide acetate into microcapsules of polylactic acid or copoly(lactic/glycolic) acid. *Chem Pharm Bull (Tokyo)* **1988,** *36* (3), 1095-103.
493. Mao, S.; Xu, J.; Cai, C.; Germershaus, O.; Schaper, A.; Kissel, T., Effect of WOW process parameters on morphology and burst release of FITC-dextran loaded PLGA microspheres. *Int J Pharm* **2007,** *334* (1-2), 137-48.
494. Patil, Y.; Panyam, J., Polymeric nanoparticles for siRNA delivery and gene silencing. *Int J Pharm* **2009,** *367* (1-2), 195-203.
495. Pantazis, P.; Dimas, K.; Wyche, J. H.; Anant, S.; Houchen, C. W.; Panyam, J.; Ramanujam, R. P., Preparation of siRNA-encapsulated PLGA nanoparticles for sustained release of siRNA and evaluation of encapsulation efficiency. *Methods Mol Biol* **2012,** *906*, 311-9.
496. Woodrow, K. A.; Cu, Y.; Booth, C. J.; Saucier-Sawyer, J. K.; Wood, M. J.; Saltzman,

W. M., Intravaginal gene silencing using biodegradable polymer nanoparticles densely loaded with small-interfering RNA. *Nature Materials* **2009,** *8* (6), 526-533.
497. Amar-Lewis, E.; Azagury, A.; Chintakunta, R.; Goldbart, R.; Traitel, T.; Prestwood, J.; Landesman-Milo, D.; Peer, D.; Kost, J., Quaternized starch-based carrier for siRNA delivery: from cellular uptake to gene silencing. *J Control Release* **2014,** *185*, 109-20.
498. Brody, J. D.; Ai, W. Z.; Czerwinski, D. K.; Torchia, J. A.; Levy, M.; Advani, R. H.; Kim, Y. H.; Hoppe, R. T.; Knox, S. J.; Shin, L. K.; Wapnir, I.; Tibshirani, R. J.; Levy, R., In situ vaccination with a TLR9 agonist induces systemic lymphoma regression: a phase I/II study. *J Clin Oncol* **2010,** *28* (28), 4324-32.
499. Aznar, M. A.; Tinari, N.; Rullan, A. J.; Sanchez-Paulete, A. R.; Rodriguez-Ruiz, M. E.; Melero, I., Intratumoral Delivery of Immunotherapy-Act Locally, Think Globally. *J Immunol* **2017,** *198* (1), 31-39.
500. Hammerich, L.; Binder, A.; Brody, J. D., In situ vaccination: Cancer immunotherapy both personalized and off-the-shelf. *Mol Oncol* **2015,** *9* (10), 1966-81.
501. Chen, Q.; Wang, C.; Zhang, X.; Chen, G.; Hu, Q.; Li, H.; Wang, J.; Wen, D.; Zhang, Y.; Lu, Y.; Yang, G.; Jiang, C.; Wang, J.; Dotti, G.; Gu, Z., In situ sprayed bioresponsive immunotherapeutic gel for post-surgical cancer treatment. *Nature Nanotechnology* **2019,** *14* (1), 89-97.
502. Park, C. G.; Hartl, C. A.; Schmid, D.; Carmona, E. M.; Kim, H. J.; Goldberg, M. S., Extended release of perioperative immunotherapy prevents tumor recurrence and eliminates metastases. *Sci Transl Med* **2018,** *10* (433).
503. Kwong, B.; Liu, H.; Irvine, D. J., Induction of potent anti-tumor responses while eliminating systemic side effects via liposome-anchored combinatorial immunotherapy. *Biomaterials* **2011,** *32* (22), 5134-5147.
504. Ishihara, J.; Fukunaga, K.; Ishihara, A.; Larsson, H. M.; Potin, L.; Hosseinchi, P.; Galliverti, G.; Swartz, M. A.; Hubbell, J. A., Matrix-binding checkpoint immunotherapies enhance antitumor efficacy and reduce adverse events. *Sci Transl Med* **2017,** *9* (415).
505. Ferritto, M. S.; Tirrell, D. A., Photoregulation of the binding of an azobenzene-modified poly(methacrylic acid) to phosphatidylcholine bilayer membranes. *Biomaterials* **1990,** *11* (9), 645-51.
506. McGinity, J. W.; O'Donnell, P. B., Preparation of microspheres by the solvent evaporation technique. *Adv Drug Deliv Rev* **1997,** *28* (1), 25-42.
507. Turley, J. L.; Moran, H. B. T.; McEntee, C. P.; O'Grady, K.; Munoz-Wolf, N.; Jin, L.; Follmann, F.; Andersen, P.; Andersson, M.; Lavelle, E. C., Chitin-derived polymer deacetylation regulates mitochondrial reactive oxygen species dependent cGAS-STING and NLRP3 inflammasome activation. *Biomaterials* **2021,** *275*, 120961.